



COM DEV LTD.

DEVELOPMENT OF MICROSTRIP ANTENNA
TECHNOLOGY FOR THE CANADIAN
MSAT PROGRAM

FINAL REPORT

RPT/MST/2500/001 REV. -

PROJECT #2500



- MICROWAVE PRODUCTS
- CONSULTING SERVICES

IC

LKC
P
91
.C654
D49
1986

P
91
C654
D48631
1986

DD 10671146

DL 10717113

REVISION RECORD

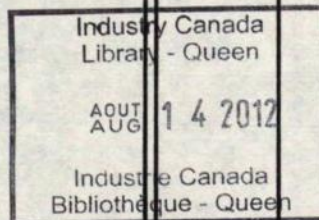
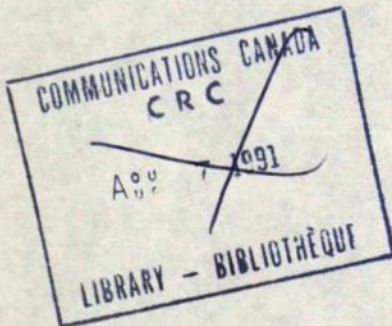
LTR

ECN

NUMBER

APPD

DATE



WRITTEN

DATE

Stephen J. Kavanagh
July 11, 1986

CHECKED

DATE

AS Raab
11 July 86

APPROVED

DATE

AS Raab
11 July 86



COM DEV

155 Sheldon Drive
Cambridge, Ontario
Canada N1R 7H6

FINAL REPORT
DEVELOPMENT OF MICROSTRIP ANTENNA
TECHNOLOGY FOR THE CANADIAN
MSAT PROGRAMME

DOCUMENT No.

REV.

MSAT
PROJECT #2500

RPT/MST/2500/001

SHEET 1 OF 200

© Her Majesty the Queen in Right of Canada (1986) as represented by the Minister of Supply And Services.

TABLE OF CONTENTS

<u>ITEM</u>	<u>DESCRIPTION</u>	<u>PAGE</u>
1.0	INTRODUCTION	10
2.0	LITERATURE SURVEY	11
3.0	ANTENNA REQUIREMENTS FOR MSAT	13
3.1	Background	13
3.2	Reflector Antenna Systems	13
3.2.1	Two Beam Configuration	13
3.2.2	Four Beam Configuration	16
3.3	Direct Radiating Arrays	17
4.0	PATCH ANTENNA ELEMENTS	31
4.1	Microstrip Patch Radiators	31
4.1.1	Description	31
4.1.2	Input Impedance	32
4.1.3	Circular Polarization	35
4.1.4	Radiating Properties	37
4.2	Single Band Patch Antenna Experiments	38
4.3	Options for Transmit/Receive Elements	40
4.3.1	MSAT Requirements	40
4.3.2	Wider Bandwidth Simple Patches	40
4.3.3	Single Patches for Dual Frequency Operation	42
4.3.4	Elements With Multiple Patch Resonators	43
4.4	Experiments with Stacked Patch Antennas	45
4.4.1	Experimental Antennas	45
4.4.2	Characteristic of Stacked Air-Dielectric Square Patch Antenna	45
4.4.3	Mutual Coupling Between Stacked Patch Antennas	48
4.5	Power Handling Capability of Patch Elements	50

TABLE OF CONTENTS

<u>ITEM</u>	<u>DESCRIPTION</u>	<u>PAGE</u>
5.0	BEAM FORMING NETWORK TECHNOLOGY	89
5.1	Transmission Line Options	89
5.2	Stripline Design	90
5.3	Experimental Coupler Design	94
5.4	Recommendations for BFN Development	95
6.0	MECHANICAL AND THERMAL DESIGN	111
6.1	Patch Element	111
6.2	Mass and Envelope Estimates for Reflector Feeds	112
6.3	Mass and Envelope for Array Antennas	113
6.4	Mechanical Design	114
6.5	Thermal Control	117
6.6	Materials	121
7.0	DESCRIPTION OF ENGINEERING MODEL	125
7.1	Construction	125
7.2	RF Performance	128
8.0	CONCLUSIONS	145
9.0	REFERENCES	148
	APPENDIX A	157
	APPENDIX B	165
	APPENDIX C	196
	APPENDIX D	208

LIST OF FIGURES

<u>ITEM</u>		<u>PAGE</u>
FIGURE 3.1	TWO BEAM FEED ARRAY FOR 4.9 m REFLECTOR	20
FIGURE 3.2	COMPUTED DIRECTIVITY CONTOURS OF 4.9 m REFLECTOR WITH 10 ELEMENT 2-BEAM MICROSTRIP FEED ARRAY AT 823 MHz	21
FIGURE 3.3	COMPUTED DIRECTIVITY CONTOURS OF 4.9 m REFLECTOR WITH 10 ELEMENT 2-BEAM MICROSTRIP FEED ARRAY AT 868 MHz	22
FIGURE 3.4	FOUR BEAM FEED ARRAY FOR 7.3 m REFLECTOR	23
FIGURE 3.5	COMPUTED 29 dB DIRECTIVITY CONTOURS OF 7.3m REFLECTOR WITH 21 ELEMENT 4-BEAM MICROSTRIP FEED ARRAY AT 823 MHz	24
FIGURE 3.6	COMPUTED 29 dB DIRECTIVITY CONTOURS OF 7.3 dB REFLECTOR WITH 21 ELEMENT 4-BEAM MICROSTRIP FEED ARRAY AT 868 MHz	25
FIGURE 3.7	FRONT FACE OF 2-BEAM ARRAY	26
FIGURE 3.8	BEAM FORMING NETWORKS FOR 2-BEAM ARRAY ANTENNA	27
FIGURE 3.9	COMPUTED DIRECTIVITY CONTOURS OF 4.2 m SQUARE PLANAR ARRAY AT 823 MHz	28
FIGURE 3.10	FOUR-BEAM ARRAY BEAMS USING TWO 2-WAY BUTLER MATRICES (-4 dB CONTOURS)	29
FIGURE 3.11	FOUR-BEAM ARRAY BEAMS USING 4-WAY BUTLER MATRIX (-4 dB CONTOURS)	30
FIGURE 4.1	TYPICAL MICROSTRIP ANTENNAS	58
FIGURE 4.2	GEOMETRY OF RECTANGULAR MICROSTRIP ANTENNA	59
FIGURE 4.3	EQUIVALENT CIRCUIT FOR RECTANGULAR MICROSTRIP WITH COAXIAL PROBE FEED	60

LIST OF FIGURES

<u>ITEM</u>		<u>PAGE</u>
FIGURE 4.4	SINGLE FEED CIRCULARLY POLARIZED MICROSTRIP ANTENNAS	61
FIGURE 4.5	TWO-FEED CIRCULARLY POLARIZED MICROSTRIP ANTENNA WITH ORTHOGONAL-PHASE FEED NETWORK	62
FIGURE 4.6	SINGLE PATCH ANTENNA WITH TWO FEEDS (SINGLE BAND BREADBOARD)	63
FIGURE 4.7	MEASURED RETURN LOSS AND ISOLATION OF BREADBOARD RECEIVE BAND ELEMENT (INPUT TO PORT 1)	64
FIGURE 4.8	MEASURED RETURN LOSS AND ISOLATION OF BREADBOARD RECEIVE BAND ELEMENT (INPUT TO PORT 2)	65
FIGURE 4.9	MEASURED RETURN LOSS AND ISOLATION OF BREADBOARD TRANSMIT BAND ELEMENT (INPUT TO PORT 1)	66
FIGURE 4.10	MEASURED RETURN LOSS AND ISOLATION OF BREADBOARD TRANSMIT BAND ELEMENT (INPUT TO PORT 2)	67
FIGURE 4.11	MEASURED E- AND H-PLANE PATTERNS OF BREADBOARD RECEIVE BAND ELEMENT AT 823 MHz	68
FIGURE 4.12	MEASURED E- AND H-PLANE PATTERNS OF BREADBOARD TRANSMIT BAND ELEMENT AT 868 MHz	69
FIGURE 4.13	PATTERN TESTING GEOMETRY	70
FIGURE 4.14	MICROSTRIP ANTENNA LOADED BY COAXIAL STUB	71
FIGURE 4.15	MICROSTRIP ANTENNA WITH COPLANAR PARASITIC RESONATORS	72
FIGURE 4.16	CIRCULARLY POLARIZED MICROSTRIP ANTENNA WITH SHORTED QUARTER-WAVE PARASITIC RESONATORS	73
FIGURE 4.17	CROSS SECTION OF STACKED PATCH ANTENNA	74
FIGURE 4.18	EXPERIMENTAL STACKED PATCH ANTENNA	75

LIST OF FIGURES

<u>ITEM</u>		<u>PAGE</u>
FIGURE 4.19	EQUIVALENT CIRCUIT FOR STACKED PATCH ANTENNA	76
FIGURE 4.20	RETURN LOSS AND BANDWIDTH OF STACKED PATCH ANTENNAS	77
FIGURE 4.21	RETURN LOSS AND ISOLATION OF A STACKED AIR-DIELECTRIC SQUARE PATCH ANTENNA. LOWER PATCH 6.4 x 6.4 INCHES, SPACED 0.35 INCH FROM GROUND PLANE; UPPER PATCH 5.5 x 5.5 INCHES, SPACED 0.50 INCH FROM LOWER PATCH	78
FIGURE 4.22	MEASURED RETURN LOSS AND PORT-TO-PORT ISOLATION OF BREADBOARD STACKED PATCH ANTENNA (INPUT TO PORT 1)	79
FIGURE 4.23	MEASURED RETURN LOSS AND PORT-TO-PORT ISOLATION OF BREADBOARD STACKED PATCH ANTENNA (INPUT TO PORT 2)	80
FIGURE 4.24	MEASURED E- AND H-PLANE PATTERNS OF BREADBOARD STACKED PATCH ELEMENT AT 823 MHz	81
FIGURE 4.25	MEASURED E-AND H-PLANE PATTERNS OF BREADBOARD STACKED PATCH ELEMENT AT 868 MHz	82
FIGURE 4.26	EFFECT OF BETA CLOTH COVER OVER BREADBOARD STACKED PATCH ANTENNA: RETURN LOSS	83
FIGURE 4.27	EFFECT OF BETA CLOTH COVER OVER BREADBOARD STACKED PATCH ANTENNA: PORT-TO-PORT ISOLATION	84
FIGURE 4.28	GEOMETRY OF E- AND H-PLANE MUTUAL COUPLING	85
FIGURE 4.29	MEASURED E- AND H-PLANE MUTUAL COUPLING VERSUS SPACING BETWEEN BREADBOARD STACKED PATCH ANTENNAS AT 820 MHz	86
FIGURE 4.30	MEASURED E- AND H-PLANE MUTUAL COUPLING VERSUS SPACING BETWEEN BREADBOARD STACKED PATCH ANTENNAS AT 870 MHz	87

LIST OF FIGURES

<u>ITEM</u>		<u>PAGE</u>
FIGURE 4.31	SEPTET COUPLING GEOMETRIES (VIEWED TOWARD FRONT FACE, ALL CASES 12 IN. CENTRE-TO-CENTRE SPACING)	88
FIGURE 5.1	TRANSMISSION LINE CANDIDATES	99
FIGURE 5.2	VACUUM-SPACED STRIPLINE GEOMETRY	100
FIGURE 5.3	ATTENUATION OF SILVER STRIPLINE VERSUS GROUND PLANE SPACING	101
FIGURE 5.4	COAXIAL TO STRIPLINE TRANSITION	102
FIGURE 5.5	EQUIVALENT CIRCUIT FOR STRIPLINE COUPLER	103
FIGURE 5.6	LAYOUT OF EXPERIMENTAL STRIPLINE COUPLER	104
FIGURE 5.7	MEASURED RETURN LOSS OF STRIPLINE COUPLER	105
FIGURE 5.8	MEASURED ISOLATION OF STRIPLINE COUPLER	106
FIGURE 5.9	MEASURED STRAIGHT-THROUGH LOSS OF STRIPLINE COUPLER	107
FIGURE 5.10	MEASURED COUPLING OF STRIPLINE COUPLER	108
FIGURE 5.11	TOTAL LOSS OF EXPERIMENTAL STRIPLINE COUPLER	109
FIGURE 5.12	MEASURED PHASE ANGLE BETWEEN STRAIGHT-THROUGH AND COUPLED PORTS OF EXPERIMENTAL STRIPLINE COUPLER	110
FIGURE 6.1	0.02 IN PATCH VIBRATION PLOT ONE g INPUT	122
FIGURE 6.2	STRIPLINE DIELECTRIC SUPPORTS	123
FIGURE 6.3	SHORTED QUARTER WAVE STUB HEAT SINK	124
FIGURE 7.1	ENGINEERING MODEL EXPLODED VIEW	132
FIGURE 7.2	PHOTOGRAPH OF ENGINEERING MODEL DURING ASSEMBLY SHOWING BFN LAYER	133

LIST OF FIGURES

<u>ITEM</u>		<u>PAGE</u>
FIGURE 7.3	PHOTOGRAPH OF ENGINEERING MODEL DURING ASSEMBLY SHOWING COUPLER LAYER	134
FIGURE 7.4	PHOTOGRAPH OF ENGINEERING MODEL BEFORE PATCH ASSEMBLY	135
FIGURE 7.5	COMPLETED ENGINEERING MODEL	136
FIGURE 7.6	FRONT FACE OF COMPLETED ENGINEERING MODEL MOUNTED IN GROUND PLANE EXTENSION	137
FIGURE 7.7	BACK FACE OF COMPLETED ENGINEERING MODEL MOUNTED IN GROUND PLANE EXTENSION	138
FIGURE 7.8	RETURN LOSS AND ISOLATION OF ENGINEERING MODEL ELEMENT (INPUT TO PORT 1)	139
FIGURE 7.9	RETURN LOSS AND ISOLATION OF ENGINEERING MODEL ELEMENT (INPUT TO PORT 2)	140
FIGURE 7.10	E- AND H-PLANE PATTERNS OF ENGINEERING MODEL ELEMENT AT 823 MHz (PORT 1)	141
FIGURE 7.11	E- AND H-PLANE PATTERNS OF ENGINEERING MODEL ELEMENT AT 823 MHz (PORT 2)	142
FIGURE 7.12	E- AND H-PLANE PATTERNS OF ENGINEERING MODEL ELEMENT AT 868 MHz (PORT 1)	143
FIGURE 7.13	E- AND H-PLANE PATTERNS OF ENGINEERING MODEL ELEMENT AT 868 MHz (PORT 2)	144

LIST OF TABLES


<u>ITEM</u>	<u>DESCRIPTION</u>	<u>PAGE</u>
TABLE 3.1	LOSS BUDGET ESTIMATE FOR 2-BEAM ARRAY	19
TABLE 4.1	MEASURED CHARACTERISTICS OF BREADBOARD SINGLE BAND PATCH ELEMENTS	52
TABLE 4.2	BEAMWIDTHS AND SQUINT OF BREADBOARD SINGLE BAND PATCH ELEMENTS	54
TABLE 4.3	PARAMETER RANGES FOR STACKED AIR-DIELECTRIC SQUARE PATCH EXPERIMENTS	54
TABLE 4.4	RETURN LOSS AND ISOLATION SUMMARY FOR BREADBOARD STACKED PATCH ANTENNA	55
TABLE 4.5	BEAMWIDTHS AND SQUINT OF BREADBOARD STACKED PATCH ELEMENT	56
TABLE 4.6	MUTUAL COUPLING BETWEEN STACKED PATCH ANTENNAS IN SEPTET CONFIGURATIONS	57
TABLE 5.1	COMPARISON OF TRANSMISSION LINE CHARACTERISTICS	98
TABLE 7.1	ENGINEERING MODEL RETURN LOSS AND ISOLATION SUMMARY	130
TABLE 7.2	ENGINEERING MODEL PATTERN SUMMARY	132

INTRODUCTION

The first generation MSAT system concept uses one satellite covering North America using transmit and receive frequencies in the UHF band (near 850 MHz) for communication with mobile stations. One or more large deployable reflectors (in the 4-9 metre diameter range) have been suggested as antennas capable of sufficient gain to minimize the size and cost of the mobile station antennas. A multibeam feed producing a small number of beams (typically 2-4) may be used. If conventional horn antennas are used in this feed the mass and volume of the feed may be excessive.

Microstrip antennas offer an alternative technology which because of their planar geometry have the potential to reduce the mass and volume requirements of the feed array. Their major drawbacks are narrow bandwidth and a lack of previously developed techniques for space applications. The primary goal of this study has been to investigate the use of a microstrip antenna feed capable of simultaneous transmit and receive operation in both right and left hand circular polarization. This could, in principle, permit the use of a single reflector at UHF.

This report contains a review of system requirements and of microstrip antenna technology, especially with regard to dual band or wideband radiators. The results of a program of development of suitable patch antenna elements and some of the necessary beam-forming network components are included, and the mechanical and thermal characteristics of these elements are described. Finally an engineering model of a radiating element constructed as part of this work is described.

DOCUMENT No.	REV.	 COM DEV
RPT/MST/2500/001	—	
		SHEET 10

The potential for low mass and volume combined with low manufacturing cost for quite sophisticated arrays has given rise to a great deal of research and development of microstrip antennas since about 1970. Their use in spacecraft applications has so far been quite limited. The best known example is that of the synthetic aperture radar arrays used on SEASAT and SIR-A described by Murphy [39] and in a report prepared by Astro Research Corporation [68].

Because of their inherently narrow bandwidth there is a strong demand for accurate theoretical models of microstrip antennas. The simplest of these is based on modelling the antenna as a transmission line. This is described by Sengupta [53] and Pues and Van de Capelle [46] among others. Other theoretical techniques include the use of a summation of modes (the "cavity" model) and moment methods. Recent work in these areas has been published by Bailey and Deshpande [2, 3, 16], Carver [6], De and Das [15], Martin and Griffin [33, 34] and Pozar [43, 45]. The square and circular patch geometries of microstrip antennas may be used for circular polarization by feeding in two places with signals 90 degrees apart in phase. The performance is limited by higher order modes as described by Chiba et al. [9]. Nearly square or elliptical patches with a single feedpoint can generate circular polarization as described by Haneishi et al. [21] and Sharma and Gupta [54], but normally maintain good axial ratio only over very narrow bandwidths. To obtain good matching over wider bands than 1 - 2 percent, it is necessary to use thick substrate materials, preferably of low permittivity. Antennas using air gaps [30], foam [25] and honeycomb [7, 57, 63] dielectrics have been described.

Narrow bandwidth has been the most serious drawback of microstrip antennas and, especially recently, has given rise to several techniques for obtaining wide band or multiple-band response. Unusual planar shapes such as the rectangular ring and H-shaped patches reported by Palanisamy and Garg [41] and stepped and wedge shaped resonators described by Poddar, et al. [42] can offer wider bandwidth. So can conical resonators [13, 23] but with greatly increased difficulty in manufacture. Matching of ordinary patch antennas can be improved with a series capacitor [17]. Other bandwidth improving techniques have included the use of auxiliary or parasitic resonances due to coplanar patches (see Kumar and Gupta [28, 29] and Wood [65]), slots in the patch (Wang and Lo [60]), reactive loading [14, 49, 50] and stacking patches in layers. This last method currently is most promising for wideband applications and empirically developed designs have been described by Chen et al. [8], Dahele and Lee [11, 12], Montgomery [37] and Sabban [52]. A review paper by Carver and Mink [7] covers the state of microstrip antenna theory and practice up to 1980.

The use of microstrip elements in arrays has been described by a number of authors including Hall [19], Haneishi et al. [21], Karlsson [25] and a 1981 review paper by Mailloux et al. [32]. Mutual coupling measurements between ordinary patch antennas have been presented by Jedlicka, et al. [24] and between stacked patches by Chen et al. [8]. Theoretical treatments of mutual coupling include those of Krowne [27], Newman et al. [40] Pozar et al. [43, 45] and Van Lil and Van de Capelle [58, 59]. Effects of finite ground planes have been studied by Huang [22] and Lier and Jakobsen [31]. Much of the early work on microstrip elements and arrays is included in the proceedings of the Workshop on Printed Circuit Technology (see ref. [39]), published in 1979.

3.0 ANTENNA REQUIREMENTS FOR MSAT

3.1 Background

A variety of system concepts for mobile communications satellites have been proposed, using either UHF frequencies (near 850 MHz) or L-Band (near 1.5 GHz), or both. Most specify coverage of CONUS and Canada and some include Alaska. Primarily because of limitations on antenna size a small number of beams is used.

We have chosen to consider the use of microstrip antennas to provide similar performance to two and four beam UHF configurations proposed by SPAR Aerospace (see Wegrowicz [61]). SPAR's 2 beam design does not cover all of Alaska and achieves an edge of coverage directivity of 28 dB using a 4.9m diameter reflector with both beams having the same polarization and no frequency reuse. Circular polarization is used. Their four beam design includes coverage of Alaska and has 29 dB directivity at the edge of coverage, using a 7.3m diameter reflector. There is frequency reuse in the eastern most and western most beams. In both designs all beams have the same sense of polarization. A satellite located at 109° west is assumed. This chapter describes the use of microstrip array fed reflectors and direct radiating microstrip arrays to provide similar levels of service.

3.2 Reflector Antenna Systems

3.2.1 Two Beam Configuration

To form two overlapping beams for both transmit and receive, there are a number of options available to trade between the number of reflectors, feed complexity and earth station



requirements. In principle the best choice is to use four reflectors which could be denoted as Beam 1 Transmit, Beam 1 Receive, Beam 2 Transmit and Beam 2 Receive. This allows full flexibility in pointing and polarization, good transmit/receive isolation and simple feeds (perhaps single horns). However, for MSAT sized reflectors the mass and volume are prohibitively high. Using two reflectors, one may be used for each beam, with each reflector operating in both receive and transmit modes. The feeds are still very simple but isolation between the transmitter and receiver is sacrificed resulting in more stringent requirements on PIM levels. Alternatively one reflector can be used for transmission and the other for reception. The transmit/receive isolation is regained but at the expense of more complicated feeds capable of producing two beams each. The beams may be separated by using different polarizations or by using a dual mode beam forming network. To reduce the mass and volume further a single reflector may be used, with a single transmit/receive feed producing two beams using a dual mode BFN or having opposite senses of polarization.

For this study the single reflector case was chosen for most of the analysis as it is potentially the most difficult and any results can be applied to the other configurations quite easily. The same reflector diameter as the SPAR design (4.9m) was chosen. It is mounted on the east side of the spacecraft and offset along the east/west axis. The two beams are of opposite senses of circular polarization. The dual mode BFN option (co-polarized beams) would be more convenient to users but would give slightly worse aperture efficiency and a more complicated feed network. The feed array is composed of a triangular grid of square vacuum-dielectric patch elements with 12 inch spacing

between centres. This spacing is driven by expected mutual coupling effects, i.e. the equivalent areas of adjacent elements should not overlap significantly. This spacing has forced the use of a long focal length ($f/D=0.85$). This is only partially offset by easier deployment and space savings afforded by a very thin feed array. The array contains two overlapping septets of patches for a total of 10 elements as shown in Figure 3.1. Each septet corresponds to a beam. Behind each element is a 3dB coupler to produce circular polarization. Each of the two inputs to this coupler produces one of the two senses of polarization. Each element is fed from the outputs of one or two beam forming networks, depending on whether the element is in the overlapping area of the septets. These BFN's can, at least in theory, be made in planar form without crossovers. Slightly more than half the power in each beam is fed to the central element with the rest divided equally among the surrounding six elements. All the elements in each septet are in phase.

The radiation patterns of the feed elements are computed according to Carver and Mink [7] using the computer program NPATPlF (see Appendix A), a modified version of earlier COM DEV software. Another existing program computes the secondary radiation patterns. The calculated directivity contours for this 10 element feed and 4.9m reflector are shown in Figures 3.2 (823 MHz) and 3.3 (868 MHz). The circular beams are very similar in performance to the SPAR design. No frequency reuse is possible as the cross-polar levels are too high for such closely spaced beams.

3.2.2

Four Beam Configuration

Similar options to the two beam case are available in choosing the number of reflectors and the feed systems for a four beam configuration. Again the single reflector with beams of alternating sense of polarization was chosen. The feed array is a 12 inch spaced triangular grid of square vacuum-dielectric patch elements and is used with a 7.3m diameter reflector (same as SPAR) with an f/D ratio of 0.85. A total of 21 elements are required, as shown in Figure 3.4. These are not organized into septets but rather into shaped beams. Many of the elements are shared between adjacent beams, the power for one beam applied at the RHCP port and for the other at the LHCP port. The computed 29dB directivity contours are shown in Figures 3.5 (823 MHz) and 3.6 (868 MHz). Computation of interference levels between the eastern most and western most beams have been carried out to evaluate the feasibility of frequency reuse. Co-polarized interference is at least 45 dB below the desired signal but cross-polarized interference is in some areas only about 20 dB down. In most systems this would be sufficient because of the cross-polar rejection available from the earth station antenna. However, the possibility of very poor axial ratio antennas being used on vehicles (due to antenna size restrictions or multipath effects) makes this performance marginal. Optimization of the sidelobe levels of the satellite antenna could improve this performance. As for the two beam feed the BFN's can, in theory, be made in single planar layer, but their complexity may make a two layer configuration more attractive. The computed performance of this antenna is similar to that proposed by SPAR although the beam shapes are somewhat different.

While considering the feasibility of using direct radiating microstrip arrays for MSAT, effort has been concentrated on obtaining comparable beam plans and performance to the reflector configurations discussed above. In order to achieve the same gain as a given reflector antenna the equivalent array must have approximately the same cross-section. For example, a two beam transmit/receive array could be configured as shown in schematic form in Figure 3.7. The antenna is a 13 by 13 array of square patch radiators on a square grid with 30 cm spacing (about 0.85λ). The overall size of the antenna would be about 4.2 m square. Each element is fed from a 3 dB hybrid located behind it to produce circular polarization of either sense. If the two beams are of orthogonal polarization then the RHCP inputs of all the elements can be fed to produce one beam and all the LHCP inputs can be used to form the other beam. The amplitude and phase distributions for the two beams are completely independent. Thus the beams can be scanned independently to any desired direction. Figure 3.8 shows the beamformers.

An initial computation of radiation patterns from such an array was made using a uniform amplitude distribution for each beam to maximize gain. The azimuth distributions have linear phase variations across the aperture to position the beams. More complex aperture distributions could be used to reduce sidelobes or to shape the beams at the expense of gain. The program JPLAP2F was used to compute patterns (see Appendix B). The computed directivity contours of this array at 823 MHz are shown in Figure 3.9. Feed losses are not included in this computation; an estimated loss budget is given in Table 3.1. The performance is very similar to that of the 4.9 m reflector. While the array is slightly smaller than the reflector and does not require the extra focal length dimension it will be substantially heavier if high performance is to be maintained. The mass of such an array is discussed in more detail in Chapter 6.

An attempt to define a single array to produce a 4-beam footprint similar to that of the 7.3 m reflector was not successful. This is a result of the characteristics of orthogonal beams. Only two arbitrary beams may be generated by one array as described above. To minimize inter-beam coupling a multi-beam feed network such as a Butler matrix must be used to excite the array. If two port Butler matrices (single 3 dB couplers) are used to excite pairs of alternate co-polarized beams the cross-over at -4 dB with respect to peak gain will be at too high a level; the increased coverage area per beam results in reduced gain for the same antenna area as the reflector (see Figure 3.10). Alternatively, all the beams could be fed from a 4-port Butler matrix. In this case the -4 dB cross-over levels between adjacent beams are too low. Coverage between the beams is insufficient (not enough overlap), as shown in Figure 3.11. Synthesis of the required patterns using narrow beams from a larger array, or using an active array (transmit/receive modules at the array face with low level BFNs) could be successful but at much higher cost. Roederer [51] and Teshirogi et al. [57] have described active arrays for spacecraft at the conceptual and engineering model stages. Alternatively a pair of two beam arrays could be used. The mass and deployment problems accompanying such a configuration seem prohibitive.

Surprisingly, microstrip arrays, which are often considered as light weight, low cost antennas appear inferior to reflectors in this application. In fact such arrays are more suited to antennas requiring a large number of beams or especially wide angle scanning. The low loss, high power beamformers and beam plans with large overlaps pose serious difficulties for such antennas for use on MSAT.

TABLE 3.1 LOSS BUDGET ESTIMATE FOR 2-BEAM ARRAY

	<u>LOSS</u>
Loss in patch element	0.1 dB
CP coupler loss	0.09
BFN Coupler Losses: 8 at 0.09 dB each	0.72
Stripline: 2 m at 0.25 dB/m	0.50
Patch return loss: 20 dB	0.05
Input return loss: 20 dB	0.05
	<hr/>
TOTAL	1.51 dB

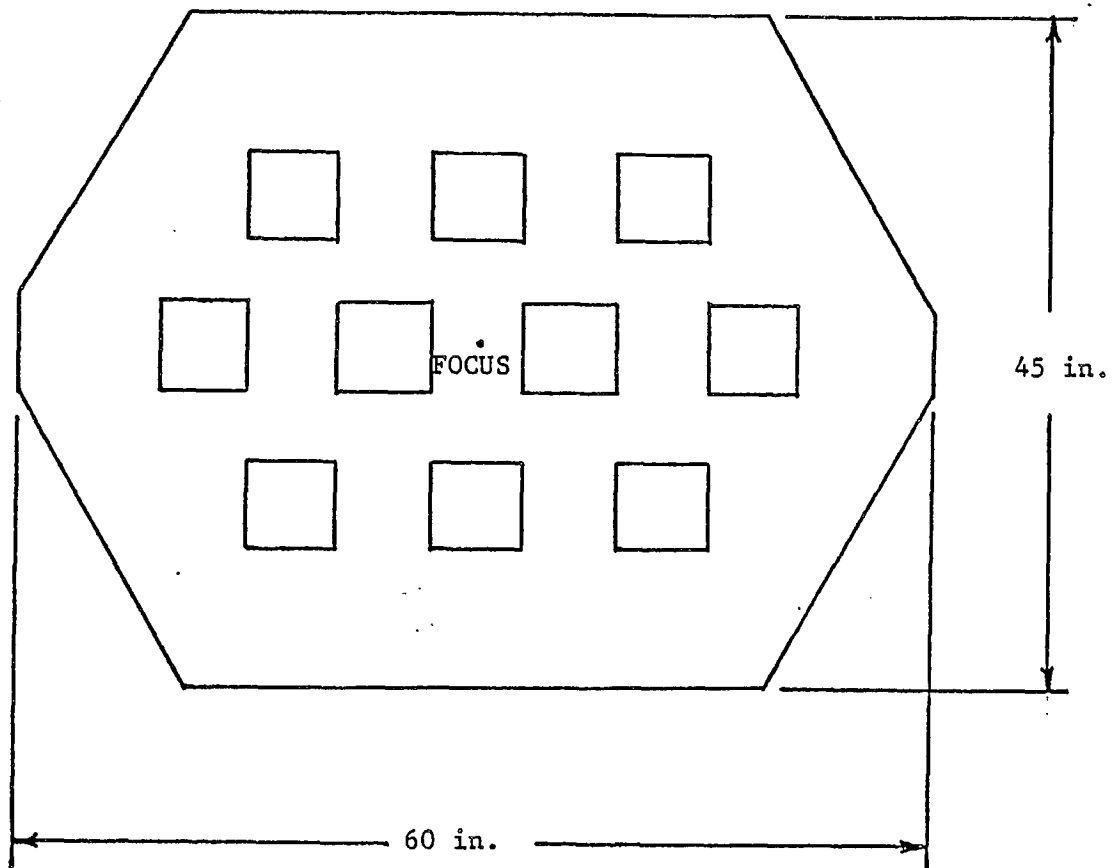


FIGURE 3.1: TWO BEAM FEED ARRAY FOR 4.9 m REFLECTOR

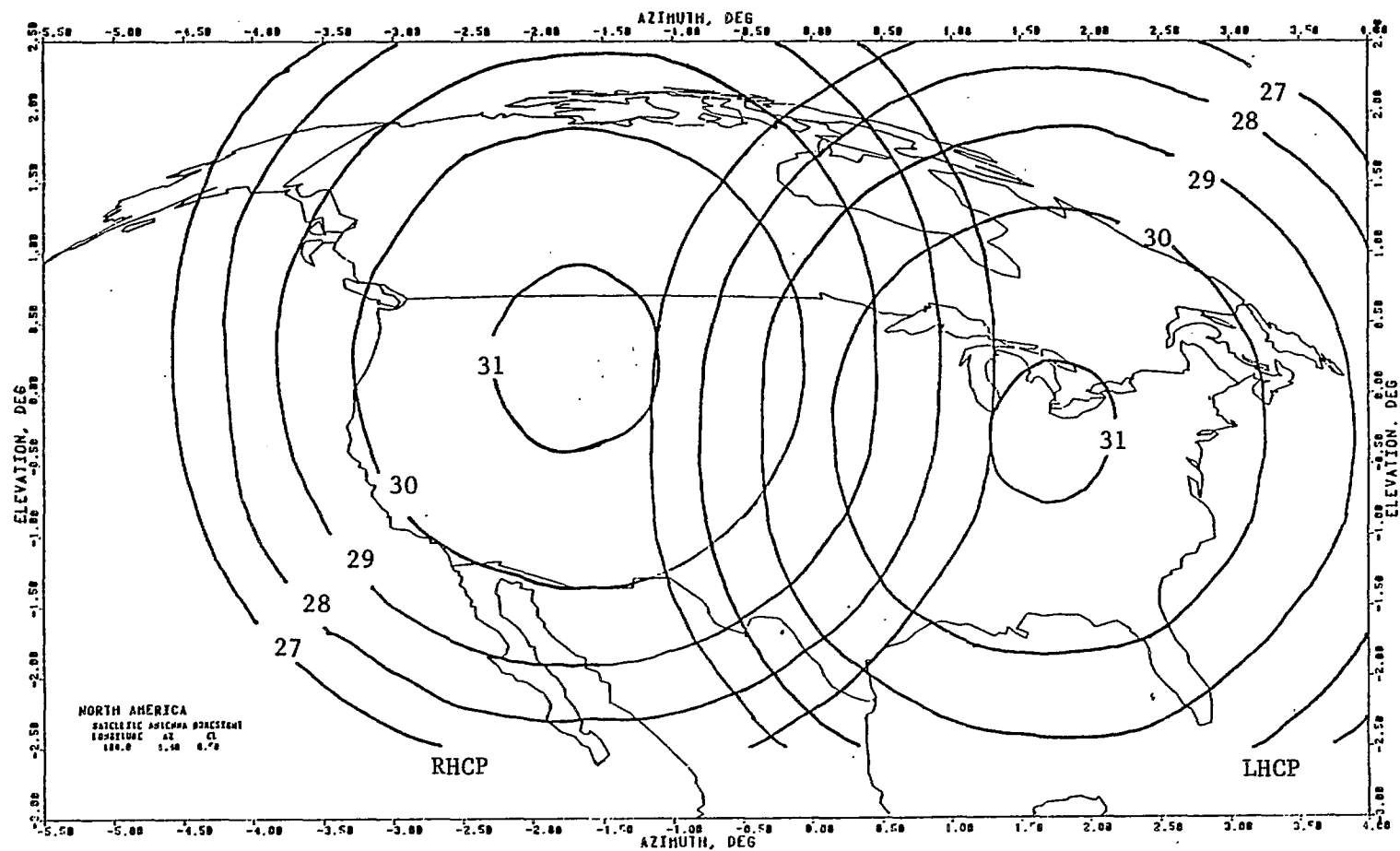


FIGURE 3.2: COMPUTED DIRECTIVITY CONTOURS OF 4.9 m REFLECTOR WITH 10 ELEMENT 2-BEAM MICROSTRIP FEED ARRAY AT 823 MHz

DOCUMENT NO.

REV.

RPT/MST/2500/001



COM DEV

SHEET

21

Her Majesty the Queen in Right of Canada (1986) as represented by the Minister of Supply And Services.

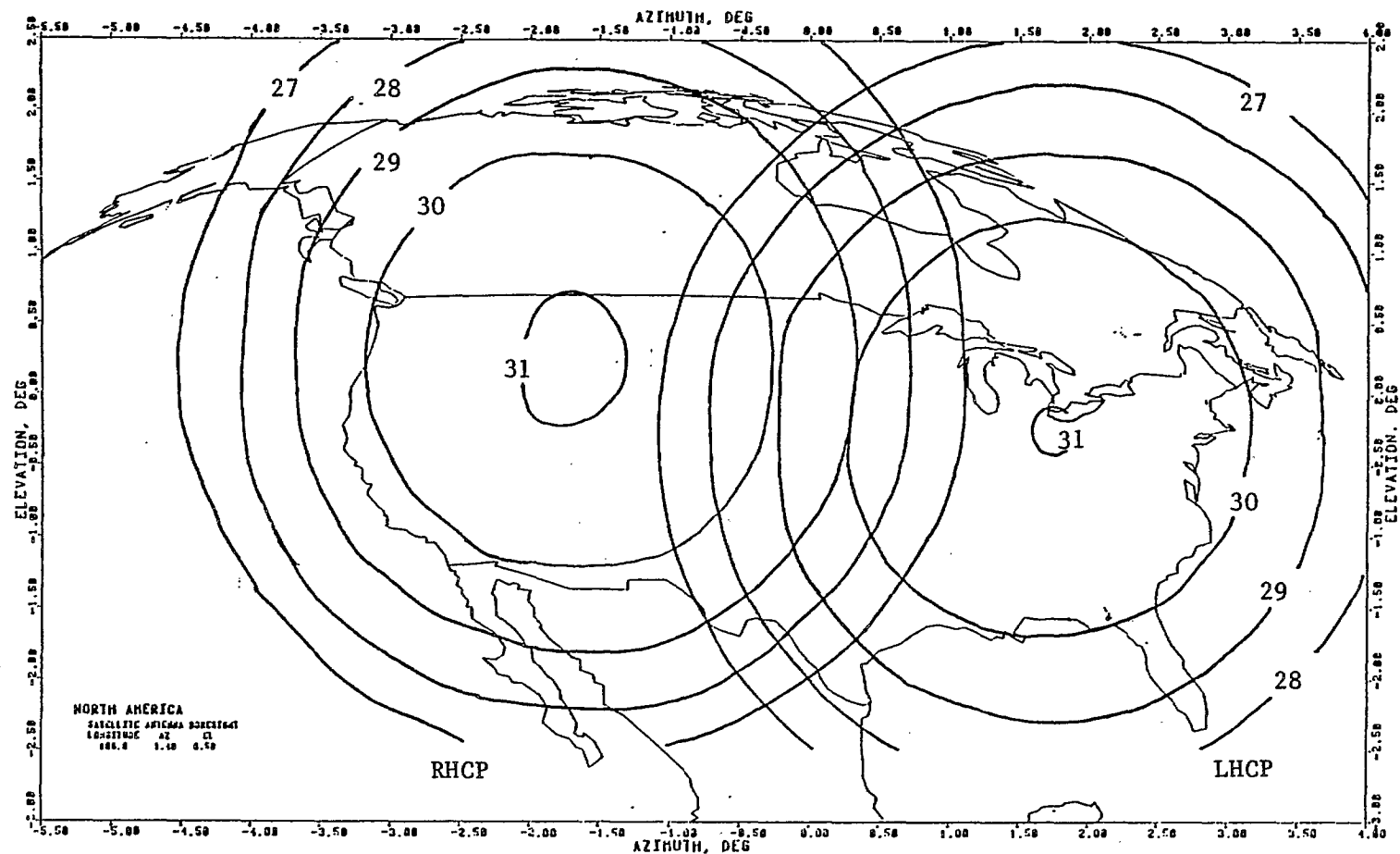


FIGURE 3.3: COMPUTED DIRECTIVITY CONTOURS OF 4.9 m REFLECTOR WITH 10 ELEMENT 2-BEAM MICROSTRIP FEED ARRAY AT 868 MHz

DOCUMENT NO.

REV.

RPT/MST/2500/001

SHEET

22

COM DEV

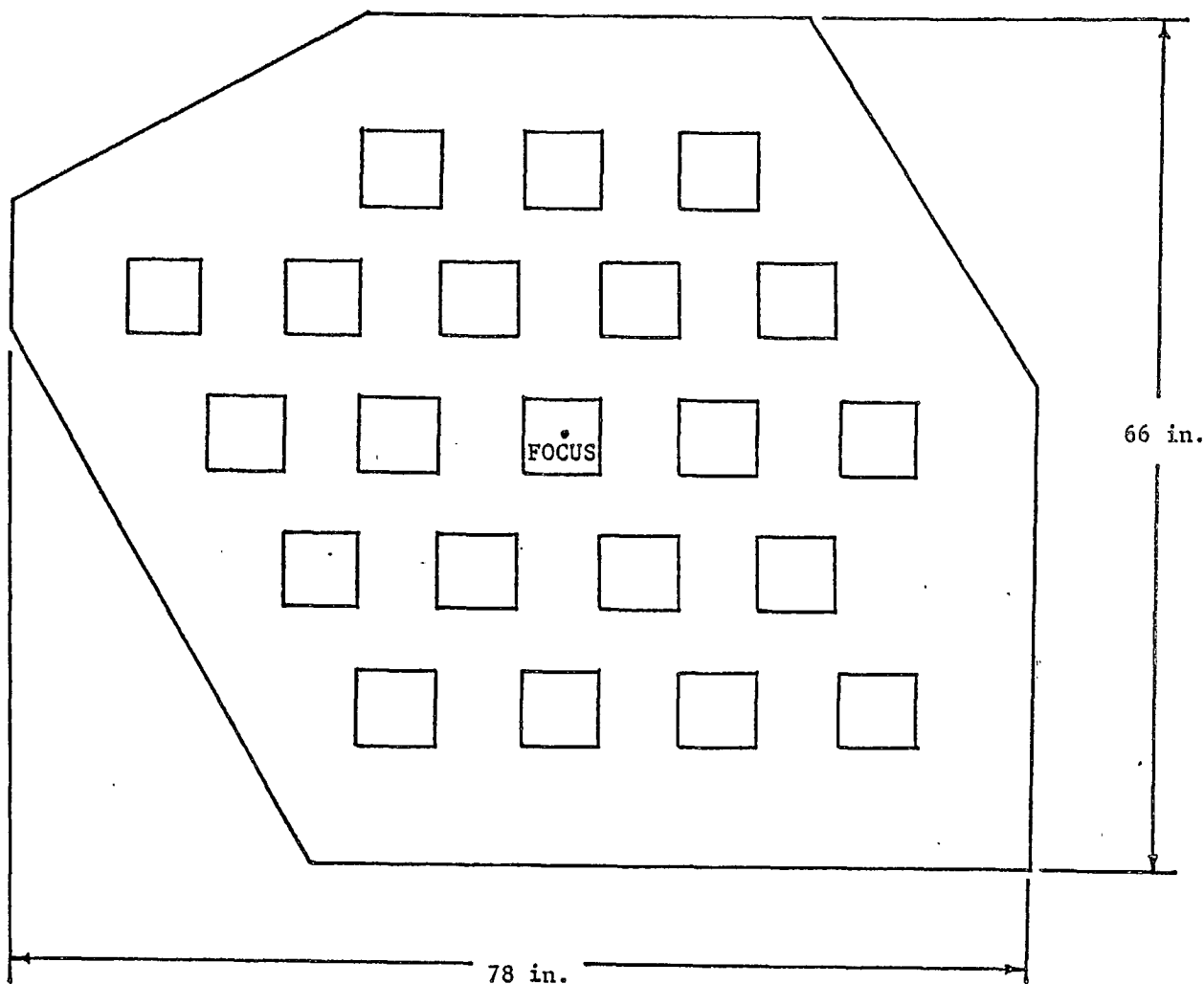


FIGURE 3.4: FOUR BEAM FEED ARRAY FOR 7.3 m REFLECTOR

Her Majesty the Queen in Right of Canada (1986) as represented by the Minister of Supply And Services.

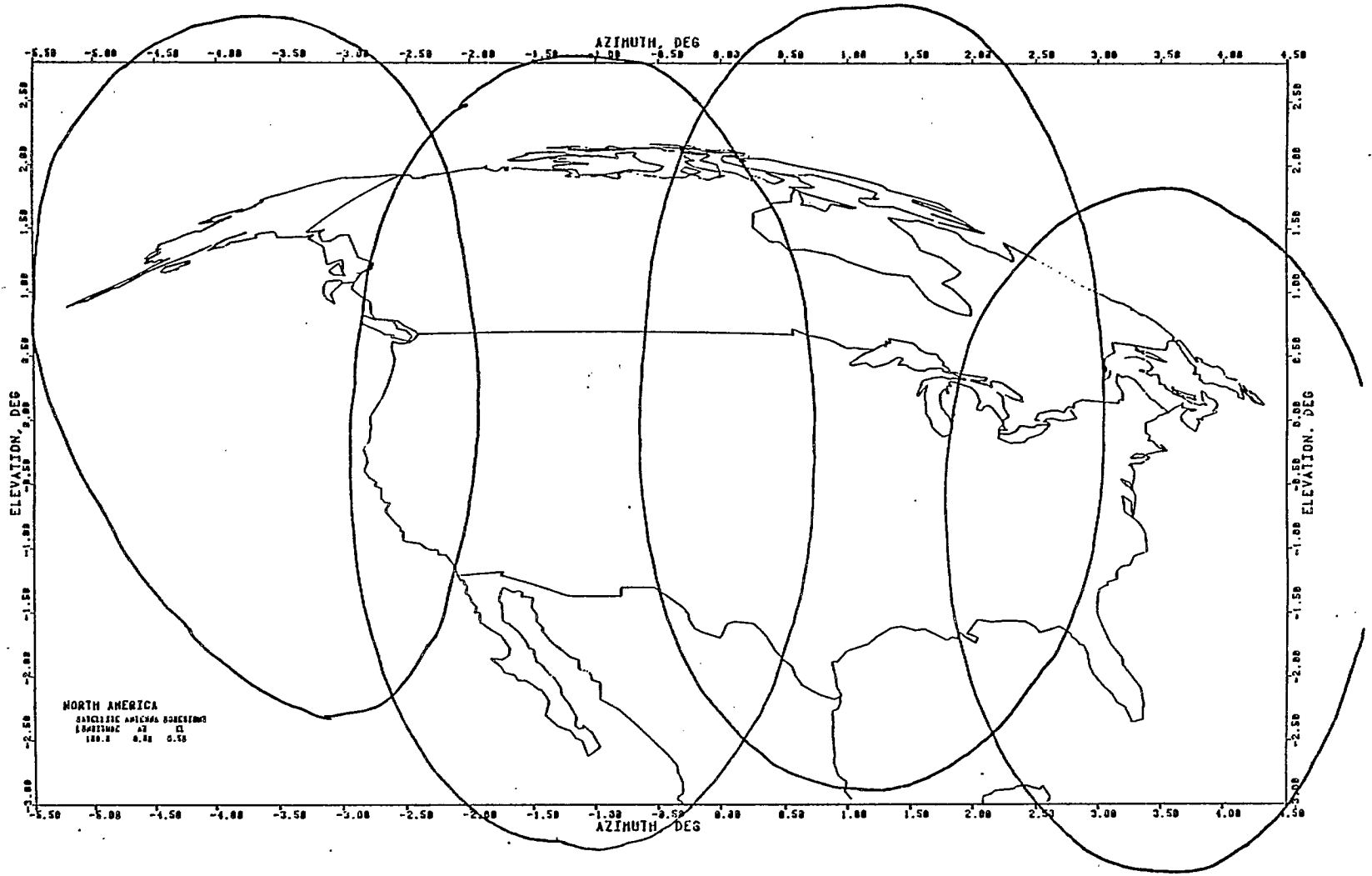


FIGURE 3.5: COMPUTED 29 dB-DIRECTIVITY CONTOURS OF 7.3 m REFLECTOR WITH 21 ELEMENT 4-BEAM MICROSTRIP FEED ARRAY AT 823 MHz

DOCUMENT NO.

REV.

RPT/MST /2500/001

Her Majesty the Queen in Right of Canada (1986) as represented by the Minister of Supply And Services.

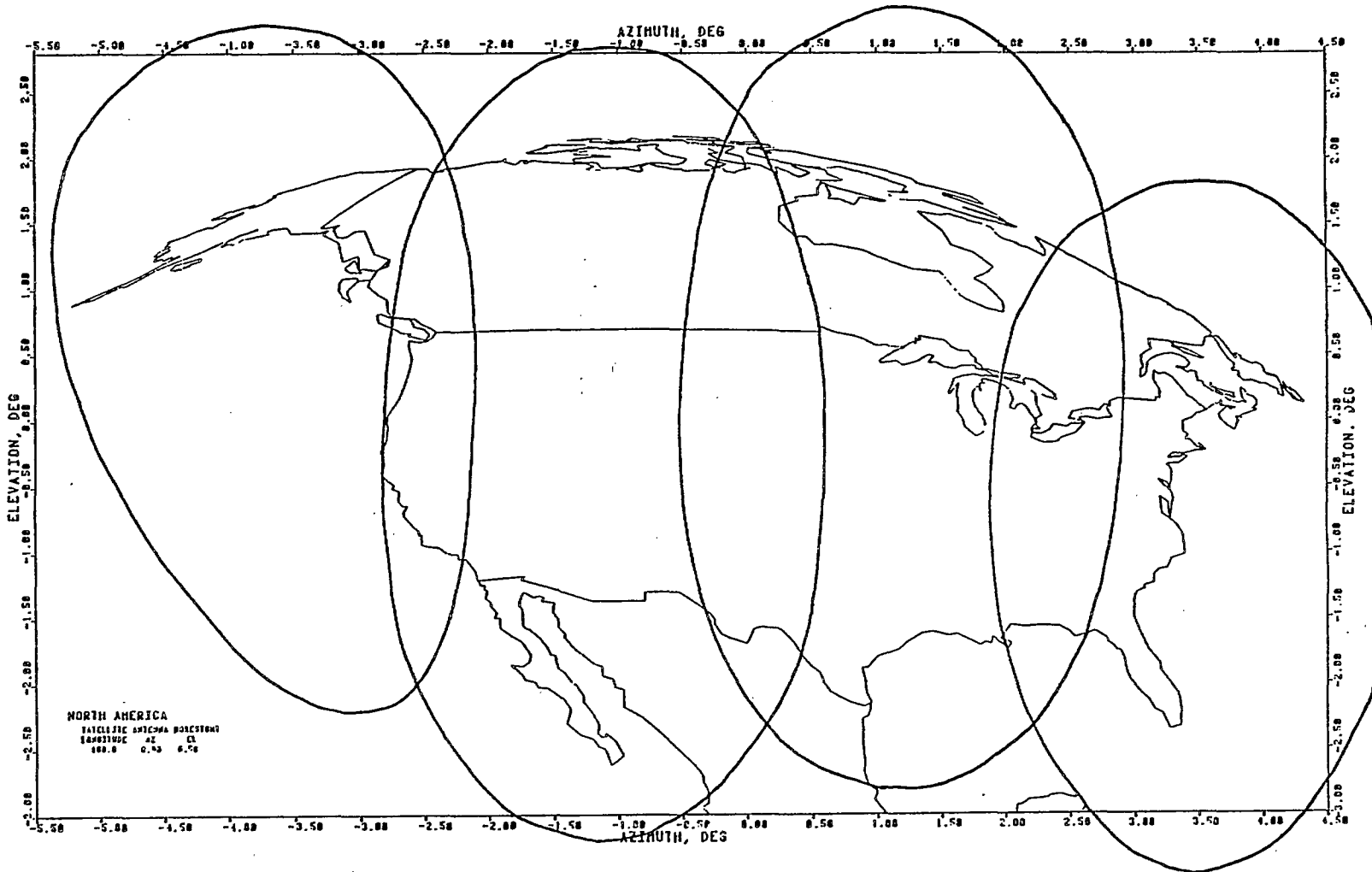


FIGURE 3.6: COMPUTED 29 dB DIRECTIVITY CONTOURS OF 7.3 m REFLECTOR WITH 21 ELEMENT 4-BEAM MICROSTRIP FEED ARRAY AT 868 MHz

DOCUMENT No.		REV.	
RPT/MST/2500/001		—	
SHEET 25		COM DEV	

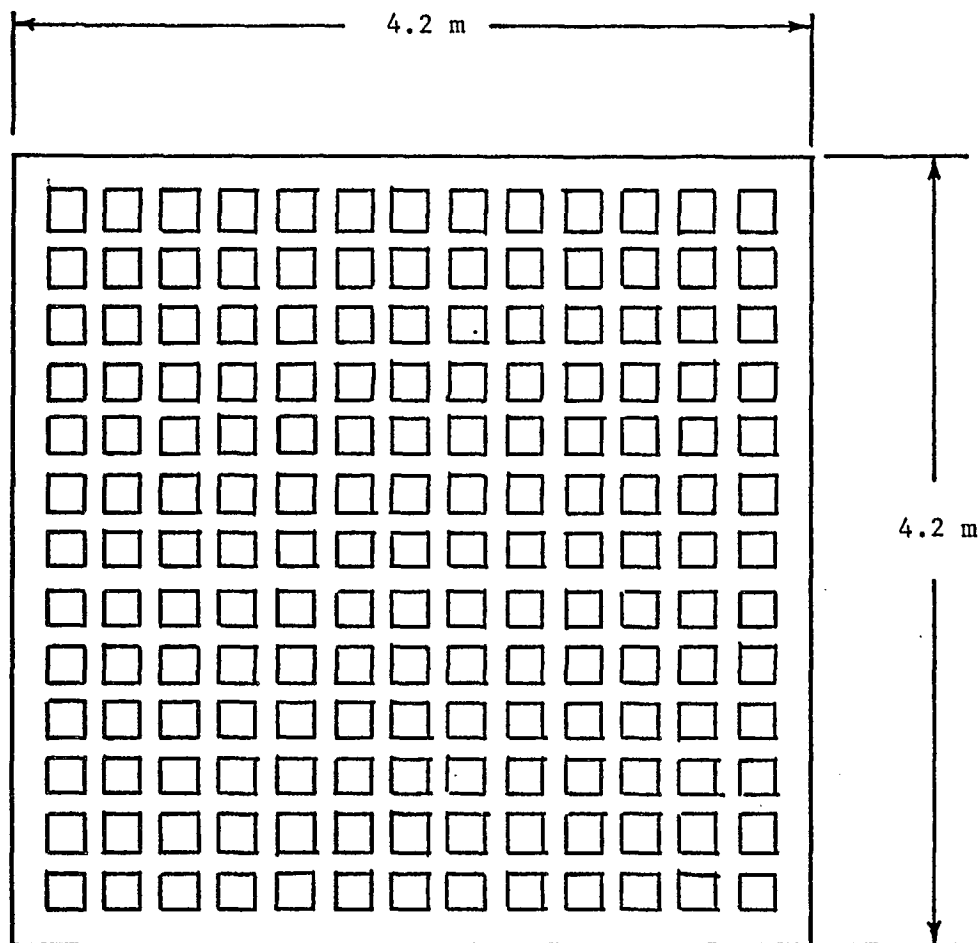


FIGURE 3.7: FRONT FACE OF 2-BEAM ARRAY

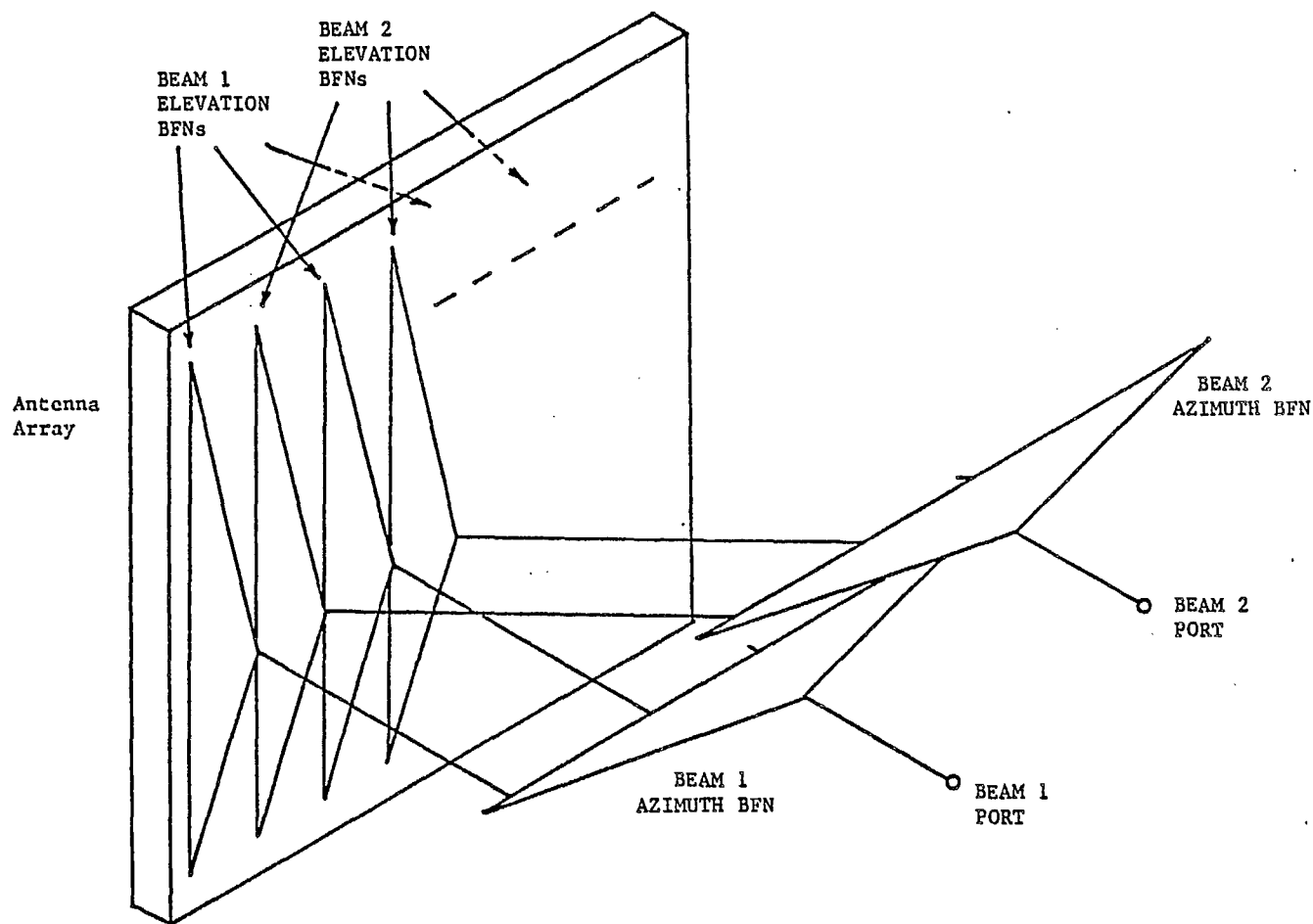


FIGURE 3.8: BEAM FORMING NETWORKS FOR 2-BEAM
ARRAY ANTENNA

Her Majesty the Queen in Right of Canada (1986) as represented by the Minister of Supply And Services.

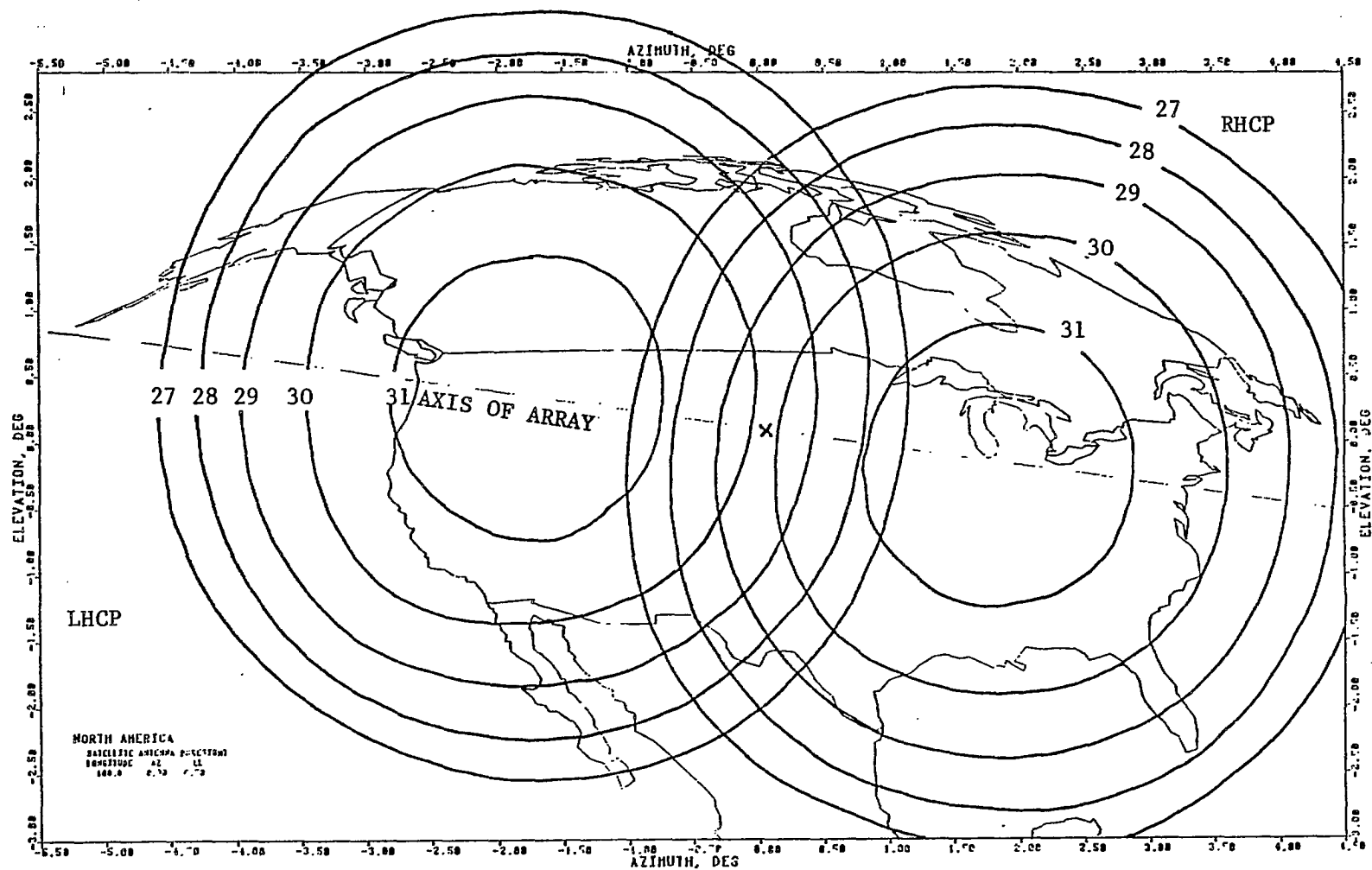


FIGURE 3.9: COMPUTED DIRECTIVITY CONTOURS OF 4.2 m SQUARE PLANAR ARRAY AT 823 MHz

DOCUMENT NO.

RPT/MST/2500/001

REV.



COM DEV

SHEET

28

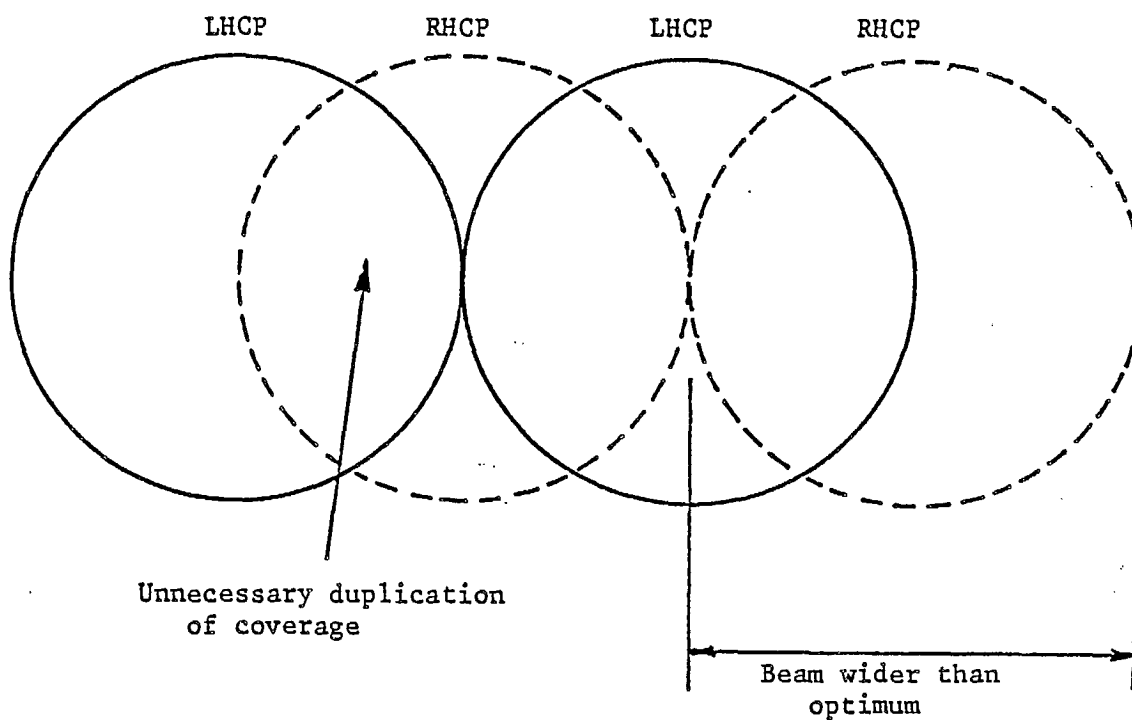


FIGURE 3.10: FOUR-BEAM ARRAY BEAMS USING TWO 2-WAY BUTLER MATRICES (-4 dB CONTOURS)

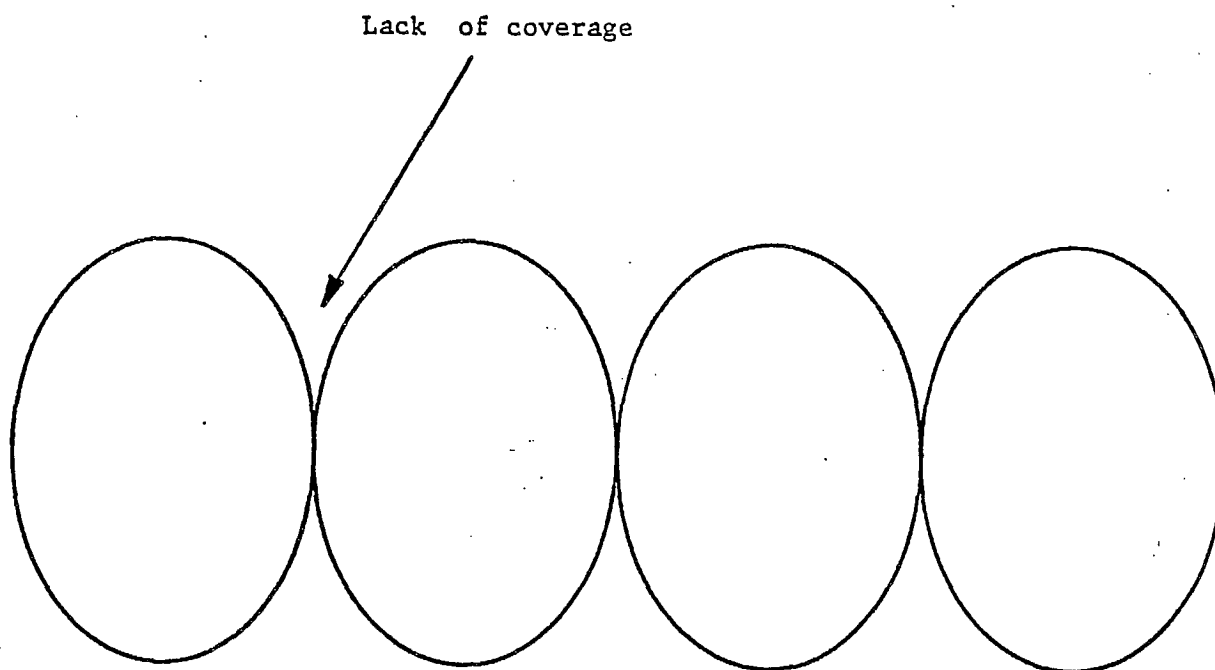


FIGURE 3.11: FOUR-BEAM ARRAY BEAMS USING 4-WAY BUTLER MATRIX (-4 dB CONTOURS)

4.0 PATCH ANTENNA ELEMENTS

4.1 Microstrip Patch Radiators

4.1.1 Description

The most common form of microstrip antenna is a patch of metal supported a small distance over a ground plane by a layer of dielectric material. The patch can be any shape although most often it is rectangular or disk-shaped. Frequently the antenna is manufactured by etching the patch on one side of double-sided copper-clad circuit board. It may be fed by a microstrip line etched on the same side of the board as the radiating patch or by a probe extending through the ground plane to circuitry on the back. Some examples of typical microstrip antennas are shown in Figure 4.1. The transverse dimensions of the patch are usually of the order of a half wavelength but the thickness is very much less.

Because of the small volume the space under the patch behaves like a high Q resonant cavity with radiation from the edges. The transverse dimensions of the patch result in a directivity of 3 to 10 dBi typically. The high Q means that substantial loss is possible in this type of antenna. In order to evaluate the use of such antenna elements for MSAT it is necessary initially to consider the matching bandwidth, the axial ratio bandwidth and method of CP feeding, the efficiency and to a lesser degree, the gain of such elements.

4.1.2 Input Impedance

The matching bandwidth will be examined first. The design band can be 821-825 MHz, 866-870 MHz or 821-870 MHz for a receive only, transmit only or combined transmit/receive element. Allowing 0.5 percent additional bandwidth for thermal contraction and expansion an appropriate specification would be 1 percent or 6.3 percent bandwidth at 20 dB return loss. The requirement for circular polarization means that the element must have the same cross-section in two orthogonal planes and be symmetric about its centre in those planes. Square or circular patches are suitable, for example. Square patches were chosen because of the relative ease of analysis and the larger body of available information compared to circular elements.

A quick evaluation of the necessary substrate thickness and permittivity needed to meet the bandwidths given above may be done using the curves given by Milligan [36] or Pues and Van de Capelle [47]. As these are given in terms of bandwidth at a VSWR of 2, it is necessary to convert between bandwidths at different VSWR (or return loss). For this purpose the patch antenna may be considered to be a single lossless tuned circuit with a response of

$$\frac{E}{E_o} = \frac{1}{\sqrt{1 + \left(Q \frac{2\Delta f}{f_o}\right)^2}} \quad (4.1)$$

E/E_o is the transmission response, Q is the loaded quality factor, $2\Delta f$ is the bandwidth and f_o is the centre frequency. The transmission response is related to the return loss by

(4.2)

$$\frac{E}{E_0} = \sqrt{1 - 10^{-RL/10}}$$

where "RL" is the return loss in decibels. By solving (4.1) for Q and equating two cases of different E/E₀ the relation between the corresponding bandwidths can be found. For example a patch with a bandwidth Δf at VSWR of 1.22 (Return Loss = 20 dB) will have a bandwidth of about 3.5 Δf at a VSWR of 2 (Return Loss = 9.5 dB). This simple conversion has been checked against measured data and found to be quite accurate for antennas well matched at centre frequency (return loss better than 25 dB).

The curves in Milligan's paper yield (for one percent bandwidth around 850 MHz at 20 dB return loss) a substrate thickness of 0.2 inch for ε_r = 1 and 0.35 inch for ε_r = 2.55. However, Pues and Van de Capelle's method yields 0.44 inch for ε_r = 1 and 0.57 inch for ε_r = 2.55. These figures do not agree very well but in any case the thickness of the ε_r = 2.55 dielectric required will result in excessive mass as materials with dielectric constants in this range normally have densities between 1 and 2.5 g/cm³. Low density/low dielectric constant substrates such as vacuum, foam, honeycomb, etc. appear necessary. For 6.3 percent bandwidth at 20 dB return loss and ε_r = 1, Pues and Van de Capelle predict a thickness of 2.8 inches. This thickness is really beyond the valid range for their model and indeed for microstrip antennas as the feeding arrangement will radiate strongly, upsetting the patch radiation patterns. We can not, therefore, obtain very good match over both transmit and receive bands with a simple patch antenna. The formulas of Pues and Van de Capelle have been incorporated into a computer program called JMPAT1F, described in Appendix C. Several square patch antennas

with 0.5 inch air spacing were constructed for the MSAT frequency range. These were found experimentally to have VSWR=2 bandwidths of about 4.8 percent, compared with predictions of 4 percent from Pues and Van de Capelle's curve and 7.4 percent from Milligan. Pues and Van de Capelle's method is closer and conservative and so may be used as a design aid.

Conceptually the simplest theoretical model for a rectangular microstrip antenna is the transmission line model. The patch is considered to be a length of microstrip transmission line with radiating slots at each end. Figure 4.2 defines the dimensions of an antenna fed by a probe protruding from the ground plane. If the thickness of the patch conductor is very small the microstrip line has an effective permittivity given by [1]

$$\epsilon_e = \epsilon_r + \frac{1}{2} + \frac{(\epsilon_r - 1)}{2} \left(\frac{1}{\sqrt{1 + 12 h/W}} \right) \quad (4.3)$$

This defines the propagation velocity and impedance of the line. The approximate resonant frequency is then found to be

$$f_r = \frac{c}{2 (L + 2\Delta l) \sqrt{\epsilon_e}} \quad (4.4)$$

where c is the speed of light in a vacuum and Δl is an equivalent length extension representing the fringing capacitance at the ends of the microstrip. Δl may be found, for quick calculations, from Figure 2 in Kirschning, Jansen and Koster [26]. Sengupta [53] uses the transmission line model to compute the resonant frequency of a microstrip antenna including the effect of a probe feed which has an inductive reactance. Pues and Van de Capelle [46] describe a transmission line model including effects of

mutual coupling between the two slots. A computer program (JATLMIF) has been written to incorporate Sengupta's probe reactance into the model of Pues and Van de Capelle. This program, described in Appendix D, computes the input impedance as a function of frequency. The equivalent circuit used in this program is shown in Figure 4.3.

For a resonant antenna with length L near a half wavelength in the dielectric the electric field under the patch is maximum across the width W at the ends of L and zero across the midline. For thin substrates the input resistance is maximum when the antenna is fed at the edge and zero in the centre. However for thick substrates, approximately greater than 0.05λ for $\epsilon_r = 1$, the probe inductance has a very marked effect and the input resistance at resonance behaves quite differently. As the substrate thickness is increased the optimum feed position for matching to 50 ohms moves toward the edge and beyond a certain thickness the probe reactance is so great that no resonance can be achieved. This effectively limits the available bandwidth of a probe fed patch. The use of front-face microstrip feedline could eliminate this problem, but such a line begins to suffer large radiation losses at similar spacing from the ground plane and can not be used.

4.1.3 Circular Polarization

There are two major techniques to obtain circular polarization from microstrip antennas. The simplest uses, for example, a nearly square patch with the feedpoint on the diagonal. The two resonant modes with directions of propagation parallel to the edges of the patch have slightly different resonant frequencies and so will be excited with different phase but almost equal amplitude at a frequency between the resonances. If the

dimensions are adjusted to make the phase difference between the two orthogonal modes equal to 90 degrees then nearly circular polarization will be radiated. Figure 4.4 shows some geometries which exhibit this property. Sharma and Gupta [54] have published a technique for theoretical analysis as well as some computed and measured examples. They achieved several axial ratios of less than 0.5 dB. However, the axial ratio bandwidths were very narrow, typically less than one percent for axial ratio of 6 dB or better. The VSWR was found to be a much more slowly varying function of frequency but typically was at least 1.5 (return loss \leq 14 dB). This poor match combined with the very narrow axial ratio bandwidth prevent the use of this technique for MSAT, unless dimensions and matching schemes can be devised to improve this performance.

Another technique to produce circular polarization makes use of the fact that the voltage distribution has a null across the middle of the microstrip patch. Two feed points can be placed orthogonally without coupling through the dominant resonant modes. This is shown in Figure 4.5. There is no bandwidth restriction on the relative excitations of the two feeds so as long as the feed network can produce two equal amplitude orthogonal phase signals over the required bandwidth circular polarization will be generated. As described by Chiba et al. [9] some coupling can exist in higher order modes which will degrade the axial ratio. This can be reduced by using balanced feeds as described in Chiba's paper, or by changing the feed network to counterbalance the effect. In a direct radiating array pairs of elements may be fed in such a manner that the ellipticities of the two elements cancel on boresight [21] but in a reflector feed each element corresponds to a certain direction of radiation so this technique is ineffective.

The radiation pattern of a linearly polarized rectangular microstrip antenna is that of two almost uniformly excited slots fed in phase and spaced apart by about a half-wavelength in the substrate dielectric. The shape of the pattern is primarily dependent on the length and spacing of the slots (radiating edges of the patch) which, at least for a square patch, are both directly dependent on the substrate permittivity. The substrate thickness has only a minor effect. Expressions for the radiation patterns are given in Carver and Mink [7], equations (45) and (46), which show that the peak of radiation is in the direction normal to the ground plane.

Because a patch with air/vacuum dielectric is larger than one with a higher permittivity it has the highest directivity. A square patch with $\epsilon_r = 1$ achieves about 10 dBi, dropping to about 7 to 8 dBi for typical dielectric materials with ϵ_r of 2 to 3. For a quick evaluation of directivity the curves of Pies and Van de Capelle are useful [47]. This has also been incorporated in the program JMPAT1F (see Appendix C).

The power gain will, of course, depend on the efficiency. Because of the adoption of vacuum for nearly all of the "substrate" dielectric this has not been considered in great detail as it is expected to be very good. However, an estimate can be obtained using Milligan's curves [36]. At 850 MHz Milligan shows a square patch on 0.25 inch Teflon fiberglass substrate ($\epsilon_r = 2.55$, loss tangent = 0.0018) to have a loss of 0.22 dB. Curves for other substrate thicknesses show that the loss is nearly halved when the thickness is doubled. Thus, a 0.5 inch Teflon fiberglass substrate should yield about 0.1 dB loss.



With vacuum dielectric the Q due to radiation is reduced and the dielectric losses eliminated so a half-inch vacuum spaced patch should lose much less than 0.1 dB due to antenna losses.

4.2

Single Band Patch Antenna Experiments

In the preceding section it was shown that ordinary microstrip antennas are incapable of achieving the matching bandwidth necessary for high performance at both the receive and transmit bands of MSAT. However, if a fairly large spacing of the patch from a ground plane is used they can cover either the transmit or the receive band (4 MHz each). The mass will be excessive, however, unless a very low density substrate material is used. To test this type of antenna a number of square patches were fabricated from 0.06 inch thick brass and supported over a 24 inch square ground plane by nylon bolts and small Rexolite spacers. An arrangement was made whereby one or two coaxial probes could be connected at various distances from the edge of the patch. Different patch sizes (side lengths in steps of 0.2 inch) were tested to find those with resonances closest to 823 MHz and 868 MHz, the two band centres. The probe positions were optimized for best match. The resulting data was interpolated to find dimensions to obtain matched antennas at 823 MHz and 868 MHz. New antennas with these dimensions were constructed with two orthogonal feeds. The patches were 6.32 inches square (fed at 1.733 inch from the edge) for 823 MHz and 5.93 inches square (fed at 1.630 inch from the edge) for 868 MHz. These were spaced 0.50 inch from the ground plane. The construction of these antennas is shown in Figure 4.6.

In Figures 4.7 to 4.10 are plotted the return losses and port-to-port isolations of these antennas. The isolation is simply the attenuation measured when a signal is applied to one feed port and detected at the other. These tests were done with the patch at the centre of a 30 by 36 inch ground plane. The 823

MHz antenna actually achieves the best match at 820.2 MHz at one port and 821.0 MHz at the other. The 868 MHz patch was resonant at 866.0 MHz at one port and 867.8 MHz at the other. In all cases the 4 MHz MSAT bands were covered with better than 20 dB return loss but the desired thermal contraction/expansion allowance was not covered by every one. One more iteration of the dimensions would permit better centering of the resonant frequencies, but to be truly useful this should be carried out in the array environment in which the element would be used. The isolation in all cases was more than 25 dB. A summary of the measured port characteristics is given in Table 4.1.

Measured E- and H-plane radiation patterns are shown in Figures 4.11 (823 MHz) and 4.12 (868 MHz). The patterns show H-plane patterns somewhat wider than the E-plane patterns. The peaky shape at boresight at 823 MHz and the dimpling at 868 MHz can be attributed to finite ground plane effects. For all of these measurements the long dimension (36 inches) of the ground plane was horizontal and the rotation was about a vertical axis, as shown in Figure 4.13. Table 4.2 summarizes the pattern measurements. The particularly wide H-plane beamwidth figure at 868 MHz is a result of the boresight dimple. The E-plane squint at 868 MHz is due to the excitation of high order modes by the asymmetric feeding arrangement. Using the formulas from Carver and Mink [7] the theoretical beamwidths are 70° (823 MHz) and 71° (868 MHz) in the E-plane and 75° (823 MHz) and 76° (868 MHz) in the H-plane.

An offset fed reflector with $f/d = 0.625$ having the edge of the reflector on the focal axis subtends an angle of 77.3 degrees at the feed. The average difference between the E- and H-plane patterns at the edges of this range is 1.7 dB at 823 MHz and 1.5 dB at 868 MHz. If a reflector with $f/D = 0.85$ is considered as in Chapter 3, then these figures drop to 0.5 dB at 823 MHz and 1.1 dB at 868 MHz.

4.3 Options for Transmit/Receive Elements

4.3.1 MSAT Requirements

For use in a transmit/receive feed array for MSAT a radiating element must operate with nearly identical properties over both the 821-825 MHz and 866-870 MHz bands. With allowance for the thermal contraction and expansion a one percent bandwidth is required at each allocation. Alternatively the element can be designed to cover the entire band from 821-870 MHz. This is a 6.3 percent bandwidth including the thermal allowance. A target of 20 dB return loss at these bandwidths was chosen. The element must be small enough to be part of an array with spacing small enough to prevent grating lobes, without suffering from strong mutual coupling effects. For microstrip patches this normally implies transverse dimensions of about a half wavelength or less. In addition the element must have the necessary symmetry to permit operation in circular polarization. The maximum average power applied to a single element will be near 60 W, with a peak value several times higher due to the multi-carrier nature of the signals.

4.3.2 Wider Bandwidth Simple Patches

The use of very thick low permittivity substrates to obtain wide bandwidth is generally unsatisfactory. This is due to the large probe reactance causing matching problems and the increased high order modes in the cavity [9] which result in asymmetric radiation patterns and difficulty in achieving good axial ratio. This has not prevented the use of such antennas in a few cases. For example Karlsson [25] has obtained 13 percent bandwidth at VSWR = 2 and a cross-polar level of -19 dB in a linearly

polarized array using a 0.15λ foam substrate. This, however, is a less stringent requirement than that for MSAT.

The matching problems associated with the large inductive reactance of the feed probe can be essentially eliminated by inserting a capacitance in series. Fong et al. [17] used this technique to improve the return loss of a patch antenna on a 0.066λ foam substrate from a best case of 10 dB to 20 dB or better over a 2.1 per cent band. Other difficulties with very thick substrates are not affected, however, and the construction of a capacitor able to handle the MSAT power levels could prove difficult.

By eliminating the feed probe, Pozar's aperture coupling technique [44] for feeding a patch from a microstrip behind the ground plane may produce lower levels of higher order modes. However, he offers little data and a way to generate circular polarization by the two feed method is not clear.

Palanisamy and Garg [41] used a rectangular ring shaped patch to obtain a bandwidth (at VSWR = 2) of 1.61 times that of a rectangular patch on the same substrate. Their experiments showed E- and H-plane beamwidths differing by a factor of about 2, making circular polarization impractical. They achieved a bandwidth (at VSWR = 2) of 1.7 percent using a substrate ($\epsilon_r = 2.50$) only 0.0057λ thick.

Others have allowed the thickness of the substrate to vary over the patch area. Poddar et al. [42], using a 0.093λ maximum substrate thickness achieved VSWR = 2 bandwidths of 25 percent for a stepped geometry and 28 percent for a wedge, compared to 13 percent for a rectangular patch. These bandwidths are of the order required for MSAT but these antennas did not have the necessary symmetry for circularly polarized operation. Using a

circular patch with the centre depressed to form a shallow cone Das and Chatterjee [13] obtained double the bandwidth of a flat circular disc of the same thickness. A very poor match, typically 4 dB return loss was obtained. Jeddari, et al. [23] achieved good matching for a conical patch using a series capacitance. The bandwidth at VSWR = 2 for a $.071 \lambda$ thickness was only 12 percent and the cross polarization level was high at about -10 dB.

Although many of these wider bandwidth elements are promising for some applications none are able to meet all the MSAT requirements simultaneously.

4.3.3 Single Patches for Dual Frequency Operation

It is possible to operate a patch antenna at both the fundamental resonance and at a higher order resonance at a higher frequency. These resonances are much too far apart in frequency to be useful for MSAT. Wang and Lo [60] have used a set of slots and shorting pins in a rectangular microstrip antenna to bring these resonances closer together but still they are too widely spaced for MSAT. In addition the patch does not possess the symmetry necessary for circular polarized operation.

An additional resonance may be introduced by loading an ordinary patch at some point with a coaxial stub as shown in Figure 4.14. The theory for this arrangement is described by Richards and Lo [49] and some experimental results are presented by Richards and Long [50]. The experimental antenna has much wider spacing between the resonances than MSAT requires. In order to achieve a good match at both frequencies a non-square patch with off-centre feed is used. This can not be used for circular polarization.

If a matched condition can be found for two closely spaced frequencies using a square patch with the feed centered along the side then this technique may be usable. Davidson et al. [14] describe a variation of this method where the loading stub is microstrip and etched on the same side of the substrate as the patch. Resonance spacing similar to that of MSAT was achieved. It is not clear if such elements could be used for circular polarization. The size of the element is quite large and would probably be excessive for arraying if it was necessary to use a very low dielectric constant. The stub-loaded patch is quite promising but as yet no antenna has been described which comes near to compliance with all the requirements of MSAT.

4.3.4 Elements With Multiple Patch Resonators

Kumar and Gupta [28 , 29] have devised a microstrip antenna where a probe-fed rectangular patch is coupled (through fringing capacitance) to additional patches etched on the same side of the substrate in close proximity to the first. They describe one arrangement with four such parasitic patches (see Figure 4.15). Unfortunately these patches are not identical and this could upset any circularly polarized use. The bandwidth is very good at 25.8 percent at VSWR = 2 for a 0.033λ thick substrate with $\epsilon_r = 2.55$. At some frequencies, however, the patterns change. As well the element is too large for arrays at 0.96 by 0.92 wavelengths.

Wood describes a very similar arrangement [65] where the auxiliary resonators are of the shorted quarter wave type. This gives double the bandwidth of an ordinary patch. He also describes a single-feed circularly polarized version using a slot and diagonal feed of the central patch to obtain the correct

phasing of two orthogonal modes. A 0.4 per cent 1 dB axial ratio bandwidth was achieved, double that of a similar antenna without the additional resonators. This antenna is shown in Figure 4.16. The antenna could also be made with two feeds for circular polarization (without the slot). However, it would still be very large.

A number of investigators have considered the use of two or more patches stacked vertically. The most promising arrangements use the upper patch as a parasitic element with only the lower one fed. Figure 4.17 shows the general form of this kind of antenna. Dahele and Lee [11] studied two identical circular discs, both etched on $\epsilon_r = 2.3$ material. The lower one was fed and rested on the ground plane and the upper one was spaced from the first with an air gap. Using the terminology of Figure 4.17, $\epsilon_{r1} = 2.3$ and $\epsilon_{r2} \approx 1$. This gave a dual frequency response but with different impedances at the two resonances. Sabban [52] used a similar arrangement but was able to achieve a wideband response with VSWR = 2 bandwidths of 9 percent for square and rectangular patches, 11.5 percent for annular rings and 15 percent for circular discs. Both linear and circular polarization were used. No dimensions were given. Chen et al. [8] describe the same type of antenna in much greater detail. They achieved a 10.8 percent bandwidth at a 20 dB return loss with 7.9 dBi gain and a half-power beamwidth of about 90 degrees. A four element CP array with 0.86λ spacing was described, giving an axial ratio better than 0.5 dB over ± 10 degrees. The patches used two orthogonal phase feeds but special measures were necessary to achieve good circularity. The results of Sabban and Chen's group were by far the best when judged by the MSAT requirements so it was decided to study the use of stacked patch elements for the transmit/receive application.

4.4 Experiments with Stacked Patch Antennas

4.4.1 Experimental Antennas

An empirical study of the characteristics of some stacked patch antennas was carried out as part of this study. Square patches were chosen in order to simplify theoretical analysis. In order to confine the study to representative antennas that would be practical for space applications the dielectric material chosen for both layers was air, except for a few support posts. This eliminates the mass and loss of a thick sheet of dielectric substrate. In practice the substrates might be honeycomb or shuttle tile with permittivities slightly greater than one. However similar behaviour to air dielectric could be expected.

The experimental antennas were constructed as shown in Figure 4.18. The two patches were made of .06 inch thick brass and were supported on four sets of Rexolite spacers slipped over nylon screws. The initial parametric study was done using a 24 inch square ground plane with slots cut to permit sliding the feed probe to different distances from the edge of the lower patch.

4.4.2 Characteristic of Stacked Air-Dielectric Square Patch Antenna

A transmission line model of the stacked patch geometry was developed. The equivalent circuit is shown in Figure 4.19. The lower patch and ground plane form one microstrip resonator, while the two patches form another. The two resonators are coupled by the fringing fields at the radiating edges. The radiation resistances, fringing field capacitances, microstrip line parameters and probe reactance are computed as for a single patch. Because of the way the upper cavity is modelled the case

where the top patch is larger than the lower one is not correctly treated. In addition, a suitable expression for the mutual admittances was not found so the simplest approximation of the average of the two slot self-admittances was used. Calculations using this model indicated that for best wideband performance the upper patch should be smaller than the lower one, the spacing between patches should be greater than between the lower patch and ground plane, and the feed probe should be connected to the lower ground plane near the edge. These trends were confirmed by experiment but the calculated input impedances were not very close to those measured. For this model to be truly useful substantial improvements are necessary. These were not pursued as empirical optimization was considered more effective.

An experimental parametric study was carried out in which the size of the upper square patch, the two spacings and the distance of the feed probe from the edge of the lower patch were variables. For each combination of patch sizes and spacings the probe was moved to the position giving the best return loss/bandwidth combination. In each case the frequency was swept from 700 MHz to 1100 MHz. Table 4.3 shows the ranges of the parameters. Figure 4.20 shows the trade-off between return loss and bandwidth for several of the more successful combinations. At 20 dB return loss the maximum bandwidth achieved was 6.3 percent, exactly the requirement for MSAT. At a VSWR of 2 the best result was 13.8 percent bandwidth, substantially better than Sabban achieved for square stacked patches [52] but still slightly less than he obtained with circular discs. The latter result was achieved with a total height above the ground plane of 1.12 inches or 0.082λ at the centre frequency of 860 MHz. Figure 4.21 shows a typical plot of return loss versus frequency. This shows clearly the dual resonance which gives rise to the

wideband characteristic when the coupling between the two resonators is correct. Also shown on this plot is the isolation between two feed probes attached to adjacent sides of the lower patch as required for circular polarization using two feedpoints. If only the dominant resonant mode existed in each of the two cavities then there would be no coupling between the probes. The existence of such coupling demonstrates that higher order modes are excited at a low level.

Based on the data accumulated in the parametric study a bread-board antenna was designed for operation between 821 and 870 MHz. This antenna used a lower patch 6.65 inches square and an upper patch 5.72 inches square with spacings of 0.350 inch (lower patch to ground plane) and 0.500 inch (between patches). The two 0.120 inch diameter probes were soldered to the lower patch at the centres of two adjacent sides, 0.08 inch from the edge. Figures 4.22 and 4.23 show the return loss and isolation measured at each input port. The element was centred in a 30 by 36 inch ground plane for these measurements. Clearly the scaling from a centre frequency of about 875 MHz (obtained in the parametric study) to 845 MHz has resulted in some deterioration of the performance. The worst case return loss between 821 and 825 MHz is 20.1 dB and between 866 and 870 MHz, 18.7 dB. The worst case isolations are 19.0 dB (821-825 MHz) and 18.5 dB (866-870 MHz). These figures do not include any thermal allowance. A more complete summary of the return loss and isolation measurements is given in Table 4.4. The plots show that careful optimization could result in each required band falling in one of the dips in the return loss curve to obtain perhaps 23 dB worst case return loss levels, using the stacked patch geometry for a dual band response. It should not be difficult to optimize these elements to meet the requirements. However, at this level it is probably necessary to perform the optimization with materials and dimensions (such as

patch thickness) as would be used for flight models and to do it in an array (or waveguide simulator) environment.

The radiation patterns of this breadboard element have been measured using the same set-up as for the single patches (Figure 4.13), at 823 MHz and 868 MHz. These are plotted in Figures 4.24 and 4.25 respectively. Again some effects of the finite ground plane are seen on the patterns near boresight. The beamwidths and squints are summarized in Table 4.5. The beamwidths are all almost identical to those measured for the single patch elements. In general the patterns are slightly more symmetrical, perhaps due to less radiation from the feed probes because of their reduced length (0.35 inch compared to 0.50 inch for the single patch).

The effect of a Beta cloth thermal blanket over the front face of the breadboard stacked patch element was checked (see section 6.5) The change in return loss and isolation caused by a single layer of Beta Cloth draped in front of the element is very small as shown in Figures 4.26 and 4.27.

4.4.3 Mutual Coupling Between Stacked Patch Antennas

Published data regarding mutual coupling between wideband or dual band stacked patch antennas is scarce. Chen et al. [8] included some experimental results in their paper. Using two of the breadboard air-dielectric stacked square patch antennas, described in the previous section, mounted on the 30 by 36 inch ground plane a number of mutual coupling measurements were carried out. Measurements of E- and H-plane coupling were made as shown in Figure 4.28, with the unused feed ports terminated. There was no observable difference in coupling with the unused ports open circuited. The measurements were made as a function of frequency between 810 MHz and 880 MHz at several spacings between the elements. The coupling changed slowly with

frequency, being slightly stronger at the lower end of the frequency range. There was no evidence of the antenna resonances in the mutual coupling data. In Figure 4.29 are shown the values of E- and H- plane coupling at 820 MHz plotted against the element spacing. Figure 4.30 contains the corresponding curves for 870 MHz. The distance scales of 8.9 - 17.9 inches correspond to $0.62 - 1.24 \lambda$ at 820 MHz and $0.66 - 1.32 \lambda$ at 870 MHz. The magnitude of the coupling is similar to that existing between single patches and to that given by Chen et al. for stacked patches. At the 12 inch spacings suggested in Chapter 3 the coupling values at 820 MHz are -23 dB (E-plane) and -27 dB (H-Plane) and at 870 MHz they are -26 dB (E-plane) and -28 dB (H-plane).

Another set of measurements were performed with two breadboard stacked patch elements positioned to correspond to locations in a 12 inch spaced triangular grid as could be used in a septet-based feed array. Three geometries were used which cover all the couplings between adjacent patches in such an array with all the feeds aligned in the same direction. These geometries are shown in Figure 4.31. The measured couplings are tabulated in Table 4.6 for the frequencies 820, 825, 865 and 870 MHz.

These mutual coupling measurements include only the port characteristics of the elements. It is possible that modes may be generated by mutual coupling which are not detected at the feedpoints. These may, nevertheless, have an effect on the radiation patterns. It will be necessary to conduct measurements of the patterns of elements in an array to determine if any significant phenomena occur.

The power level at which the single or stacked patch elements can safely operate is potentially limited by the temperature rise due to power dissipation, passive intermodulation and multipactor discharge. With suitable choice of materials and proper attention to making a good connection between the patch and feed probes there should be no difficulty with PIM in the antenna element itself. The beam forming network will probably be the worst area for PIM.

The power dissipation ability of the patches is severely limited by the minimal thermal contact between the layers. In addition the actual loss of the elements is not known although at least in the case of the single patch it is reasonable to assume less than 0.1 dB loss, corresponding to 1.4 W dissipation for 60 W input. The stacked patch will probably have greater loss than the single patch because of the two resonators. Development of a good theoretical model of the stacked patch element would lead to a prediction of loss. The loss values are too small to be conveniently determined by gain measurement. Alternatively the temperature rise could be measured with high RF power applied, preferably under vacuum. While currently difficult to quantify, it is not expected that power dissipation will be a major problem.

Multipactor discharge, discussed in more detail in Chapter 5, is another condition which is very difficult to test for in an antenna. As it only occurs under vacuum, the tests must be held in a hard-to-find vacuum anechoic environment. Potentially a breakdown could occur between the lower patch and ground plane of the stacked patch antenna. The maximum voltage occurs near the feed point which is matched to 50 ohms so it may be assumed that the power at which breakdown occurs corresponds to the expected

breakdown voltage of at least 250 V for a 0.35 inch gap between parallel plates at 868 MHz, corresponding to a power of 1.25 kW, which should be sufficient. However, Clancy [10] shows possible breakdown at only about 300W which leaves little margin for a multi-carrier signal of 60W average power. Therefore it would probably be useful to attempt a measurement. The single patch with a wider 0.50 inch spacing should require about twice the power to produce multipaction, compared to the stacked patch. If, instead of using a small number of dielectric posts, the patch was supported on a continuous layer of material such as shuttle tile, having a low dielectric constant but very small voids, the danger of multipactor breakdown could probably be eliminated completely.


DOCUMENT No.	REV.	 COM DEV
RPT/MST/2500/001	—	
		SHEET 51

TABLE 4.1 MEASURED CHARACTERISTICS OF BREADBOARD
SINGLE BAND PATCH ELEMENTS

	Receive Element		Transmit Element	
	Port 1	Port 2	Port 1	Port 2
Nominal Centre Freq. (MHz)	823	823	868	868
Measured Centre Freq. (MHz)	820.2	821.0	866.0	867.8
Return Loss in 4 MHz MSAT Band (dB)	20.3	21.8	22.0	23.5
Return Loss in 1% Band (dB)	21.8	21.8	21.7	21.3
Bandwidth at 20 dB Match (%)	1.27	1.25	1.29	1.24
Isolation in 4 MHz MSAT Band (dB)	25.6	25.3	26.1	25.8
Isolation in 1% Band (dB)	25.8	25.3	26.0	25.4

TABLE 4.2 BEAMWIDTHS AND SQUINT OF BREADBOARD
SINGLE BAND PATCH ELEMENTS

	Half-Power Beamwidth (degrees)	Squint (degrees)
Receive element (823 MHz)		
E-plane	63	2.5
H-plane	66	2.0
Transmit element (868 MHz)		
E-plane	63	5.5
H-plane	78	0.0

TABLE 4.3 PARAMETER RANGES FOR STACKED AIR-DIELECTRIC
SQUARE PATCH EXPERIMENTS

<u>Parameter</u>	<u>Range (in)</u>	<u>Step Size (in)</u>
Lower patch side length	6.40	---
Upper patch side length	5.50-6.50	0.20
Lower patch-ground plane spacing	0.15-0.45	0.10
Inter-patch spacing	0.15-0.55	0.10
Probe distance from edge	0.15-1.20	0.15

TABLE 4.4: RETURN LOSS AND ISOLATION SUMMARY
FOR BREADBOARD STACKED PATCH ANTENNA

Frequency Band (MHz)	Return Loss (dB)		Isolation (dB)
	Port 1	Port 2	
821 - 825	21.6	20.1	19.0
866 - 870	20.0	18.7	18.5
821 - 870	17.3	16.1	17.7
with thermal allowance			
819 - 827	20.4	19.6	18.8
864 - 872	19.0	17.8	18.4
819 - 872	17.3	16.1	17.7

TABLE 4.5 BEAMWIDTHS AND SQUINT OF BREADBOARD
STACKED PATCH ELEMENT


	Half-Power Beamwidth <u>(degrees)</u>	Squint <u>(degrees)</u>
823 MHz		
E-plane	61	0.5
H-plane	68	2.0
868 MHz		
E-plane	61	0.5
H-plane	79	1.5

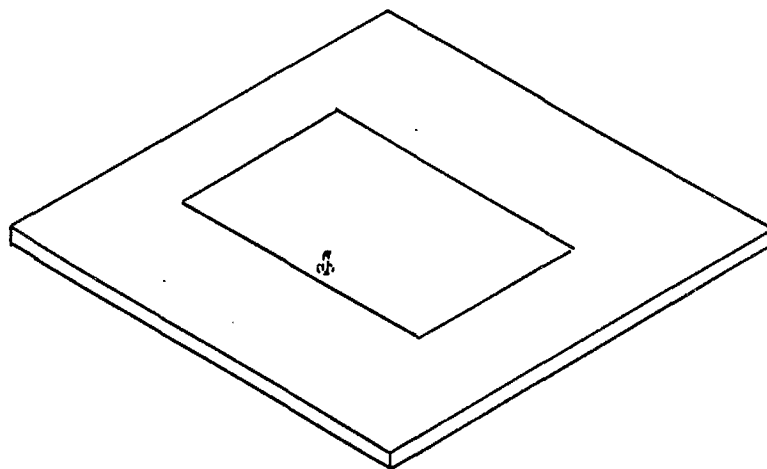


TABLE 4.6: MUTUAL COUPLING BETWEEN STACKED PATCH ANTENNAS IN SEPTET CONFIGURATIONS

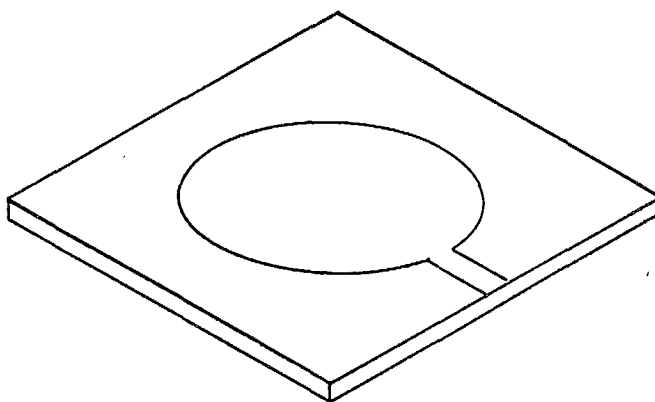
Frequency (MHz)	S ₁₃		S ₁₄		S ₂₃		S ₂₄	
	Loss (dB)	Angle (deg.)	Loss (dB)	Angle (deg.)	Loss (dB)	Angle (deg.)	Loss (dB)	Angle (deg.)
Case 1								
820	27.2	-45.5	36.7	45.4	36.6	159.9	23.6	30.3
825	27.4	-60.7	36.3	38.1	36.5	154.9	24.0	23.8
865	29.0	-165.4	36.7	-30.4	42.6	92.8	25.8	-65.2
870	28.0	175.7	36.7	-42.0	48.1	74.7	25.9	-91.8
Case 2								
820	27.3	35.8	25.8	83.3	25.6	72.6	34.2	-31.4
825	28.1	29.9	26.1	73.1	25.8	62.4	39.1	-41.4
865	30.9	-62.5	28.7	-17.5	27.6	-23.4	39.9	-144.8
870	31.9	-99.5	29.1	-36.3	28.2	-40.8	33.7	-170.5
Case 3								
820	28.7	-28.6	30.7	-95.6	26.7	-127.3	25.0	19.6
825	30.7	-36.2	30.6	-104.8	26.4	-136.2	25.7	10.5
865	31.8	-134.1	33.8	159.9	28.4	145.4	28.1	-84.6
870	29.7	-160.4	35.2	141.7	29.5	132.7	28.6	-114.2

Her Majesty the Queen in Right of Canada (1986) as represented by the Minister of Supply And Services.

DOCUMENT No.	REV.	 COM DEV
RPT/MST/2500/001	—	
SHEET 5/		



RECTANGULAR PATCH WITH COAXIAL PROBE FEED



CIRCULAR PATCH WITH MICROSTRIP LINE FEED

FIGURE 4.1: TYPICAL MICROSTRIP ANTENNAS

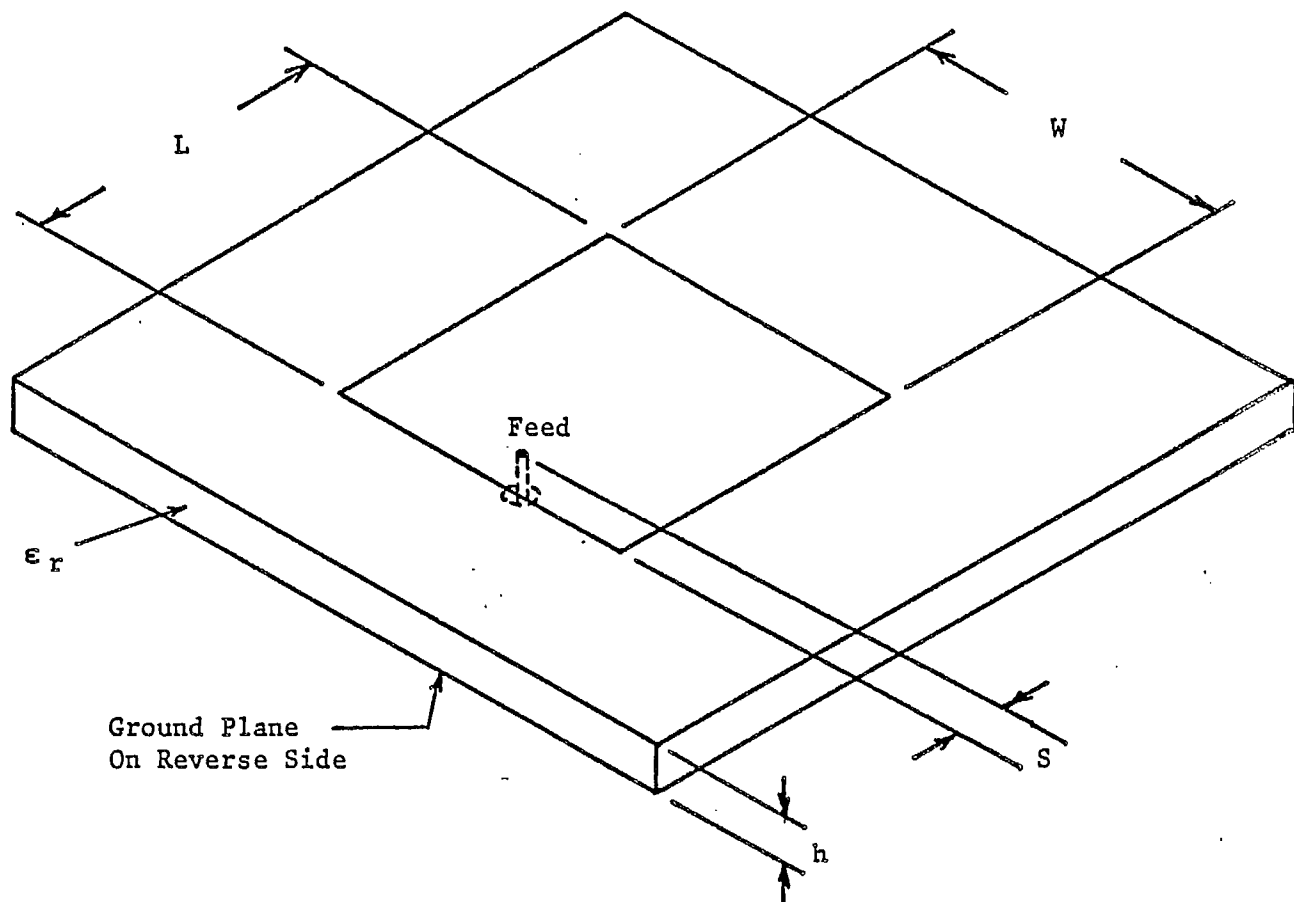
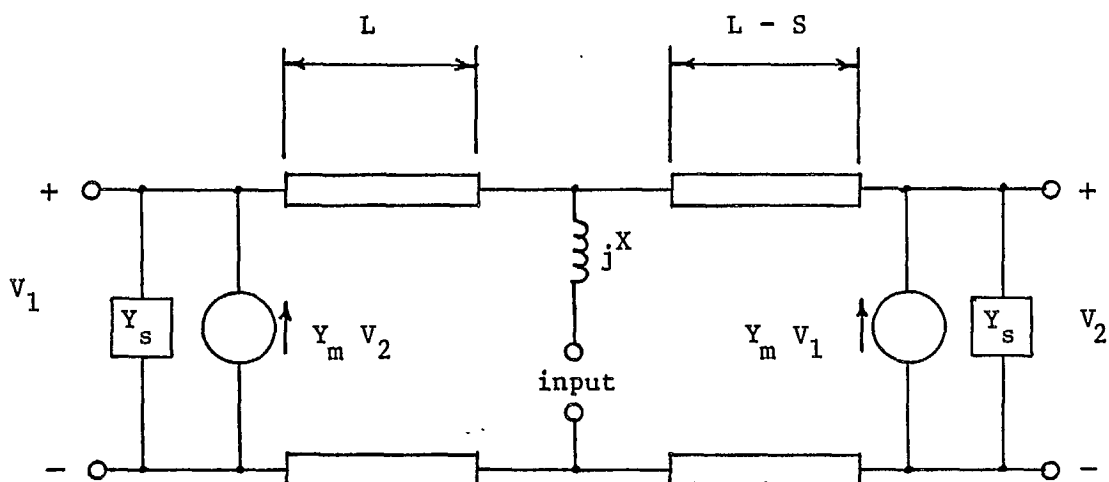
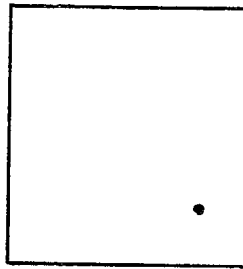


FIGURE 4.2: GEOMETRY OF RECTANGULAR MICROSTRIP ANTENNA

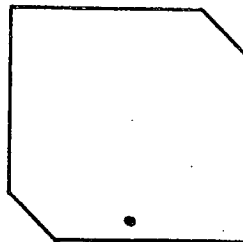


Y_m : Mutual Admittance Between Slots
 Y_s : Self Admittance of Slot
 jX : Feed Probe Reactance

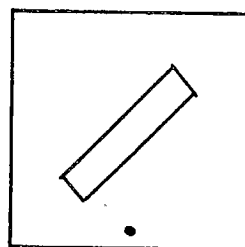
FIGURE 4.3: EQUIVALENT CIRCUIT FOR RECTANGULAR MICROSTRIP WITH COAXIAL PROBE FEED



DIAGONAL-FED NEARLY SQUARE ANTENNA



TRUNCATED CORNERS ANTENNA



SQUARE ANTENNA WITH DIAGONAL SLOT

FIGURE 4.4: SINGLE FEED CIRCULARLY POLARIZED MICROSTRIP ANTENNAS

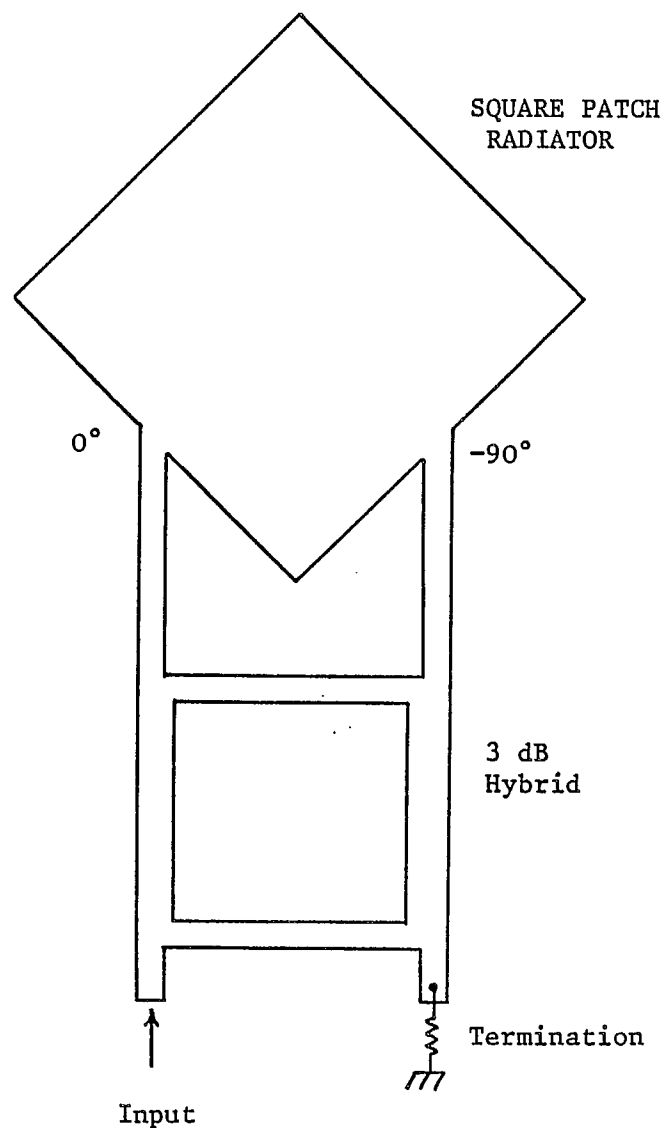


FIGURE 4.5: TWO-FEED CIRCULARLY POLARIZED MICROSTRIP ANTENNA WITH ORTHOGONAL-PHASE FEED NETWORK

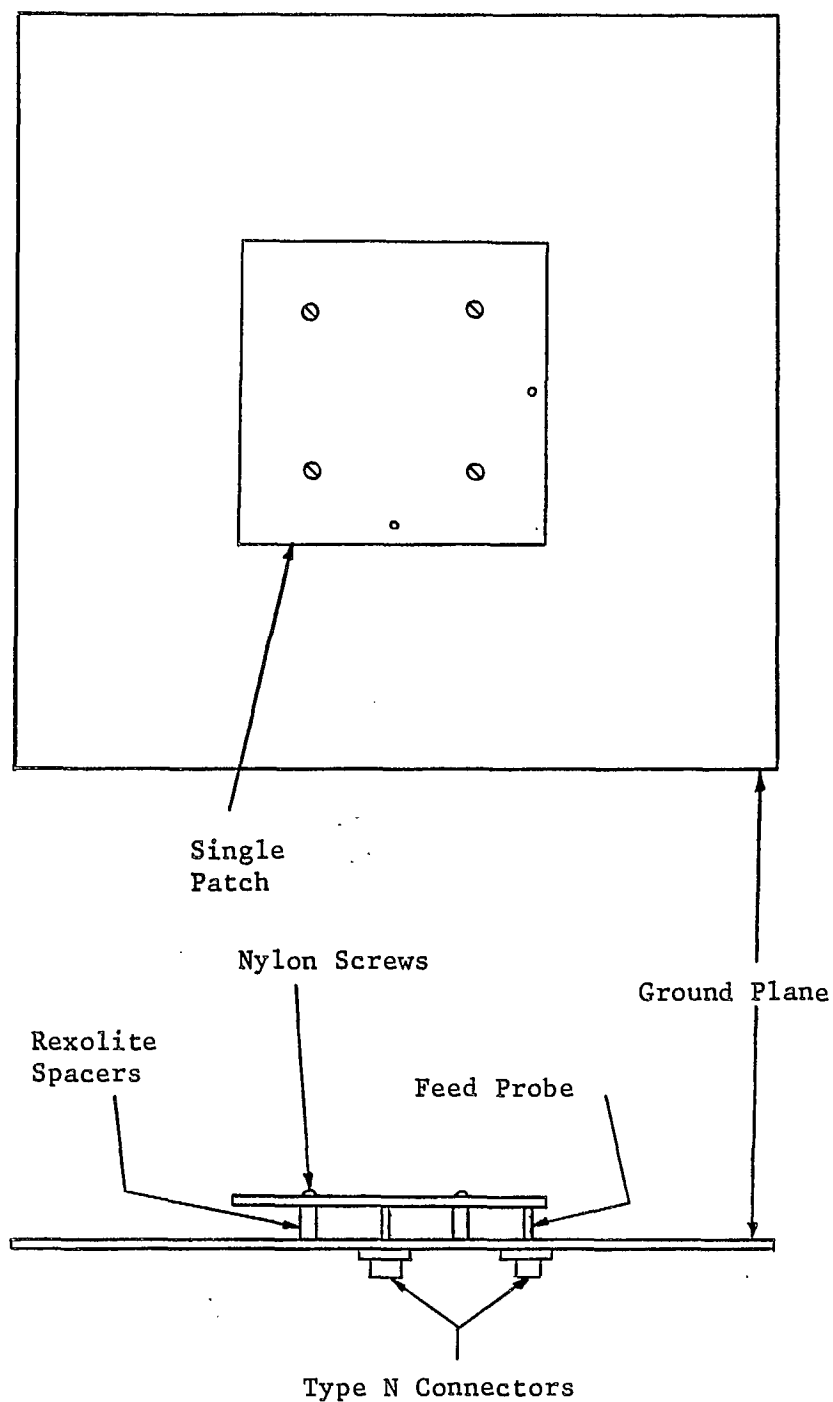


FIGURE 4.6: SINGLE PATCH ANTENNA WITH TWO FEEDS
(SINGLE BAND BREADBOARD)

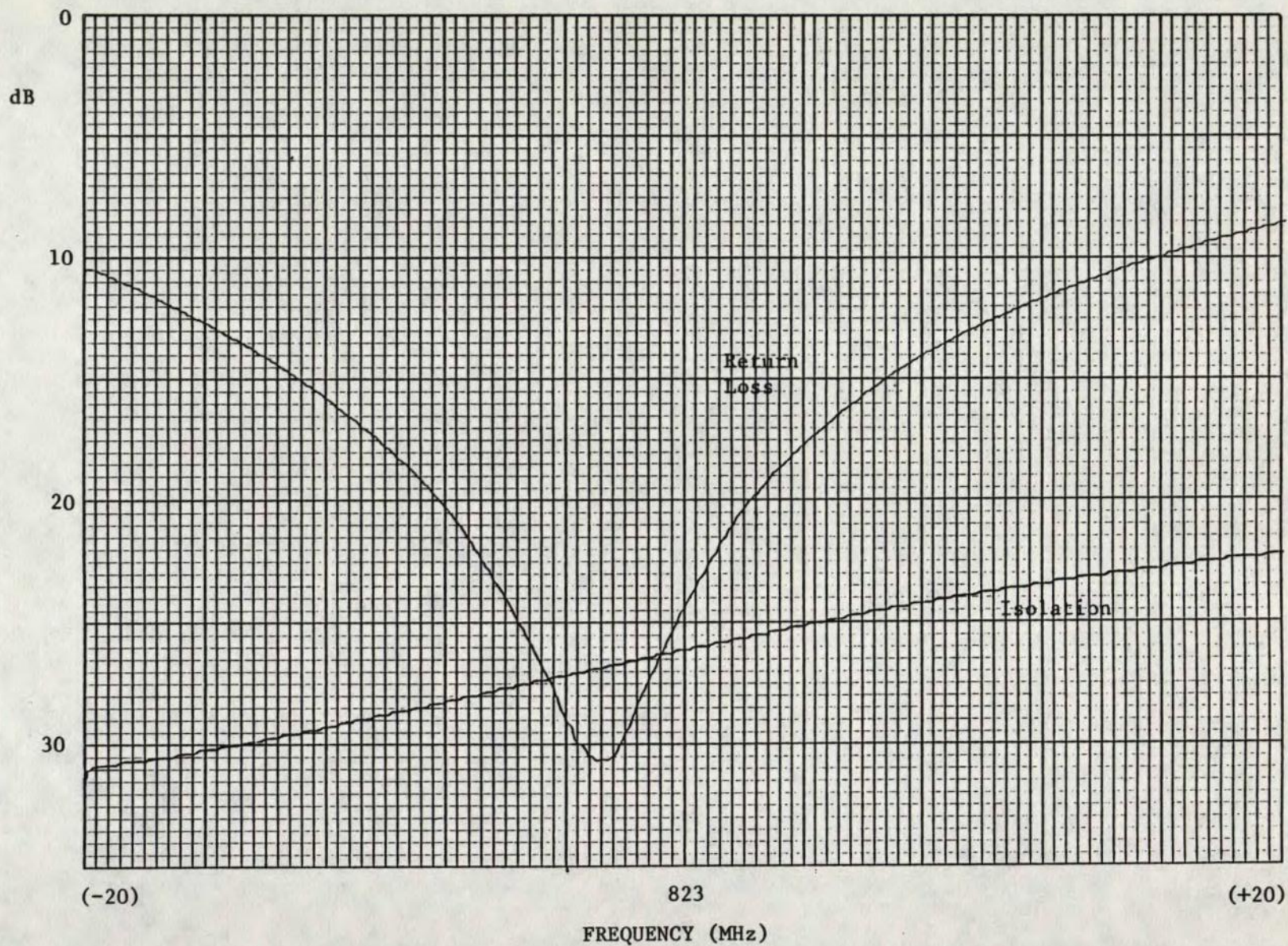


FIGURE 4.7: MEASURED RETURN LOSS AND ISOLATION OF BREADBOARD RECEIVE BAND ELEMENT (INPUT TO PORT 1)

DOCUMENT NO.
RPT/MST/2500/001

REV.

COM DEV
SHEET 64

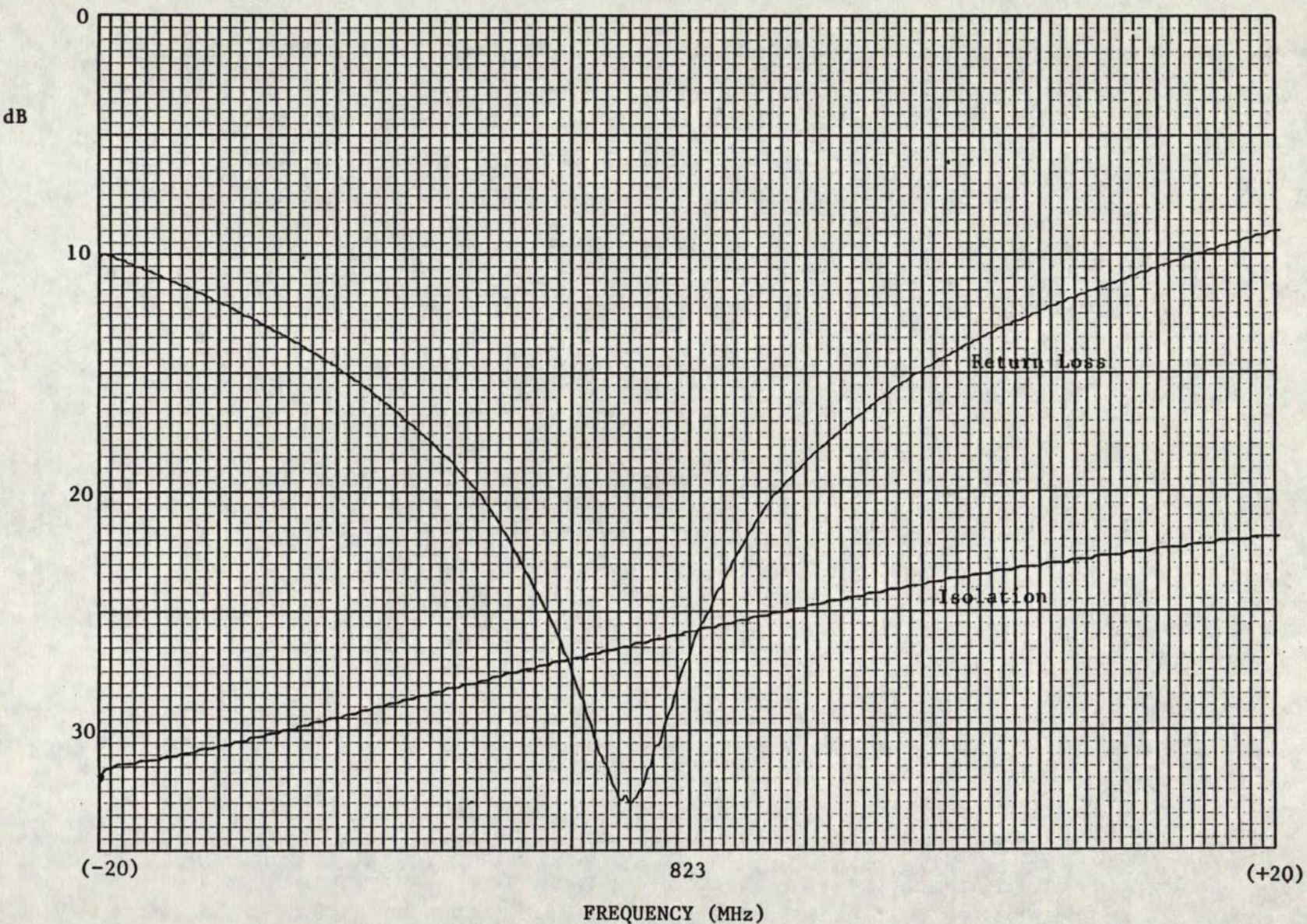


FIGURE 4.8: MEASURED RETURN LOSS AND ISOLATION OF BREADBOARD RECEIVE BAND ELEMENT (INPUT TO PORT 2)

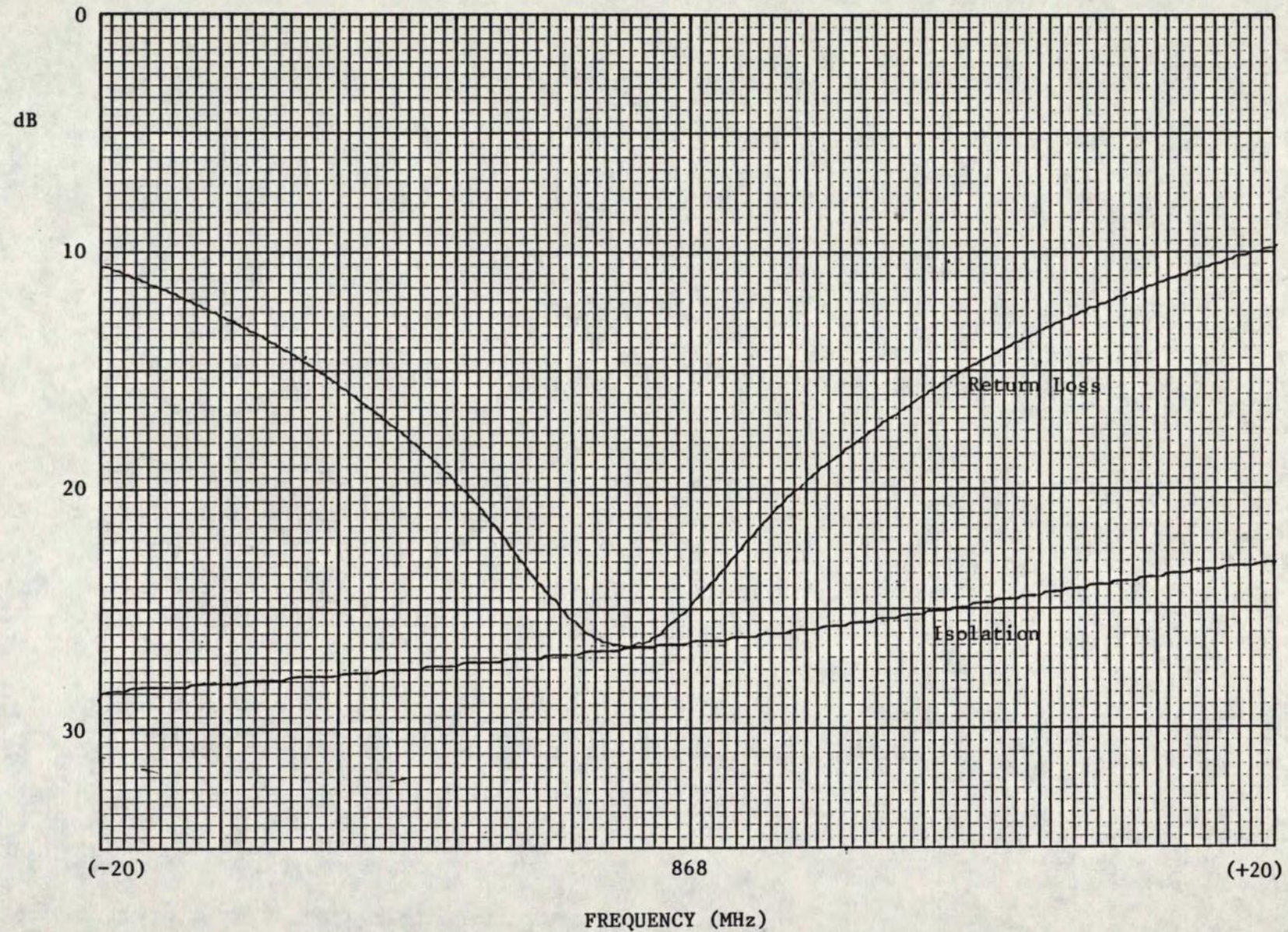



FIGURE 4.9: MEASURED RETURN LOSS AND ISOLATION OF BREADBOARD TRANSMIT BAND ELEMENT (INPUT TO PORT 1)

Her Majesty the Queen in Right of Canada (1986) as represented by the Minister of Supply And Services.

DOCUMENT No.	REV.	 COM DEV
RPT/MST/2500/001	—	
		SHEET 67

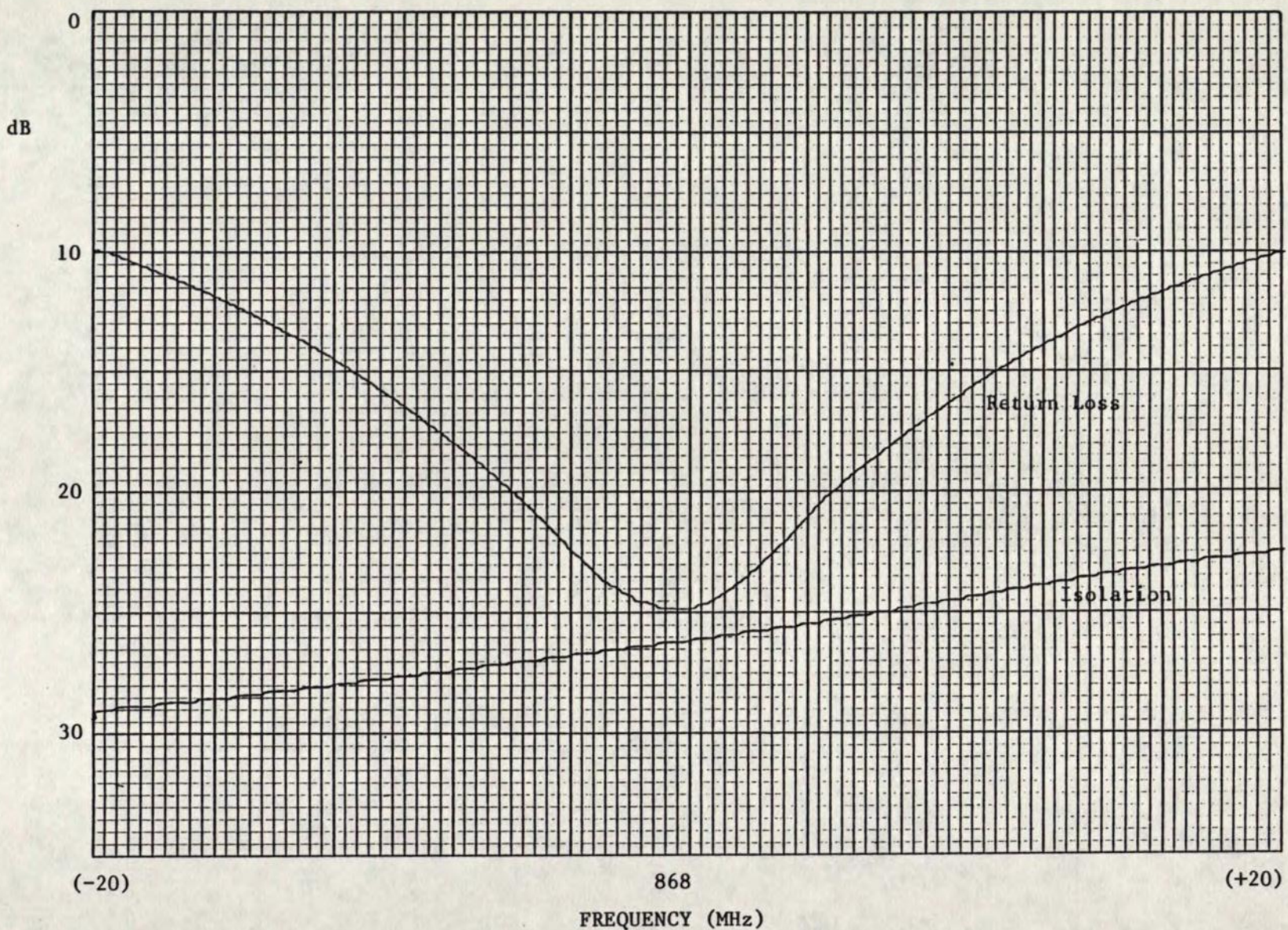


FIGURE 4.10: MEASURED RETURN LOSS AND ISOLATION OF BREADBOARD TRANSMIT BAND ELEMENT (INPUT TO PORT 2)

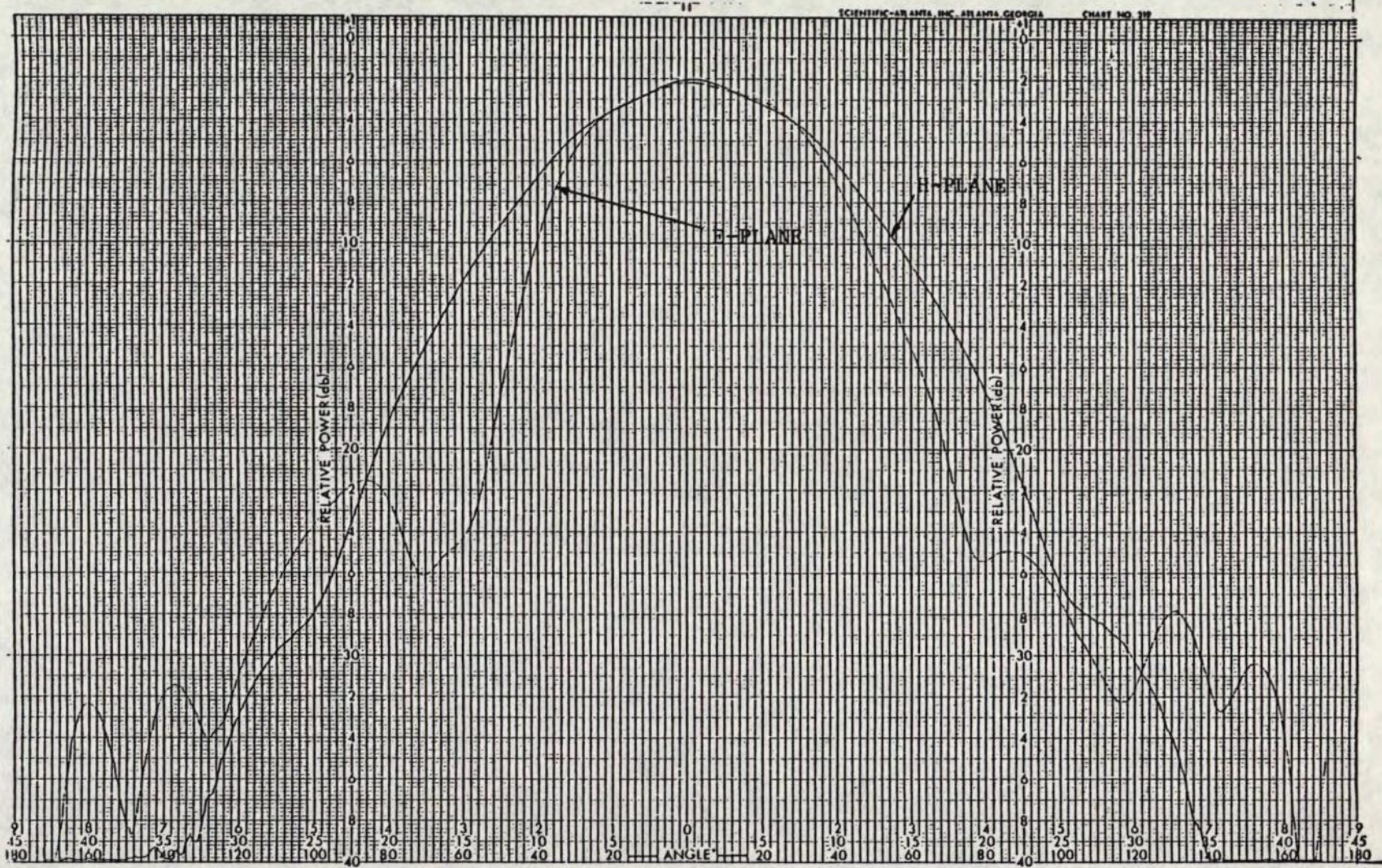


FIGURE 4.11: MEASURED E- AND H-PLANE PATTERNS OF BREADBOARD RECEIVE BAND ELEMENT AT 823 MHz

RPT/MST/2500/001

DOCUMENT NO.

REV.

SHEET

69



COM DEV

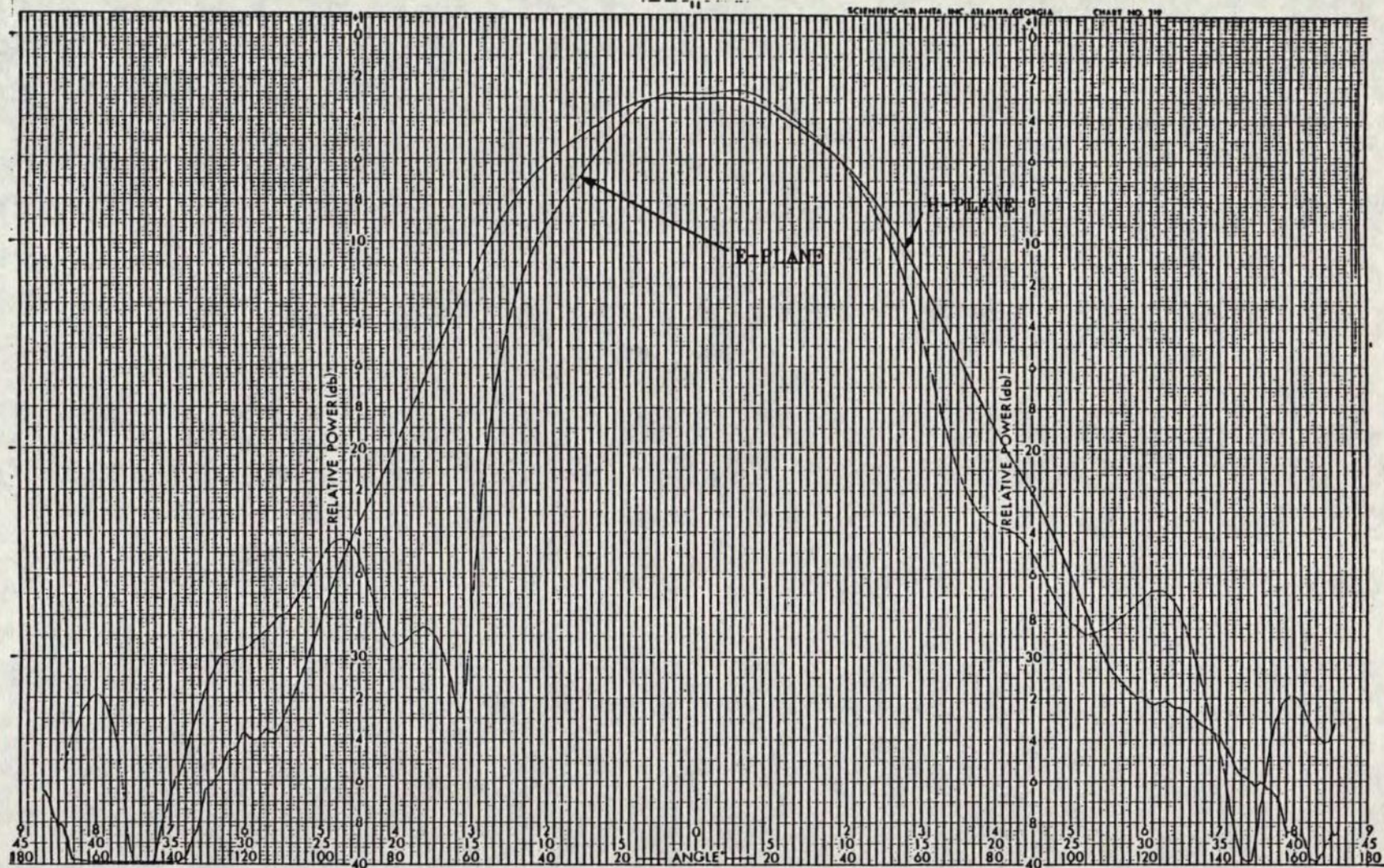


FIGURE 4.12: MEASURED E- AND H-PLANE PATTERNS OF BREADBOARD TRANSMIT BAND ELEMENT AT 868 MHz

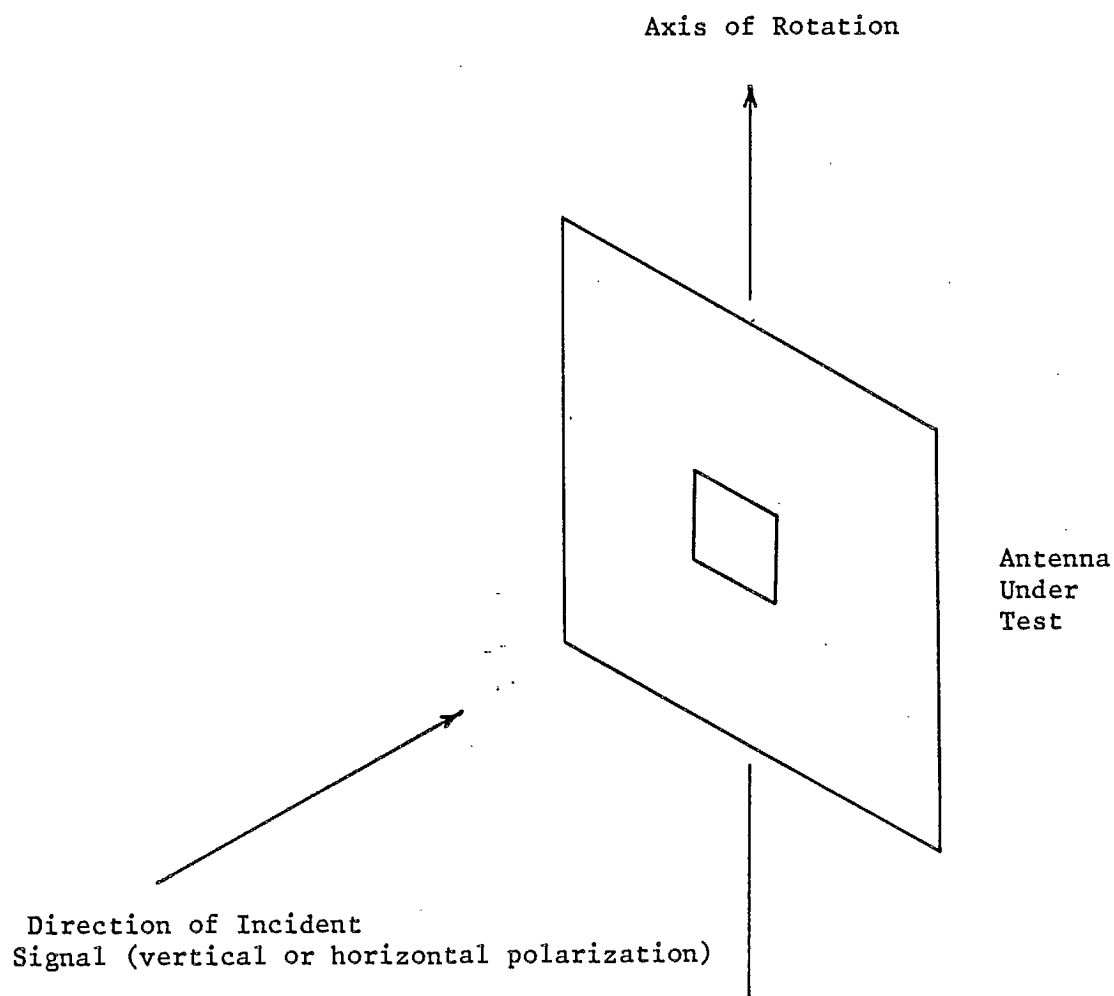


FIGURE 4.13: PATTERN TESTING GEOMETRY

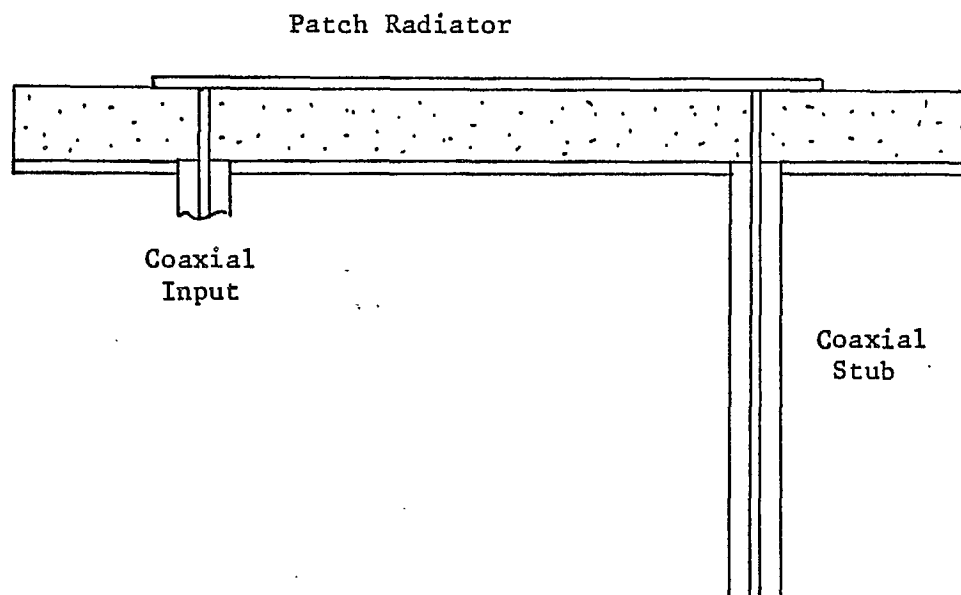


FIGURE 4.14: MICROSTRIP ANTENNA LOADED BY COAXIAL STUB

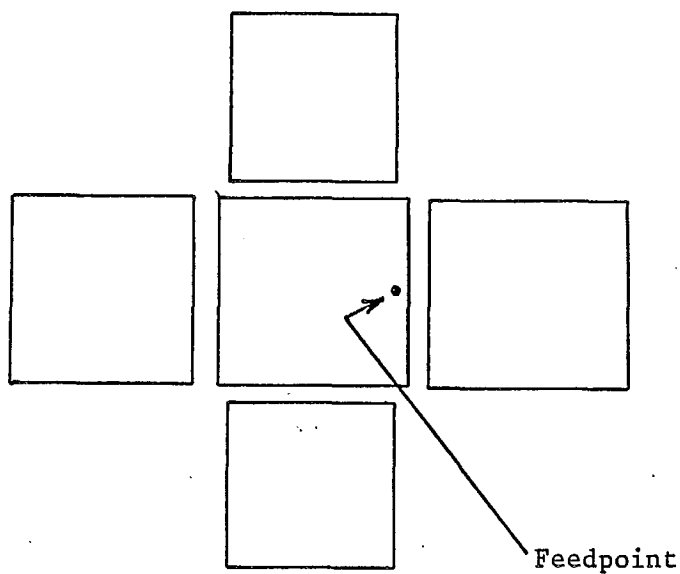


FIGURE 4.15: MICROSTRIP ANTENNA WITH COPLANAR PARASITIC RESONATORS

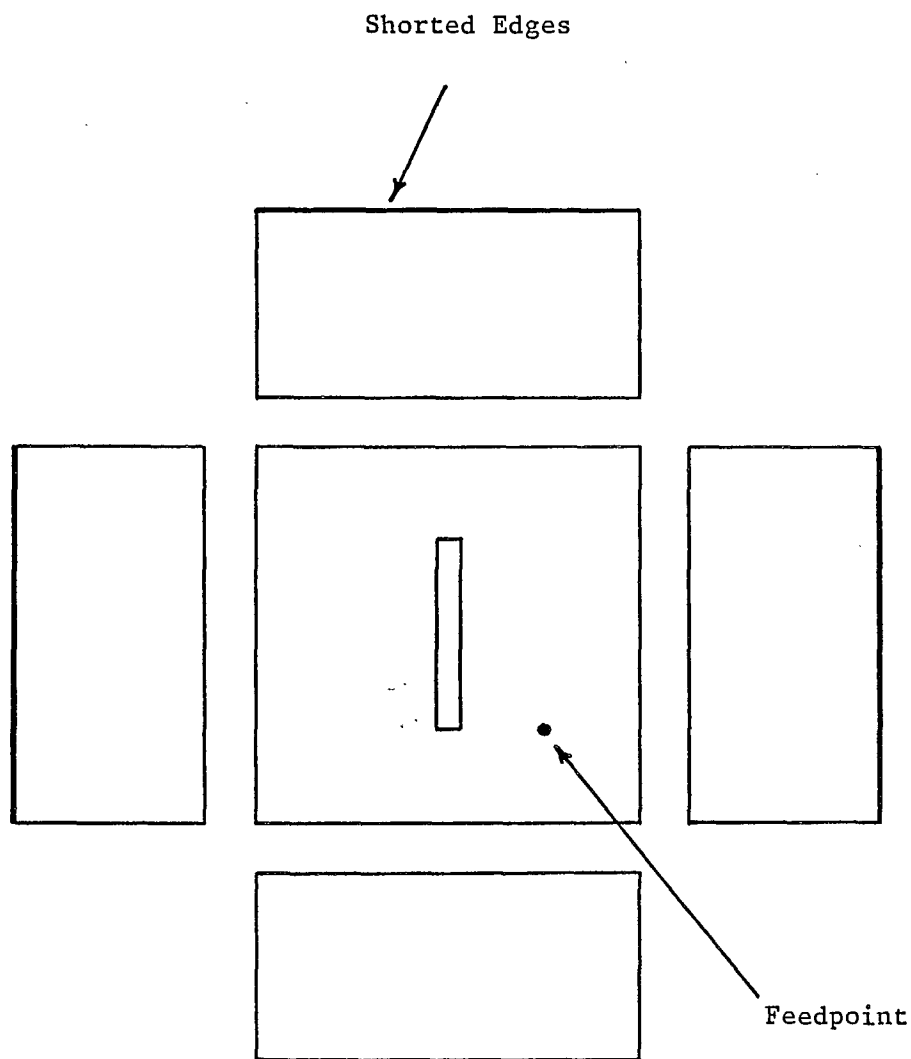


FIGURE 4.16: CIRCULARLY POLARIZED MICROSTRIP ANTENNA WITH SHORTED QUARTER-WAVE PARASITIC RESONATORS

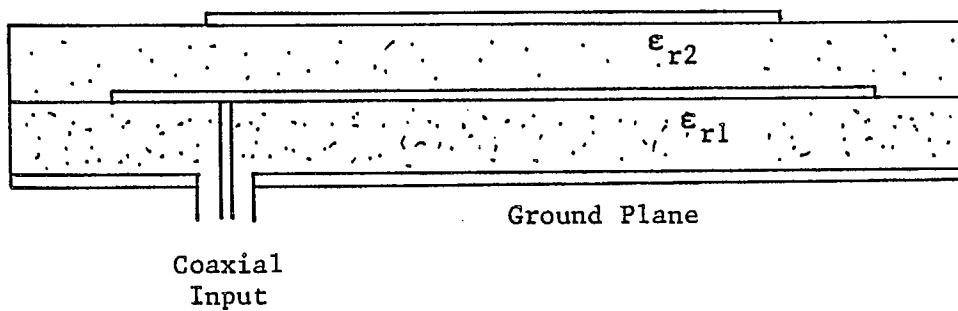


FIGURE 4.17: CROSS SECTION OF STACKED PATCH ANTENNA

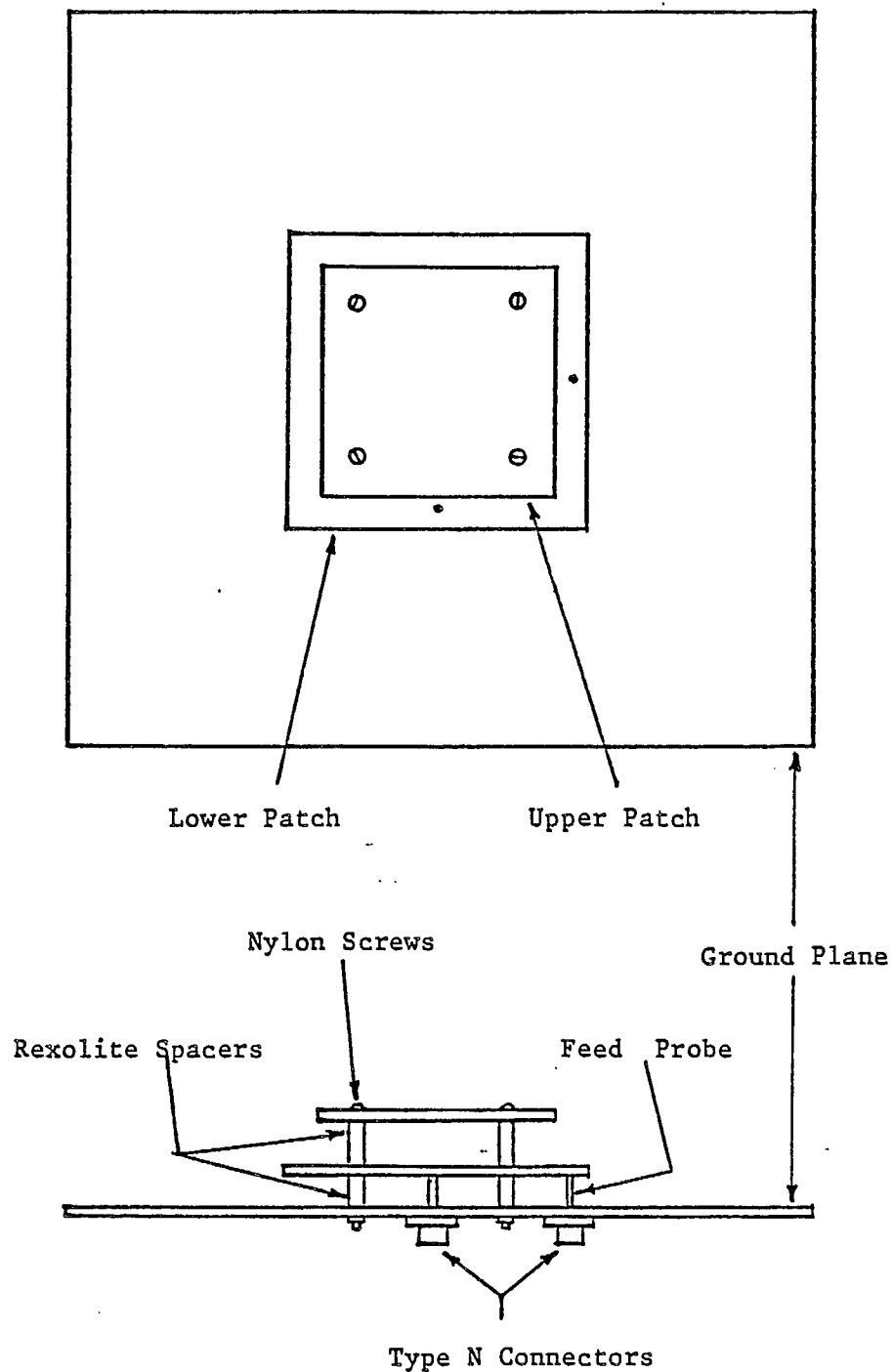
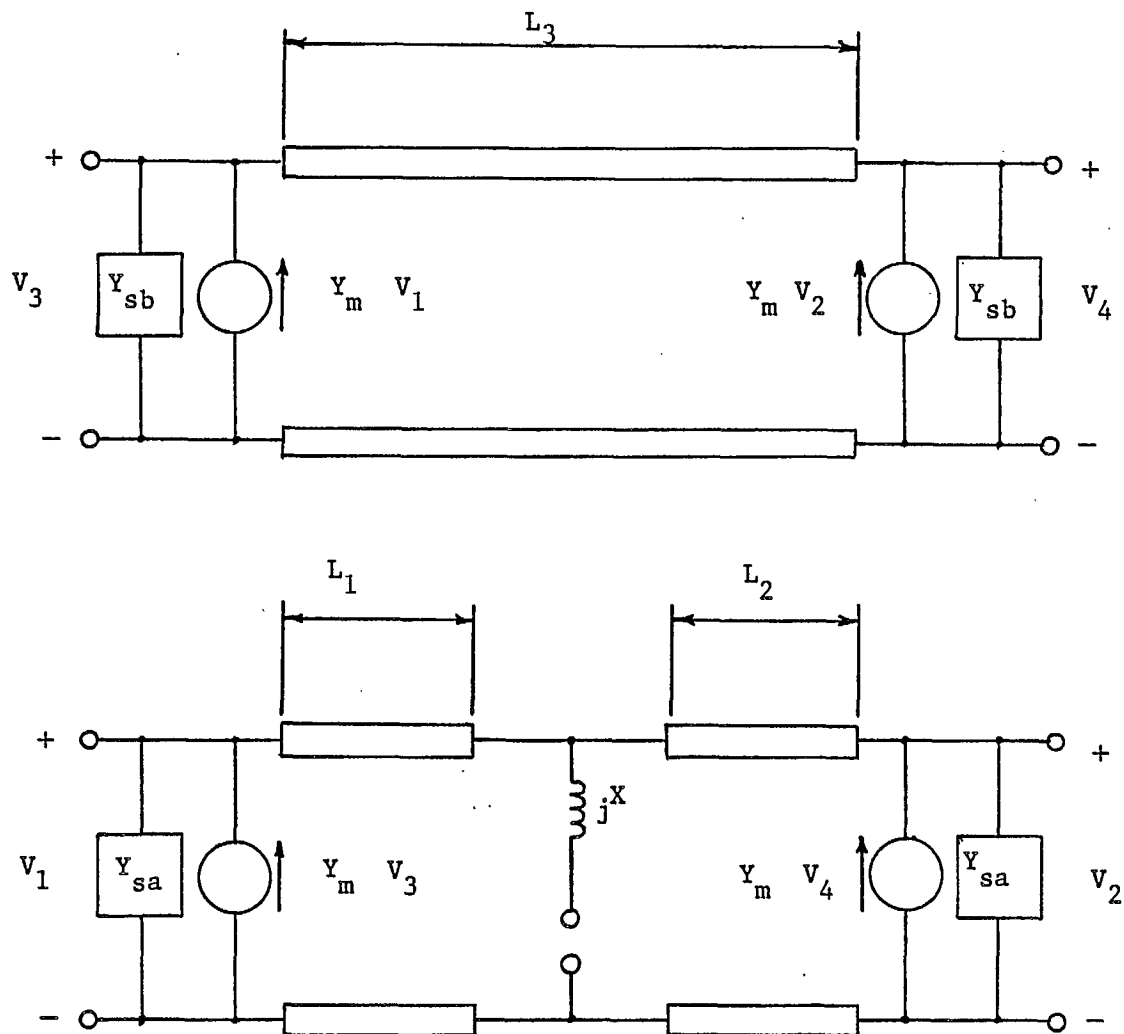
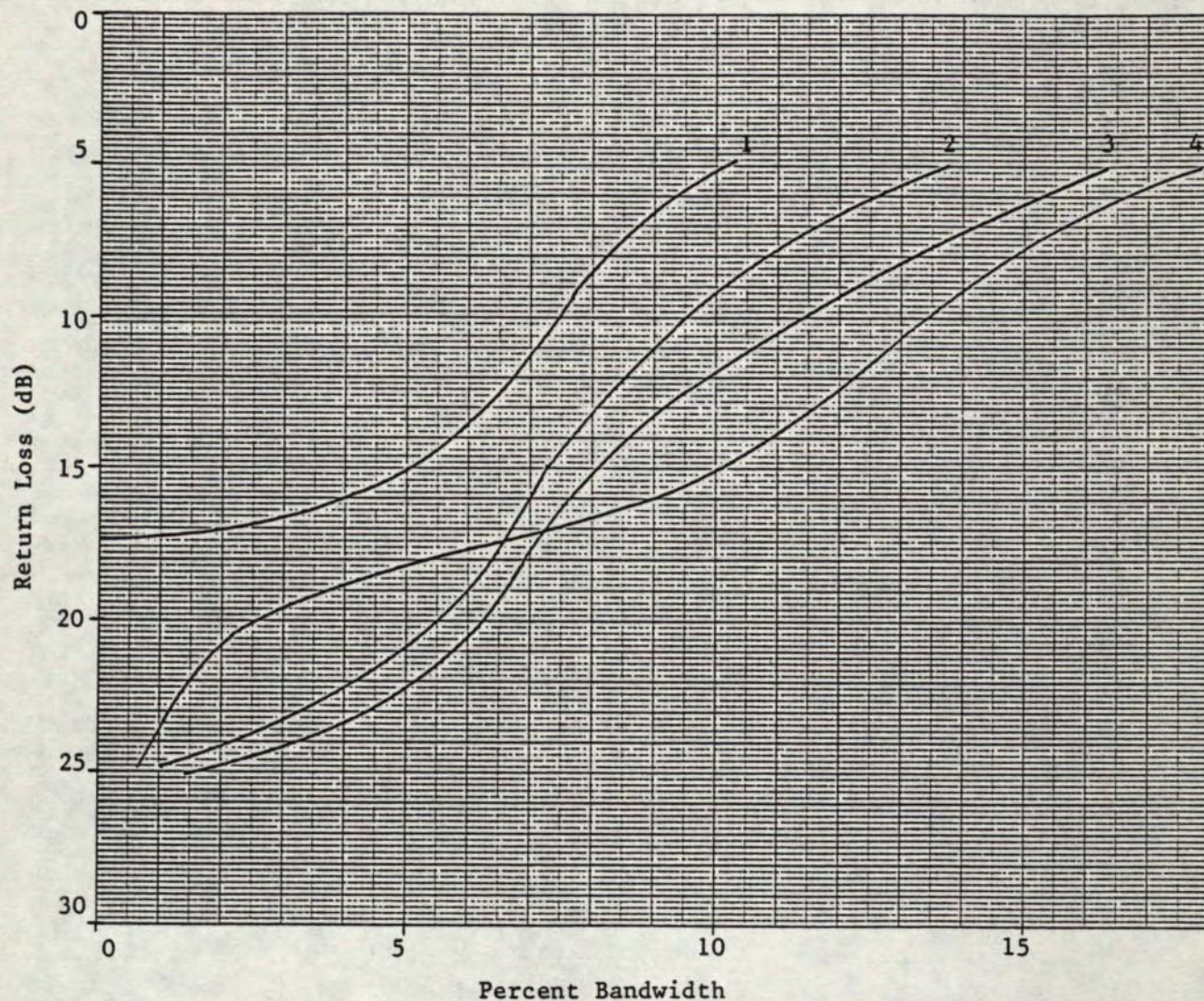


FIGURE 4.18: EXPERIMENTAL STACKED PATCH ANTENNA



- L_1 : Lower Patch Length From Edge to Feed
 L_2 : Lower Patch Length From Other Edge to Feed
 L_3 : Upper Patch Length
 Y_m : Mutual Admittance Between Upper and Lower Slots
 Y_{sa} : Self Admittance of Lower Slots
 Y_{sb} : Self Admittance of Upper Slots
 jX : Feed Probe Reactance

FIGURE 4.19: EQUIVALENT CIRCUIT FOR STACKED PATCH ANTENNA



All cases: Lower patch 6.4 inches square, upper patch 5.5 inches square

- 1: Lower spacing 0.15 inch, upper spacing 0.45 inch
- 2: Lower spacing 0.25 inch, upper spacing 0.55 inch
- 3: Lower spacing 0.35 inch, upper spacing 0.55 inch
- 4: Lower spacing 0.45 inch, upper spacing 0.55 inch

FIGURE 4.20: RETURN LOSS AND BANDWIDTH OF STACKED PATCH ANTENNAS

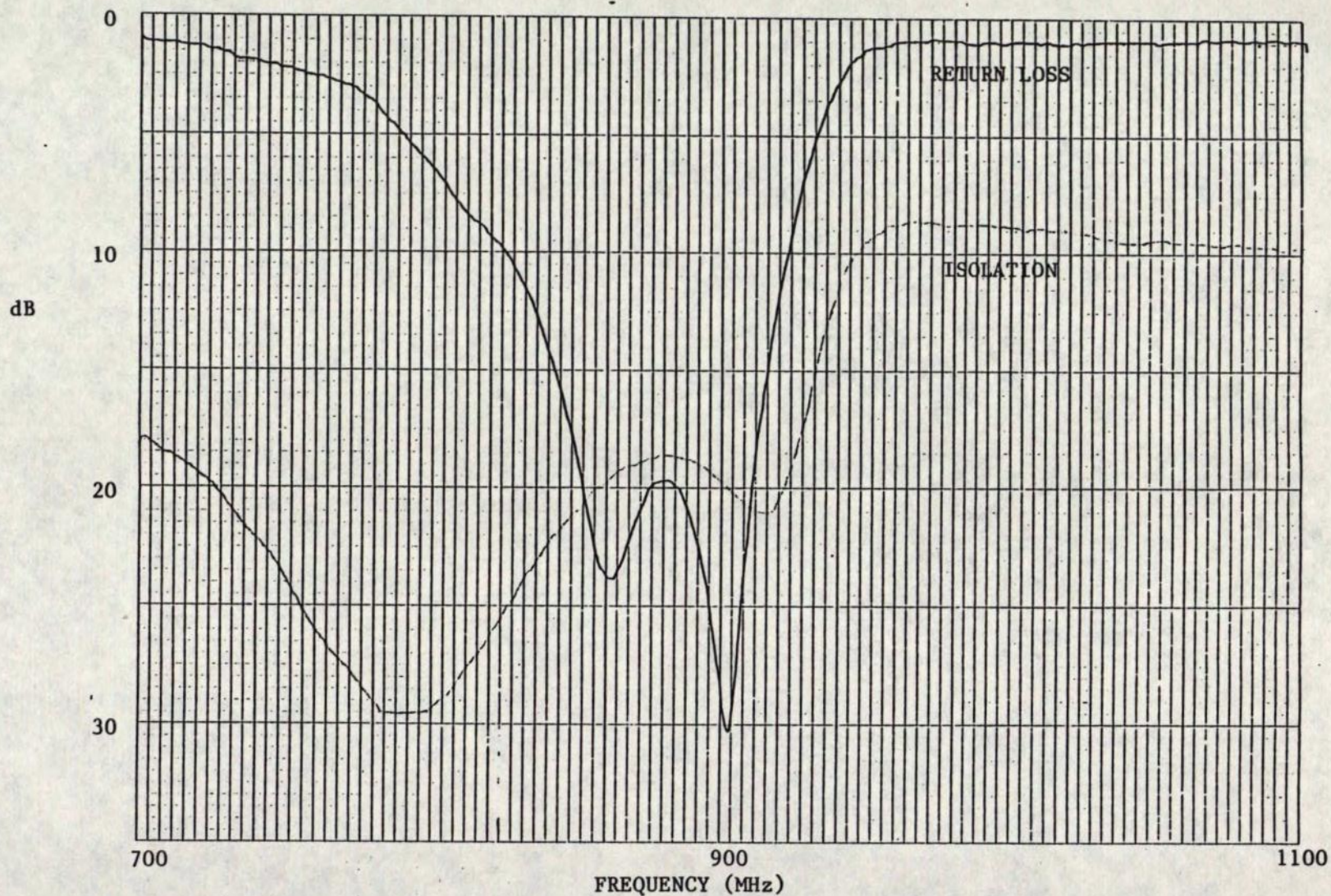


FIGURE 4.21: RETURN LOSS AND ISOLATION OF A STACKED AIR-DIELECTRIC SQUARE PATCH ANTENNA. LOWER PATCH 6.4 x 6.4 INCHES, SPACED 0.35 INCH FROM GROUND PLANE; UPPER PATCH 5.5 x 5.5 INCHES, SPACED 0.50 INCH FROM LOWER PATCH

DOCUMENT No.

REV.

RPT/MST/2500/001

COM DEV
SHEET 78

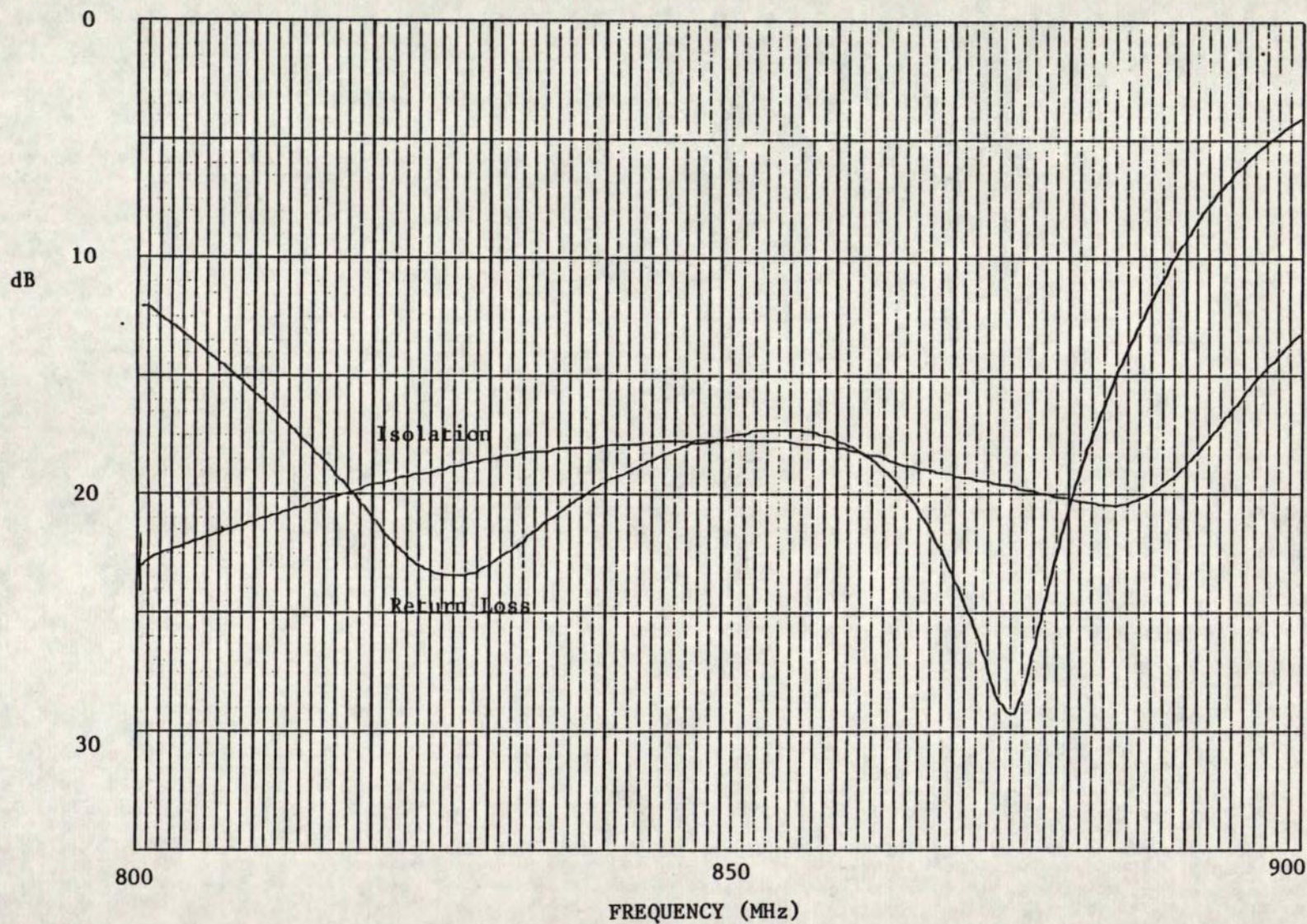


FIGURE 4.22: MEASURED RETURN LOSS AND PORT-TO-PORT ISOLATION OF BREADBOARD STACKED PATCH ANTENNA (INPUT TO PORT 1)

DOCUMENT NO.

REV.

RPT/MST/2500/001

COM DEV
SHEET 79

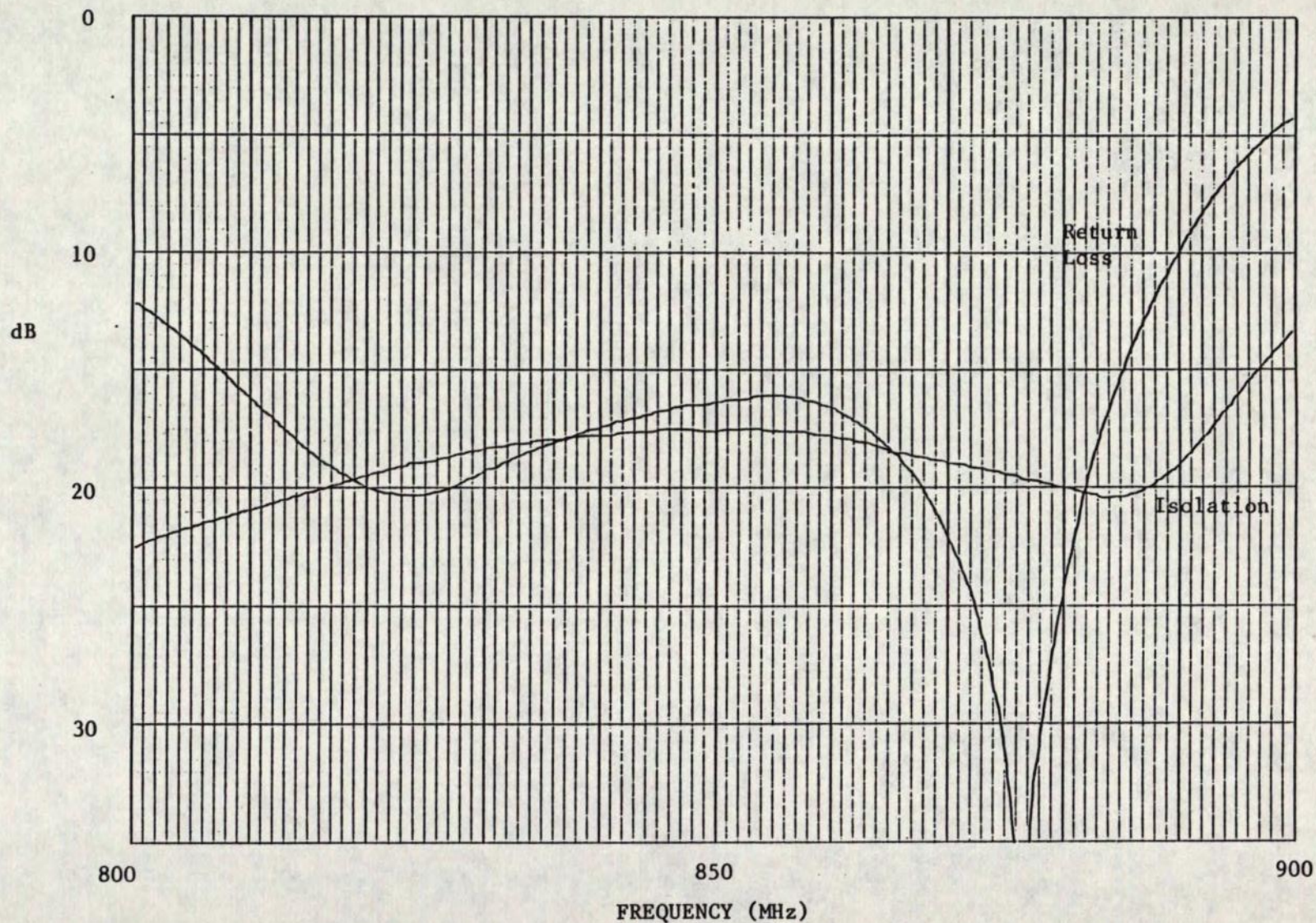


FIGURE 4.23: MEASURED RETURN LOSS AND PORT-TO-PORT ISOLATION OF BREADBOARD STACKED PATCH ANTENNA (INPUT TO PORT 2)

DOCUMENT NO.

RPT/MST/2500/001

REV.

—



COM DEV

SHEET

80

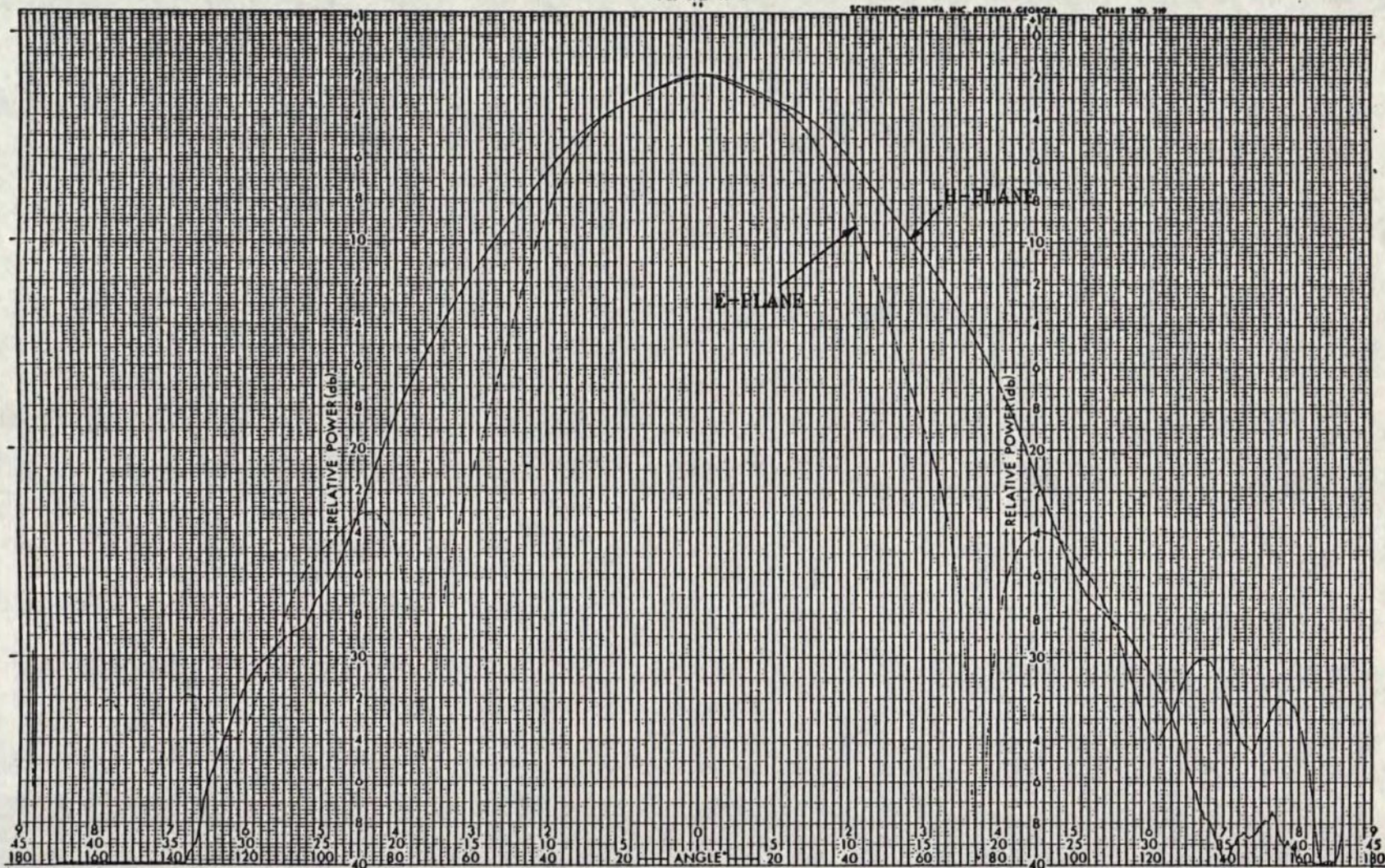


FIGURE 4.24: MEASURED E- AND H-PLANE PATTERNS OF BREADBOARD STACKED PATCH ELEMENT AT 823 MHz

DOCUMENT NO.

REV.

RPT/MST/2500/001

SHEET

81

COM DEV

DOCUMENT No.

REV.

RPT/MST/2500/001

SHEET

82



COM DEV

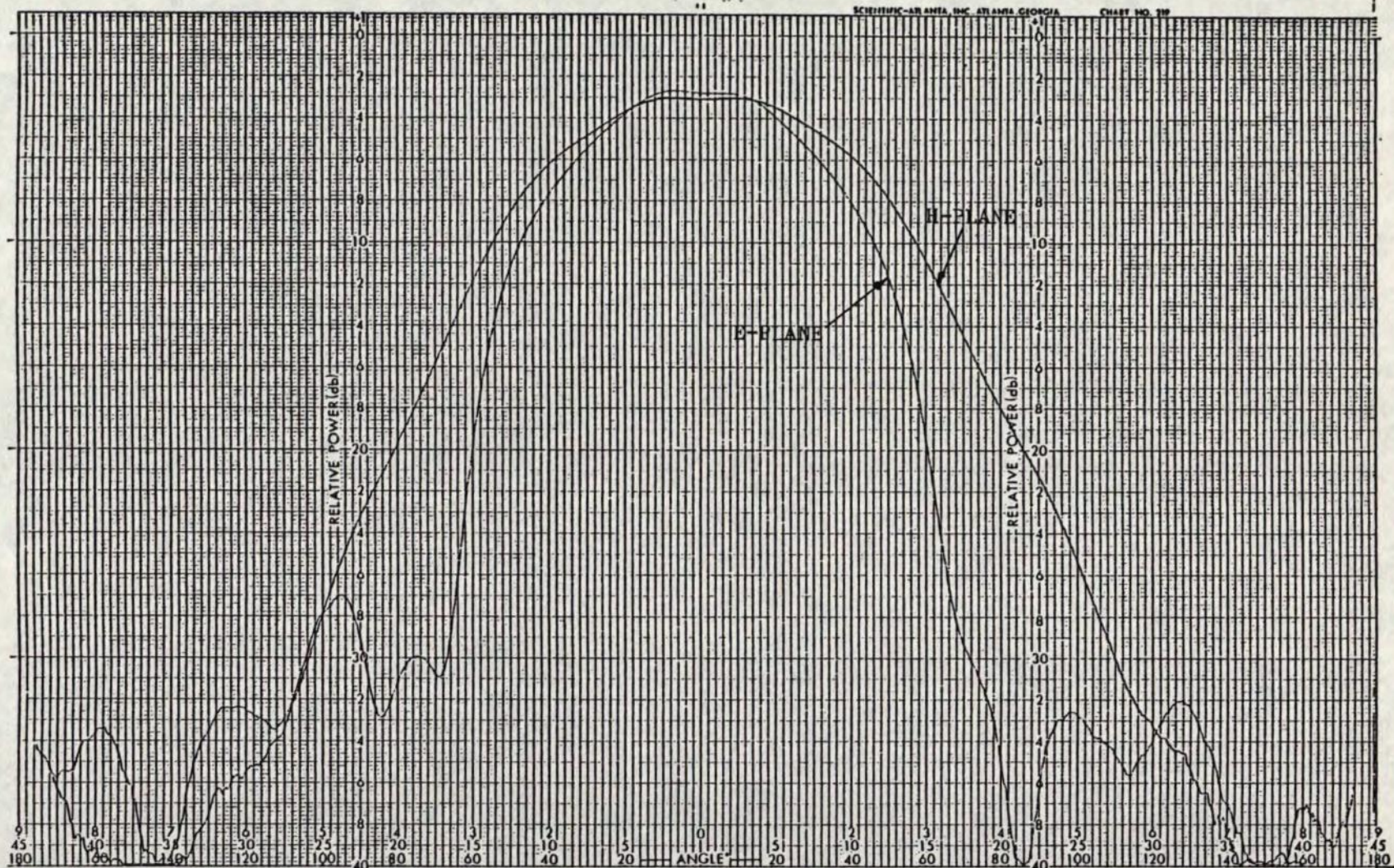


FIGURE 4.25: MEASURED E- AND H-PLANE PATTERNS OF BREADBOARD STACKED PATCH ELEMENT AT 868 MHz

Her Majesty the Queen in Right of Canada (1986) as represented by the Minister of Supply And Services.

DOCUMENT No.	REV.	 COM DEV
RPT/MST/2500/001	---	
		SHEET 83

COM DEV LTD

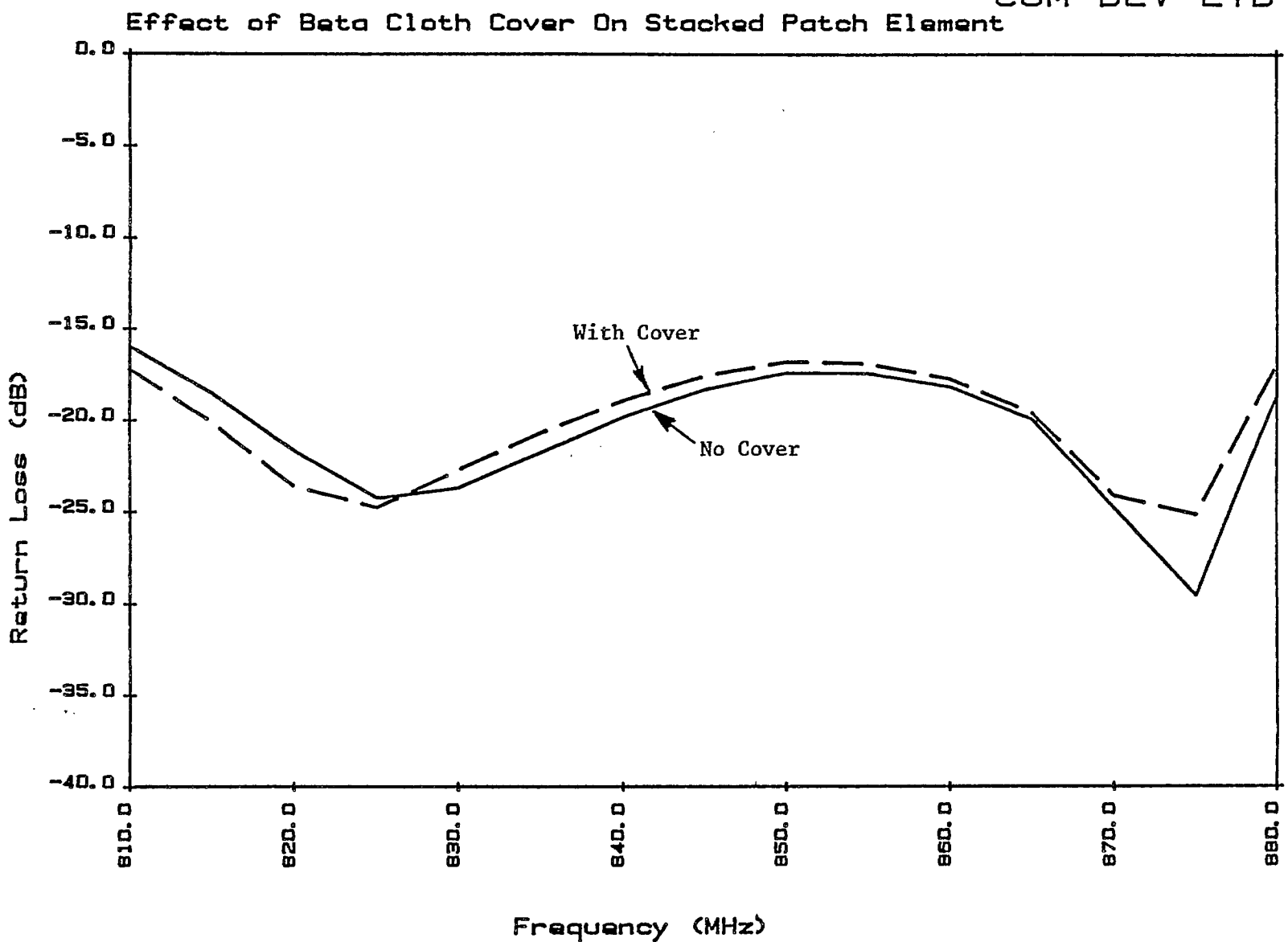


FIGURE 4.26: EFFECT OF BETA CLOTH COVER OVER BREADBOARD STACKED PATCH ANTENNA : RETURN LOSS

Effect of Beta Cloth Cover On Stacked Patch Element

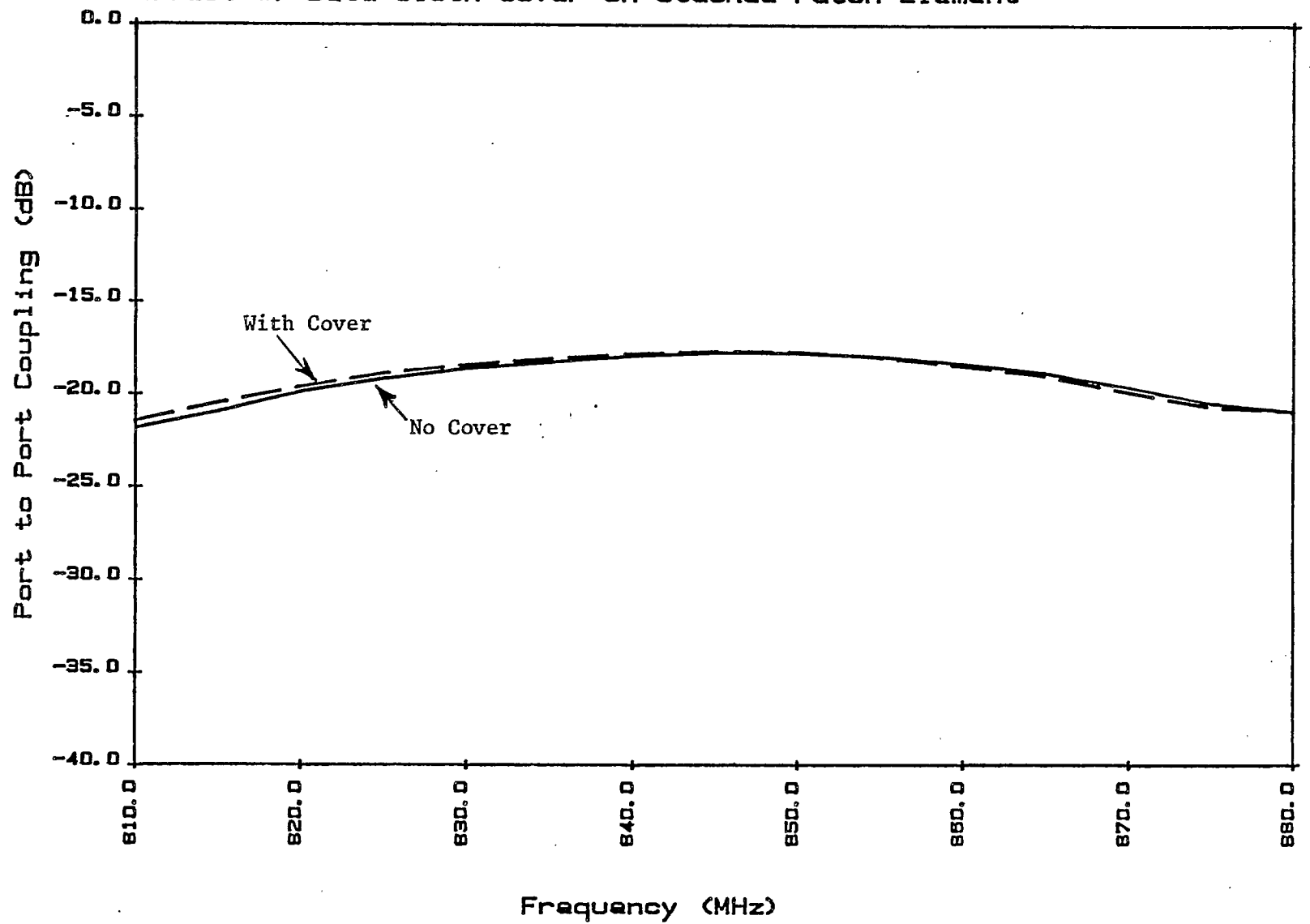



FIGURE 4.27: EFFECT OF BETA CLOTH COVER OVER BREADBOARD STACKED PATCH ANTENNA: PORT-TO-PORT ISOLATION

Her Majesty the Queen in Right of Canada (1986) as represented by the Minister of Supply And Services.

DOCUMENT NO.	REV.	 COM DEV
RPT/MST/2500/001	—	
SHEET 84		

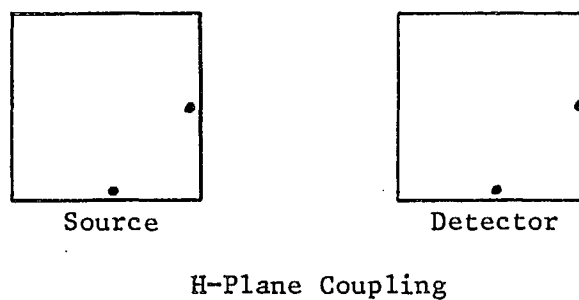
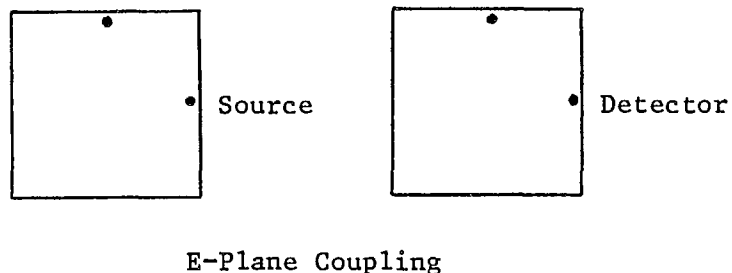



FIGURE 4.28: GEOMETRY OF E- and H-PLANE MUTUAL COUPLING

Her Majesty the Queen in Right of Canada (1986) as represented by the Minister of Supply And Services.

DOCUMENT NO.	REV.	 COM DEV
RPT/MST/2500/001	—	
SHEET		86

COM DEV LTD

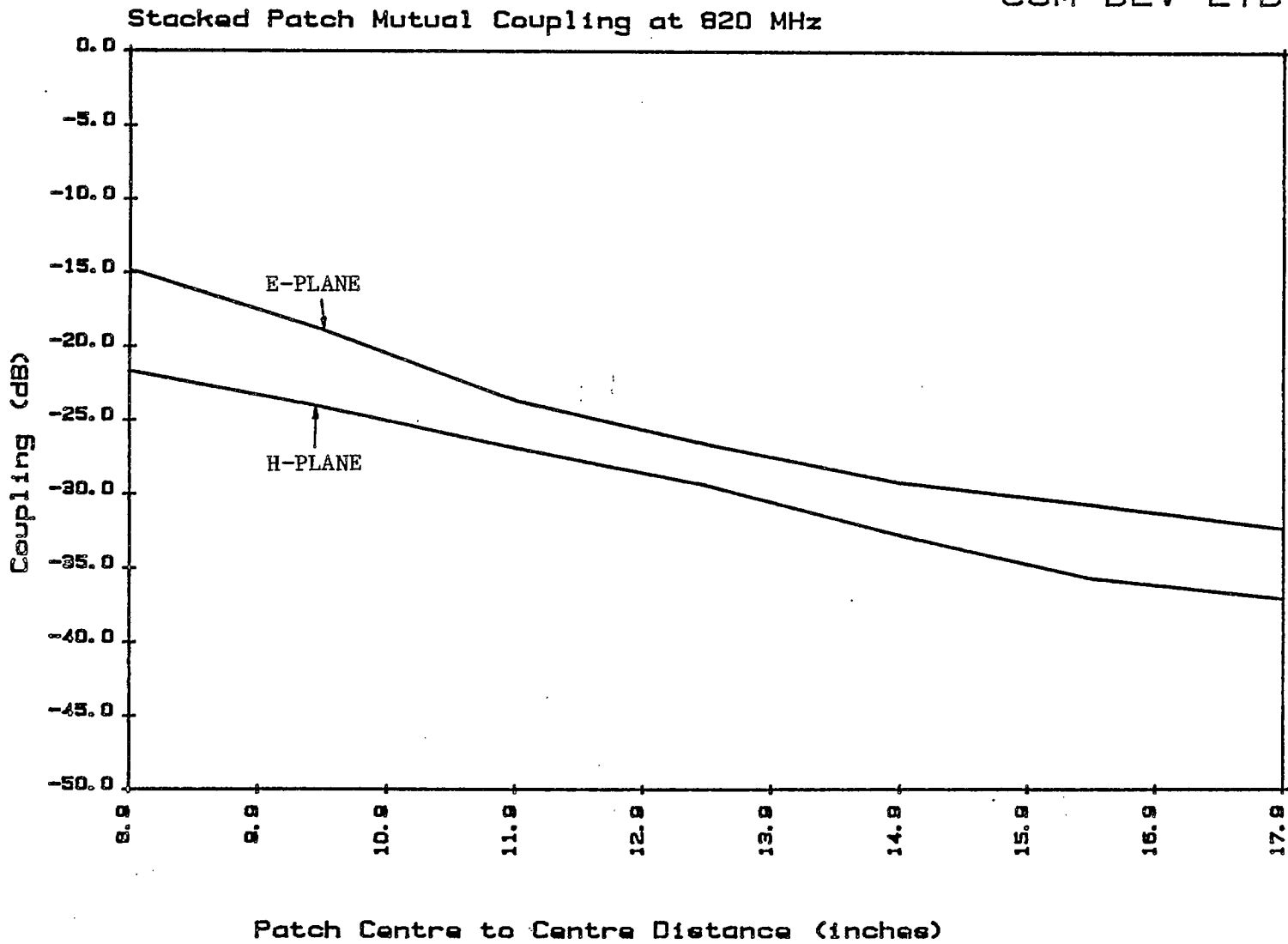



FIGURE 4.29: MEASURED E- AND H-PLANE MUTUAL COUPLING VERSUS SPACING BETWEEN BREADBOARD STACKED PATCH ANTENNAS AT 820 MHz

DOCUMENT No.	REV.	 COM DEV
RPT/MST/2500/001	—	
SHEET 87		

COM DEV LTD

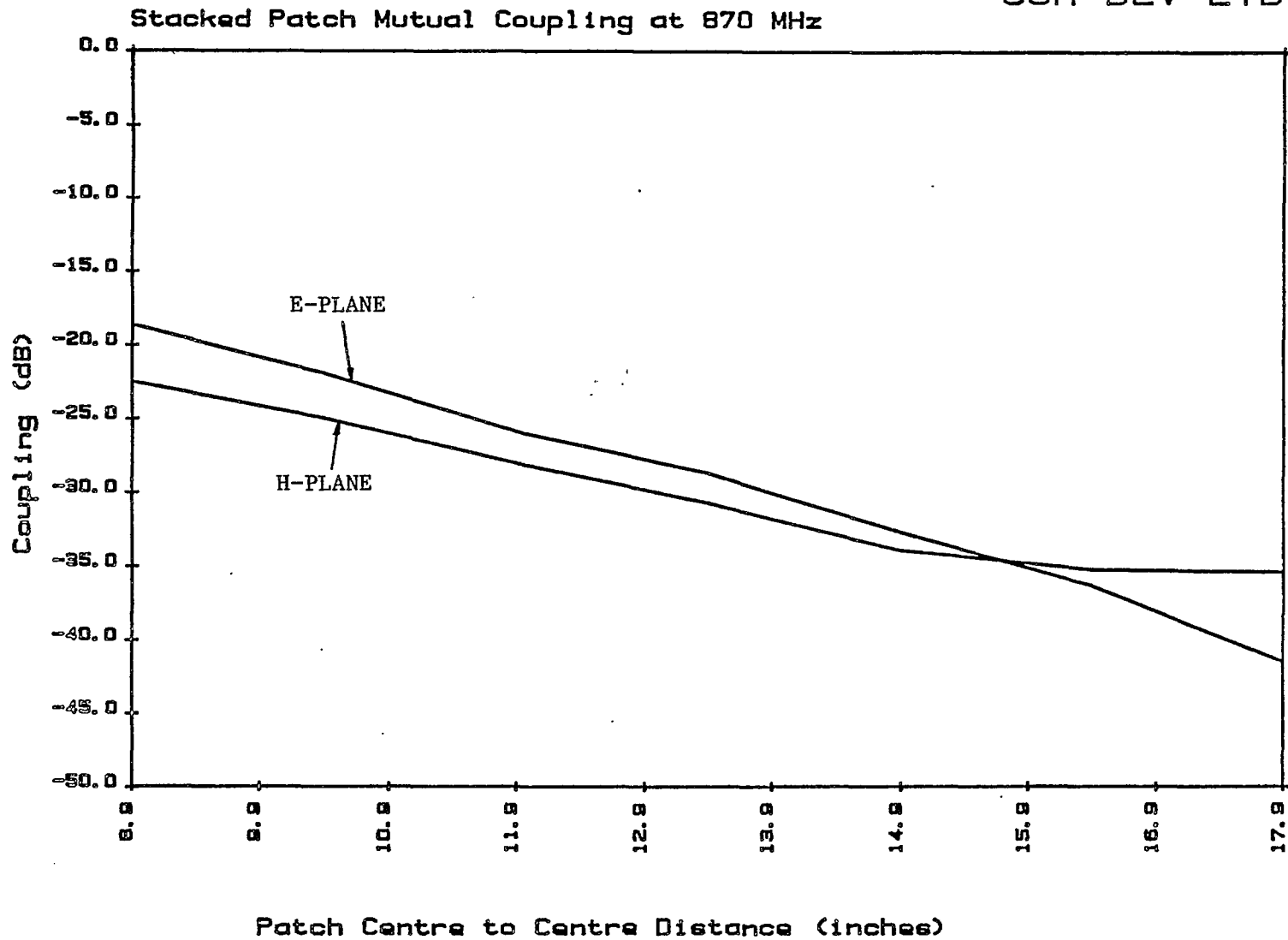
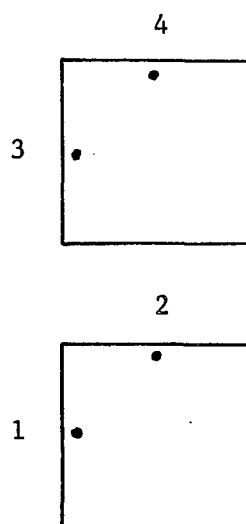
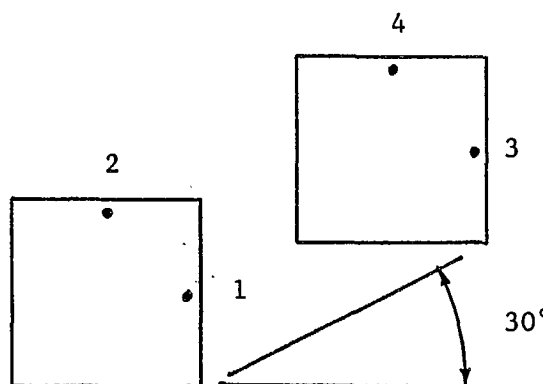


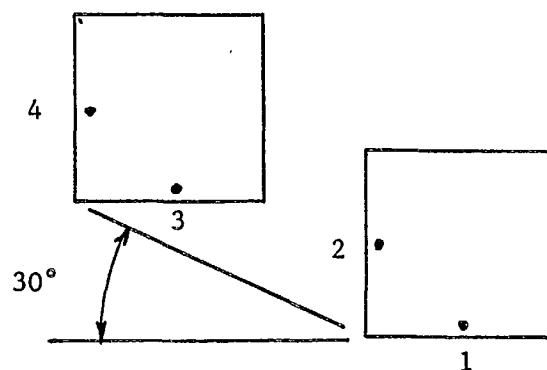
FIGURE 4.30: MEASURED E- AND H-PLANE MUTUAL COUPLING VERSUS SPACING BETWEEN BREADBOARD STACKED PATCH ANTENNAS AT 870 MHz



Case 1



Case 2



Case 3

FIGURE 4.31: SEPTET COUPLING GEOMETRIES (VIEWED TOWARD FRONT FACE, ALL CASES 12 IN. CENTRE-TO-CENTRE SPACING)

5.0 BEAM FORMING NETWORK TECHNOLOGY

5.1 Transmission Line Options

Each beam forming network required for MSAT will consist of a multi-way power divider network with unequal output powers and well controlled phases. It will be made up of a number of two-output power dividers interconnected with transmission lines (including bends and possibly fixed phase shifters and connections between layers of a multilayer structure). The two-way power dividers will probably be in the form of directional couplers with good isolation between the output ports in order to minimize effects due to reflections and mutual coupling of the array elements.

A variety of transmission line types may be considered including waveguide, coaxial cable, "squarax" (TEM-line), vacuum-spaced stripline, dielectric spaced stripline and microstrip (see Figure 5.1). These may be evaluated for attenuation, volume, mass, applicability to long interconnecting lines and to fabrication of components, potential for high power problems such as passive intermodulation and multipactor breakdown, unwanted coupling between components, and suitability for the space environment. These characteristics are tabulated in Table 5.1. Waveguide can be dropped from consideration because it has much greater mass and volume than the other candidates. Interconnections in coaxial cable (especially T-junctions) are rather difficult and potentially could cause higher susceptibility to PIM and multipactor. It would be very difficult to manufacture large parts of a BFN in a single piece using coaxial geometry. Microstrip on a typical teflon/glass substrate has high loss compared to other geometries. The most promising technologies are square coaxial ("squarax" or TEM line) type or stripline (also known as triplate), preferably with vacuum dielectric for

low loss (apart from a few supports). These are reasonably lightweight and do not suffer from excessive loss. The major drawbacks for both are the potential problems at high power levels, PIM and multipactor discharge. The tradeoff between squarax and stripline is dependent on loss (better for squarax) and mass (better for stripline). We elected to consider stripline in detail because of the possibility of very lightweight construction.

5.2 Stripline Design

The dimensions of a stripline are defined in Figure 5.2. Using the ratios $t/w=.272$ and $t/h=.237$ the loss of stripline with silver conductors has been computed as a function of the ground plane spacing h , at 820 and 880 MHz. The TOUCHSTONE [67] software package was used to obtain these values, which are plotted in Figure 5.3. The curves may be approximated very closely by the simple relation

$$\text{Loss (dB/inch)} = .00163/h \text{ (inches)}$$

where the result is an average value for the MSAT transmit and receive bands. In practice, for the larger value of h the thickness of the strip (t) might not be as large as assumed above, in order to reduce mass. In this case the loss would be slightly lower. These losses are conduction losses only. Any dissipation in dielectric supports would add to these values but is expected to be small.

In the feed array panel envisaged in this report each patch element is fed by two probes passing through the ground plane from a stripline coupler underneath it which is in turn fed by a beam-forming network occupying one or more layers underneath

that. The probe coupling between layers requires careful consideration. The abrupt change in transmission line characteristics from the stripline to, for example, a round pin at right angles to the strip results in a considerable reactance. In addition the asymmetry of the transition tends to excite propagation of the parallel-plate waveguide (TEM) mode between the upper and lower ground planes of the stripline. This was observed experimentally with stripline coupler circuits having coupling, return loss and isolation that varied with movement of one's hand around the edges of the ground planes. This unwanted mode may be eliminated by connecting the two ground planes together near the probe transition. These connections must be made far enough from the stripline to avoid changing its impedance excessively. Any residual effect can be lumped with the other mismatches of the probe.

Based on measured characteristics of a section of stripline with TNC connectors at each end an equivalent circuit for the stripline-to-coaxial transition was developed. Modifications to this equivalent circuit were made and the performance recalculated in order to find a simple matching technique. It was found that a good narrowband match could be obtained by extending the stripline 0.3 inch past the centre of the connector probe. The configuration of this transition is shown in Figure 5.4. This modification was made to the test line and resulted in much improved match.

It is important to consider the behaviour of vacuum-dielectric stripline at high power levels. Two potential problems are of concern: multipactor breakdown and passive intermodulation.

Multipactor breakdown occurs between two surfaces with an RF voltage between them, and only under vacuum conditions. Any electrons released by one surface are accelerated by the electric field across the gap. On impact with the other surface a number of secondary electrons are released. If the AC field reverses direction at the appropriate time the secondary electrons will be accelerated back across the gap. If the average number of secondary electrons released by the impact of one electron is greater than one the discharge can build up to a level that causes deterioration of return loss of a component and release of gases which may result in catastrophic ionization breakdown. The voltage necessary to cause breakdown is dependent on the frequency, gap size and properties of the two surfaces.

To consider these effects on stripline components a baseline 50 ohm design with a gap between the strip and the ground plane of 0.1 inch was chosen. A number of publications contain figures showing the region of existence of multipactor plotted on axes of voltage (or power) and frequency-gap product. While these curves are all of similar shape the predicted voltages at which onset of discharge will be observed varies greatly. For example Woo [64] predicts that at 868 MHz the baseline stripline should breakdown at 162 watts and Clancy [10] shows 63 watts to be the minimum for multipaction. These levels assume that breakdown for stripline will occur at the same levels as for coaxial line. This should be approximately true as Woo has shown similar behaviour for coaxial and parallel plate geometries.

A report prepared at Hughes [69] shows that different metals have generally similar behaviour. Although the variations in onset levels are not insignificant they do not follow any clear trend. Prediction of multipactor, therefore, seems quite inexact.

A preliminary experiment was carried out using a section of brass stripline between aluminum ground planes with the baseline dimensions (0.1 inch strip-ground plane gap, 0.262 inch between ground planes). This was placed in an evacuated chamber. Power at 868 MHz was gradually increased until breakdown was observed (as a sudden increase of reflected power), initially at 159 Watts. Power was shut off and increased again but no breakdown was observed until 224 W was reached. On the third attempt 345 W was required. The test piece was not cleaned between these tests. On disassembly one ground plane only was found to be severely discoloured under the stripline.

The initial measured breakdown agrees well with Woo's data. Therefore, it would seem advisable to use a larger spacing or some dielectric material to increase the threshold for use on MSAT. The Hughes report [69] shows considerable improvement when metal surfaces are completely coated with thin layers of Teflon or epoxy. Alternatively, a material such as shuttle tile which has low dielectric constant and low loss could be used to fill the entire gap. To be successful the voids in a material such as this must be too small to support multipactor.

There is potential for passive intermodulation in several parts of a stripline network. If silver plated aluminum parts are used it is important to ensure that any intermediate nickel plating layer is not exposed to significant field strengths. The silver plating must be thick enough to prevent penetration into the nickel. PIM may be generated in connections between separately manufactured sections of the network. Connections between stripline pieces and with probes between layers of the network must be welded or well soldered and must be resistant to vibration and shock. Another possible problem area is the pins

for suppression of the parallel plate waveguide mode. Suitable prevention methods may include smearing of bolted joints with conductive adhesive (which may suffer from problems at low temperatures) or use of fastening techniques such as dip-brazing. With due care any excessive PIM levels can be eliminated.

5.3 Experimental Coupler Design

As part of the investigation of technology suitable for the MSAT beam-forming network a stripline branch-line coupler was developed. For compactness a two-branch design was adopted, using as a baseline air-spaced stripline with a ground plane spacing of 0.262 inch. Suppression of the parallel-plate waveguide mode (using several pins around connector probes) and matching using stripline extensions beyond the connector probes were found to be necessary for acceptable performance to be achieved.

Each of the four ports was brought out to a type TNC connector for testing. The TOUCHSTONE [67] microwave modelling software package was used to optimize the dimensions of the coupler. The elements of the model are shown in Figure 5.5. This software was very useful but was not completely accurate using the circuit shown. The most significant difference with measurements was in the centre frequency of the coupler. Allowing for a frequency correction the design was chosen so as to equalize the power split at the two MSAT bands: 821- 825 MHz and 866 - 870 MHz. The experimental coupler is shown in Figure 5.6.

The measured performance of this coupler is shown in Figure 5.7 (Return Loss), 5.8 (Isolation), 5.9 (Straight-through Loss) and 5.10 (Coupled Port Loss). These measurements include the

degradation due to coaxial adapters between the TNC type connectors used for the coupler and the APC-7 types of the Hewlett-Packard 8408B automatic network analyzer used to make the tests. The overall loss of the coupler, including reflection, dissipation and radiation losses can be defined as:

$$\text{LOSS} = -10 \log_{10} \left(10^{-\frac{\text{COUPLING}}{10}} + 10^{-\frac{\text{STRAIGHT THROUGH}}{10}} \right)$$

where "coupling" and "straight through" are the loss measured at the coupled and straight through ports (in dB). This value of overall loss is plotted in Figure 5.11. A smoothed curve is in good agreement with TOUCHSTONE predictions of about 0.09 dB loss. Figure 5.12 shows the phase difference between the coupled and straight through ports. As expected for this type of coupler the phase difference is almost exactly 90 degrees over the useful bandwidth of the device.

An ideal coupler of this type has return loss and isolation curves that track exactly and reach a value of 19 dB at six percent above the centre frequency. For a centre frequency of 845 MHz this corresponds to about 896 MHz. The measured return loss of 17.8 dB and isolation of 18.9 dB at 895 MHz demonstrate that the experimental coupler closely approaches the theoretical limit [48].

5.4 Recommendations for BFN Development

This preliminary work on stripline with largely air/vacuum dielectric has demonstrated that it should be considered a viable medium for UHF spacecraft beam formers. However, there are a number of clear limitations which will have to be taken into account in the design of an actual BFN and feed array.

For power levels such as proposed for MSAT multipactor breakdown is a real possibility. For this reason, and also to obtain lower loss, it is probable that in general a larger ground plane spacing than the 0.262 inch used experimentally is preferable. Doubling this dimension leads to breakdown powers of about 450W (from Woo [64]) and a halving of the loss. A coupler loss of about 0.05 dB should be achievable. Further increases in dimensions, however, would lead to intolerably wide striplines, large mismatches at transitions between layers and substantially increased mass. If higher power handling capability is required the higher loss of stripline with dielectric such as Teflon or glass/Teflon circuit board materials may be difficult to avoid. The use of low density, low permittivity materials such as space shuttle tile should be investigated.

The power dissipated in the stripline components at MSAT power levels will be significant, primarily because the stripline geometry provides a poor thermal path from the strip to the ground planes. This problem is common to microstrip, squarax and coaxial cables. It may be necessary to provide special heat sinking devices, such as shorted quarter wave stubs shunting the line. (See Figure 6.3).

The possible generation of PIM in the BFN components should be investigated. The primary candidates for PIM generation are the pins for suppression of the parallel-plate waveguide mode, connections between layers of the BFN/feed assembly and connections within a layer of the BFN.

It will be necessary to consider power dividers other than the two-branch branchline hybrid, for cases where smaller size or higher performance are required. Reactive power dividers, Wilkinson hybrids, rat-race and 3-branch branchline couplers may be useful and can be implemented in stripline. Coupled-line types may also be useful but care must be taken not to cause multipactor breakdown between lines in close proximity. It is likely that a mixture of types would be optimum.


DOCUMENT No.	REV.	 COM DEV
RPT/MST/2500/001	—	
		SHEET 97

TABLE 5.1: COMPARISON OF TRANSMISSION LINE CHARACTERISTICS

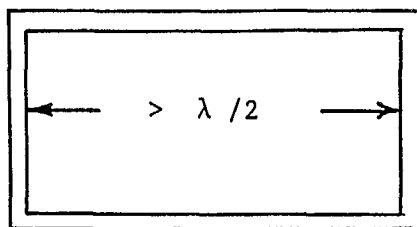
Characteristics	Waveguide	Coaxial Cable	Squarax	Vacuum Stripline	Dielectric Stripline	Microstrip
Loss	1	2 - 3	2	2 - 3	3 - 4	4
Volume	4	2	2	2	2	1
Mass	4	2	3	2	3	1
Suitability for Long Transmission Line	1	1	2	2	2	2
Suitability for Couplers	2	4	2	2	2	1
Potential for PIM	1	3	3	3	3	2
Potential for Multipactor	1	1 - 3	2 - 3	2 - 3	1	1
Space Environment Compatibility	1	2	2	2	3	3
Unwanted Couplings	1	1	2	2	2	3

1 = very good

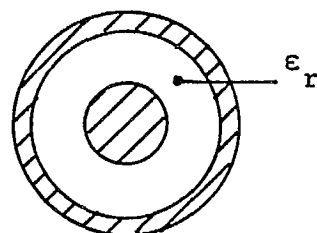
2 = good

3 = fair

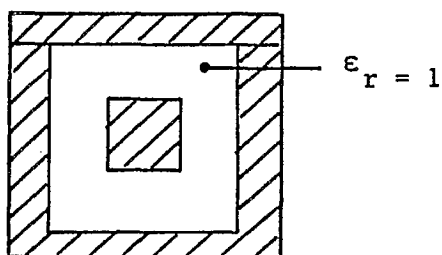
4 = poor



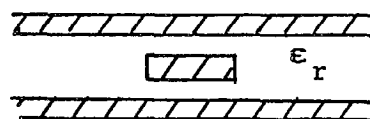
Waveguide



Coaxial Cable



Squarax



Stripline



Microstrip

FIGURE 5.1: TRANSMISSION LINE CANDIDATES

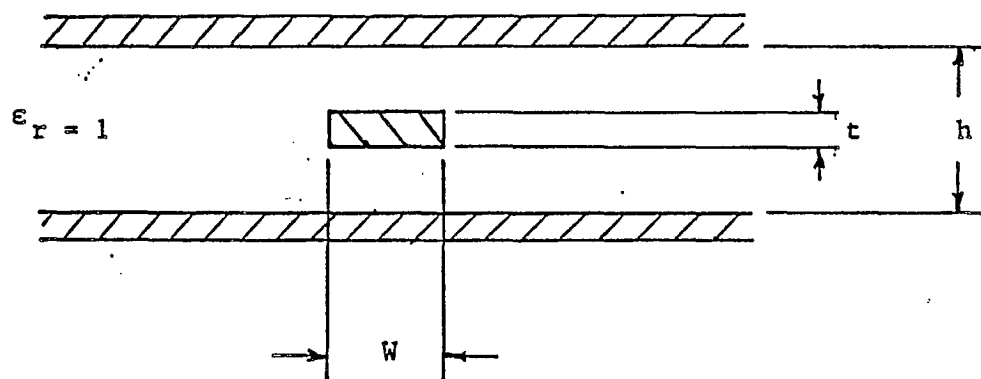


FIGURE 5.2: VACUUM-SPACED STRIPLINE GEOMETRY

LOSS
(dB/inch)

.016

.012

.008

.004

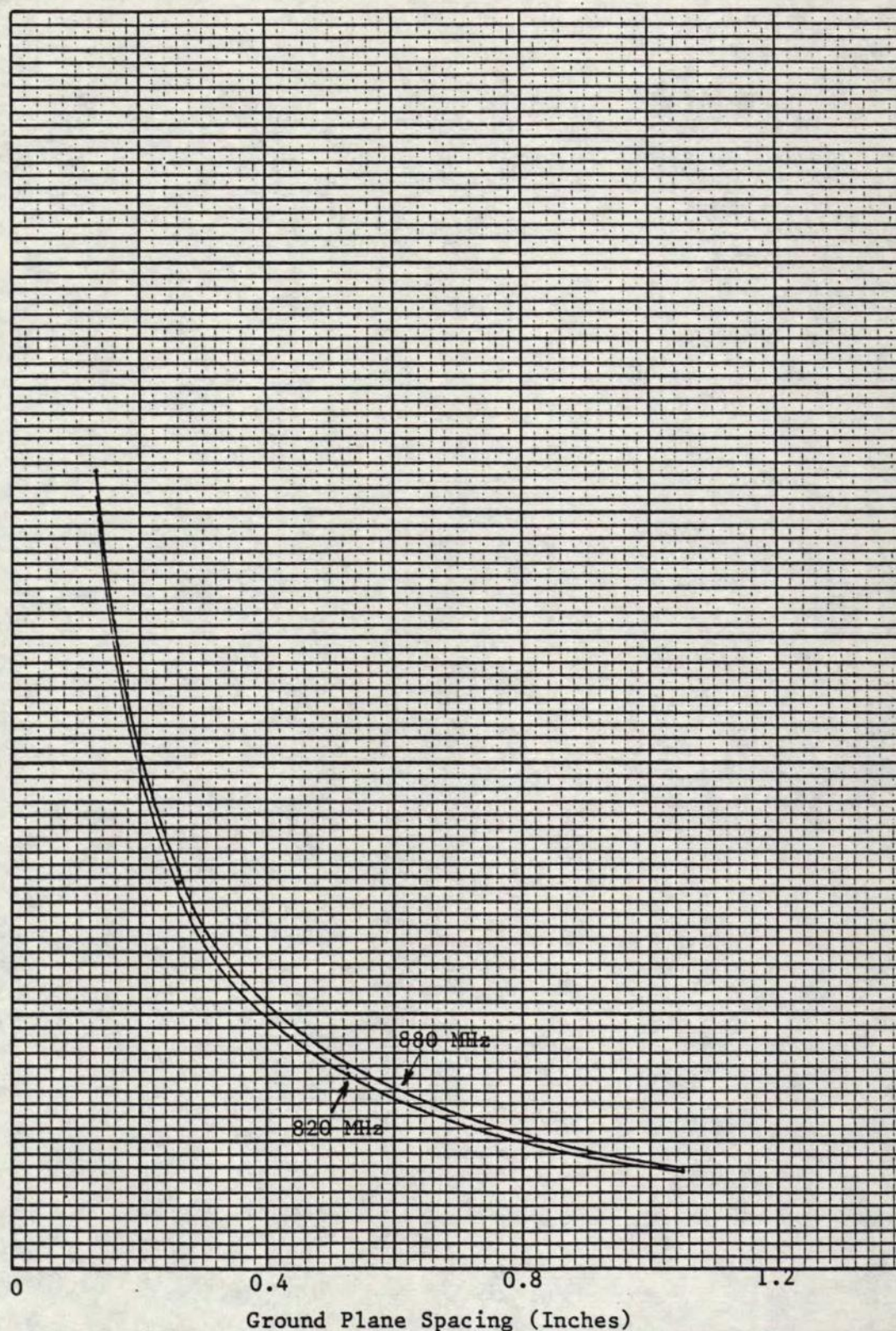


FIGURE 5.3: ATTENUATION OF SILVER STRIPLINE VERSUS GROUND PLANE SPACING

DOCUMENT No.

REV.



COM DEV

RPT/MST/2500/001

SHEET

101

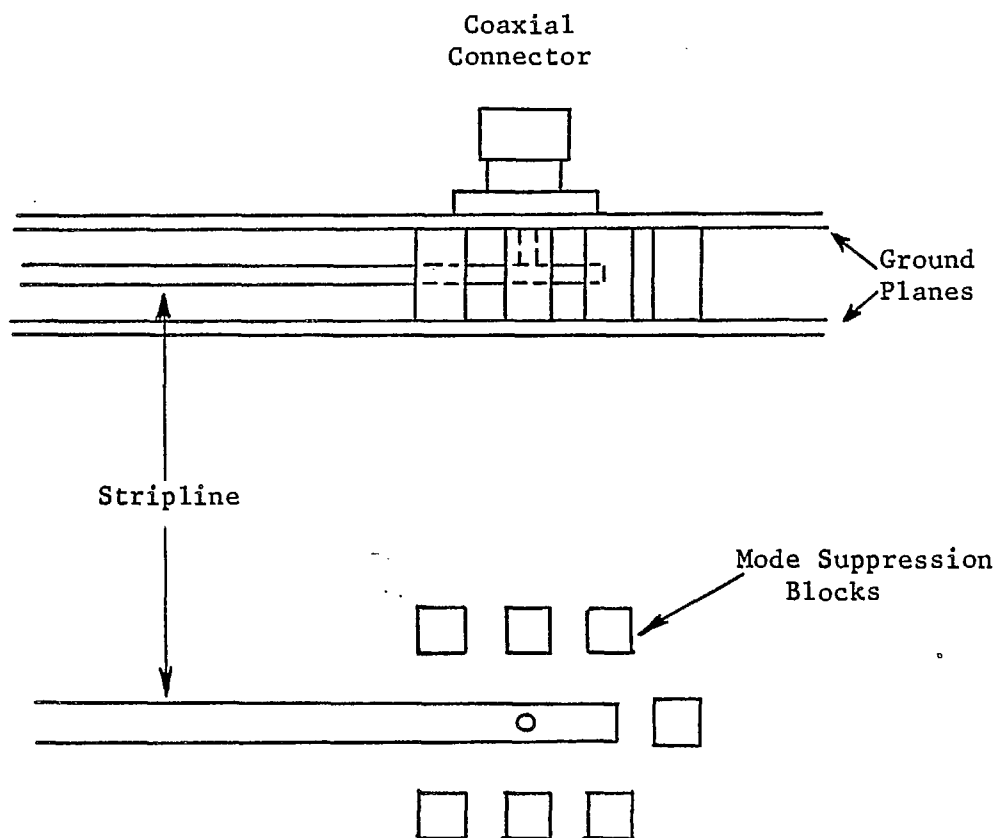


FIGURE 5.4: COAXIAL TO STRIPLINE TRANSITION

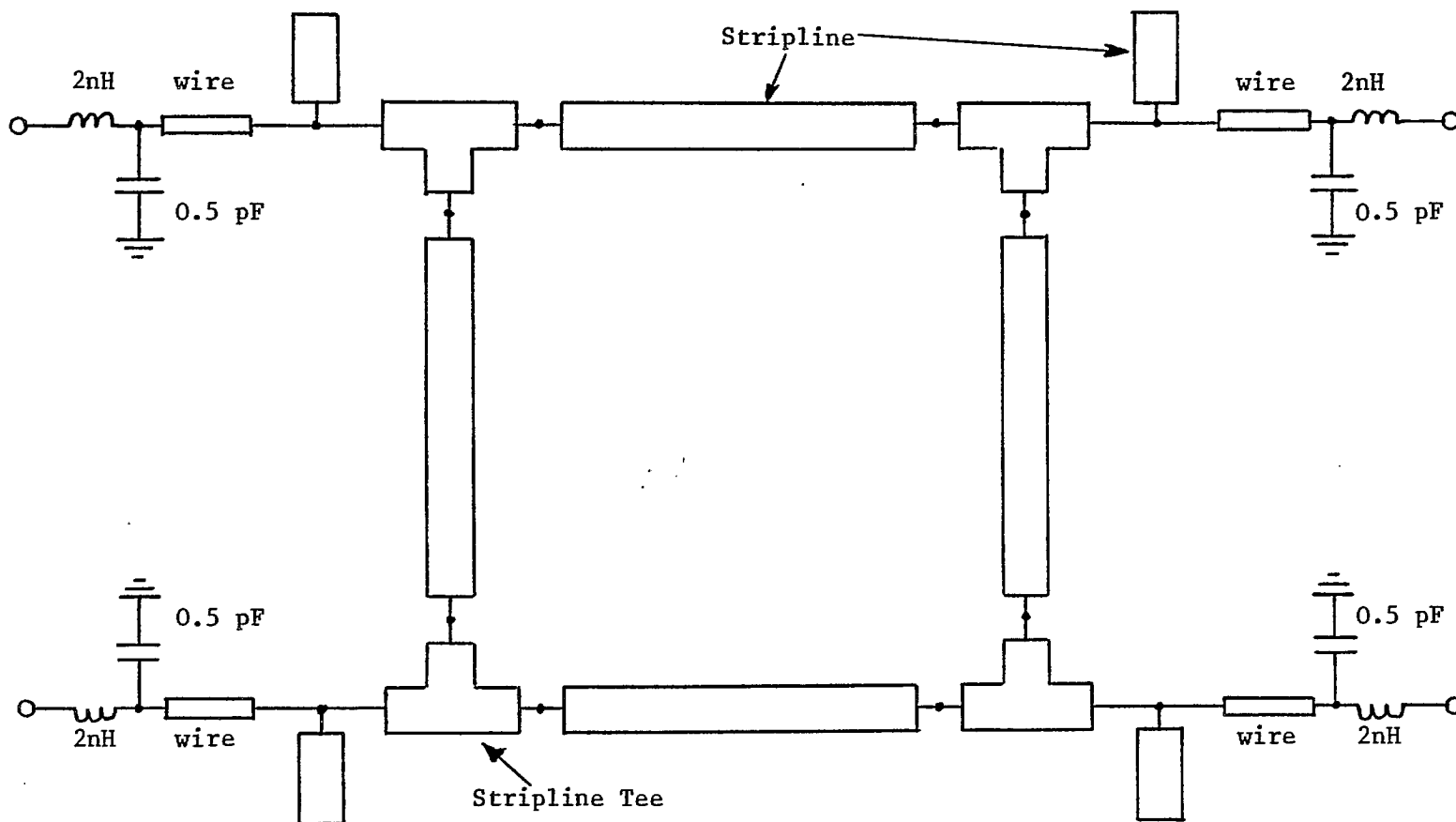


FIGURE 5.5: EQUIVALENT CIRCUIT FOR STRIPLINE COUPLER

DOCUMENT No.

RPT/MST/2500/001

REV.

—



COM DEV

SHEET 103

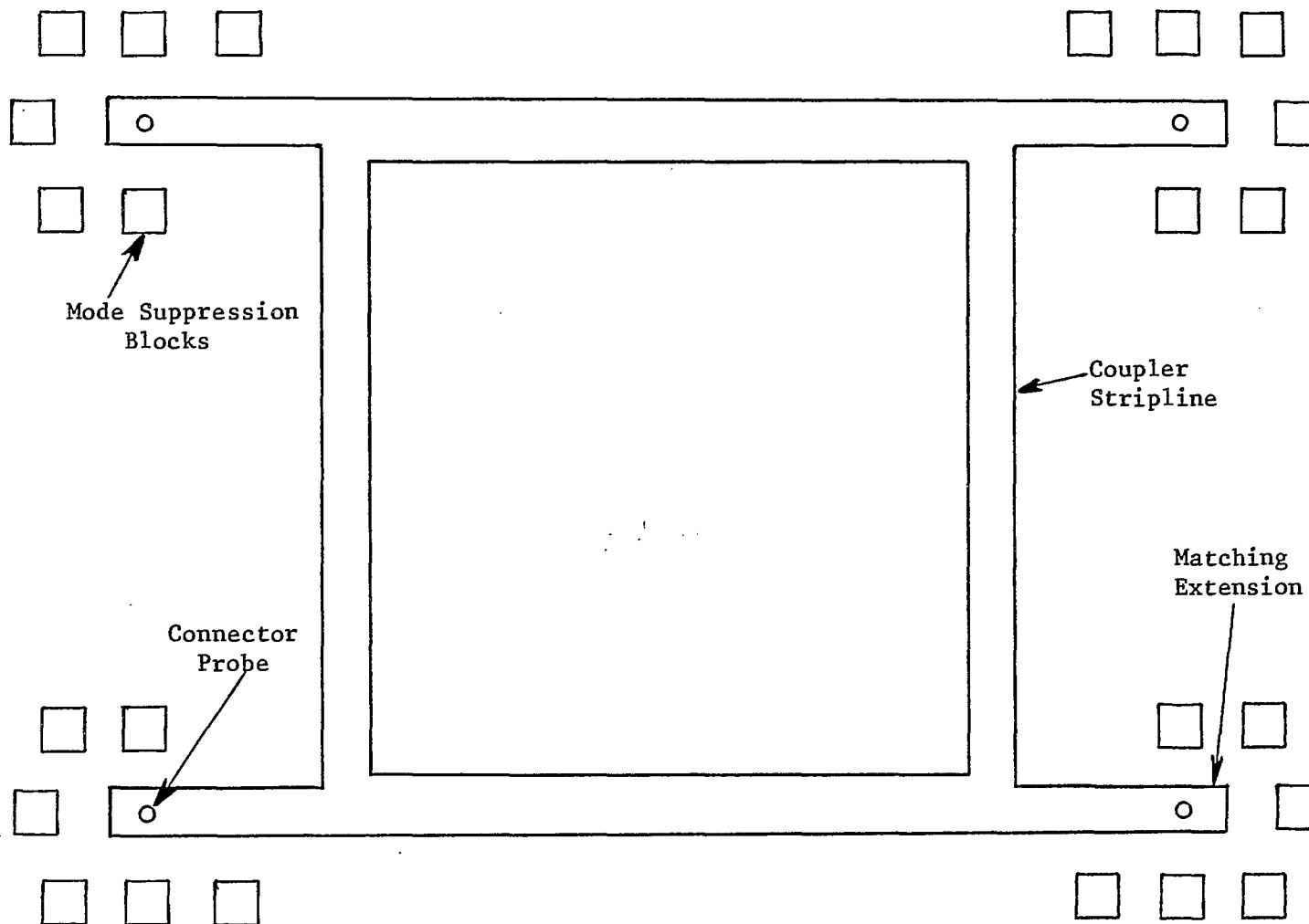


FIGURE 5.6: LAYOUT OF EXPERIMENTAL STRIPLINE COUPLER

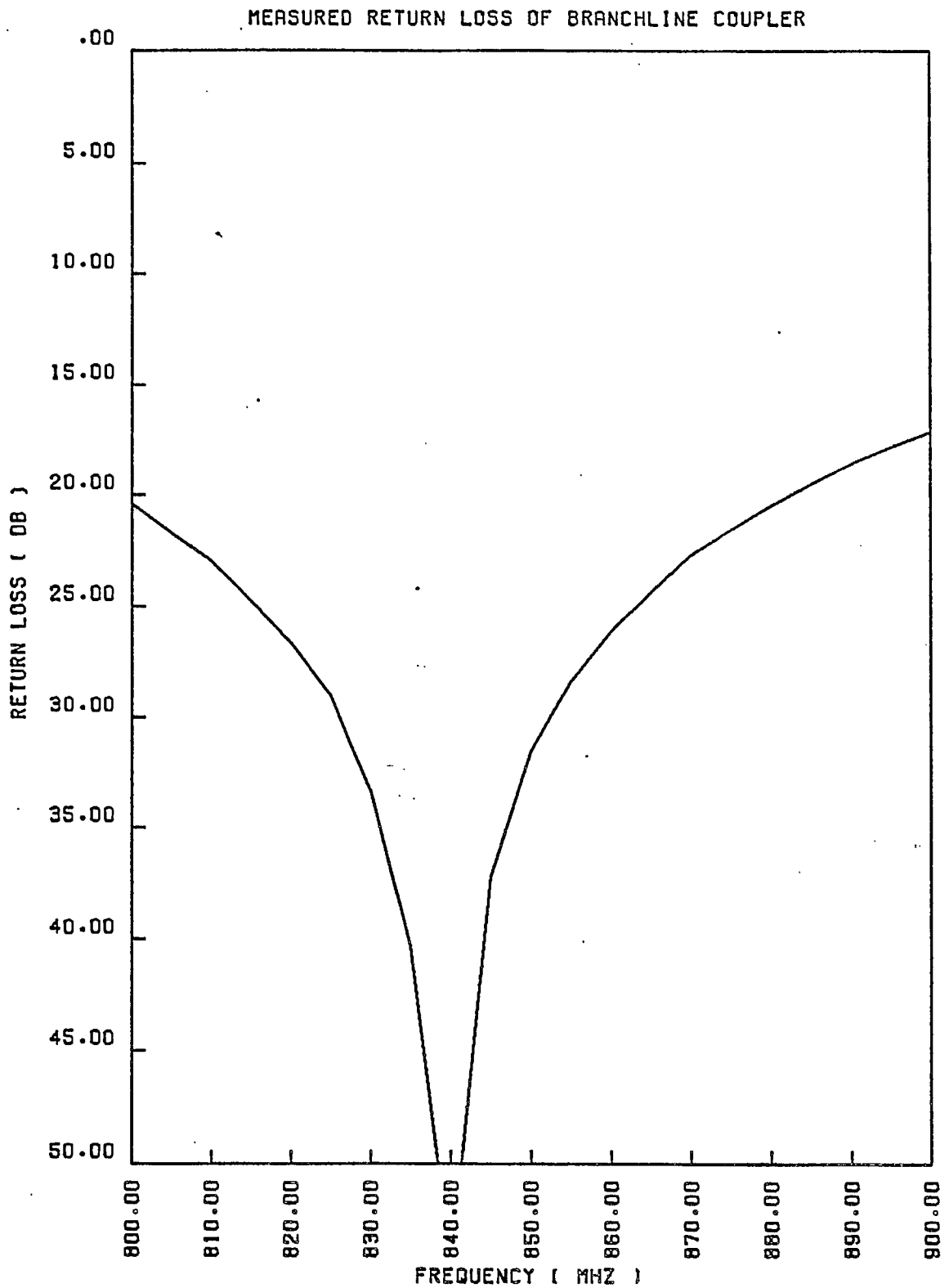


FIGURE 5.7: MEASURED RETURN LOSS OF STRIPLINE COUPLER

MEASURED ISOLATION OF BRANCHLINE COUPLER

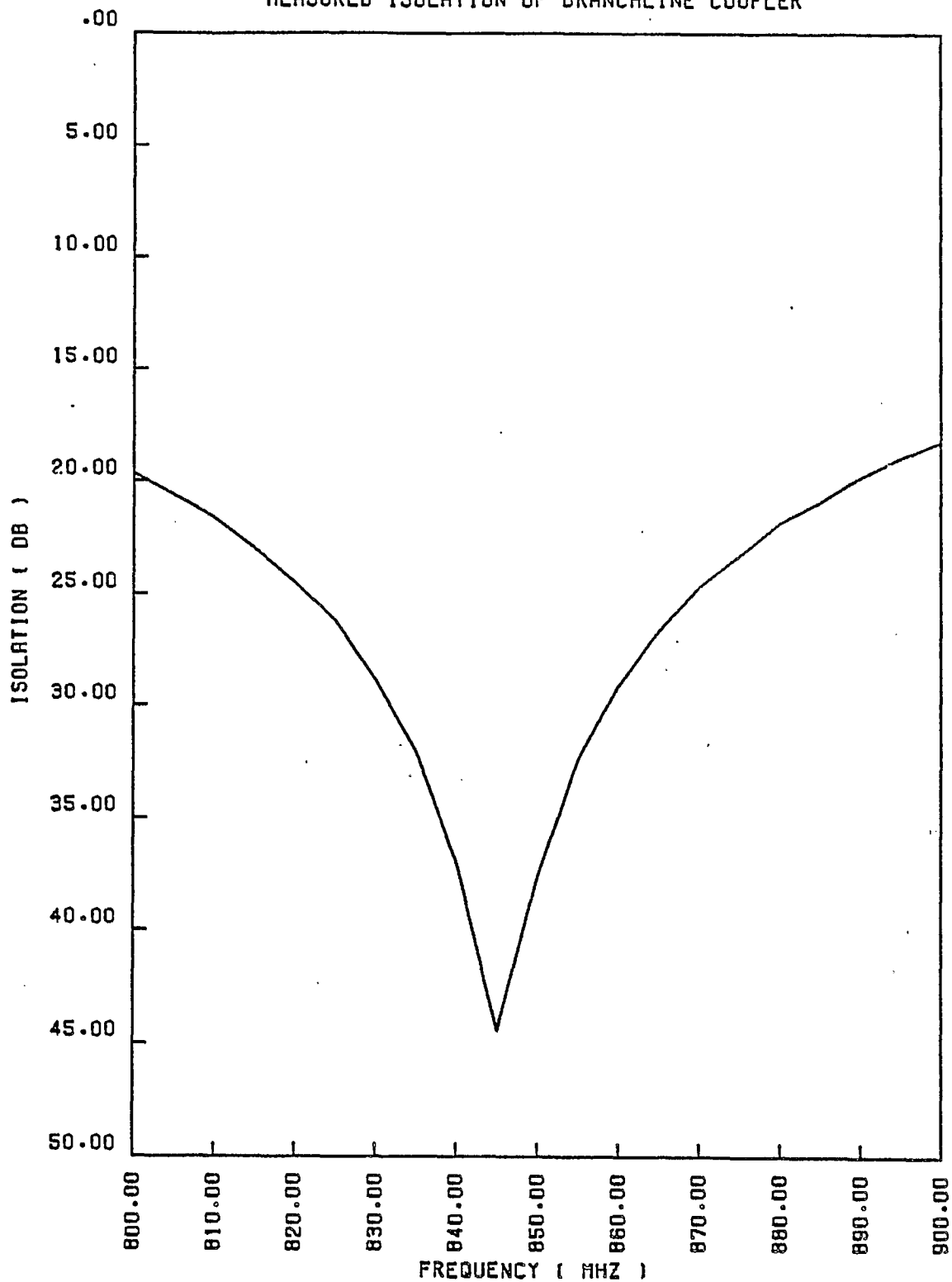


FIGURE 5.8: MEASURED ISOLATION OF STRIPLINE COUPLER

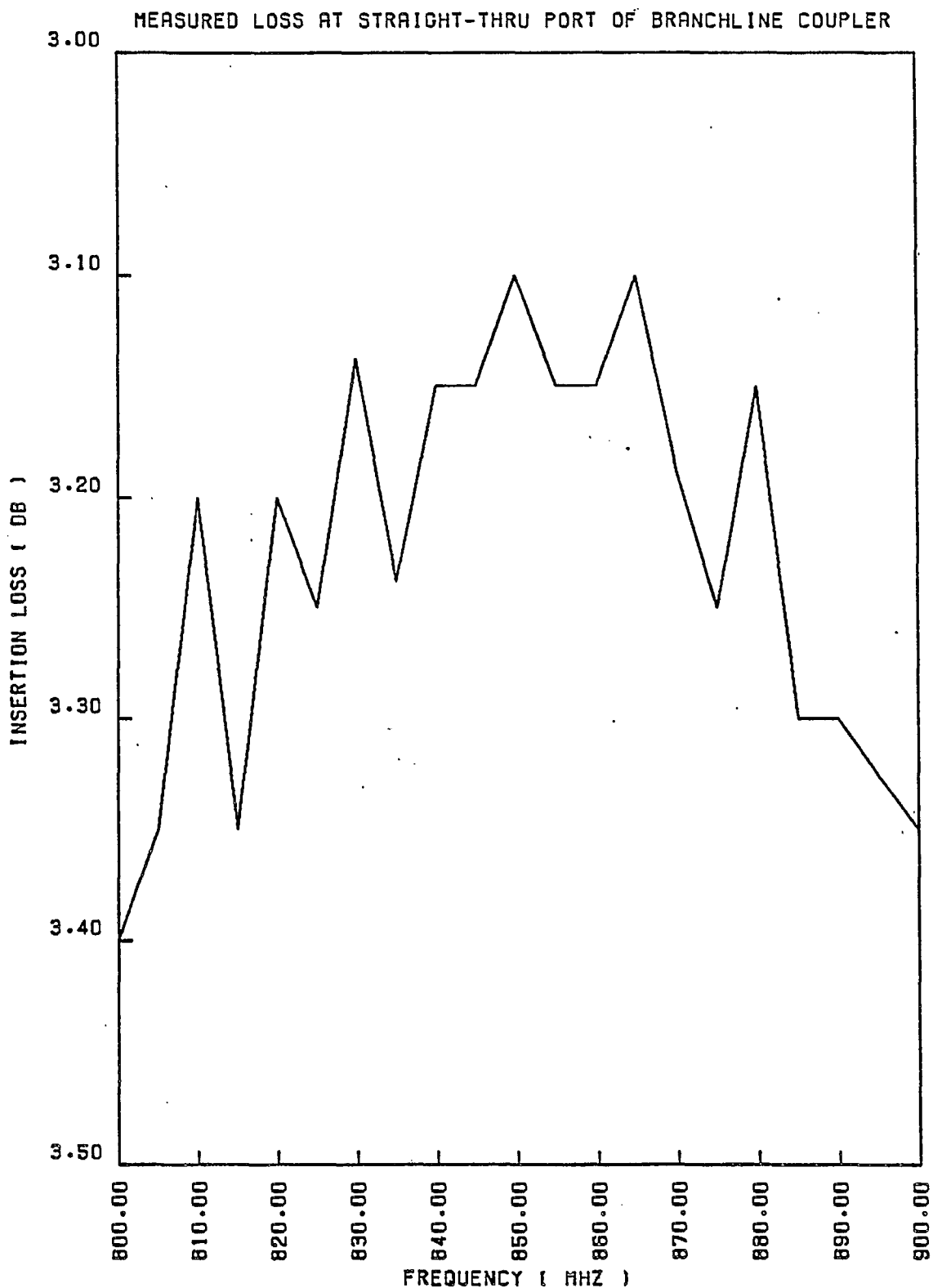


FIGURE 5.9: MEASURED STRAIGHT-THROUGH LOSS OF STRIPLINE COUPLER

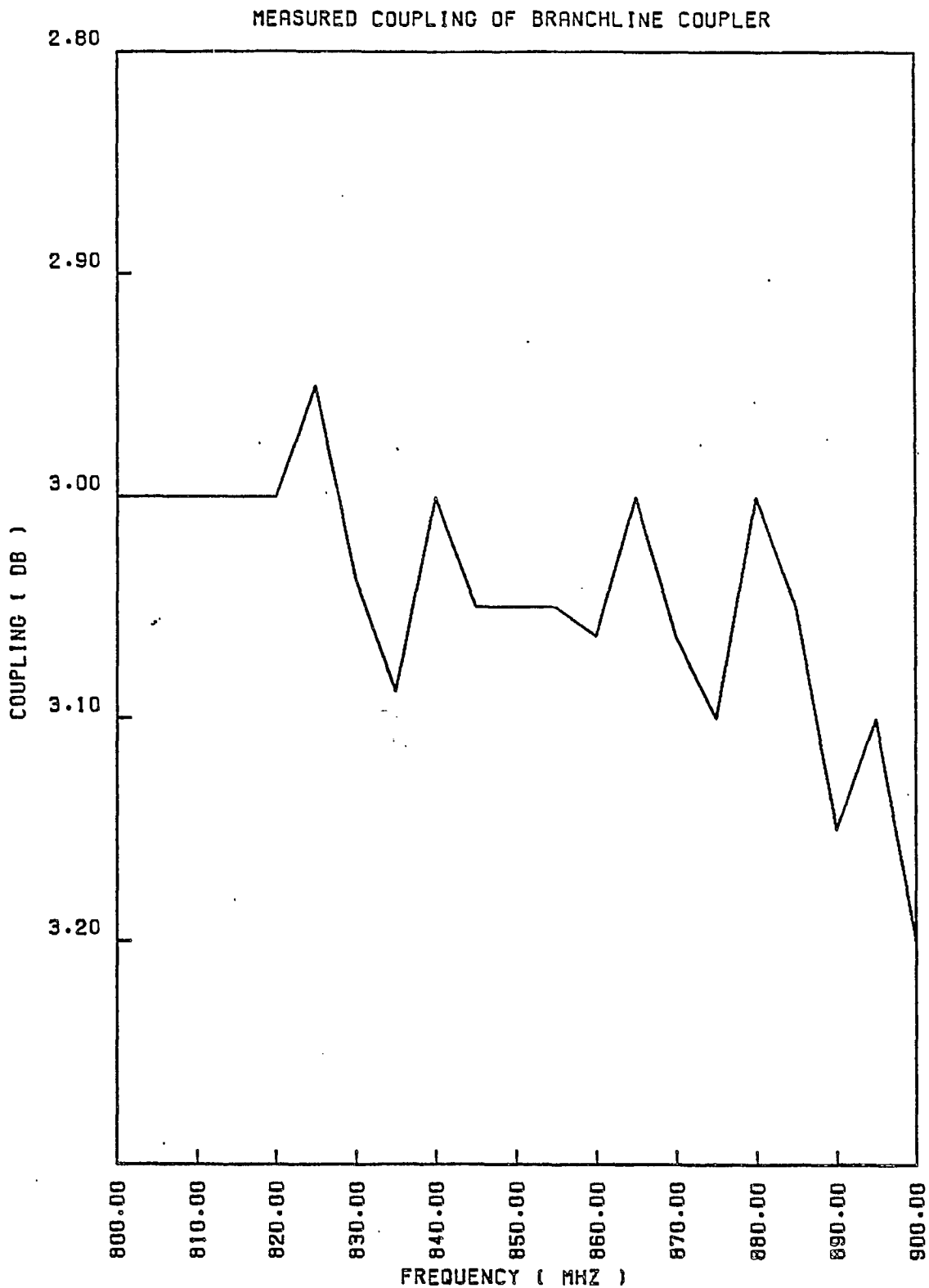


FIGURE 5.10: MEASURED COUPLING OF STRIPLINE COUPLER

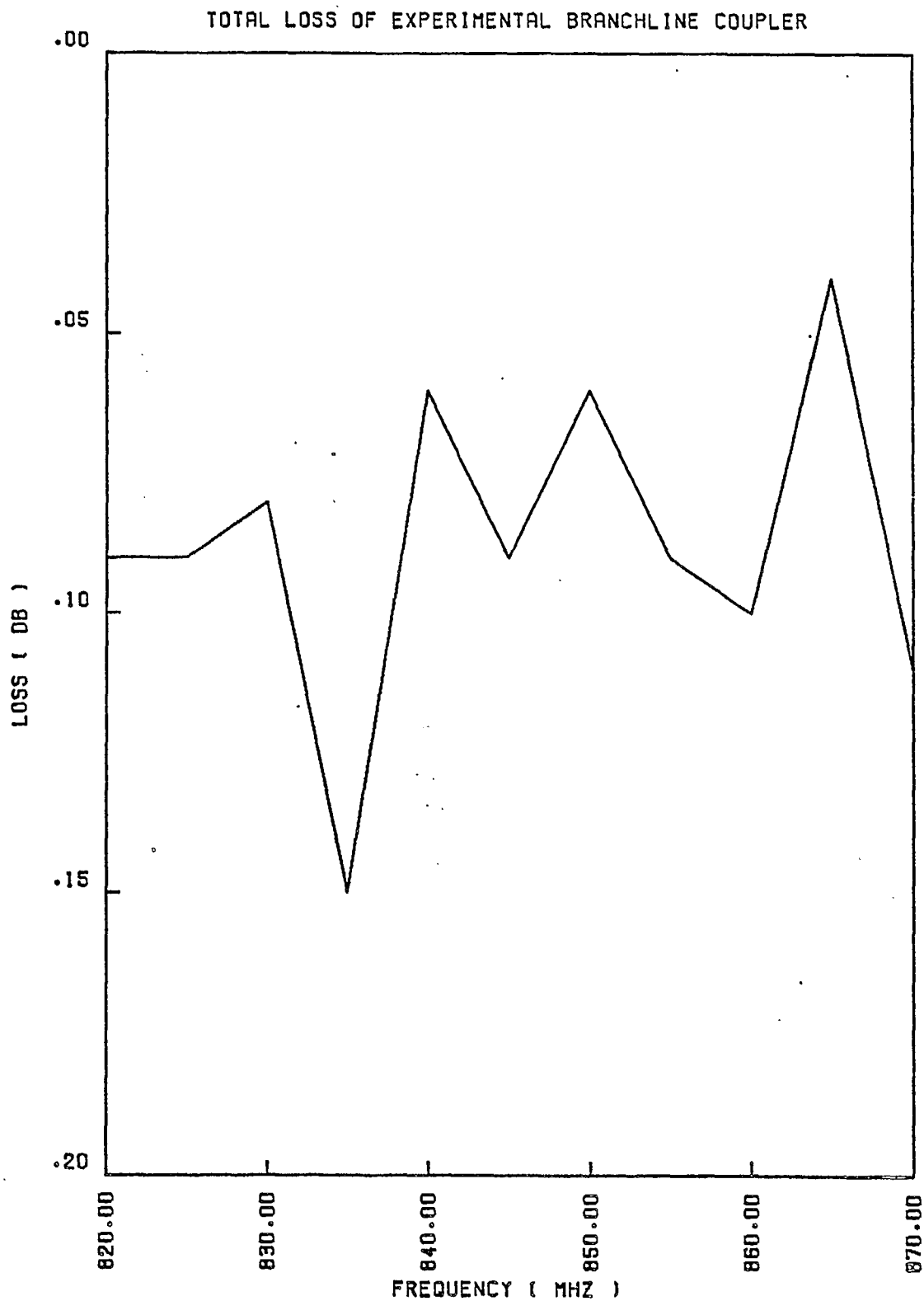


FIGURE 5.11: TOTAL LOSS OF EXPERIMENTAL STRIPLINE COUPLER

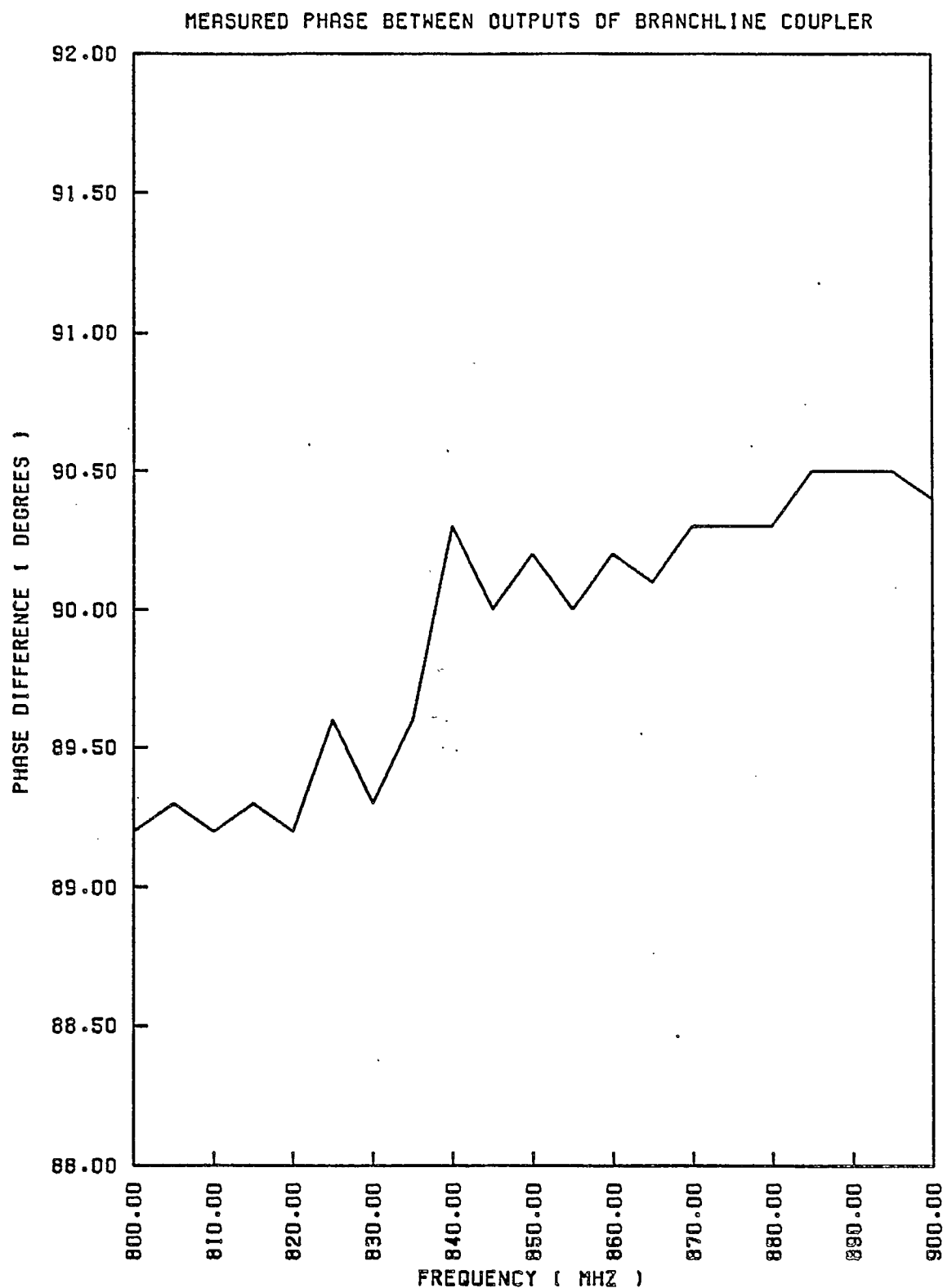


FIGURE 5.12: MEASURED PHASE ANGLE BETWEEN STRAIGHT-THROUGH AND COUPLED PORTS OF EXPERIMENTAL STRIPLINE COUPLER

6.0 MECHANICAL AND THERMAL DESIGN

6.1 Patch Element

The mechanical requirements on the patch elements are that they be flat to 0.01 in., be less than 0.06 in. thick, have facility for coupler probe electrical connection and be mounted with a dielectric material. To meet these requirements various options have been considered. An original concept considered was to use printed circuit board material with a copper layer forming the feed elements. However, this idea was not pursued due to the development time required to assess patches with dielectric material and the higher mass implications.

A second concept of using thin aluminum honeycomb panel was discarded due to complications of coupler probe attachment. However, the use of dielectric honeycomb panel (NOMEX) is considered feasible for future development with the patches etched on the upper and lower metal-clad dielectric faceskins.

A third option considered was to use 0.06 in. aluminum sheet weight relieved to leave 0.02 in. stiffening walls. This design allowed easier electrical connections but was considered to have too high a mass.

A fourth option utilized thin aluminum sheet of thickness 0.02 in. and 0.03 in. Calculated resonant frequencies were 226 Hz and 337 Hz for the 0.02 in. and 0.03 in. plates respectively. The value for the 0.02 in. plate was confirmed by testing, see Figure 6.1.

The resonant frequency of the 0.02 in. plate is considered to be acceptable and this option has been incorporated in the engineering model.

Electrical connections between the coupler and lower patch element are made by a combination of mechanical attachment (using a countersunk 0-80 flat head screw through the patch into the end of the coupler probe) and soldering.

The patch elements are mounted on five dielectric supports. Four of the supports are spaced in from the patch corners at locations that minimize deflection of the patch during vibration [5]. The fifth support is at the patch centre and has an aluminum charge leak tube over it which is soldered to the upper and lower patches.

The five dielectric supports pass through the complete antenna array assembly with spring washers on the antenna back face to provide preload and a pinned dielectric collar fixing at the upper patch.

The four corner dielectric supports extend beyond the upper patch to provide standoffs for the front face thermal blanket.

6.2

Mass and Envelope Estimate for Reflector Feeds

The actual measured mass of one module from a feed array is 632 g. This includes two stacked patches, a coupler, a simplified BFN and associated ground planes stiffening members and hardware. With the proposed method of interconnecting modules to form the array only half of the mass of the edge attachments is included per module.

The BFN included in the measured mass comprised two 3.2 in. lengths of stripline each terminated by a coaxial connector. The flight feed assembly will not have connectors for each antenna

patch but will have a heavier BFN. An additional mass (equal to twice the coupler mass) of 35 g will account for these differences. The front and rear face thermal blankets are estimated to weigh 24 g each per patch module.

This results in an overall module mass of 715 g.

It is envisaged that the actual feed array will have a 6 in. wide strip of ground plane around its perimeter in addition to that provided by each patch module. The mass per square foot of this extended ground plane is estimated to be 540 g. Since the ground planes at the coupler and BFN level are no longer electrically needed at the perimeter some weight relieving can be carried out without adversely effecting the mechanical stiffness.

For the 2-beam feed array the number of patch modules will be 10, see Figure 3.1. The required ground plane perimeter area is 7 ft.². Therefore the estimated 2 beam antenna feed mass is 10.9 kg.

With a 4-beam feed array the number of patch modules will be 21, see Figure 3.4, and the required ground plane perimeter area is 11 ft². Therefore the estimated 4 beam antenna feed mass is 20.9 kg.

The proposed thickness of both the 2-beam and 4-beam feed arrays including thermal blankets is 2.6 in.

6.3. Mass and Envelope for Array Antennas

A mass estimate for an array antenna can be projected from the mass of a reflector feed. Since an antenna patch module will be 12 in. x 12 in. instead of 12 in. x 10.4 in. the module mass will

be increased to 785 g. The antenna array will comprise 13 x 13 patches, see Figure 3.7, with a resultant mass of 132.7 kg.

The BFN will comprise 26 x 13 way power dividers in elevation plus 2 x 13 way power dividers in azimuth. There are 12 couplers in each 13 way power divider. Therefore the total number of couplers would be 336. The mass per coupler is 18 g giving a total mass of 6.05 kg. To approximate interconnecting stripline the mass can be doubled to 12.1 kg.

Since the BFN will occupy two layers, instead of one layer with the reflector feed, a ground plane on the rear antenna face has to be added. The ground plane would only cover approximately 20% of the antenna area and have a mass of 3.5 kg.

The antenna will have a ground plane extension of 6 in. around its perimeter which will result in an additional mass of 11.3 kg.

Therefore the total mass of an array antenna without stiffening or deployment structure is 160 kg.

The estimated antenna thickness including thermal blankets is 3.0 in.

6.4 Mechanical Design

The mechanical design objectives are to provide a light weight rigid structure which provides the required stripline and patch mounts with associated ground planes.

The mechanical design of the feed assembly is complicated by the electrical connections that are required between the patches, couplers and BFN. These connections are at different levels and

are separated by ground planes. As a consequence honeycomb panel was not considered practical except as a method of providing stiffening at the back face of the feed assembly.

The proposed mechanical design utilizes the three levels of ground planes as shear panels with stiffening walls and spacers coupling the panels together. With ground planes of 0.02 in. aluminum sheets the assembly forms a box structure which is rigid in both bending and torsion.

Since there will be no interconnections between patch modules at the coupler level the upper and lower coupler ground planes can be attached to an aluminum stiffening frame around the module perimeter. With the complete feed array this stiffening frame can form a continuous welded structure.

At the BFN level the stripline will be passing between modules and therefore separate ground plane spacers are used. This will allow for the removal of certain spacers to allow interconnection of the BFN.

Within the module perimeter spacers and stiffening frame the ground planes are rigidly coupled together via stripline charge leak pins, stripline mounts and the five dielectric patch mounts and spacers. These coupling points ensure the ground plane flatness is preserved and that the minimum resonant frequencies and associated deflections are acceptable [5].

Various methods of attachment of the 0.02 in. ground planes to the spacers, charge leak pins and stiffening walls have been considered. The use of TIG or torch welding caused the ground planes to distort and melt. A dip brazing process would be acceptable but would complicate the assembly process. The method

adopted for the engineering model involves the use of 0-80 flat head screws set in countersunk holes. This ensures an uninterrupted smooth ground plane on the side of the bolt head. Further development would incorporate a combination of dip brazing and mechanical fixing methods.

Stripline in the coupler and BFN are held by machined dielectric blocks. The blocks are mounted onto the ground planes using 0-80 screws. The screws are countersunk into the ground planes and pass through holes at the ends of the dielectric blocks, to tap into small aluminum pieces, see Figure 6.2. Two of the coupler mounts utilize two of the dielectric patch supports that pass through the antenna assembly. The stripline mounts also provide additional stiffening between the ground planes.

Stiffening of the antenna back face can be provided by cross braces of weight relieved aluminum sections or by honeycomb panel. The first option would entail attachment of aluminum beam sections to the back ground plane either with 0-80 countersunk screws or by dip brazing. The advantage of this method is that the BFN mounts, mode suppression pins and ground plane spacers are easy to attach with socket head 0-80 screws from the back face of the antenna ground plane. This method has been adopted for the engineering model with a typical machined cross brace. The option with the honeycomb panel would have the advantage of providing a very rigid continuous antenna back face requiring little additional support structure. One face skin would provide the BFN stripline lower ground plane. A disadvantage would be the increased complication of providing inserts at the stripline mounts mode suppression pins and ground plane spacers to allow for their attachment.

The primary requirement of the thermal control method adopted is to minimize the temperature extremes experienced by the antenna during periods of maximum solar exposure and eclipse conditions.

The proposed method of thermal control comprises a covering of quartz cloth on the antenna front face and a multilayer insulation (MLI) blanket the antenna rear face.

Coverage of the front face of the antenna poses a problem of conflicting requirements to avoid static discharge and to provide an RF transparent surface. The use of mylar or kapton layers with no metallization can result in detrimental static discharge through and between the layers [4, 35]. The static discharge problem is not reduced by etching aluminum squares in the insulation layers since any metallic edges enhances static build up.

A possible solution to provide an RF transparent thermal insulation layer which does not promote static discharge is to select a woven non-electrically conductive material. The process of weaving fibres tends to hinder the propagation of static discharge reducing it to non-detrimental levels. Possible materials are Astro Quartz cloth and Beta cloth.

Quartz cloth has been used extensively on antenna and other space thermal insulation applications. The surface finish has a low solar absorbance (0.2) and high infrared emittance (0.8). This allows the quartz cloth to run cool during conditions of solar illumination.

Without the restriction of RF transparency the antenna rear face can be covered by a conventional MLI blanket. The proposed blanket comprises 0.002" singly aluminized Kapton outer layer which is black painted with 9 inner layers of 0.00025" doubly aluminized mylar. All blanket layers will be electrically grounded via aluminum foil strips to avoid static build up. The layers of mylar will be crinkled so that they only touch at discrete points rather than over the entire surface. This reduces the amount of heat that can be conducted between layers.

Radiative coupling with the quartz blanket will be minimized by the low emittance surface finishes of the antenna comprising chemical film on the ground plane and silver plated patches. This will ensure that temperature extremes experienced by the blanket are not transmitted to the antenna. Preliminary thermal modelling has considered an antenna feed in both hot and cold orbital conditions.

The hottest orbital condition is with a winter solstice sun (1420 W/m^2) normal to the high absorbance black painted MLI blanket. The resultant mean antenna temperature in this condition is 35°C .

The coldest condition occurs during equinox eclipse. Just prior to eclipse the antenna will be solar illuminated (1329 W/m^2). A worst case condition of a solar vector 66° to the normal of the antenna incident on the low absorbance quartz blanket face has been assumed. The average antenna temperature in this condition is -80°C . The rate of temperature decrease during eclipse is dependent on the antenna thermal capacity. The eclipse condition is considered to last approximately 72 minutes. At the end of this period the average antenna temperature will decrease by 10°C to -90°C . Therefore the resultant expected maximum antenna temperature variation is 125°C .

It has been identified that thermal dissipation will occur in the patches. With 1 W dissipation per patch module the resultant maximum and minimum antenna temperatures are modified to 50°C and -50°C respectively giving an antenna temperature variation of 100°C.

Therefore the worst case operating temperature range is 50°C hot case with patch dissipation to a minimum power cold eclipse case temperature of -90°C. This gives a maximum antenna temperature range of 140°C.

Dissipation in the patches will be transferred by a combination of radiation to the quartz blanket, radiation to the ground plane and conduction. The upper and lower patches are conductively coupled together via the central charge leak pin. The lower patch has conductive links at the coupler connections. However, it may be advantageous to continue the charge leak pin to couple the lower patch to the ground plane. Also a thermally conductive dielectric material for the spacers between patches and between the lower patch and the ground plane could be used.

Additional dissipation will occur in the stripline couplers. The maximum dissipation occurs at the BFN input coupler which has an input of approximately 100 W. With a loss of 0.1 dB the coupler dissipation would be 2.3 W. Since the coupler is conductively isolated at the dielectric mounts and has low radiative coupling with the ground planes the primary heat flow path will be through the connectors. The anticipated temperature rise of the coupler above the ground planes is 35°C giving a maximum coupler temperature of 85°C. This is assuming adequate heat sinking at the input connectors. Without this heat sinking the remaining

couplers present a critical thermal problem. The circularly polarized coupler for the central patch of a 2-beam antenna septet has 52 W input for primary polarization and an additional 8 W for the other polarization. The resultant dissipation at 0.1 dB loss is 1.4 W. In order to maintain an acceptable temperature rise of the coupler above the ground planes conductive links between the couplers and ground planes will be required. These links could take the form of shorted quarter wave stubs as illustrated in Figure 6.3. The ends of the stubs would be connected via pins to the ground planes. With 1.4 W dissipation in a coupler and four stubs the approximate coupler temperature rise above the ground planes would be 40°C.

Additional heat sinking of the patches could be provided by using a material with high thermal conductivity such as Boron Nitride to electrically insulate the stripline probes from the ground planes. The Boron Nitride grommets could be bonded in place with thermally conductive epoxy to provide a heat path from the stripline to the ground planes.

To allow the ground planes to radiate the power absorbed from the stripline they should have a surface finish which provides an emittance of 0.2 or better. Possible surface finishes are chemical film or clear anodize.

The selection of materials for support of stripline and patches presented the problem of requiring a dielectric material that was usable at low temperatures. The required electrical properties are that the material have a dielectric constant of 2-3 and have a loss tangent at 800 MHz of no greater than 0.005 over the required temperature range. Mechanically the material should be tough at low temperatures (typically -100°C), be resistant to ultra violet radiation, meet the required outgassing specification and be easily machined.

A material that meets the electrical requirements is rexolite. However, its mechanical properties at low temperatures and resistance to ultra violet radiation are not clear at this stage. Rexolite has been selected for stripline supports in the engineering model due to its acceptable dielectric properties. When considering problems of multipaction it is envisaged that the stripline will be required to be surrounded by a low dielectric constant material. A favourable material for this application is the all-silica insulation material used on the space shuttle.

Due to the required tensile loading of the dielectric patch mounting rods rexolite was not considered acceptable. A glass reinforced resin (G10) has been used for this application on the engineering model. For a flight model a resin selection will be required for low temperature use. The glass fibres ensure that mechanical strength is maintained under tensile loading.

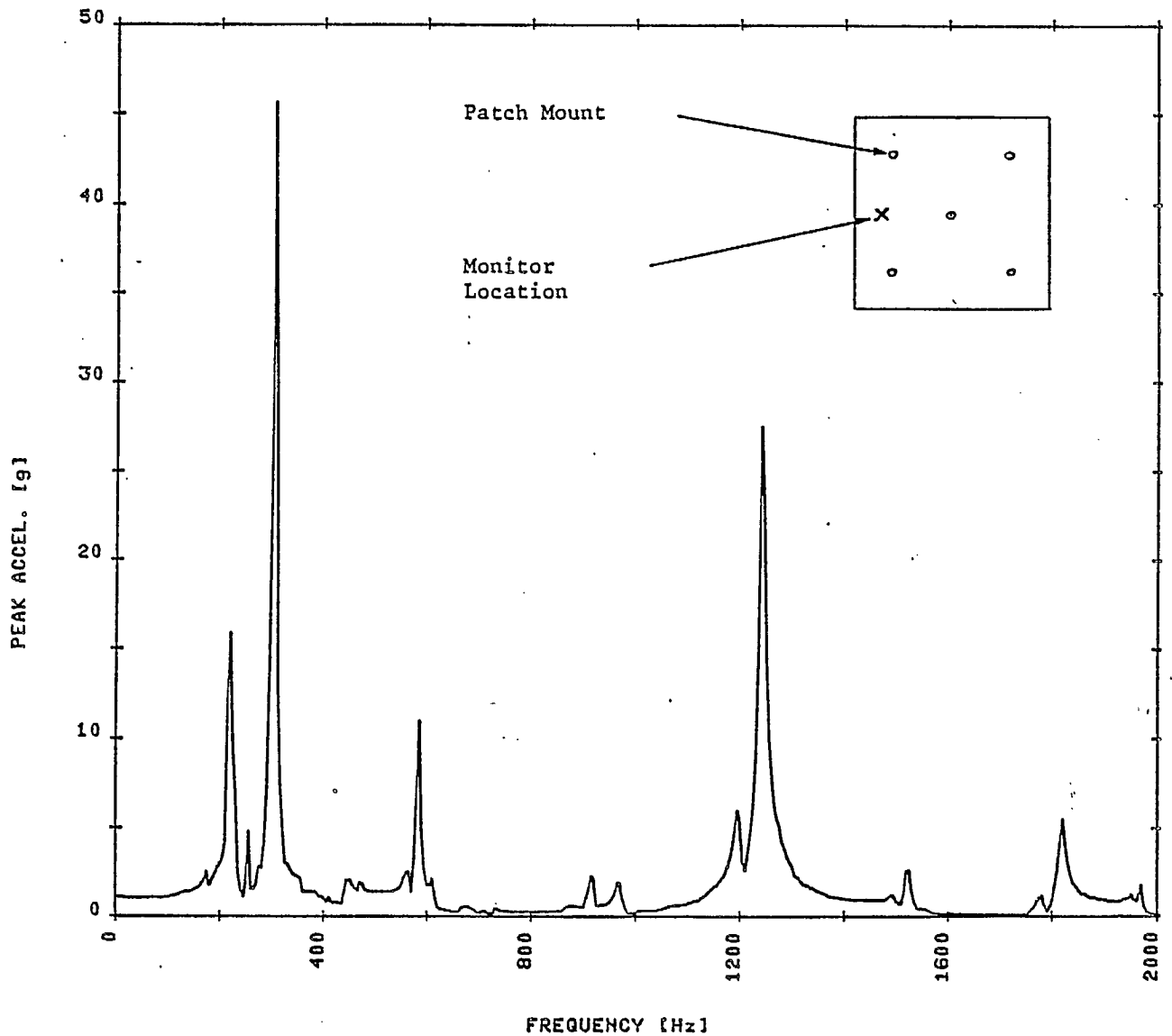
Aluminum sheet of thickness 0.02 in. has been selected for the ground planes and patches. To avoid distortion over temperature the aluminum will be stress relieved.



10/06/86

SINE VIBRATION TEST

COM DEV LTD



LOW LEVEL SINE INITIAL M-SAT PATCH ANT.(20 THOU) SWEEP RATE 2 octaves/min
 Z AXIS S/N XXXXXX
 P/N XXXXX
 OPERATOR 90 MONITOR 2
 FLAT WEIGHING

FIGURE 6.1: 0.02 IN PATCH VIBRATION PLOT ONE g INPUT

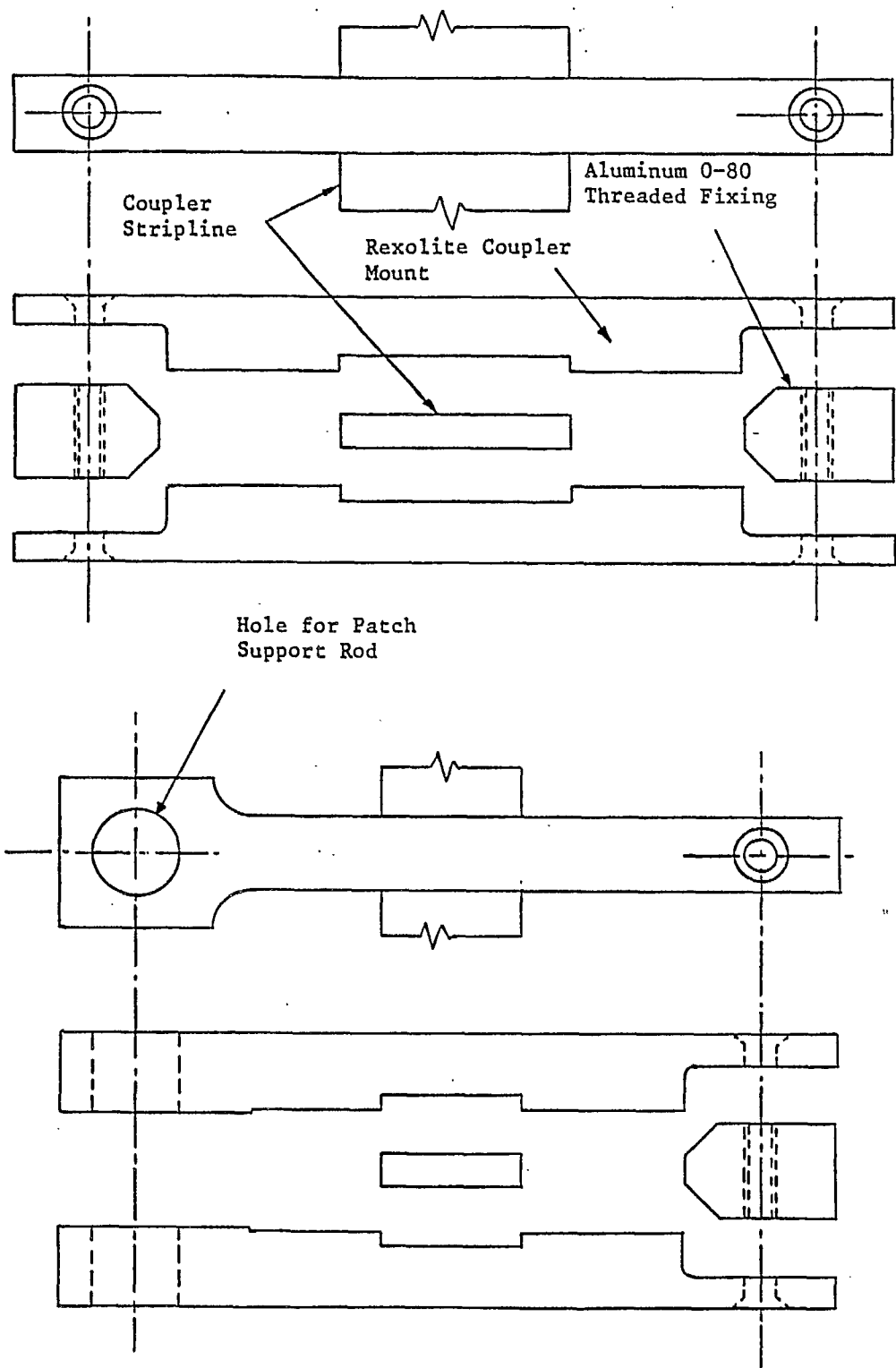


FIGURE 6.2: STRIPLINE DIELECTRIC SUPPORTS

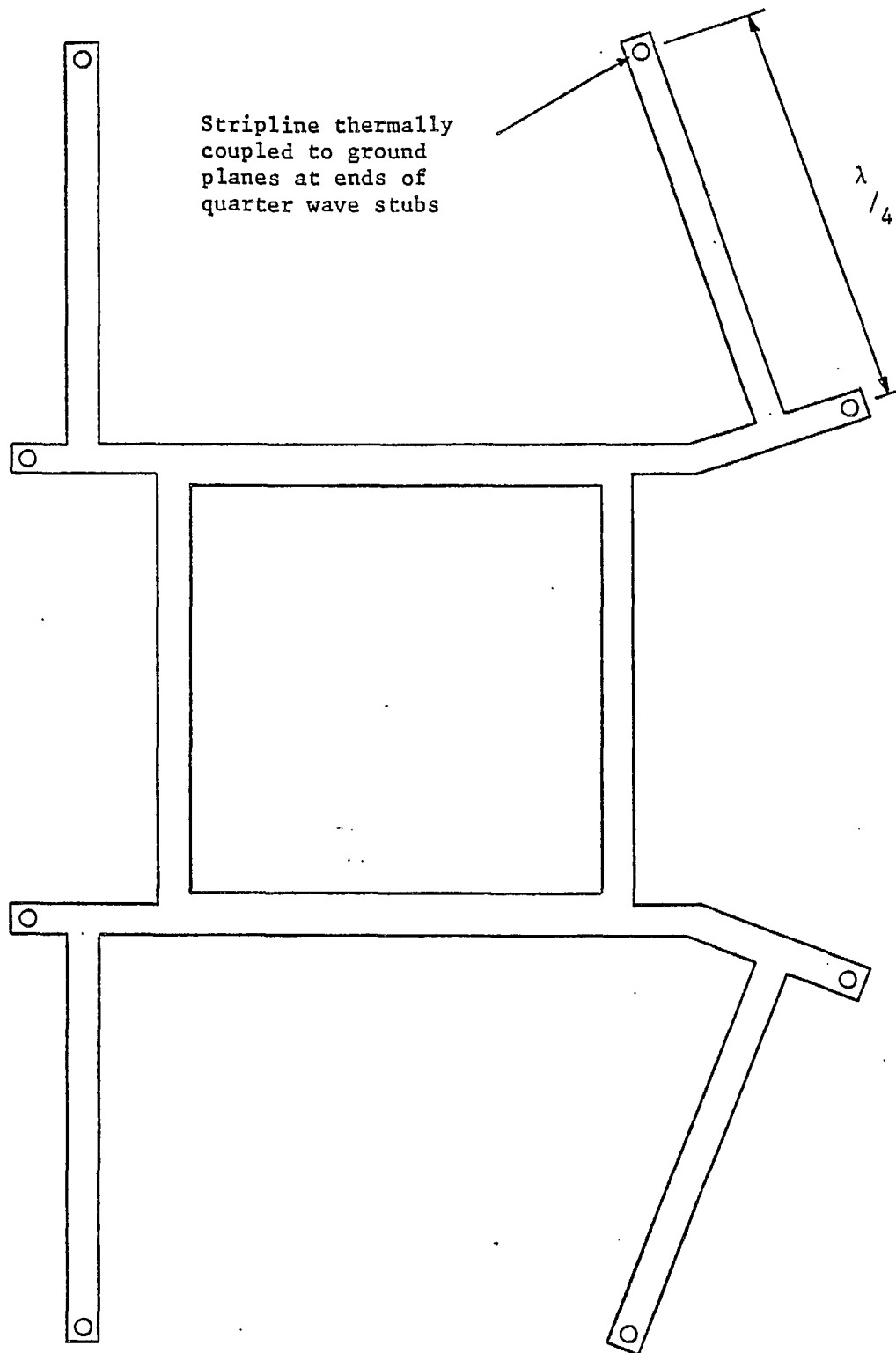


FIGURE 6.3: SHORTED QUARTER WAVE STUB HEAT SINK

7.0 DESCRIPTION OF ENGINEERING MODEL

7.1 Construction

An engineering model antenna was designed and fabricated to be representative of a single stacked patch element that could make up part of the flight version of an array. This model includes a stacked patch radiator fed from a stripline coupler, making up a module that could be repeated across the array. Also included is an additional layer representing a portion of a beam-forming network fabricated with the antenna array in an integrated panel. An exploded view of the engineering model is illustrated in Figure 7.1.

The upper and lower patch elements are 0.02 in. thick silver plated aluminum sheet, 5.72 inches and 6.65 inches square respectively. They are mounted using five glass fibre rods. The rods have a head at one end and pass through the antenna assembly from the back face. An insulated stainless steel spring washer between the head of each rod and the antenna rear ground plane stiffening structure ensure positive location of the patches over temperature. The rods pass through the patches with four near the corners and one at the centre. Each rod is secured above the upper patch using a glass fibre collar with an aluminum pin pushed through a hole in the collar and dielectric rod. To maintain the required spacing between patches and ground planes the support pins pass through glass fibre tubes. At the centre location between the two patches the support pin passes through an aluminum tube which is bonded with a silver loaded epoxy to the upper and lower patches. This provides a charge leak and a thermally conductive coupling between patches.



The structure of the engineering model comprises three ground plane layers of 0.02 in. aluminum sheet of dimensions 12 in. x 10.4 in. spaced apart by an aluminum frame at the coupler level and individual spacers at the BFN layer. The ground planes and spacers have chemical film finish.

Two probes connected to the lower patch pass through holes in the upper ground plane to be attached to the coupler below. Electrical connection to the patch is made by a combination of a 0-80 screw tapped into the end of the probe and solder. The probes are attached to the coupler by TIG welding. The two probes between the coupler and BFN pass through the middle ground plane and are soldered to the coupler and TIG welded to the BFN stripline. Where the probes pass through the ground planes electrical insulation is provided by RTV grommets. The BFN and coupler striplines with their welded probes are silver plated as separate assemblies.

The coupler is machined from a sheet of aluminum and has thickness of 0.062 in. The arms that carry the patch probes are angled through 20° to accommodate the patch attachment locations.

The BFN layer is represented by two 3.2 in. lengths of stripline machined from aluminum sheet to a thickness of 0.062 in.

Each probe connection has six or seven aluminum mode suppression pins around it which are fastened between the ground planes with a 0-80 flat head screw at each end.

The coupler is held at four locations between an upper and lower machined rexolite block. At two of the locations the blocks are attached with 0-80 flat head screws at either end. The screws are countersunk into the ground planes and pass through the ends

of the blocks to tap into small aluminum blocks. The remaining two coupler mounts use a 0-80 screw at one end while the other end is held by a fibre glass patch mounting rod that passes through the antenna.

Each of the two BFN strips are held near their centre by rexolite blocks with 0-80 screws at either end.

The aluminum frame that connects the upper and middle ground planes together around their perimeter comprises four weight relieved lengths of aluminum which are TIG welded at the corners. Each side of the frame is machined to an "I" section with 0.03 in. web and 0.06 in. upper and lower flanges. The cross brace structure on the antenna back face is assembled from two machined "I" section lengths welded at their centre to form an 'X'. To ensure accuracy of the weld configuration both the frame and cross brace are welded while held in a machined aluminum jig.

The upper ground plane is bolted to the frame with 38 x 0-80 flat head screws which are countersunk into the ground plane, to provide a flush surface, and tapped into the frame. The middle and rear ground planes are secured with 38 x 0-80 socket head bolts. Each bolt passes through the rear ground planes, an aluminum spacer, the middle ground plane and taps into the rear side of the frame. The frame and the lower to middle ground plane spacers extend beyond the 12 in. x 10.4 in. ground plane perimeter to allow attachment of adjacent patch antenna modules.

Each of the BFN strips are terminated at a coaxial connector. The central conductor pin is soldered to the BFN strip. The connectors are mounted on aluminum stiffening plates bolted to the rear ground plane.

To allow for attachment of the rear thermal MLI blanket there are four glass fibre blanket support pins. After punching four holes in the blanket they will be pushed over the pins and secured with teflon washers. In order to hold the front thermal blanket clear of the patches four of the glass fibre rods extend well beyond the patches.

Figure 7.2 is a photograph of the engineering model during assembly with the layer of stripline representing the BFN exposed. In Figure 7.3 the middle ground plane has been added and the circular polarization producing coupler stripline is in place. Figure 7.4 includes the top ground plane. Figure 7.5 shows the completed antenna. Figures 7.6 and 7.7 show it mounted in an extended ground plane used for testing.

7.2

RF Performance

For all tests the engineering model antenna was mounted in the centre of a 24 inch square ground plane. Figures 7.8 and 7.9 show the return losses and isolations between input ports measured with input to Port 1 (LHCP) and Port 2 (RHCP) respectively. The data is summarized in Table 7.1. The differences in the two return loss curves appear to be caused by some residual asymmetry in the fabrication. The rather low isolation at the lower end of the frequency range is a combination of the coupler isolation level and the coupling between the feed probes of the antenna itself. The E- and H-plane radiation patterns for each input port at 823 MHz and 868 MHz are shown in Figure 7.10 through 7.13. These were measured with a linearly polarized source horn defining the plane of the E-vector. The beamwidths and squints are summarized in Table 7.2, along with measured axial ratios. The unexpectedly poor axial ratio can be largely attributed to the effect of the inter-probe coupling. The coupling level (about -20 dB at -90 degrees phase) is such as to add directly in phase to the

excitation of one linear polarization and to subtract from the other. Using this average value for the coupling an axial ratio contribution of 1.74 dB can be explained. In order to reduce the axial ratio to usable levels it is proposed that a coupler with unequal power split be used to counterbalance the effect of the coupling between the feed probes. From the return loss curves it appears that there is some residual asymmetry which may also contribute to the axial ratio. Teshirogi et al. [57] achieved 1 dB axial ratio over a good bandwidth using notches in the sides of two-feed patches. It is expected that a very considerable improvement can be achieved using one or more of these techniques. Also included in Table 7.2 are average values of gain, measured by comparison with a standard gain horn. The values of 9.0 - 10.0 dBi are in agreement with Pues and Van de Capelle's values for single patches [47].

TABLE 7.1: ENGINEERING MODEL RETURN LOSS AND
ISOLATION SUMMARY

	Return Loss (dB)		Isolation Between
	<u>Port 1</u>	<u>Port 2</u>	<u>CP Ports (dB)</u>
Without thermal allowance			
821-825 MHz	20.6	17.5	15.3
866-870 MHz	21.0	16.6	24.0
With thermal allowance			
819-827 MHz	20.4	17.4	15.0
864-872 MHz	20.2	16.4	23.7

TABLE 7.2: ENGINEERING MODEL PATTERN SUMMARY

	Beamwidth (degrees)		Axial Ratio (db)	Gain (db)
	<u>E-Plane</u>	<u>H-Plane</u>		
Port 1, 823 MHz	47	64	2.6	9.2
Port 1, 868 MHz	57	73	2.6	10.0
Port 2, 823 MHz	48	65	2.3	9.0
Port 2, 868 MHz	57	73	2.7	9.7

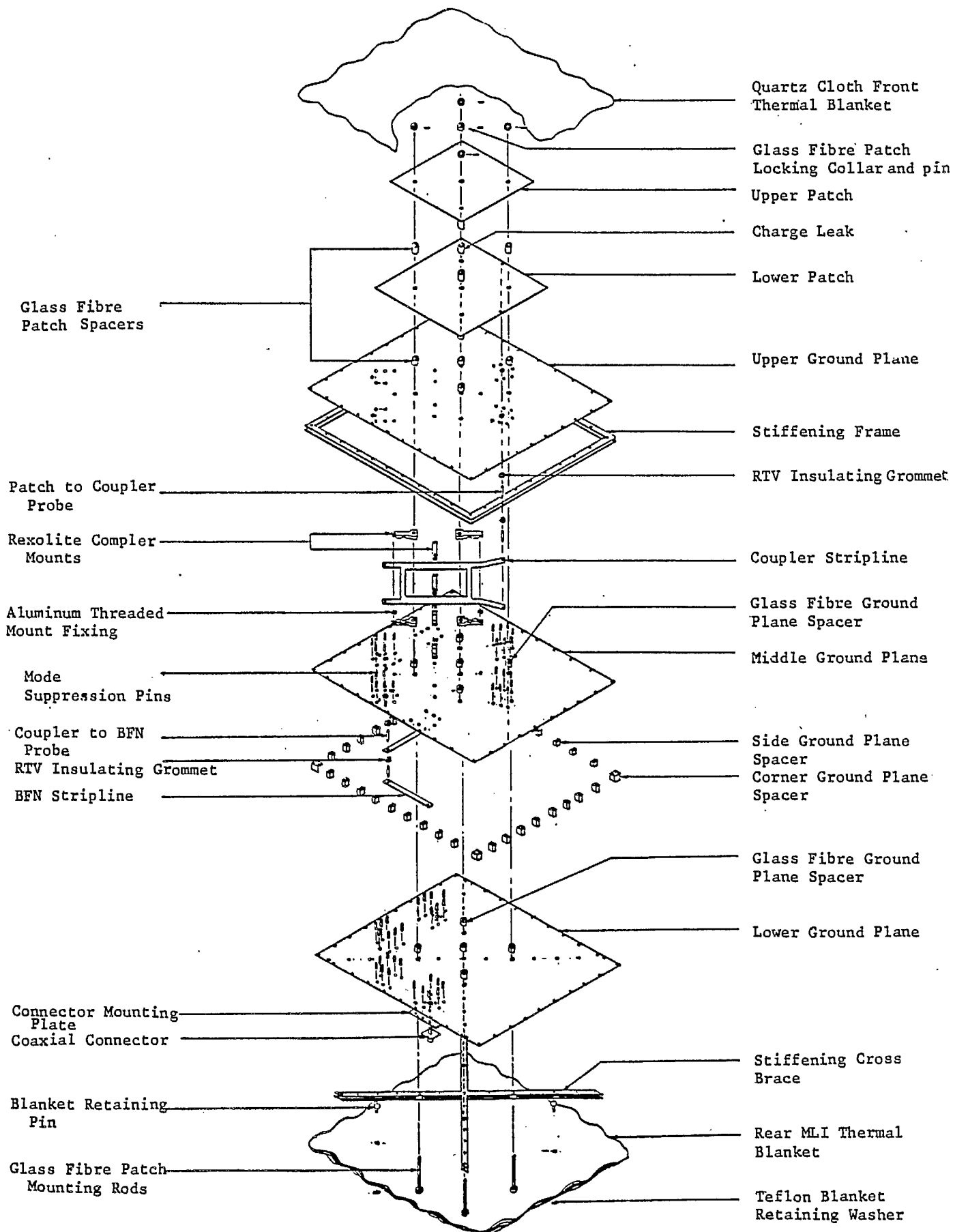


FIGURE 7.1: ENGINEERING MODEL
EXPLODED VIEW

© Her Majesty the Queen in Right of Canada (1986) as represented by the Minister of Supply And Services.

DOCUMENT No.	REV.	COM DEV
RPT/MST/2500/001	—	
		SHEET 132

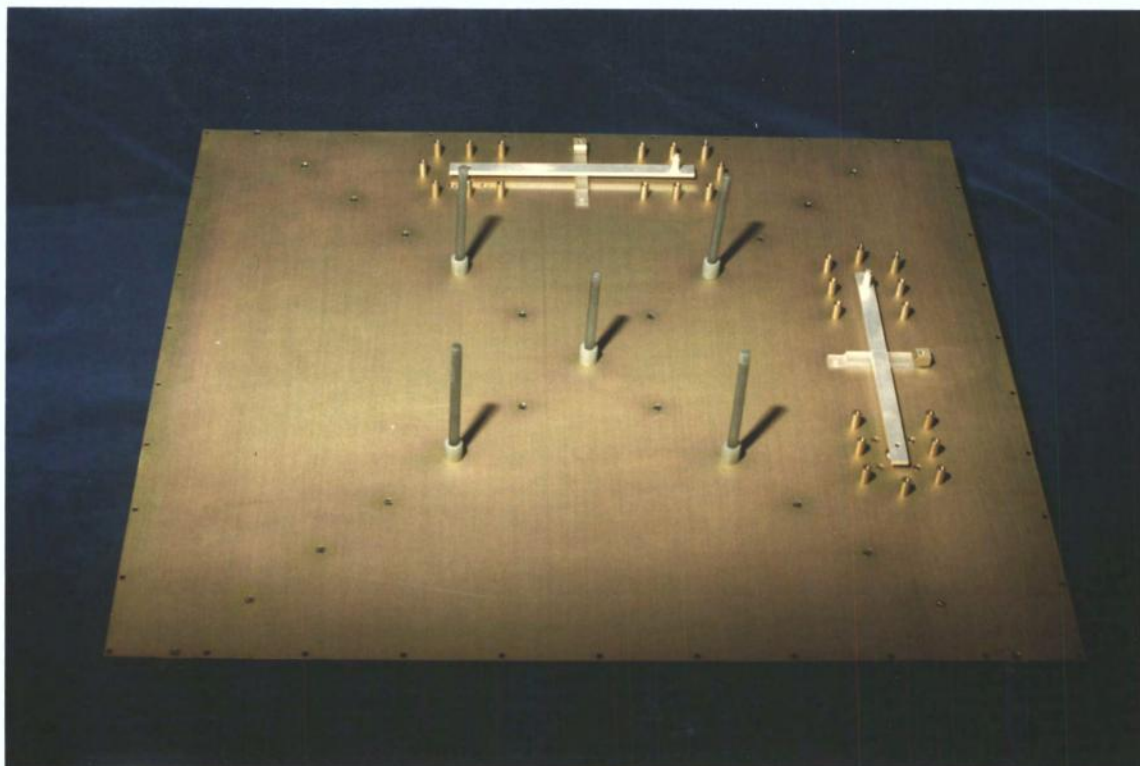


FIGURE 7.2: PHOTOGRAPH OF ENGINEERING MODEL DURING ASSEMBLY
SHOWING BFN LAYER

DOCUMENT No.

RPT/MST/2500/001

REV.

—



COM DEV

SHEET 133

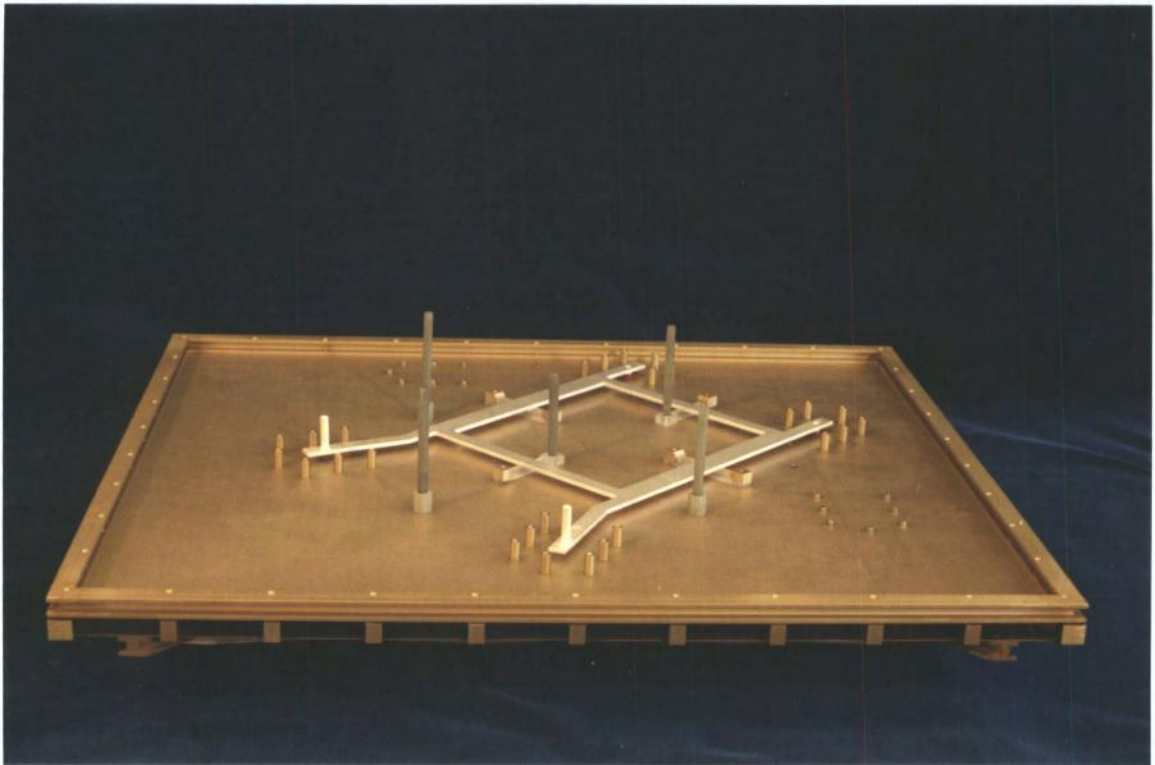


FIGURE 7.3: PHOTOGRAPH OF ENGINEERING MODEL DURING ASSEMBLY
SHOWING COUPLER LAYER

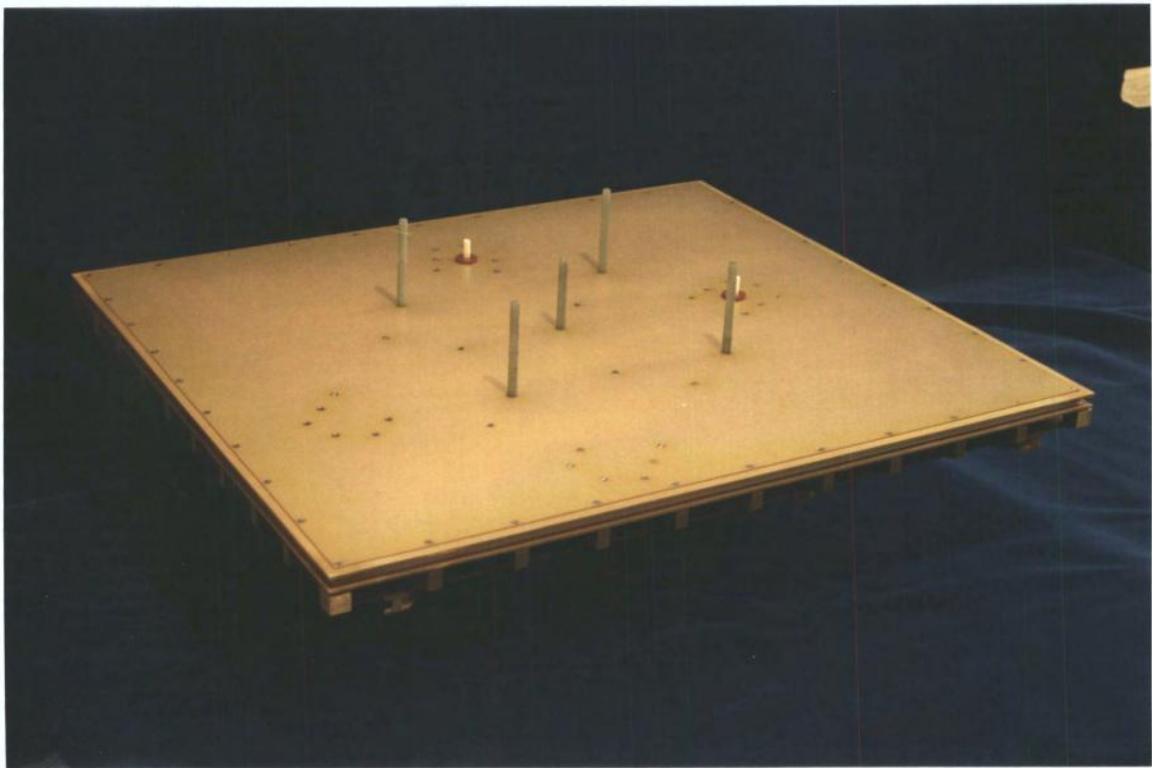


FIGURE 7.4: PHOTOGRAPH OF ENGINEERING MODEL BEFORE PATCH ASSEMBLY

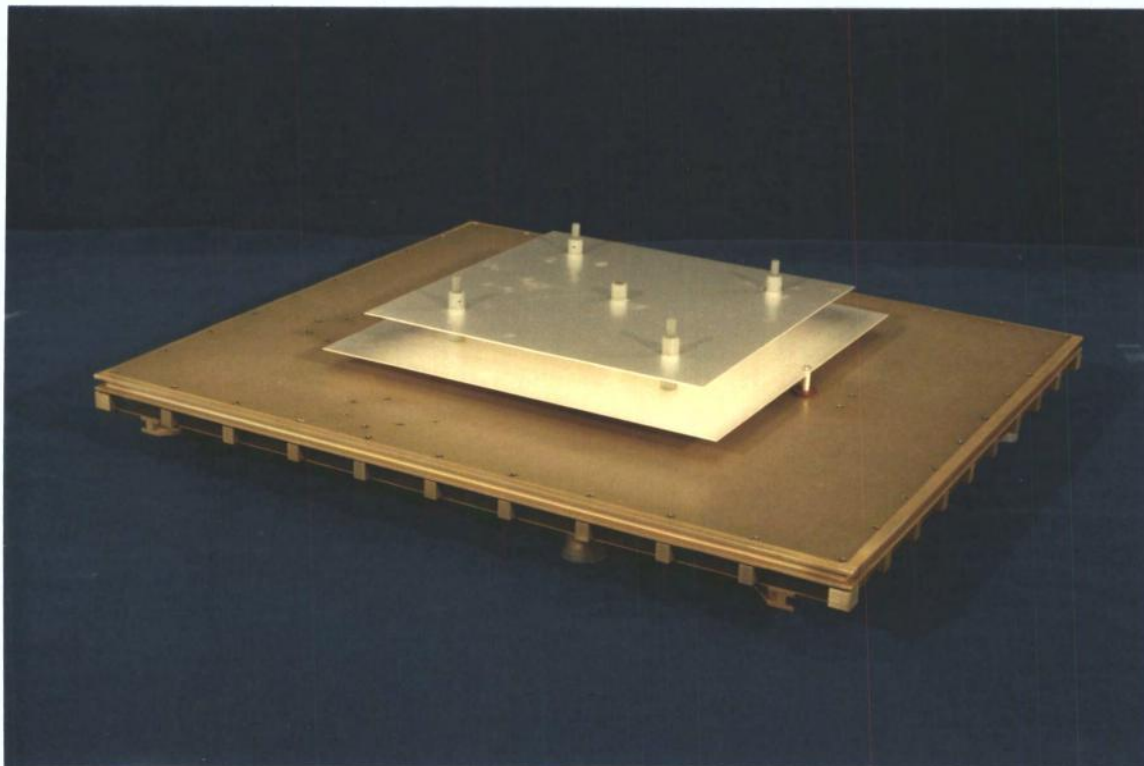


FIGURE 7.5: COMPLETED ENGINEERING MODEL

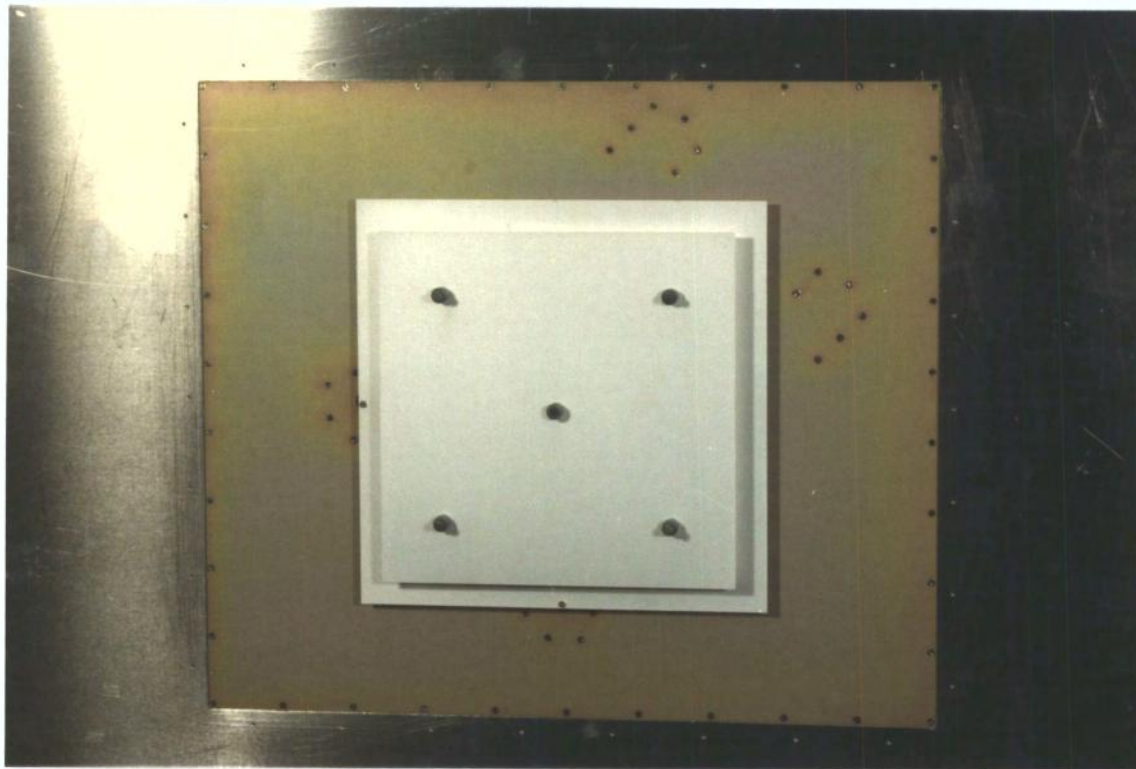


FIGURE 7.6: FRONT FACE OF COMPLETED ENGINEERING MODEL MOUNTED
IN GROUND PLANE EXTENSION

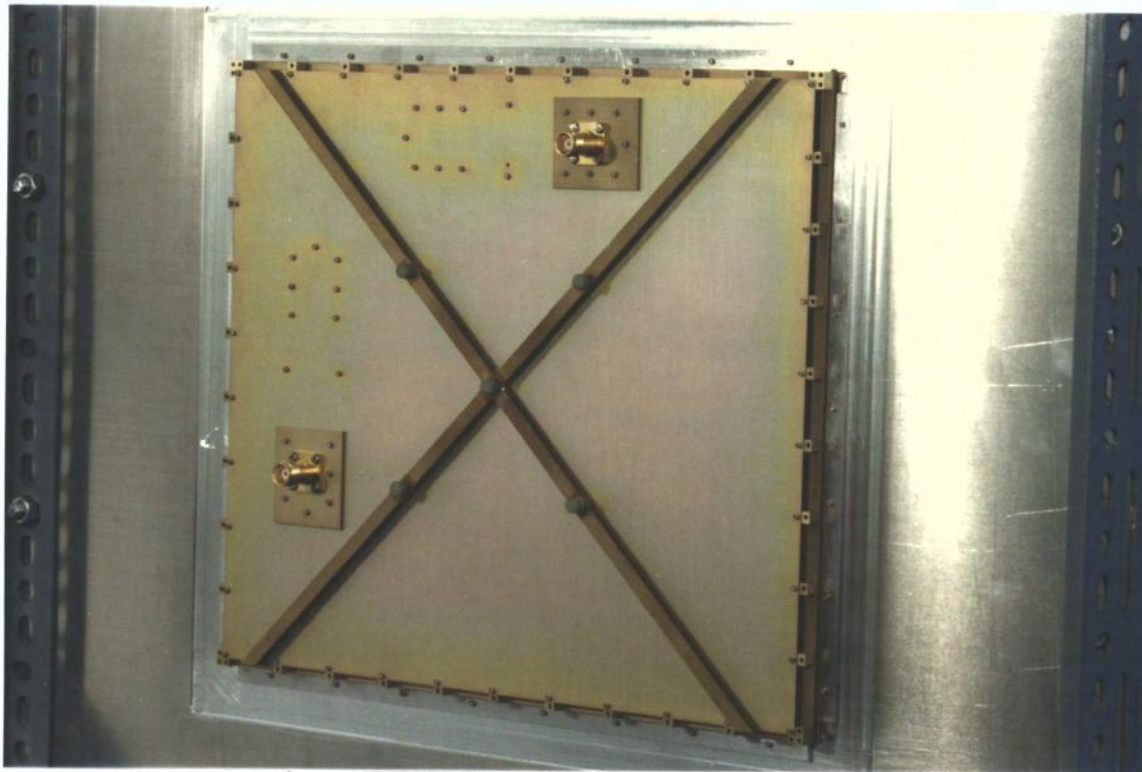


FIGURE 7.7: BACK FACE OF COMPLETED ENGINEERING MODEL MOUNTED
IN GROUND PLANE EXTENSION

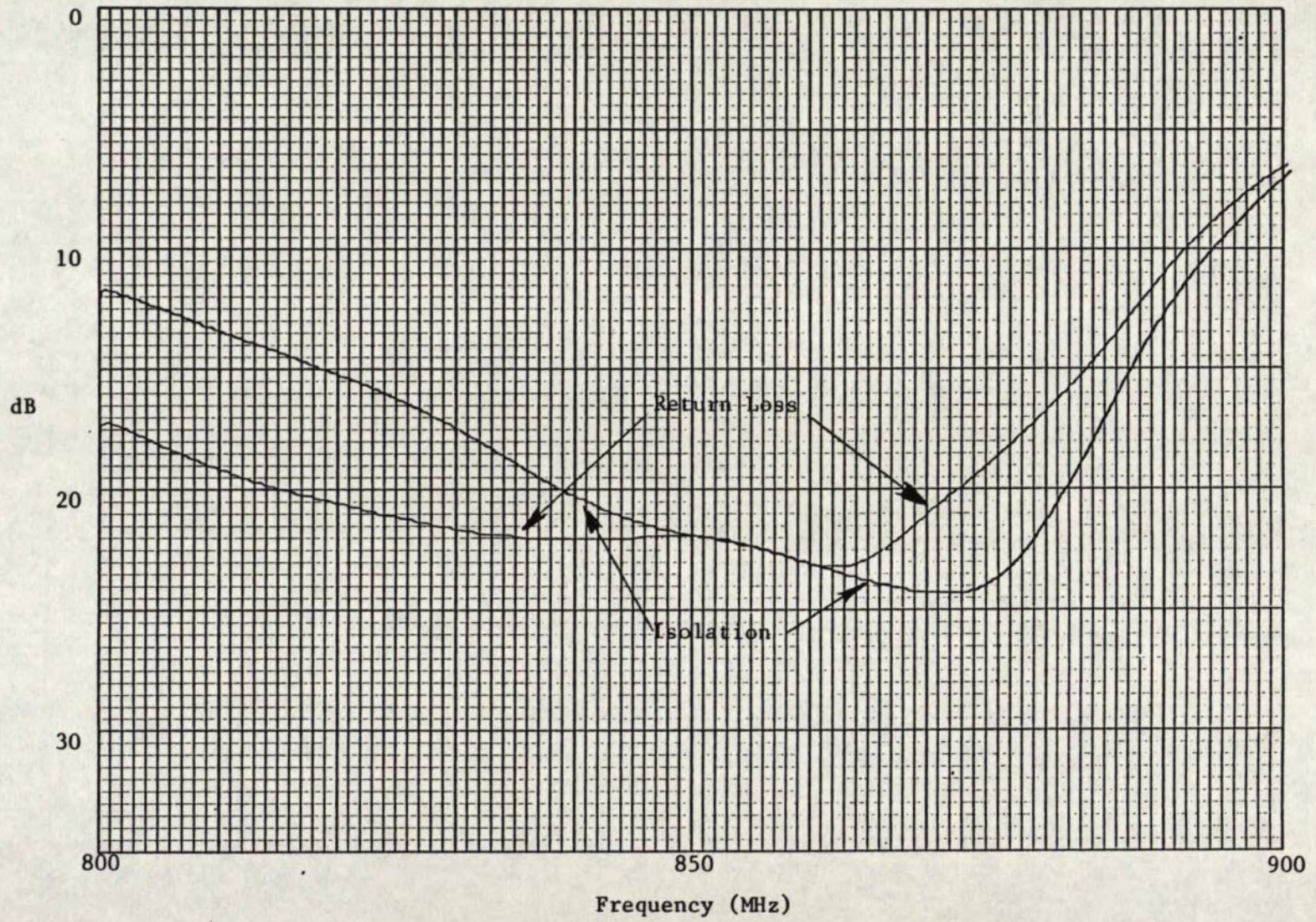


FIGURE 7.8: RETURN LOSS AND ISOLATION OF ENGINEERING MODEL ELEMENT
(INPUT TO PORT 1)

DOCUMENT NO.

REV.

RPT/MST/2500/001

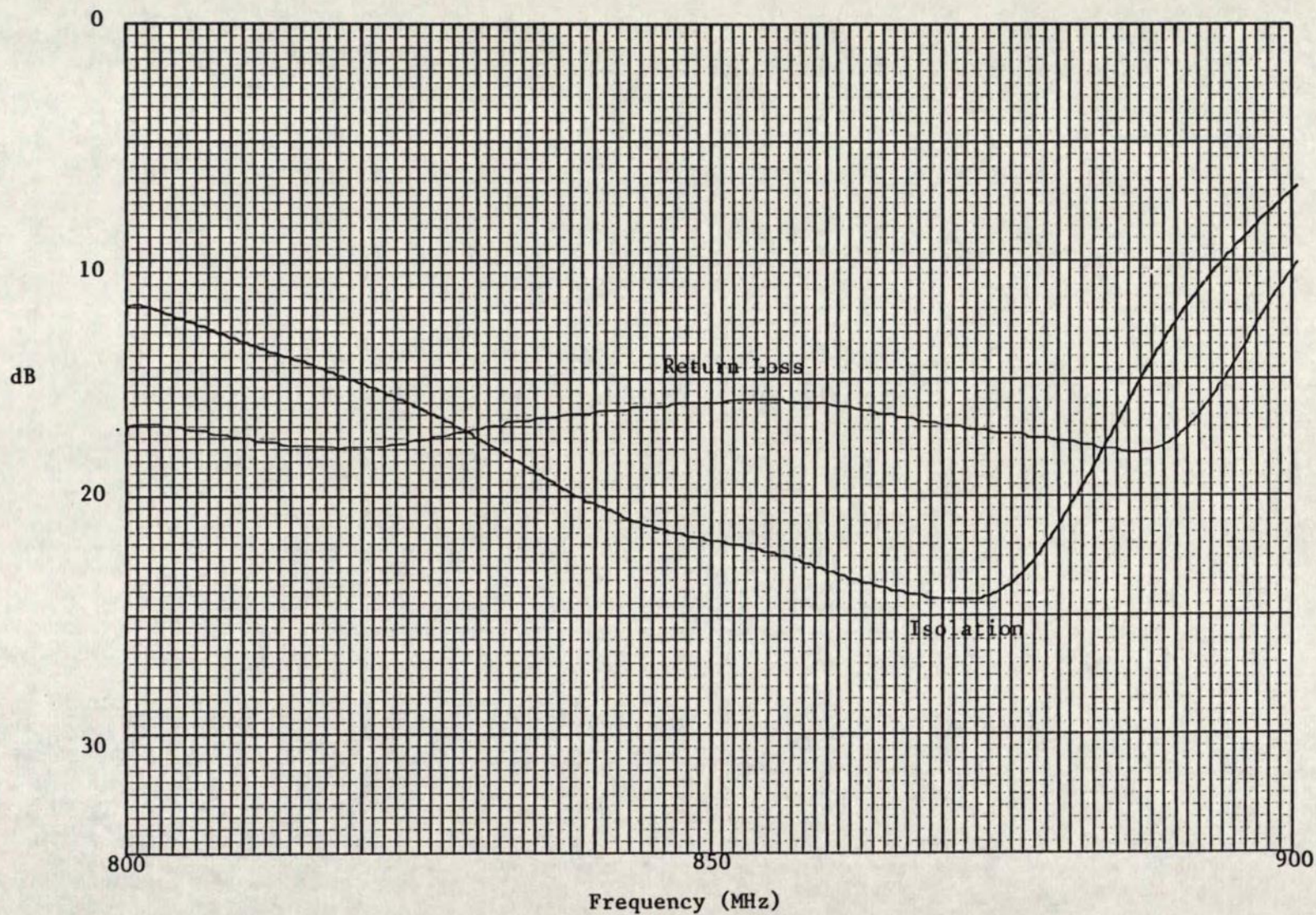


FIGURE 7.9: RETURN LOSS AND ISOLATION OF ENGINEERING MODEL ELEMENT
(INPUT TO PORT 2)

DOCUMENT NO.

REV.

RPT/MST/2500/001




COM DEV

SHEET

140

Her Majesty the Queen in Right of Canada (1986) as represented by the Minister of Supply And Services.

DOCUMENT No.	REV.
RPT/MST/2500/001	—
 COM DEV	
SHEET 141	

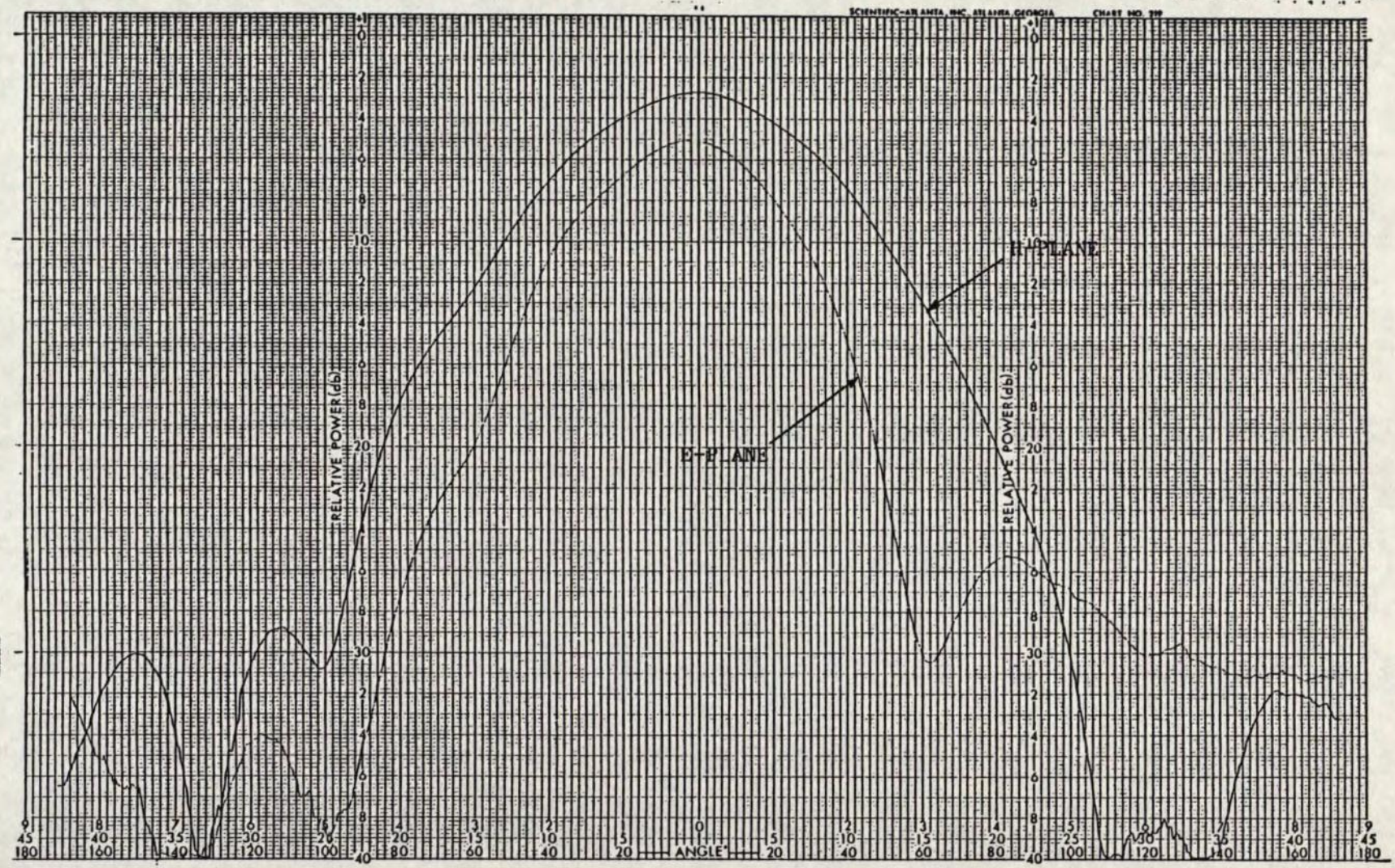


FIGURE 7.10: E- AND H-PLANE PATTERNS OF ENGINEERING MODEL ELEMENT AT 823 MHz (PORT 1)

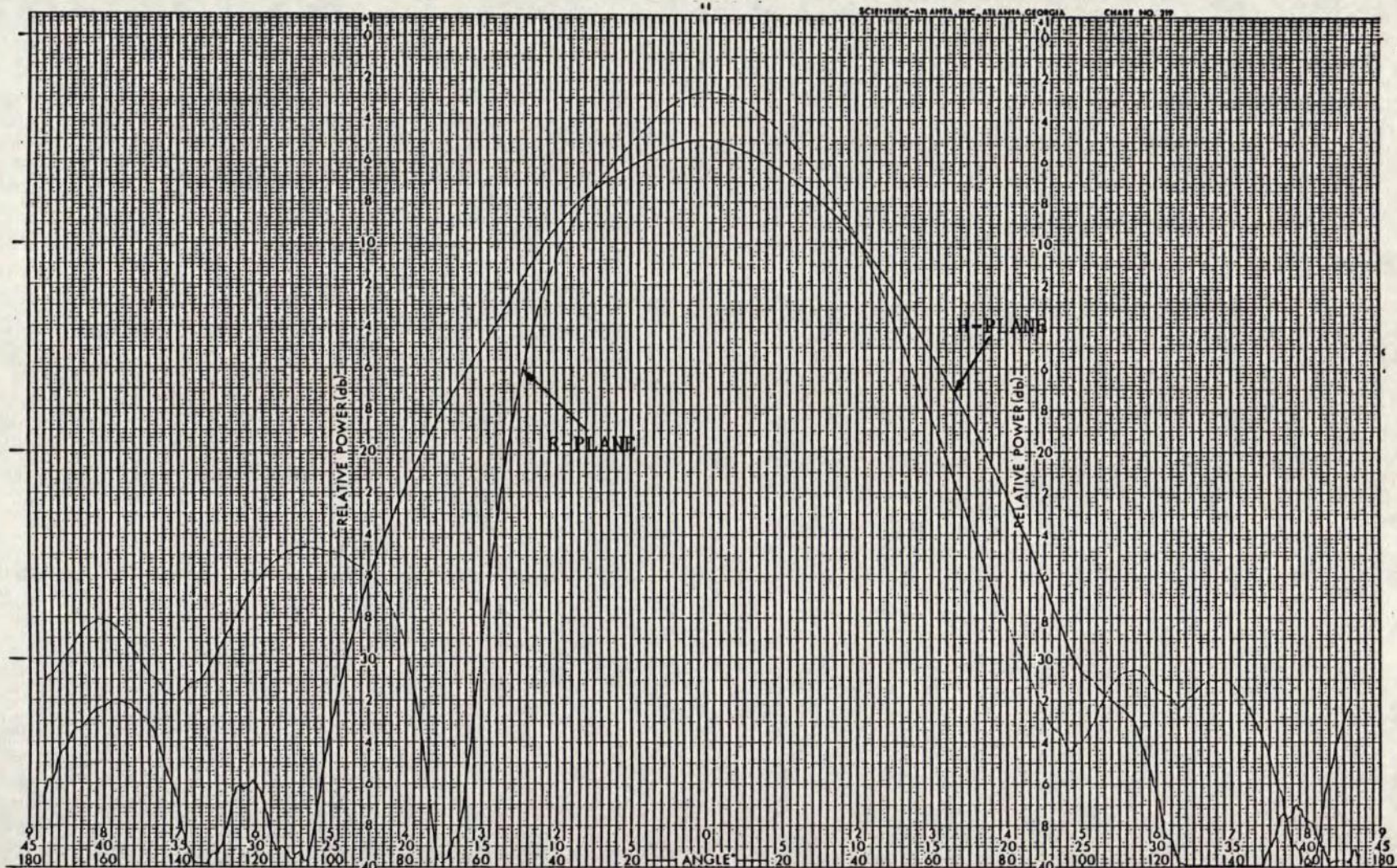


FIGURE 7.11: E- AND H-PLANE PATTERNS OF ENGINEERING MODEL ELEMENT
AT 823 MHz (PORT 2)

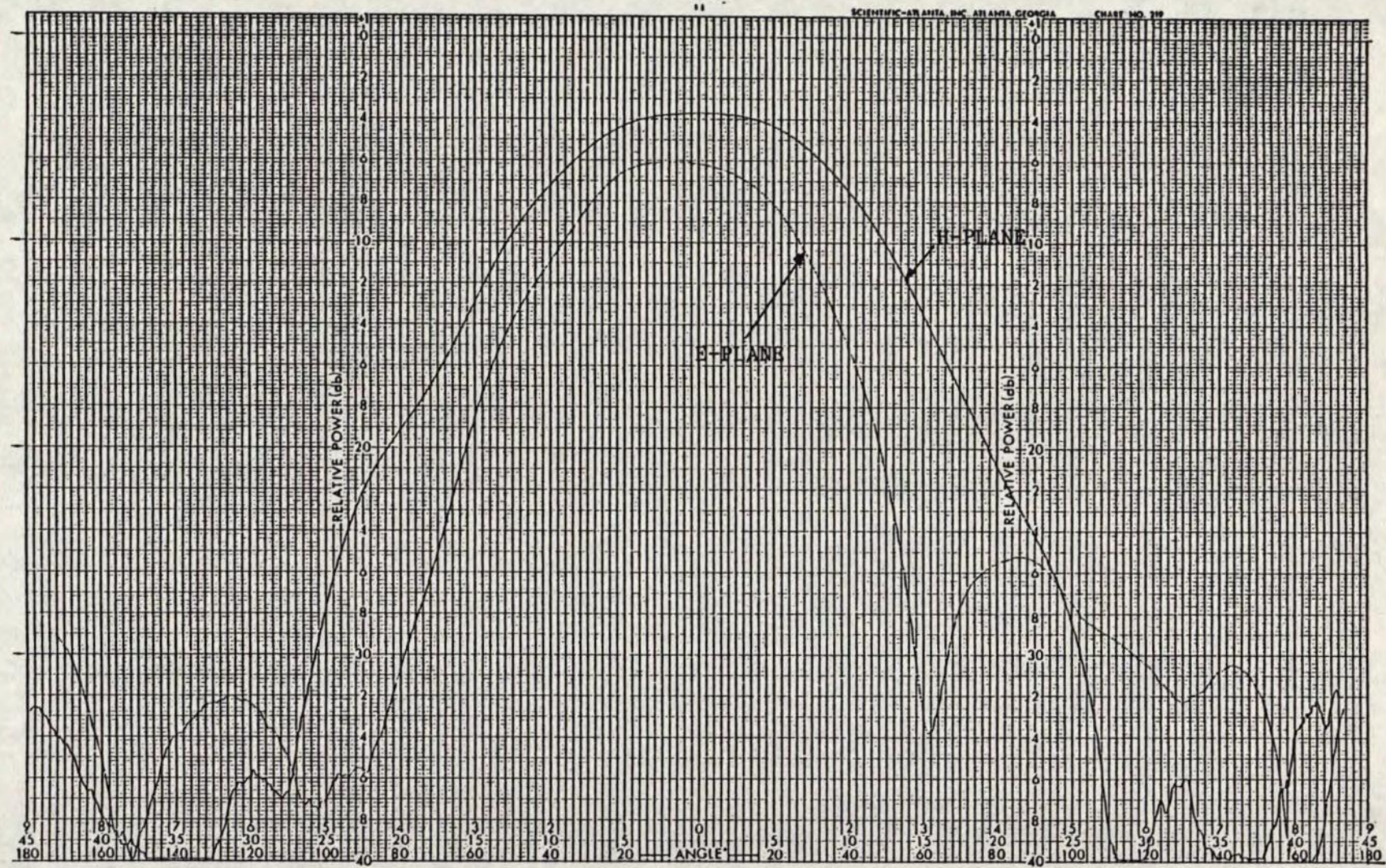


FIGURE 7.12: E- AND H-PLANE PATTERNS OF ENGINEERING MODEL ELEMENT AT 868 MHz (PORT 1)

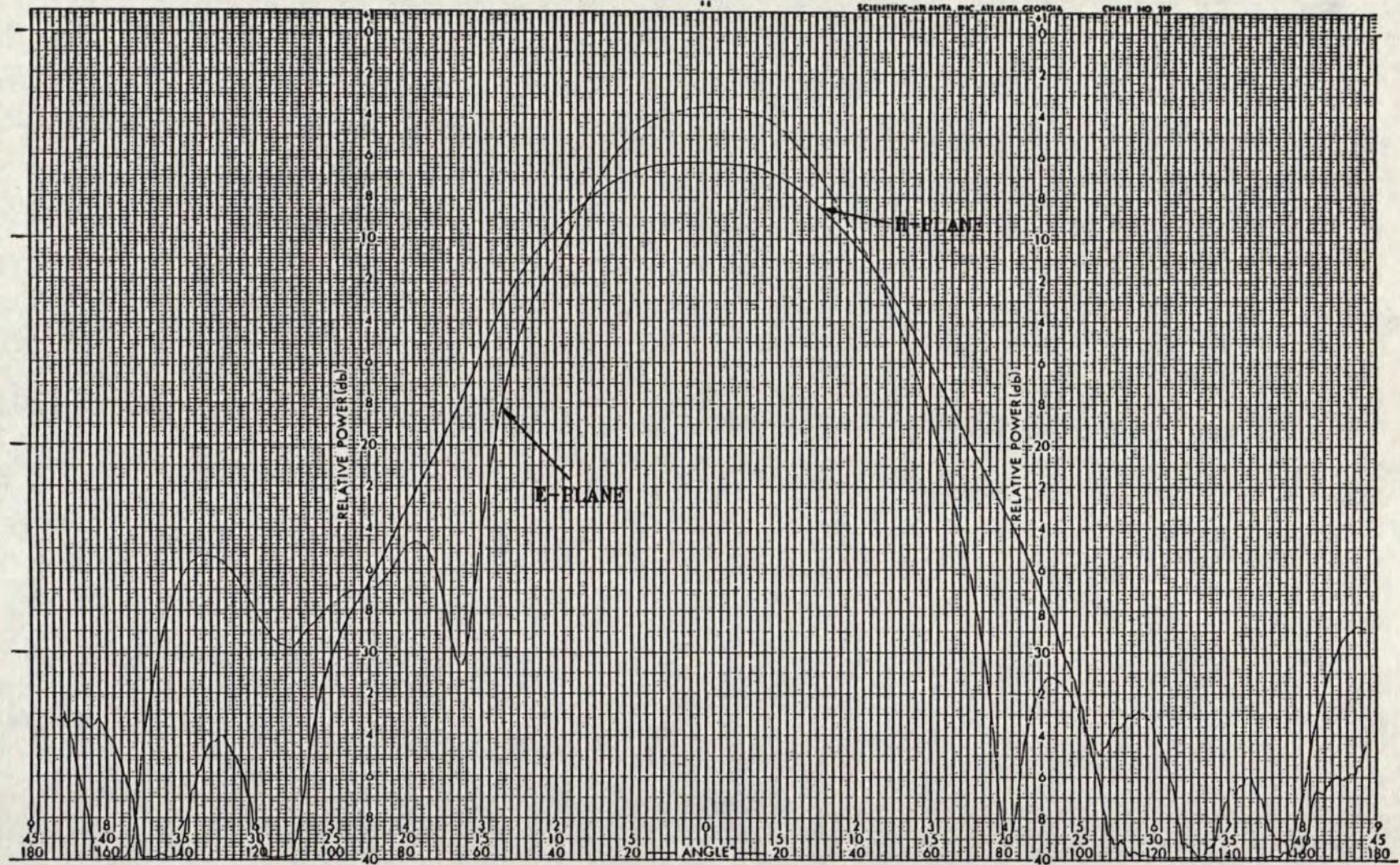


FIGURE 7.13: E- AND H-PLANE PATTERNS OF ENGINEERING MODEL ELEMENT AT 868 MHz (PORT 2)

DOCUMENT NO.

REV.

RPT/MST/2500/001

CONCLUSION

In this study the feasibility of using microstrip array antennas and feeds for the MSAT spacecraft at UHF has been investigated. Technology development has been carried out to show the practicality of such antennas and the areas where further development is required for manufacture of a flight antenna have been identified.

Direct radiating microstrip arrays appear to be unsatisfactory for MSAT. Using the construction technique developed during this study, which can handle transmit power with low loss high level beam forming, the estimated mass for a 2-beam array is 160 kg, not including deployment and mounting structures. This is considerably more than would be expected for a wire mesh construction reflector system. In an array there must be continuous ground planes of solid metal to avoid leakage between layers of the beam-formers. As well, there is considerable mass in the extensive BFN's. The large transverse dimensions (at least 4 m, although only about 8cm thick) will probably require the array to be deployed, with the associated problems of high power, low PIM RF motional joints. A four beam array will require active transmit/receive modules at the subarray level, and low level beam forming. Deployment would be difficult as the overall size would be near 4 by 8 metres.

On the other hand, the use of microstrip antennas in the feed array for a reflector is quite feasible and can offer some advantages over conventional horns. Prior to this study the essential obstacle to the use of microstrip antenna techniques for transmit/receive feeds for MSAT has been bandwidth. However, with development of stacked patch antennas this is no longer a

problem. As part of this project such elements were constructed which meet a specification of 20 dB return loss over both transmit and receive bands of MSAT, with radiation patterns that change very slowly with frequency. While good axial ratio has not yet been achieved it appears that it will not be difficult to obtain with minor changes to the feed system of the engineering model. Mutual coupling measurements carried out during this study will permit the prediction of the performance of an array of these elements.

The thickness of such an array has been estimated at 6.6 cm, including thermal blankets on both surfaces, although this might have to be increased (perhaps to 8 cm) to improve power ratings. A 2-beam feed array will have transverse dimensions of 1.14 by 1.52 metres and a mass of 10.9 kg while a 4-beam feed measures 1.68 by 1.98 m with a mass of 20.9 kg. These designs are conservative in the sense that the element spacing has been chosen to keep mutual coupling effects to a minimum. The sizes may be reduced with careful design including mutual coupling effects. This could permit a reduction in reflector f/D from the assumed value of 0.85 required by these feeds. Simplification of the feeds (especially the two-beam version) could also reduce the feed size and reflector f/D while allowing less control of sidelobes than possible with full septet feeds. The estimated in-service temperature range that would be seen by these arrays is -90° C to +50°C. Performance of an antenna system will be similar to that with horn feeds, but with a lighter feed which is more easily stowable because of its reduced thickness.

A number of critical areas have been identified which require resolution or offer possible improved characteristics. Initially the axial ratio of the engineering model should be improved. Construction techniques should be examined further including the possible use of copper clad dielectric honeycomb as a patch

antenna substrate and aluminum honeycomb as antenna array stiffening on the back face. Fastening methods should be considered to reduce the number of screw junctions, in part to minimize passive intermodulation. Identification of suitable materials for space applications must be considered in more detail, particularly with respect to low temperature, low loss dielectrics and the front face thermal blanket. Further work on qualification of power carrying ability of the components will be required. Multipactor discharge, PIM and power dissipation will all be significant factors in design but none are expected to prohibit operation at MSAT power levels. There is potential for improvement of the stacked patch element. Theoretical modelling of such antennas with accurate methods would be useful. A comparison of circular and square patches should be made, with regard to bandwidth, return loss and mutual coupling. If a suitable 4-phase power divider can be found a four feed element should be considered to improve axial ratio.

The patch array feed concept offers equivalent performance to conventional horn arrays with the advantage of lower volume and competitive mass. With further optimization of the engineering model design, volume and mass reduction is feasible and a fully space-qualifiable technology will be developed.

REFERENCES


1. Bahl, I.J. and P. Bhartia, Microstrip Antennas, Artech House, Dedham, MA, 1981.
2. Bailey, M.C. and M.D. Deshpande, Integral Equation Formulation of Microstrip Antennas, IEEE Trans. Antenna and Propagat., Vol. AP-30, No. 4, pp 651 - 656, July 1982.
3. Bailey, M.C. and M.D. Deshpande, Analysis of Elliptical and Circular Microstrip Antennas Using Moment Method, IEEE Trans Antennas and Propagat., Vol. AP-33, No. 9, pp 954 - 959, Sept. 1985.
4. Balmain, K.G., Surface Discharge Effects, in Space Systems and their Interations with Earth's Space Environment, Progress in Astronautics and Aeronautics, Vol. 71.
5. Blevins, R.D., Formulas for Natural Frequency and Mode Shape, Van Nostrand Reinhold, New York, 1979.
6. Carver, K.R., Input Impedance to Probe-Fed Microstrip Antennas, IEEE 1980 AP-S International Symposium Digest, pp 617 - 620.
7. Carver, K.R. and J.W. Mink, Microstrip Antenna Technology, IEEE Trans. Antennas and Propagat., Vol, AP-29, No. 1, pp 2 - 24, Jan. 1981.
8. Chen, C.H., A. Tulintseff and R.M. Sorbello, Broadband Two-Layer Microstrip Antenna, IEEE 1984 AP-S International Symposium Digest, pp 251 - 254.

9. Chiba, T., Y. Suzuki and N. Miyano, Suppression of Higher Order Modes and Cross Polarized Component for Microstrip Antennas, IEEE 1982, AP-S International Symposium Digest, pp 285 - 288.
10. Clancy, P.F., Multipactor Control in Microwave Space Systems, Microwave Journal, March 1978, pp 77 - 83.
11. Dahele, J.S. and K.F. Lee, A Tunable Dual-Frequency Stacked Microstrip Antenna, IEEE 1982 AP-S International Symposium Digest, pp 308 - 311.
12. Dahele, J.S. and K.F. Lee, Experimental Study of the Effect of Substrate Thickness on Single and Stacked Circular-Disc Microstrip Antenna, IEEE 1982 AP-S International Symposium Digest, pp 66 - 69.
13. Das, N. and J.S. Chatterjee, Conically Depressed Microstrip Patch Antenna, IEE Proc. Vol 130, Pt. H, No. 3, pp 193 - 196, Apr. 1983.
14. Davidson, S.E., S.A. Long and W.F. Richards, Dual-Band Microstrip Antennas with Monolithic Reactive Loading, Electronics Letters, Vol. 21, No. 20, pp 936 - 937, 26 Sept. 1985.
15. De, A. and B.N. Das, Input Impedance of Probe-Excited Rectangular Microstrip Patch Radiator, IEE Proc., Vol. 131, Pt. H, No. 1, pp 31 - 34, Feb. 1984.
16. Deshpande, M.D. and M.C. Bailey, Input Impedance of Microstrip Antennas, IEEE Trans. Antennas and Propagat., Vol. AP-30, No. 4, pp 645 - 650, July 1982.

17. Fong, K.S., H.F. Pues and M.J. Withers, Wideband Multilayer Coaxial-Fed Microstrip Antenna Element, Electronics Letters, Vol. 21, No. 11, pp 497 - 499, 23 May 1985.
18. Gregorwich, W.S., The Space Shuttle Tile: A New Electronic Substrate and Radome Material, IEEE 1983 AP-S International Symposium Digest, pp 350 - 352.
19. Hall, P.S. and C.J. Prior, Microstrip Array for Reflector Feed Applications, Proc. of 14th European Microwave Conference, pp 631 - 636, 1984.
20. Hammerstad, E. and O. Jensen, Accurate Models for Microstrip Computer-Aided Design, IEEE 1980 MTT-S International Symposium Digest, pp 407-409.
21. Haneishi, M., S. Yoshida and N. Goto, "A Broadband Microstrip Array Composed of Single-Feed Type Circularly Polarized Microstrip Antennas, IEEE 1982 AP-S International Symposium Digest, pp 160 - 163.
22. Huang, J., The Finite Ground Plane Effect on the Microstrip Antenna Radiation Patterns, IEEE Trans. Antennas and Propagat., Vol. AP-31, No. 4, pp 649 - 653, July 1983.
23. Jeddari, L., K. Mahdjoubi, C. Terret and J.P. Daniel, Broadband Conical Microstrip Antenna, Electronics Letters, Vol. 21, No. 20, pp 896 - 898, 26 Sept. 1985.
24. Jedlicka, R.P., M.T. Poe and K.R. Carver, Mutual Coupling Between Rectangular and Circular Microstrip Elements, IEEE 1980 AP-S International Symposium Digest, pp 750 - 753.

25. Karlsson, I., Broadband Microstrip Array Antenna, IEEE 1980 AP-S International Symposium Digest, pp 593 - 596.
26. Kirschning, M., R.H. Jansen and N.H.L. Koster, Accurate Model for Open End Effect of Microstrip Lines, Electronics Letters, Vol, 17, No. 3, pp 123 - 125, 5 Feb. 1981.
27. Krowne, C.M., Dielectric and Width Effect on H-Plane and E-Plane Coupling Between Rectangular Microstrip Antennas, IEEE Trans. Antennas and Propagat., Vol, AP-31, No. 1, pp 39 - 47, Jan. 1983.
28. Kumar, G. and K.C. Gupta, Broad-Band Microstrip Antennas Using Additional Resonators Gap-Coupled to the Radiating Edges, IEEE Trans. Antennas and Propagat., Vol, AP-32, No. 12, pp 1375 - 1379, Dec. 1984.
29. Kumar, G. and K.C. Gupta, Nonradiating Edges and Four Edges Gap-Coupled Multiple Resonator Broad-Band Microstrip Antennas, IEEE Trans. Antennas and Propagat., Vol, AP-33, No. 2, pp 173 - 178, Feb. 1985.
30. Lee, K.F., K.Y. Ho and J.S. Dahele, Circular-Disk Microstrip Antenna with an Air Gap, IEEE Trans. Antennas and Propagat, Vol. AP-32, No. 8, pp 880 - 884, Aug. 1984.
31. Lier, E. and K.R. Jakobsen, Rectangular Microstrip Patch Antennas with Infinite and Finite Ground Plane Dimensions, IEEE Trans. Antennas and Propagat., Vol. AP-31, No. 6, pp 978 - 984, Nov. 1983.
32. Mailloux, R.J., J.F. McIlvenna and N.P. Kernweis, Microstrip Array Technology, IEEE Trans. Antennas and Propagat., Vol AP-29, No. 1, pp 25 - 37, Jan. 1981.


FORM 351/86

DOCUMENT No.	REV.	 COM DEV
RPT/MST/2500/001	—	
		SHEET 151

33. Martin, N.M. and D.W. Griffin, New Empirically Determined Parameters for Modelling Rectangular Microstrip Antennas, IEEE 1983 AP-S International Symposium Digest, pp 150 - 153.
34. Martin, N.M. and D.W. Griffin, A Tapered Transmission Line Model for the Feed-Probe of a Microstrip Patch Antenna, IEEE 1983 AP-S International Symposium Digest, pp 154 - 157.
35. Meulenberg, A., Electrical Discharge on Spacecraft at Synchronous Altitude, COMSAT Technical Review, Vol. 6, No. 1, pp 189 - 193, Spring 1976.
36. Milligan, T.A., Bandwidth and Efficiency of a Microstrip Patch Antenna, IEEE 1980 AP-S International Symposium Digest, pp 585 - 588.
37. Montgomery, N.W., Triple-Frequency Stacked Microstrip Element, IEEE 1984 AP-S International Symposium Digest, pp 255 - 258.
38. Moore, R.L., W.P. Cooke, D.S. Eggers and S.D. Lenett, Broadband Dielectric Measurements of Space Shuttle Tiles, IEEE 1983 AP-S International Symposium Digest, pp 353 - 356.
39. Murphy, L.R., SEASAT and SIR-A Microstrip Antennas, Proc. Workshop on Printed Circuit Antenna Technology, Las Cruces, New Mexico, pp 18-1 to 18-20, 1979.
40. Newman, E.H., J.H. Richmond and B.W. Kwan, Mutual Impedance Computation Between Microstrip Antennas, IEEE Trans. Microwave Theory and Tech., Vol. MTT-31, No. 11, pp 941 - 945, Nov. 1983.

41. Palanisamy, V. and R. Garg, Rectangular Ring and H-Shaped Microstrip Antennas - Alternatives to Rectangular Patch Antenna, Electronics Letters, Vol. 21, No. 19, pp 874 - 876, 12 Sept. 1985.
42. Poddar, D.R., J.S. Chatterjee and S.K. Chowdhury, On Some Broad-Band Microstrip Resonators, IEEE Trans. Antennas and Propagat., Vol. AP-31, No. 1, pp 193 - 194, Jan. 1983.
43. Pozar, D.M., M.C. Bailey and M.D. Deshpande, Calculated Self and Mutual Impedance of Rectangular Microstrip Antennas, IEEE 1982 AP-S International Symposium Digest, pp 62 - 65.
44. Pozar, D.M., Microstrip Antenna Aperture-Coupled to a Microstripline, Electronics Letters, Vol. 21, No. 2 pp.49 - 50, 17 Jan. 1985.
45. Pozar, D.M., Input Impedance and Mutual Coupling of Rectangular Microstrip Antennas, IEEE Trans. Antennas and Propagation, Vol. AP-30, No. 6, pp 1191 - 1196, Nov. 1982.
46. Pues, H. and A. Van de Capelle, Accurate Transmission-line Model for the Rectangular Microstrip Antenna, IEE Proc., Vol. 131, Pt. H, No. 6, pp 334 - 340, Dec. 1984.
47. Pues, H. and A. Van de Capelle, Functional Dependence of the Bandwidth and Gain of a Rectangular Microstrip Antenna on its Structural Parameters, IEEE 1982 AP-S International Symposium Digest, pp 77-80.
48. Reed, J. and G.J. Wheeler, A Method of Analysis of Symmetrical Four-Port Networks, IRE Trans. Microwave Theory and Tech. Vol. MTT-4, No. 4, pp 246-252, October 1956.

49. Richards, W.F. and Y.T. Lo, A Simple Theory for Reactively Loaded Microstrip Antennas, IEEE 1984 AP-S International Symposium Digest, pp 259 - 262.
50. Richards, W.F. and S.A. Long, An Experimental Investigation of Loaded Microstrip Antennas, IEEE 1984 AP-S International Symposium Digest, pp 263 - 266.
51. Roederer, A., A Foldable Multibeam Array for Satellite Communication, Proceedings of ISAP '85, Kyoto, pp 385-388, Aug. 1985.
52. Sabban, A., A New Broadband Stacked Two-Layer Microstrip Antenna, IEEE 1983 AP-S International Symposium Digest, pp 63 -66.
53. Sengupta, D.L., The Transmission Line Model for Rectangular Patch Antennas, IEEE 1983 AP-S International Symposium Digest, pp 158 - 161.
54. Sharma, P.C. and K.C. Gupta, Analysis and Optimized Design of Single Feed Circularly Polarized Microstrip Antennas, IEEE Trans. Antennas and Propagat., Vol. AP-31, No. 6, pp 949 - 955, Nov. 1983.
55. Siddiqi, S., A.I. Zaghloul, S.M. Chou and R.E. Eaves, An L-Band Active Array System for Global Coverage, COMSAT Technical Review, Vol. 15, No. 1, pp 39 - 69, 1985.
56. Sindoris, A.R. and C.M. Krowne, Calculation of H-Plane Mutual Coupling Between Rectangular Microstrip Antennas, IEEE 1980 AP-S International Symposium Digest, pp 738 - 741.

DOCUMENT No.	REV.	 COM DEV
RPT/MST/2500/001	—	
		SHEET 154

57. Teshirogi, T., W. Chujo, H. Komuro, A. Akaishi and H. Hirose, Development of 19 Multibeam Array Antenna for Data Relay Satellite, Proceedings of ISAP'85, Kyoto, pp 381-384, Aug. 1985.
58. Van Lil, E. and A. Van de Capelle, Comparison of Models for Calculating Mutual Coupling in Microstrip Arrays, IEEE 1984 AP-S International Symposium Digest, pp 745 - 748.
59. Van Lil, E.H. and A.R. Van de Capelle, Transmission Line Model for Mutual Coupling Between Microstrip Antennas, IEEE Trans. Antennas and Propagat., Vol. AP-32, No. 8, pp 816 - 821, Aug. 1984.
60. Wang, B.F. and Y.T. Lo, Microstrip Antenna for Dual-Frequency Operation, IEEE 1984 AP-S International Symposium Digest, pp 551 - 554.
61. Wegrowicz, L.A., Antennas for Mobile Communication Satellite, Digest Supplement, International Symposium on Antennas and Electromagnetic Theory, Beijing, pp 7-12, 1985.
62. Wolfson, R.I. and W.G. Sterns, A High-Performance, Microstrip, Dual-Polarized Radiating Element, IEEE 1984 AP-S International Symposium Digest, pp 555 - 558.
63. Woo, K., Ground Vehicle Antenna Development for Land Mobile Satellite Service, IEEE 1984 AP-S International Symposium Digest, pp 66 - 69.
64. Woo, R., Final Report on RF Voltage Breakdown in Coaxial Transmission Lines, JPL Technical Report 32 - 1500, Jet Propulsion Laboratory, California Institute of Technology, Pasadena, October 1970.

65. Wood, C., Improved Bandwidth of Microstrip Antennas Using Parasitic Elements, IEE Proc., Vol, 127, Pt, H, No. 4, pp 231 - 234, Aug. 1980.
66. Wood, P.J., TEM Line Technology for Satellite Antenna Feed Applications, Proc. Satellite Communications Conference, Ottawa, pp 29.6.1 - 29.6.4, 1983.
67. Manual for TOUCHSTONE 002 (Version 1.4), prepared by EEsof Inc., 31194 LaBaya Drive, Suite 205, Westlake Village, CA, 1985.
68. SEASAT Antenna Extendible Support Structure, prepared by Astro Research Corporation, August 1978.
69. The Study of Multipactor Breakdown in Space Electronic Systems, prepared by Hughes Aircraft Company, NASA CR-448, 1966.

APPENDIX A

NPATP1F
Computer Program to Compute
Radiation Patterns of Square Microstrip
Feed Elements for Use in Offset
Reflector Radiation Pattern Calculation

Prepared by: S. Kavanagh
Date: June 1986

RPT/MST/2500/001

PROGRAM DESCRIPTION

NPATPlF computes the far-field E- and H-plane radiation patterns of a set of square microstrip patch antennas at a single frequency. The output data is intended to be used by program NCIRY2F to describe a feed array for an offset fed reflector. The geometry of the array is not incorporated in NPATPlF; only the patterns of each element are calculated using the formulas of Carver and Mink [1]. NCIRY2F will compute the secondary pattern of an offset-fed paraboloidal reflector with a multi-element feed. The input data is read from local file TAPE1 and output is to TAPE2. Optionally, the output in suitable format for printing is sent to TAPE6. The input file is in the following format.

```
FREQ, NEL, T, ER, IPRINT
AINCH(1), AINCH(2), ..., AINCH(NEL)
```

The variables are defined as below

FREQ	(REAL)	Frequency in GHz
NEL	(INTEGER)	Number of patch elements in feed array
T	(REAL)	Substrate thickness of all elements in inches
ER	(REAL)	Dielectric constant of substrate
IPRINT	(INTEGER)	Flag for writing output to TAPE6 in suitable format for printing (0=no print, 1=print)
AINCH	(REAL)	One dimensional array of side lengths of square patches in inches

The output data includes the start and end angles between which the pattern is to be computed (in degrees), the number of angles, the patch side lengths, a normalized power used in NCIRY2F in calculating gain and the E-plane and H-plane patterns (in dB and degrees phase).

Running NPATP1F Under NOS at COM DEV

This program may be run using the procedure KPATP1P shown below. The input data must be stored in a permanent file named PATP##D where ## is any two alphanumeric characters. The compiled version of NPATP1F must be available as KPATP1B. To run type:

-,KPATP1P,##

where ## are the same characters as in the desired data file name. The output for NCIRY2F will be stored in file PATP##G. The printable output (if specified) will remain in the local file TAPE6.

Procedure file KPATP1P

```
.PROC,KPATP1P,HNUM.  
GET,TAPE1=PATP_HNUM_D.  
GET,KPATP1B.  
KPATP1B.  
REWIND,TAPE2.  
REPLACE,TAPE2=PATP_HNUM_G.  
RETURN,TAPE1,TAPE2,KPATP1B.
```

REFERENCE

1. Carver, K.R. and J.W. Mink, Microstrip Antenna Technology, IEEE Trans. Antennas and Propagat., Vol. AP-29, No. 1, pp 2-24, Jan. 1981.

Typical Input Data File PATP01D

0.868 1 0.5 1.00 0
6.4

Frequency = 868 MHz

1 patch element

Substrate 0.5 inch thick, $\epsilon_r = 1$

No print file to be created

Patch is 6.4 inches square

TYPICAL OUTPUT DATA FILE PATP01G

 COM DEV

90.000 179.995 91

5.400

.19437443E-02

-20.400	.0
-20.379	.0
-20.317	.0
-20.214	.0
-20.072	.0
-19.894	.0
-19.680	.0
-19.435	.0
-19.161	.0
-18.861	.0
-18.537	.0
-18.194	.0
-17.834	.0
-17.459	.0
-17.073	.0
-16.678	.0
-16.275	.0
-15.868	.0
-15.457	.0
-15.044	.0
-14.630	.0
-14.218	.0
-13.807	.0
-13.399	.0
-12.994	.0
-12.593	.0
-12.197	.0
-11.806	.0
-11.421	.0
-11.041	.0
-10.658	.0
-10.301	.0
-9.940	.0
-9.586	.0
-9.239	.0
-8.898	.0
-8.564	.0
-8.237	.0
-7.917	.0
-7.604	.0
-7.298	.0
-6.999	.0
-6.706	.0
-6.420	.0
-6.141	.0
-5.869	.0
-5.604	.0
-5.345	.0
-5.093	.0
-4.847	.0
-4.608	.0
-4.375	.0
-4.149	.0
-3.929	.0
-3.716	.0
-3.509	.0
-3.308	.0
-3.113	.0
-2.925	.0
-2.742	.0
-2.566	.0
-2.396	.0
-2.232	.0
-2.074	.0
-1.922	.0
-1.775	.0
-1.635	.0
1.501	.0
1.372	.0

RPT/MST/2500/001

-1.250	.0
-1.133	.0
-1.022	.0
-.917	.0
-.817	.0
-.724	.0
-.636	.0
-.554	.0
-.477	.0
-.407	.0
-.342	.0
-.282	.0
-.229	.0
-.181	.0
-.138	.0
-.102	.0
-.071	.0
-.045	.0
-.025	.0
-.011	.0
-.003	.0
.000	.0
-100.000	180.0
-38.358	.0
-32.336	.0
-28.811	.0
-26.307	.0
-24.364	.0
-22.773	.0
-21.426	.0
-20.257	.0
-19.224	.0
-18.297	.0
-17.457	.0
-16.888	.0
-15.978	.0
-15.318	.0
-14.703	.0
-14.125	.0
-13.580	.0
-13.065	.0
-12.575	.0
-12.109	.0
-11.685	.0
-11.239	.0
-10.831	.0
-10.439	.0
-10.082	.0
-9.698	.0
-9.347	.0
-9.007	.0
-8.679	.0
-8.361	.0
-8.053	.0
-7.754	.0
-7.463	.0
-7.181	.0
-6.907	.0
-6.640	.0
-6.381	.0
-6.128	.0
-5.882	.0
-5.643	.0
-5.410	.0
-5.183	.0
-4.961	.0
-4.746	.0
-4.536	.0
-4.331	.0
-4.132	.0
-3.938	.0
-3.750	.0
-3.566	.0
-3.388	.0
-3.214	.0
-3.045	.0
-2.881	.0
-2.722	.0
-2.567	.0
-2.418	.0

-2.273	.0
-2.132	.0
-1.996	.0
-1.865	.0
-1.738	.0
-1.616	.0
-1.498	.0
-1.385	.0
-1.276	.0
-1.172	.0
-1.072	.0
-.977	.0
-.886	.0
-.800	.0
-.718	.0
-.640	.0
-.567	.0
-.498	.0
-.434	.0
-.374	.0
-.319	.0
-.268	.0
-.222	.0
-.180	.0
-.142	.0
-.109	.0
-.080	.0
-.055	.0
-.036	.0
-.020	.0
-.009	.0
-.002	.0
.000	.0

 COM DEV

APPENDIX B



JPLAP2F
Computer Program to Calculate
the Radiation Pattern of a
Planar Array Antenna

Version 2.2

Prepared by: S. Kavanagh
Date: June 1986

RPT/MST/2500/001

PROGRAM DESCRIPTION

JPLAP2F is a program to compute the radiation patterns and approximate gain of a planar array of elements arranged in a rectangular grid. Version 2.2 includes either isotropic or rectangular microstrip patch elements with amplitude and phase excitations specified individually or according to one of several simplified distributions. The program reads data from a local file (TAPE5) and output is to local files TAPE6 for printing and TAPE7, TAPE8 for contour plots of co-polarized and cross-polarized fields respectively. TAPE7 and TAPE8 outputs may also be used by a pattern integration routine. The geometry of the array is shown in Figure 1. The basic formulation is similar to that of Elliot [1] and the microstrip element patterns are computed according to Carver and Mink [2]. Mutual coupling between elements is not considered.

INPUT DATA FORMAT FOR JPLAP2F

Input file to program is "TAPE5". Alternate names may be defined in the procedure call.

Input file format

UNITS

NX1, DX1, NY1, DY1

(data read by subroutine READEL)

(data read by subroutine READEX)

F

AZSD, AZED, NAZ, ELSD, ELED, NEL

IPAD, IPEP, IPGT

Variables read by program JPLAP2F

<u>NAME</u>	<u>TYPE</u>	<u>DESCRIPTION</u>
UNITS	CHAR*2	Indicates units for linear dimensions. Choose from MM, CM, M, IN, FT.
NX1, NY1	INTEGER	Numbers of elements in X(azim.) and Y(elev.) directions. Must be odd numbers.
DX1, DY1	REAL	Element spacings in X and Y directions
F	REAL	Frequency in MHz
AZSD, AZED	REAL	Start, end values of azimuth angle range (degrees)
ELSD, ELED	REAL	Start, end values of elevation angle range (degrees)
NAZ, NEL	INTEGER	Numbers of azimuth and elevation angles
IPAD	INTEGER	Print flag for element positions and excitations: 0 = short form (separable excitations only), otherwise long.
IPEP	INTEGER	Print flag for element pattern. Print if IPEP = 1.
IPGT	INTEGER	Print flag for gain table. Write to TAPE6 if IPGT = 1

RPT/MST/2500/001

Variables read by subroutine READEL (Element Description)

JEL

IPOL, (ELDATA(I), I = 2,5) only if JEL = 1

<u>NAME</u>	<u>TYPE</u>	<u>DESCRIPTION</u>
JEL	INTEGER	Type of element: 0 = isotropic (radiating into half-space only) 1 = rectangular microstrip patch If JEL = 0, no more data is read by READEL
IPOL	INTEGER	Source polarization and observer co-polarization direction/sense: 1 = Azimuth (x) linear 2 = Elevation (y) linear 3 = Right-hand circular 4 = Left-hand circular
ELDATA(2)	REAL	Patch dimension parallel to x-axis
ELDATA(3)	REAL	Patch dimension parallel to y-axis Note: If IPOL = 3 or 4, ELDATA(2) and ELDATA(3) must be equal (square patch)
ELDATA(4)	REAL	Microstrip substrate thickness
ELDATA(5)	REAL	Microstrip substrate permittivity

Variables read by subroutine READDEX (excitations)

Currently, the element excitation data can be entered in 5 formats according to the value of JEX (Type INTEGER).

<u>JEX</u>	<u>Excitations Specified</u>
1	Uniform amplitudes, equal phases
2	Uniform amplitudes, constant element-to-element phase differences
3	Separable amplitude distributions, constant element-to-element phase differences
4	Separable amplitude and phase distributions
5	Arbitrary amplitudes and phases, specified for each element

<u>NAME</u>	<u>TYPE</u>	<u>DESCRIPTION</u>
-------------	-------------	--------------------

(IF JEX = 1)

JEX	INTEGER	Type of excitations (no further data read)
-----	---------	--

(IF JEX = 2)

JEX	INTEGER	Type of excitations
DXIXD,DXIYD	REAL	Phase differences between adjacent elements in x- and y- directions (degrees)

(IF JEX = 3)

JEX	INTEGER	Type of excitations
(AX(MM),MM=1,NX1)	REAL	Relative element amplitudes in x-direction
(AY(NN),NN=1,NY1)	REAL	Relative element amplitudes in y-direction
DXIXD,DXIYD	REAL	As for JEX=2

(IF JEX = 4)

JEX	INTEGER	Type of excitations
(AX(MM),MM=1,NX1)	REAL	Relative element amplitudes in x-direction
(AY(NN),NN=1,NY1)	REAL	Relative element amplitudes in y-direction
(XIXD(MM),MM=1,NX1)	REAL	Relative phases in x-direction

<u>NAME</u>	<u>TYPE</u>	<u>DESCRIPTION</u>
(XIYD(NN),NN=1,NY1)	REAL	Relative phases in y-direction
<u>(IF JEX=5)</u>		
JEX	INTEGER	Type of excitation
(A(MM,1),MM=1,NX1)	REAL	Element amplitudes
(A(MM,2),MM=1,NX1)		
.		
.		
(A(MM,NY1),MM=1,NX1)	REAL	Element phases (degrees)
(XID(MM,1),MM=1,NX1)		
(XID(MM,2),MM=1,NX1)		
.		
.	REAL	Element phases (degrees)
(XID(MM,NY1),MM=1,NX1)		

Limits in JPLAP2F (Version 2.2)

Number of elements in x-direction	≤ 35
Number of elements in y-direction	≤ 35
Number of observation angles in azimuth	≤ 20
Number of observation angles in elevation	≤ 20

Running JPLAP2F Under NOS at COM DEV

To run the program the procedure file KPLAP2P may be used. In this case the compiled version of JPLAP2F must be available in file KPLAP2B. In addition the contour plotting program (in compiled form) must be available in file CONTB, and the printing program JSPRN1F must be available in compiled form in file KSPRN1B.

PROCEDURE CALL

To run, type:

-,KPLAP2P,<datafil,><contfil>,ID=<id>,COPOL =<copol>

<datafil> is permanent file containing input data for JPLAP2F.
Default is TAPE5

<contfil> is permanent file containing control data for CONTF
(contour generation program). Default is KCONT1D.

<id> is destination for printout (0 = computer room printer,
1 = Printonix printer outside computer room. Default
is zero.

<copol> is destination file for a copy of the co-polarized gain
table file in the format used for contour plotting or
pattern integration. This file is made permanent by
the procedure. Default is KPLAPØC.

Output listing from JPLAP2F (TAPE6) and contour plots of co- and
cross-polarized patterns are routed to a printer. No permanent
copies are kept except for <copol>.

Procedure file KPLAP2P

```
. PROC,KPLAP2P,DATAFIL=TAPE5,CONFIL=KCONT1D,ID=0,COPOL=KPLAPOC.
GET,TAPE5=DATAFIL.
GET,KPLAP2B.
REWIND,TAPE6,TAPE7,TAPE8.
KPLAP2B.
REWIND,TAPE2,TAPE3,TAPE6,TAPE7,TAPE8.
GET,TAPE1=CONFIL.
COPY,TAPE7,TAPE2.
REWIND,TAPE2,TAPE7.
REPLACE,TAPE7=COPOL.
GET,CONTB/UN=IRWIN.
CONTB.
REWIND,TAPE1,TAPE2.
COPY,TAPE8,TAPE2.
REWIND,TAPE2.
CONTB.
REWIND,TAPE3,TAPE91.
COPY,TAPE6,TAPE91.
REWIND,TAPE91,TAPE99.
COPY,Q,TAPE99.
BLOCK,TAPE99,,4./USER/PLANAR/ARRAY/DATAFIL/.
BLOCK,TAPE99,,1./USER/PLANAR/ARRAY/DATAFIL/.
REWIND,KSPRN1B.
KSPRN1B.
COPYSBF,TAPE3,TAPE99.
REWIND,TAPE99.
PACK,TAPE99.
ROUTE,TAPE99,DC=PR,#ID=ID.
RETURN,TAPE1,TAPE2,TAPE3,TAPE5,TAPE6,TAPE7,TAPE8,TAPE91,TAPE98,TAPE99.
RETURN,Q,KPLAP1B,CONTB.
. DATA,TAPE98.
O
S
TAPE6
O
O
O
O
. DATA,Q.
Q
```


REFERENCES

1. Elliot, R.S., Chapter 1 of Microwave Scanning Antennas (Vol. II), R.C. Hansen (Ed.), Academic Press, New York, 1966.
2. Carver, K.R. and J.W. Mink, Microstrip Antenna Technology, IEEE Trans. Antennas and Propagat., Vol, AP-29, No. 1, pp 2-24, Jan. 1981.

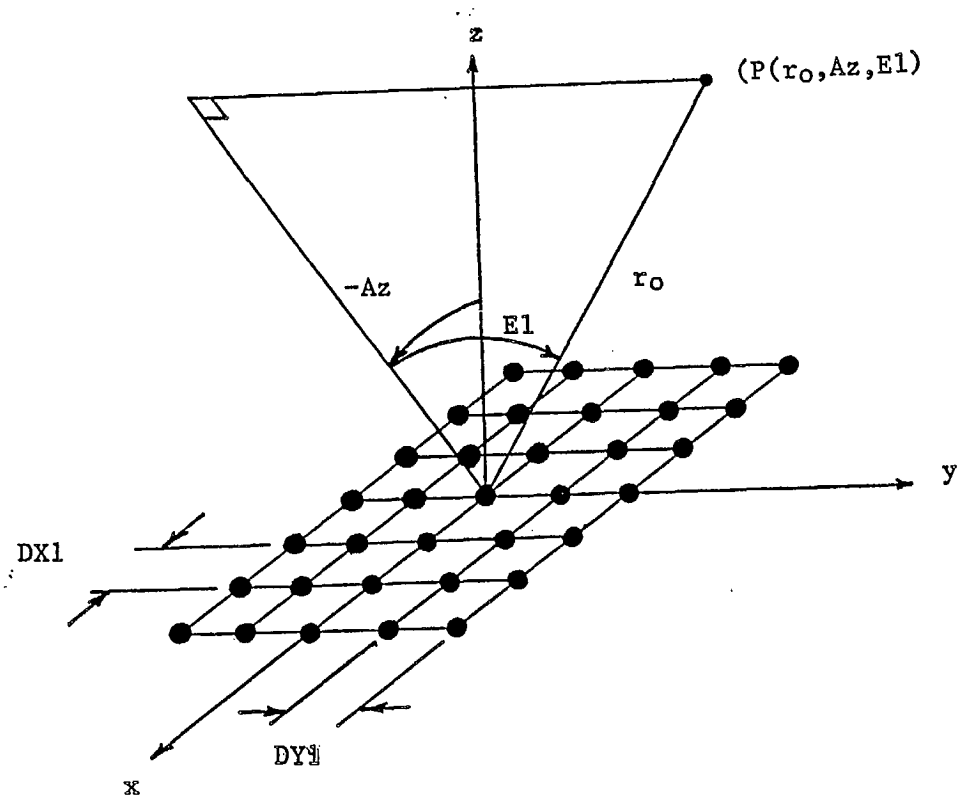


FIGURE 1: PLANAR ARRAY GEOMETRY

TYPICAL OUTPUT

*** FILE: TAPE6 *** 86/01/29. 08.59.52. PAGE 1

JPLAF2F (VERSION 2.0): PLANAR ARRAY PATTERN COMPUTATION
86/01/29. 08.59.23.

ELEMENT POSITIONS AND EXCITATIONS

ELEMENT		POSITION (CM)		AMPLITUDE		PHASE
M	N	X	Y	NUMERICAL	DB	DEGREES
-4	-4	-60.000	-60.000	1.00000	.00	.000
-4	-3	-60.000	-45.000	1.00000	.00	.000
-4	-2	-60.000	-30.000	1.00000	.00	.000
-4	-1	-60.000	-15.000	1.00000	.00	.000
-4	0	-60.000	.000	1.00000	.00	.000
-4	1	-60.000	15.000	1.00000	.00	.000
-4	2	-60.000	30.000	1.00000	.00	.000
-4	3	-60.000	45.000	1.00000	.00	.000
-4	4	-60.000	60.000	1.00000	.00	.000
-3	-4	-45.000	-60.000	1.00000	.00	.000
-3	-3	-45.000	-45.000	1.00000	.00	.000
-3	-2	-45.000	-30.000	1.00000	.00	.000
-3	-1	-45.000	-15.000	1.00000	.00	.000
-3	0	-45.000	.000	1.00000	.00	.000
-3	1	-45.000	15.000	1.00000	.00	.000
-3	2	-45.000	30.000	1.00000	.00	.000
-3	3	-45.000	45.000	1.00000	.00	.000
-3	4	-45.000	60.000	1.00000	.00	.000
-2	-4	-30.000	-60.000	1.00000	.00	.000
-2	-3	-30.000	-45.000	1.00000	.00	.000
-2	-2	-30.000	-30.000	1.00000	.00	.000
-2	-1	-30.000	-15.000	1.00000	.00	.000
-2	0	-30.000	.000	1.00000	.00	.000
-2	1	-30.000	15.000	1.00000	.00	.000
-2	2	-30.000	30.000	1.00000	.00	.000
-2	3	-30.000	45.000	1.00000	.00	.000
-2	4	-30.000	60.000	1.00000	.00	.000
-1	-4	-15.000	-60.000	1.00000	.00	.000
-1	-3	-15.000	-45.000	1.00000	.00	.000
-1	-2	-15.000	-30.000	1.00000	.00	.000
-1	-1	-15.000	-15.000	1.00000	.00	.000
-1	0	-15.000	.000	1.00000	.00	.000
-1	1	-15.000	15.000	1.00000	.00	.000
-1	2	-15.000	30.000	1.00000	.00	.000
-1	3	-15.000	45.000	1.00000	.00	.000
-1	4	-15.000	60.000	1.00000	.00	.000
0	-4	.000	-60.000	1.00000	.00	.000
0	-3	.000	-45.000	1.00000	.00	.000
0	-2	.000	-30.000	1.00000	.00	.000
0	-1	.000	-15.000	1.00000	.00	.000
0	0	.000	.000	1.00000	.00	.000
0	1	.000	15.000	1.00000	.00	.000
0	2	.000	30.000	1.00000	.00	.000
0	3	.000	45.000	1.00000	.00	.000
0	4	.000	60.000	1.00000	.00	.000
1	-4	15.000	-60.000	1.00000	.00	.000
1	-3	15.000	-45.000	1.00000	.00	.000
1	-2	15.000	-30.000	1.00000	.00	.000

RPT/MST/2500/001

*** FILE: TAPE6 *** 86/01/29. 08.59.52. PAGE 2

1	-1	15.000	-15.000	1.00000	.00	.000
1	0	15.000	.000	1.00000	.00	.000
1	1	15.000	15.000	1.00000	.00	.000
1	2	15.000	30.000	1.00000	.00	.000
1	3	15.000	45.000	1.00000	.00	.000
1	4	15.000	60.000	1.00000	.00	.000
2	-4	30.000	-60.000	1.00000	.00	.000
2	-3	30.000	-45.000	1.00000	.00	.000
2	-2	30.000	-30.000	1.00000	.00	.000
2	-1	30.000	-15.000	1.00000	.00	.000
2	0	30.000	.000	1.00000	.00	.000
2	1	30.000	15.000	1.00000	.00	.000
2	2	30.000	30.000	1.00000	.00	.000
2	3	30.000	45.000	1.00000	.00	.000
2	4	30.000	60.000	1.00000	.00	.000
3	-4	45.000	-60.000	1.00000	.00	.000
3	-3	45.000	-45.000	1.00000	.00	.000
3	-2	45.000	-30.000	1.00000	.00	.000
3	-1	45.000	-15.000	1.00000	.00	.000
3	0	45.000	.000	1.00000	.00	.000
3	1	45.000	15.000	1.00000	.00	.000
3	2	45.000	30.000	1.00000	.00	.000
3	3	45.000	45.000	1.00000	.00	.000
3	4	45.000	60.000	1.00000	.00	.000
4	-4	60.000	-60.000	1.00000	.00	.000
4	-3	60.000	-45.000	1.00000	.00	.000
4	-2	60.000	-30.000	1.00000	.00	.000
4	-1	60.000	-15.000	1.00000	.00	.000
4	0	60.000	.000	1.00000	.00	.000
4	1	60.000	15.000	1.00000	.00	.000
4	2	60.000	30.000	1.00000	.00	.000
4	3	60.000	45.000	1.00000	.00	.000
4	4	60.000	60.000	1.00000	.00	.000

ELEMENTS ARE RECTANGULAR MICROSTRIP PATCHES

POLARIZATION : LHCP
 AZIM.DIMENSION : 14.000 CM
 ELEV.DIMENSION : 14.000 CM
 SUBSTRATE THICKNESS : .500 CM
 SUBSTR.DIEL.CONST. : 1.000

FREQUENCY : 1000.0 MHZ
 AZIMUTH SCAN : -28.00 TO 28.00 DEGREES (15 POINTS)
 ELEVATION SCAN : -28.00 TO 28.00 DEGREES (15 POINTS)

CO-POLARIZED ELEMENT PATTERX GAIN TABLE (DBI)

		AZIMUTH														
ELEV.)		-28.00	-24.00	-20.00	-16.00	-12.00	-8.00	-4.00	.00	4.00	8.00	12.00	16.00	20.00	24.00	28.00
28.00 :		-3.59	-3.17	-2.82	-2.52	-2.29	-2.13	-2.03	-2.00	-2.03	-2.13	-2.29	-2.52	-2.82	-3.17	-3.59
24.00 :		-3.16	-2.71	-2.34	-2.02	-1.78	-1.61	-1.50	-1.47	-1.50	-1.61	-1.78	-2.02	-2.34	-2.71	-3.16
20.00 :		-2.80	-2.33	-1.93	-1.60	-1.35	-1.16	-1.05	-1.02	-1.05	-1.16	-1.35	-1.60	-1.93	-2.33	-2.80
16.00 :		-2.51	-2.02	-1.60	-1.26	-.99	-.80	-.69	-.65	-.69	-.80	-.99	-1.26	-1.60	-2.02	-2.51
12.00 :		-2.28	-1.78	-1.34	-.99	-.72	-.52	-.41	-.37	-.41	-.52	-.72	-.99	-1.34	-1.78	-2.28
8.00 :		-2.12	-1.60	-1.16	-.80	-.52	-.32	-.20	-.16	-.20	-.32	-.52	-.80	-1.16	-1.60	-2.12

*** FILE: TAPE6 ***

86/01/29. 08.59.52. PAGE 3

4.00 :	-2.03	-1.50	-1.05	-.69	-.41	-.20	-.08	-.04	-.08	-.20	-.41	-.69	-1.05	-1.50	-2.03
0.00 :	-2.00	-1.47	-1.02	-.65	-.37	-.16	-.04	.00	-.04	-.16	-.37	-.65	-1.02	-1.47	-2.00
-4.00 :	-2.03	-1.50	-1.05	-.69	-.41	-.20	-.08	-.04	-.08	-.20	-.41	-.69	-1.05	-1.50	-2.03
-8.00 :	-2.12	-1.60	-1.16	-.80	-.52	-.32	-.20	-.16	-.20	-.32	-.52	-.80	-1.16	-1.60	-2.12
-12.00 :	-2.28	-1.78	-1.34	-.99	-.72	-.52	-.41	-.37	-.41	-.52	-.72	-.99	-1.34	-1.78	-2.28
-16.00 :	-2.51	-2.02	-1.60	-1.26	-.99	-.80	-.69	-.65	-.69	-.80	-.99	-1.26	-1.60	-2.02	-2.51
-20.00 :	-2.80	-2.33	-1.93	-1.60	-1.35	-1.16	-1.05	-1.02	-1.05	-1.16	-1.35	-1.60	-1.93	-2.33	-2.80
-24.00 :	-3.16	-2.71	-2.34	-2.02	-1.78	-1.61	-1.50	-1.47	-1.50	-1.61	-1.78	-2.02	-2.34	-2.71	-3.16
-28.00 :	-3.59	-3.17	-2.82	-2.52	-2.29	-2.13	-2.03	-2.00	-2.03	-2.13	-2.29	-2.52	-2.82	-3.17	-3.59

CO-POLARIZED ELEMENT PATTERN PHASE TABLE(DEG.)

ELEV. :	AZIMUTH														
	-28.00	-24.00	-20.00	-16.00	-12.00	-8.00	-4.00	.00	4.00	8.00	12.00	16.00	20.00	24.00	28.00
28.00 :	179.85	179.77	179.73	179.74	179.78	179.84	179.92	180.00	-179.92	-179.84	-179.78	-179.74	-179.73	-179.77	-179.85
24.00 :	-179.95	179.94	179.88	179.85	179.87	179.90	179.95	180.00	-179.95	-179.90	-179.87	-179.86	-179.88	-179.94	179.95
20.00 :	-179.83	-179.95	179.92	179.94	179.94	179.95	179.97	180.00	-179.97	-179.95	-179.94	-179.94	-179.98	179.95	179.83
16.00 :	-179.78	-179.89	-179.96	179.99	179.98	179.98	179.99	180.00	-179.99	-179.98	-179.98	-179.99	179.96	179.89	179.78
12.00 :	-179.78	-179.88	-179.94	-179.98	180.00	179.99	179.99	180.00	-179.99	-179.99	-180.00	179.98	179.94	179.88	179.78
8.00 :	-179.63	-179.90	-179.95	-179.98	-179.99	180.00	180.00	180.00	-180.00	-180.00	179.99	179.98	179.95	179.90	179.83
4.00 :	-179.91	-179.94	-179.97	-179.98	-179.99	-180.00	180.00	180.00	-180.00	180.00	179.99	179.98	179.97	179.94	179.91
0.00 :	-180.00	-180.00	-180.00	-180.00	-180.00	-180.00	-180.00	-180.00	180.00	180.00	180.00	180.00	180.00	180.00	180.00
-4.00 :	179.91	179.94	179.97	179.93	179.99	180.00	-180.00	-180.00	180.00	-180.00	-179.99	-179.98	-179.97	-179.94	-179.91
-8.00 :	179.63	179.90	179.95	179.98	179.99	-180.00	-180.00	-180.00	180.00	180.00	-179.99	-179.98	-179.95	-179.90	-179.83
-12.00 :	179.78	179.88	179.94	179.98	-180.00	-179.99	-179.99	-180.00	179.99	179.99	180.00	-179.98	-179.94	-179.88	-179.78
-16.00 :	179.78	179.89	179.96	-179.99	-179.98	-179.98	-179.99	-180.00	179.99	179.98	179.98	179.99	-179.96	-179.89	-179.78
-20.00 :	179.83	179.95	-179.98	-179.94	-179.94	-179.95	-179.97	-180.00	179.97	179.95	179.94	179.94	179.96	-179.95	-179.83
-24.00 :	179.95	-179.94	-179.88	-179.86	-179.87	-179.90	-179.95	-180.00	179.95	179.90	179.87	179.86	179.88	179.94	-179.95
-28.00 :	-179.85	-179.77	-179.73	-179.74	-179.78	-179.84	-179.92	-180.00	179.92	179.84	179.78	179.74	179.73	179.77	179.85

CROSS-POLARIZED ELEMENT PATTERN GAIN TABLE (DB)

ELEV. :	AZIMUTH														
	-28.00	-24.00	-20.00	-16.00	-12.00	-8.00	-4.00	.00	4.00	8.00	12.00	16.00	20.00	24.00	28.00
28.00 :	-21.79	-22.83	-24.04	-25.62	-27.51	-29.78	-32.18	-33.44	-32.18	-29.78	-27.51	-25.62	-24.09	-22.83	-21.79
24.00 :	-22.58	-23.64	-24.94	-26.54	-28.55	-31.07	-33.97	-35.66	-33.97	-31.07	-28.55	-26.54	-24.94	-23.64	-22.58
20.00 :	-23.65	-24.74	-26.08	-27.75	-29.88	-32.64	-36.12	-38.44	-36.12	-32.64	-29.88	-27.75	-26.08	-24.74	-23.65
16.00 :	-25.05	-26.19	-27.59	-29.34	-31.58	-34.59	-38.71	-42.01	-38.71	-34.59	-31.58	-29.34	-27.59	-26.19	-25.05
12.00 :	-26.69	-28.11	-29.61	-31.46	-33.64	-37.08	-41.88	-46.77	-41.88	-37.08	-33.64	-31.46	-29.61	-28.11	-26.69
8.00 :	-29.23	-30.65	-32.34	-34.40	-37.00	-40.52	-46.01	-53.65	-46.01	-40.52	-37.00	-34.40	-32.34	-30.65	-29.23
4.00 :	-31.92	-33.74	-35.92	-38.55	-41.78	-45.97	-52.34	-65.59	-52.34	-45.97	-41.78	-38.55	-35.92	-33.74	-31.92
0.00 :	-33.44	-35.66	-38.44	-42.01	-46.77	-53.65	-65.59	-100.00	-65.59	-53.65	-46.77	-42.01	-38.44	-35.66	-33.44
-4.00 :	-31.92	-33.74	-35.92	-38.55	-41.78	-45.97	-52.34	-65.59	-52.34	-45.97	-41.78	-38.55	-35.92	-33.74	-31.92
-8.00 :	-29.23	-30.65	-32.34	-34.40	-37.00	-40.52	-46.01	-53.65	-46.01	-40.52	-37.00	-34.40	-32.34	-30.65	-29.23
-12.00 :	-26.69	-28.11	-29.61	-31.46	-33.64	-37.08	-41.88	-46.77	-41.88	-37.08	-33.64	-31.46	-29.61	-28.11	-26.69
-16.00 :	-25.05	-26.19	-27.59	-29.34	-31.58	-34.59	-38.71	-42.01	-38.71	-34.59	-31.58	-29.34	-27.59	-26.19	-25.05
-20.00 :	-23.65	-24.74	-26.08	-27.75	-29.88	-32.64	-36.12	-38.44	-36.12	-32.64	-29.88	-27.75	-26.08	-24.74	-23.65
-24.00 :	-22.58	-23.64	-24.94	-26.54	-28.55	-31.07	-33.97	-35.66	-33.97	-31.07	-28.55	-26.54	-24.94	-23.64	-22.58
-28.00 :	-21.79	-22.83	-24.09	-25.62	-27.51	-29.78	-32.18	-33.44	-32.18	-29.78	-27.51	-25.62	-24.09	-22.83	-21.79

CROSS-POLARIZED ELEMENT PATTERN PHASE TABLE(DEG.)

*** FILE: TAPE6 *** 86/01/29. 08.59.53. PAGE 4

ELEV. ↓	AZIMUTH														
	-28.00	-24.00	-20.00	-16.00	-12.00	-8.00	-4.00	.00	4.00	8.00	12.00	16.00	20.00	24.00	28.00
28.00 :	-92.90	-96.37	-100.79	-106.59	-114.73	-127.24	-148.06	180.00	148.06	127.24	114.73	106.59	100.79	96.37	92.90
24.00 :	-86.75	-92.17	-96.44	-101.98	-109.72	-121.80	-143.27	180.00	143.27	121.80	109.72	101.98	96.44	92.17	88.75
20.00 :	-83.67	-87.31	-91.52	-96.88	-104.23	-115.71	-137.34	180.00	137.34	115.71	104.23	96.88	91.52	87.31	83.67
16.00 :	-77.78	-81.36	-85.66	-90.97	-96.03	-106.79	-129.91	180.00	129.91	108.79	98.03	90.97	85.66	81.36	77.78
12.00 :	-69.54	-73.42	-78.01	-83.53	-90.55	-100.69	-120.47	180.00	120.47	100.69	90.55	83.53	78.01	73.42	69.54
8.00 :	-57.01	-61.30	-66.44	-72.59	-80.14	-90.24	-108.19	180.00	108.19	90.24	80.14	72.59	66.44	61.30	57.01
4.00 :	-35.43	-39.46	-44.66	-51.43	-60.29	-72.15	-90.06	180.00	90.06	72.15	60.29	51.43	44.66	39.46	35.43
.00 :	.00	.00	.00	.00	.00	.00	.00	.00	.00	.00	.00	.00	.00	.00	.00
-4.00 :	35.43	39.46	44.66	51.43	60.29	72.15	90.06	-180.00	-90.06	-72.15	-60.29	-51.43	-44.66	-39.46	-35.43
-8.00 :	57.01	61.30	66.44	72.59	80.14	90.24	108.19	-180.00	-108.19	-90.24	-80.14	-72.59	-66.44	-61.30	-57.01
-12.00 :	69.54	73.42	78.01	83.53	90.55	100.69	120.47	-180.00	-120.47	-100.69	-90.55	-83.53	-78.01	-73.42	-69.54
-16.00 :	77.78	81.36	85.66	90.97	96.03	106.79	129.91	-180.00	-129.91	-108.79	-98.03	-90.97	-85.66	-81.36	-77.78
-20.00 :	83.67	87.31	91.52	96.88	104.23	115.71	137.34	-180.00	-137.34	-115.71	-104.23	-96.88	-91.52	-87.31	-83.67
-24.00 :	86.75	92.17	96.44	101.98	109.72	121.80	143.27	-180.00	-143.27	-121.80	-109.72	-101.98	-96.44	-92.17	-88.75
-28.00 :	92.90	96.37	100.79	106.59	114.73	127.24	148.06	-180.00	-148.06	-127.24	-114.73	-106.59	-100.79	-96.37	-92.90

ARRAY CG-POLARIZED PATTERN GAIN TABLE (DBI)

ELEV. ↓	AZIMUTH														
	-28.00	-24.00	-20.00	-16.00	-12.00	-8.00	-4.00	.00	4.00	8.00	12.00	16.00	20.00	24.00	28.00
28.00 :	-26.85	-18.20	-16.77	-24.45	-16.93	-7.78	-3.93	-2.78	-3.93	-7.78	-16.93	-24.45	-16.77	-18.20	-26.85
24.00 :	-27.79	-14.38	-11.69	-17.07	-13.76	-3.28	.89	2.12	.89	-3.28	-13.76	-17.07	-11.69	-14.38	-27.79
20.00 :	-33.93	-7.99	-4.11	-7.99	-7.93	3.94	8.40	9.71	8.40	3.94	-7.93	-7.98	-4.11	-7.99	-33.93
16.00 :	-28.94	-10.36	-5.34	-8.16	-10.78	2.51	7.22	8.58	7.22	2.51	-10.78	-8.16	-5.34	-10.36	-28.94
12.00 :	-30.53	-19.56	-13.53	-15.58	-20.42	-5.79	-.87	.54	-.87	-5.79	-20.42	-15.58	-13.53	-19.56	-30.53
8.00 :	-11.04	-3.68	3.17	1.64	-4.91	10.86	15.93	17.38	15.93	10.86	-4.91	1.64	3.17	-3.68	-11.04
4.00 :	-4.63	.86	8.26	7.04	-.62	15.94	21.10	22.58	21.10	15.94	-.62	7.04	8.26	.86	-4.63
.00 :	-2.78	2.12	9.71	8.58	.54	17.38	22.58	24.06	22.58	17.38	.54	8.58	9.71	2.12	-2.78
-4.00 :	-4.63	.86	8.26	7.04	-.62	15.94	21.10	22.58	21.10	15.94	-.62	7.04	8.26	.86	-4.63
-8.00 :	-11.04	-3.68	3.17	1.64	-4.91	10.86	15.93	17.38	15.93	10.86	-4.91	1.64	3.17	-3.68	-11.04
-12.00 :	-30.53	-19.56	-13.53	-15.58	-20.42	-5.79	-.87	.54	-.87	-5.79	-20.42	-15.58	-13.53	-19.56	-30.53
-16.00 :	-28.94	-10.36	-5.34	-8.16	-10.78	2.51	7.22	8.58	7.22	2.51	-10.78	-8.16	-5.34	-10.36	-28.94
-20.00 :	-33.93	-7.99	-4.11	-7.98	-7.93	3.94	8.40	9.71	8.40	3.94	-7.93	-7.98	-4.11	-7.99	-33.93
-24.00 :	-27.79	-14.38	-11.69	-17.07	-13.76	-3.28	.89	2.12	.89	-3.28	-13.76	-17.07	-11.69	-14.38	-27.79
-28.00 :	-26.85	-18.20	-16.77	-24.45	-16.93	-7.78	-3.93	-2.78	-3.93	-7.78	-16.93	-24.45	-16.77	-18.20	-26.85

ARRAY CROSS-POLARIZED PATTERN GAIN TABLE (DBI)

ELEV. ↓	AZIMUTH														
	-28.00	-24.00	-20.00	-16.00	-12.00	-8.00	-4.00	.00	4.00	8.00	12.00	16.00	20.00	24.00	28.00
28.00 :	-45.04	-37.65	-38.04	-47.55	-42.15	-35.43	-34.08	-34.22	-34.08	-35.43	-42.15	-47.55	-38.04	-37.65	-45.04
24.00 :	-47.21	-35.30	-34.29	-41.59	-40.54	-32.75	-31.58	-32.07	-31.58	-32.75	-40.54	-41.59	-34.29	-35.30	-47.21
20.00 :	-54.78	-30.40	-28.25	-34.13	-36.46	-27.54	-26.66	-27.72	-26.66	-27.54	-36.46	-34.13	-28.25	-30.40	-54.78
16.00 :	-51.48	-34.53	-31.33	-36.23	-41.37	-31.28	-30.80	-32.78	-30.80	-31.28	-41.37	-36.23	-31.33	-34.53	-51.48
12.00 :	-55.13	-45.90	-41.79	-46.05	-53.54	-42.35	-42.35	-45.87	-42.35	-42.35	-53.54	-46.05	-41.79	-45.90	-55.13
8.00 :	-38.15	-32.73	-28.61	-31.96	-41.39	-29.33	-29.88	-36.10	-29.88	-29.33	-41.39	-31.96	-28.61	-32.73	-38.15
4.00 :	-34.52	-31.37	-26.60	-30.82	-41.99	-29.82	-31.15	-42.97	-31.15	-29.82	-41.99	-30.82	-26.60	-31.37	-34.52

*** FILE: TAPE6 *** 86/01/29. C8.59.53. PAGE 5

.00 :	-34.22	-32.07	-27.72	-32.78	-45.87	-36.10	-42.97	-99.00	-42.97	-36.10	-45.87	-32.78	-27.72	-32.07	-34.22
-4.00 :	-34.52	-31.37	-26.60	-30.82	-41.99	-29.82	-31.15	-42.97	-31.15	-29.82	-41.99	-30.82	-26.60	-31.37	-34.52
-8.00 :	-38.15	-32.73	-28.01	-31.96	-41.39	-29.33	-29.88	-36.10	-29.88	-29.33	-41.39	-31.96	-28.01	-32.73	-38.15
-12.00 :	-55.13	-45.90	-41.79	-46.05	-53.54	-42.35	-42.35	-45.87	-42.35	-42.35	-53.54	-46.05	-41.79	-45.90	-55.13
-16.00 :	-51.48	-34.53	-31.33	-36.23	-41.37	-31.28	-30.80	-32.78	-30.80	-31.28	-41.37	-36.23	-31.33	-34.53	-51.48
-20.00 :	-54.78	-30.40	-28.25	-34.13	-36.46	-27.54	-26.66	-27.72	-26.66	-27.54	-36.46	-34.13	-28.25	-30.40	-54.78
-24.00 :	-47.21	-35.30	-34.29	-41.59	-40.54	-32.75	-31.58	-32.07	-31.58	-32.75	-40.54	-41.59	-34.29	-35.30	-47.21
-28.00 :	-45.04	-37.65	-38.04	-47.55	-42.15	-35.43	-34.08	-34.22	-34.08	-35.43	-42.15	-47.55	-38.04	-37.65	-45.04

JPLAP2F(VERS.2.0):FLANAR ARRAY PATTERN-CROSS-POLARIZED
DE LOSS (SUBTR. FROM GAINS BEFORE PRINTING) = .00

GAIN MATRIX (DB)

```

-26.85-18.20-16.77-24.45-16.93 -7.78 -3.93 -2.78 -3.93 -7.78-16.93-24.45-16.77-18.20-26.85
-27.79-14.38-11.69-17.07-13.76 -3.28 .89 2.12 .89 -3.28-13.76-17.07-11.69-14.38-27.79
-33.93 -7.99 -4.11 -7.98 -7.93 3.94 8.40 9.71 8.40 3.94 -7.93 -7.98 -4.11 -7.99-33.93
-28.94-10.36 -5.34 -8.16-10.78 2.51 7.22 8.58 7.22 2.51-10.78 -8.16 -5.34-10.36-28.94
-30.53-19.56-13.53-15.58-20.42 -5.79 -.87 .54 -.87 -5.79-20.42-15.58-13.53-19.56-30.53
-11.04 -3.68 3.17 1.64 -4.91 10.86 15.93 17.38 15.93 10.86 -4.91 1.64 3.17 -3.68-11.04
-4.63 .86 8.26 7.04 -.62 15.94 21.10 22.58 21.10 15.94 -.62 7.04 8.26 .86 -4.63
-2.78 2.12 9.71 8.58 .54 17.38 22.58 24.06 22.58 17.38 .54 8.58 9.71 2.12 -2.78
-4.63 .86 8.26 7.04 -.62 15.94 21.10 22.58 21.10 15.94 -.62 7.04 8.26 .86 -4.63
-11.04 -3.68 3.17 1.64 -4.91 10.86 15.93 17.38 15.93 10.86 -4.91 1.64 3.17 -3.68-11.04
-30.53-19.56-13.53-15.58-20.42 -5.79 -.87 .54 -.87 -5.79-20.42-15.58-13.53-19.56-30.53
-28.94-10.36 -5.34 -8.16-10.78 2.51 7.22 8.58 7.22 2.51-10.78 -8.16 -5.34-10.36-28.94
-33.93 -7.99 -4.11 -7.98 -7.93 3.94 8.40 9.71 8.40 3.94 -7.93 -7.98 -4.11 -7.99-33.93
-27.79-14.38-11.69-17.07-13.76 -3.28 .89 2.12 .89 -3.28-13.76-17.07-11.69-14.38-27.79
-26.85-18.20-16.77-24.45-16.93 -7.78 -3.93 -2.78 -3.93 -7.78-16.93-24.45-16.77-18.20-26.85

```

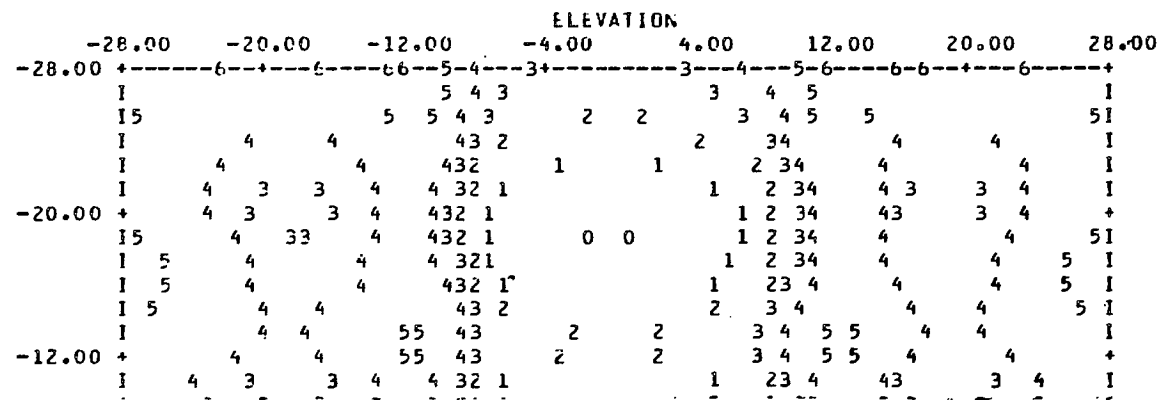
AZIMUTH AXIS SCALE = 8.00000 DEG/INCH

ELEVATION AXIS SCALE = 8.00000 DEG/INCH

BORESIGHT AZ = .000 EL = .000 DEG

CONTCUR SYMBOLS AND CORRESPONDING DB VALUES

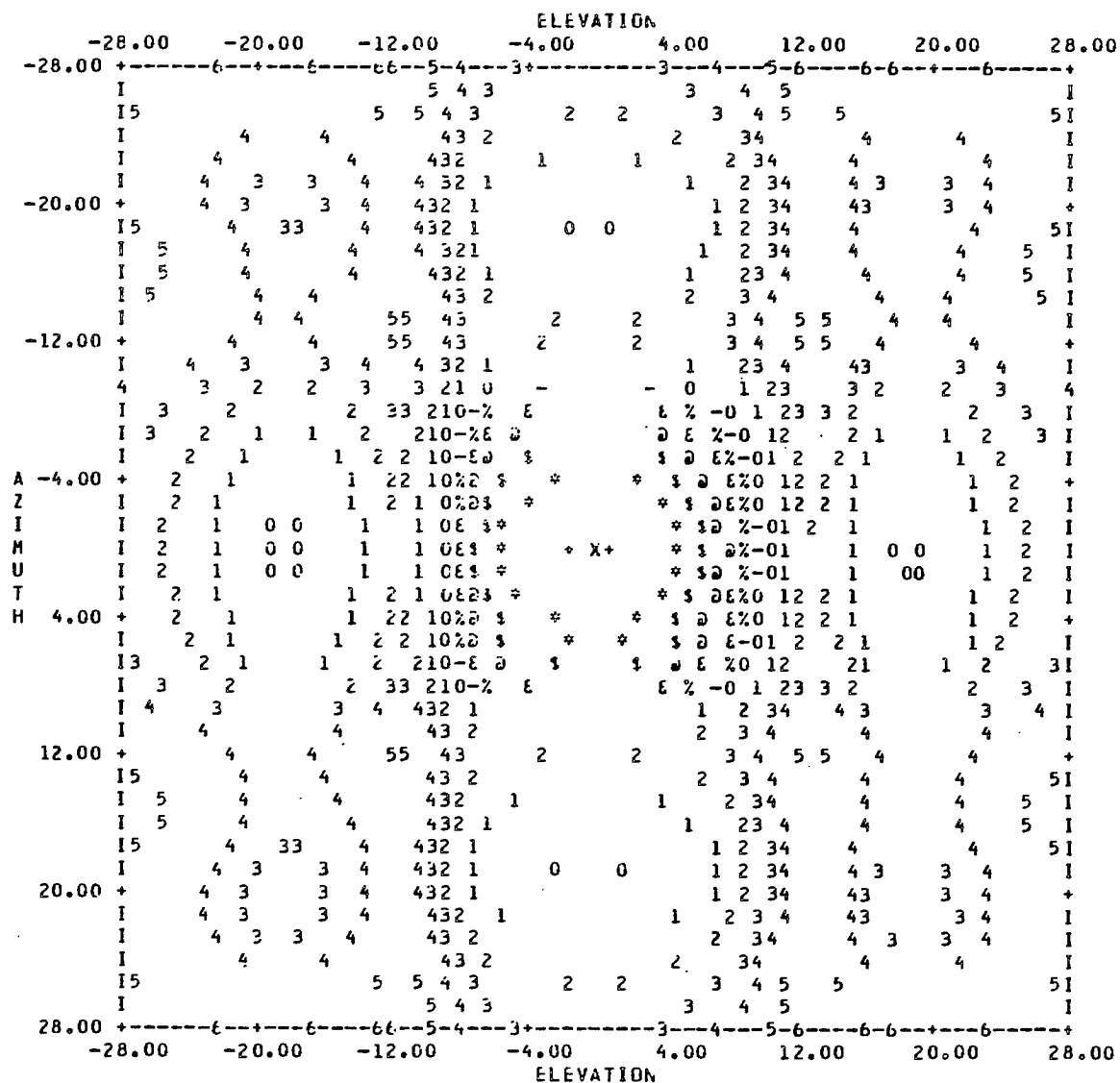
SYMBOL	#	+	*	%	@	E	%	-	0	1	2	3	4	5	6
DB VALUE	26.00	24.00	22.00	20.00	18.00	16.00	14.00	12.00	10.00	5.00	.00	-5.00	-10.00	-20.00	-30.00



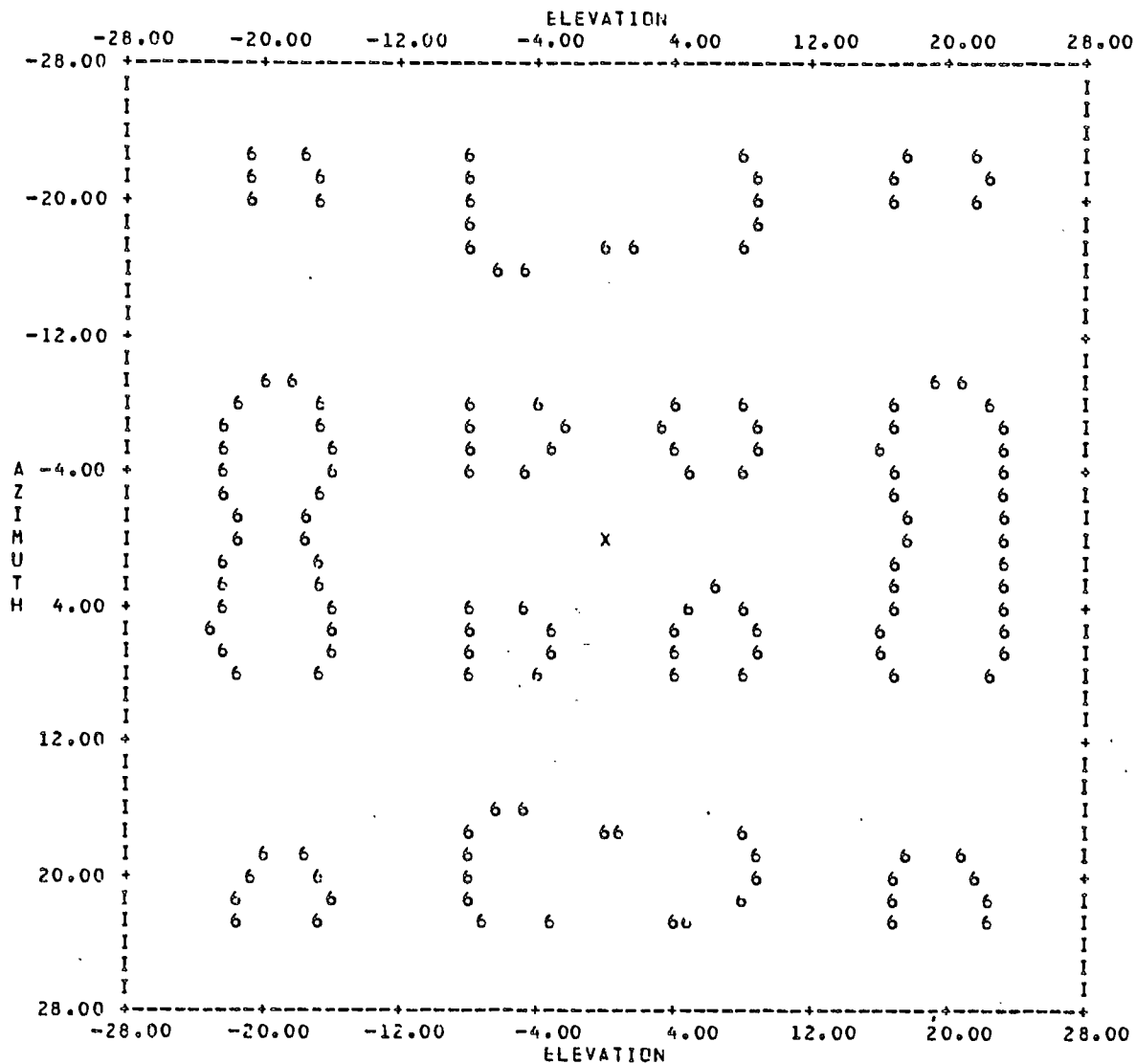
RDR: HT AZ = .000 EL = .000 DEG

CONTOUR SYMBOLS AND CORRESPONDING DB VALUES

SYMBOL	#	+	*	%	0	1	2	3	4	5	6
DB VALUE	26.00	24.00	22.00	20.00	18.00	16.00	14.00	12.00	10.00	5.00	.00 -5.00-10.00-20.00-30.00



CON DEV



09.01.14.UCLP, AA, TFRNT01,

0.570KLS.

** END OF LISTING **


```

7104 FORMAT(1X,'JPLAP2F(VERS.2.3):PLANAR ARRAY PATTERN-',
2      'COMPUTATION')
      TODAY=DATE()
      NOW=TIME()
      WRITE(6,6110) TODAY,NOW
6110 FORMAT(25X,A,10X,A/)
      READ(5,5120) UNITS
5120 FORMAT(A2)
      READ(5,*) NX1,DX1,NY1,DY1
      CALL READL(JEL,ELDATA)
      CALL READL(JEX,NX1,NY1,A,XI,XIO,AX,AY,XIXD,XIYO)
      READ(5,*) F
      READ(5,*) AZSD,AZEO,NAZ,ELSD,ELEO,NEL
      READ(5,*) IPAD,IPEP,IPGT
C
C NORMALIZE ELEMENT POWERS
C
      PSUM=0.
      DO 140 MM=1,NX1
        DO 130 NN=1,NY1
          P(MM,NN)=A(MM,NN)**2
          PSUM=PSUM+P(MM,NN)
        130 CONTINUE
      140 CONTINUE
      DO 160 MM=1,NX1
        DO 150 NN=1,NY1
          P(MM,NN)=P(MM,NN)/PSUM
        150 CONTINUE
      160 CONTINUE
C
C CONVERT OX,OY TO METRES
C
      DX=CONVERT(DX1,UNITS)
      DY=CONVERT(DY1,UNITS)
C
C ECHO ARRAY GEOMETRY AND EXCITATION DATA
C
      CALL WRITAO(IPAD,NX1,OX1,NY1,OY1,A,XID,AX,AY,XIXO,XIYO,UNITS,JEX)
C
C ECHO ELEMENT DESCRIPTION
C
      CALL WRITEL(JEL,ELOATA,UNITS)
C
      WRITE(6,6170) F
6170 FORMAT(/16X,'FREQUENCY : ',F7.1,' MHZ')
      WRITE(6,6180) AZSD,AZEO,NAZ
6180 FORMAT(16X,'AZIMUTH SCAN : ',F7.2,' TO ',F7.2,' DEGREES ( ',
1      I2,' POINTS )')
      WRITE(6,6190) ELSD,ELEO,NEL
6190 FORMAT(16X,'ELEVATION SCAN : ',F7.2,' TO ',F7.2,' DEGREES ( ',
1      I2,' POINTS )')
C
C CONVERT AZ,EL DATA TO RADIANs
C
      AZS=AZSD/RAD
      AZE=AZEO/RAD
      ELS=ELSD/RAD
      ELE=ELEO/RAD
C
C COMPUTE ELEMENT PATTERN
C
      CALL EP(JEL,ELOATA,F,AZS,AZE,NAZ,ELS,ELE,NEL,GE1,GE2,
2      ALPHA1,ALPHA2,UNITS)
      IF(IPEP.EQ.1) CALL WRITEP(AZSD,AZEO,NAZ,ELSD,ELEO,NEL,GE1,GE2,
2      ALPHA1,ALPHA2)
C
C START ANGLE LOOP
C
      BETA=2.*PI*F/C
      GEPEAK=BETA*BETA*OX*DY/PI
      OAZ=(AZE-AZS)/(NAZ-1)
      DEL=(ELE-ELS)/(NEL-1)
      DO 290 I=1,NAZ
        AZ=AZS+(I-1)*DAZ
        DO 280 J=1,NEL
          EL=ELS+(J-1)*DEL
          CALL CHANGE(AZ,EL,TH,PH)
          ST=SIN(TH)
          SP=SIN(PH)
          CP=COS(PH)

```

```

SUM1=CMPLX(0.,0.)
SUM2=CMPLX(0.,0.)
C
C START ELEMENT LOOP
C
      DO 250 MM=1,NX1
        M=MM-(NX1+1)/2
        DO 240 NN=1,NY1
          N=NN-(NY1+1)/2
          PS1=XI(MM,NN)+ALPHA1(I,J)+BETA*ST*(M*DX*CP+N*DY*SP)
          SUM1=SUM1+SQRT(P(MM,NN))*CEXP(CMPLX(0.,PS1))
          PS2=XI(MM,NN)+ALPHA2(I,J)+BETA*ST*(M*DX*CP+N*DY*SP)
          SUM2=SUM2+SQRT(P(MM,NN))*CEXP(CMPLX(0.,PS2))
240        CONTINUE
250      CONTINUE
          G=GEPEAK*GE1(I,J)*CABS(SUM1)**2
          GDB1(I,J)=10.*BLOG10(G,1.2589254E-10)
          G=GEPEAK*GE2(I,J)*CABS(SUM2)**2
          GDB2(I,J)=10.*BLOG10(G,1.2589254E-10)
280      CONTINUE
290    CONTINUE
C
C OUTPUT TO CONTOUR PLOTTING FILES : CD-POL TO TAPE7,CRDSS-POL TO TAPE8
C
      WRITE(7,7310) AZSD,AZED,NAZ,ELSD,ELED,NEL
7310  FORMAT(' ',2F10.3,I6,2F10.3,I6)
      DD 330 J=NEL,1,-1
      WRITE(7,7320) (GDB1(I,J),I=1,NAZ)
7320  FORMAT(17(1X,F7.2))
330    CONTINUE
C
      WRITE(8,8340) AZSD,AZED,NAZ,ELSD,ELED,NEL
8340  FORMAT(' ',2F10.3,I6,2F10.3,I6)
      DD 360 J=NEL,1,-1
      WRITE(8,8350) (GDB2(I,J),I=1,NAZ)
8350  FORMAT(17(1X,F7.2))
360    CONTINUE
C
C OPTIONAL OUTPUT TO MAIN OUTPUT FILE
C
      IF(IPGT.EQ.1) THEN
        WRITE(6,6370)
6370    FORMAT(/T15,'ARRAY CO-POLARIZED PATTERN GAIN TABLE (DBI)')
        CALL WRITGT(AZSD,AZED,NAZ,ELSD,ELED,NEL,GDB1,6)
        WRITE(6,6380)
6380    FORMAT(/T15,'ARRAY CRDSS-POLARIZED PATTERN GAIN TABLE (DBI)')
        CALL WRITGT(AZSD,AZED,NAZ,ELSD,ELED,NEL,GDB2,6)
      END IF
C
      STOP
      END

      FUNCTION BLOG10(X,BOUND)
*
* COMPUTES BASE 10 LOGARITHM OF X UNLESS X LESS THAN BOUND
* IN WHICH CASE RETURNS LOG OF BOUND.PREVENTS LOG(0) ERRORS.
*
      IF(X.LE.BOUND)GO TO 10
      BLOG10=ALOG10(X)
      RETURN
10    BLOG10=ALOG10(BOUND)
      RETURN
      END

      SUBROUTINE CHANGE(AZ,EL,TH,PH)
C
C TRANSFORMS AZIM./ELEV. COORDINATES INTO EQUIVALENT
C THETA/PHI COORDINATES. ALL VALUES ARE IN RADIAN.
C WRITTEN DEC.3/85 - S.KAVANAGH
C
      TH=ACOS(COS(EL)*COS(AZ))
C
      IF(TH.LT.0.001) THEN
        TH=0.
        PH=0.
        RETURN
      ELSE
        IF(AZ.LT.-0.001) THEN

```

```

        PH=ASIN(SIN(EL)/SIN(TH))
        RETURN
    ELSE IF(AZ.GT.0.001) THEN
        PH1=ASIN(SIN(EL)/SIN(TH))
        PH=3.141592654-PH1
        RETURN
    ELSE
        PH=1.570796327
        IF(EL.LT.0.) PH=-1.570796327
        RETURN
    END IF
END IF
C
END

FUNCTION CONVERT(X,UNITS)
C
C CONVERTS X ( IN MM,CM,M,INCHES OR FEET ) TO METRES
C WRITTEN NOV.29/85 - S.KAVANAGH
C
    CHARACTER*2 UNITS
C
    IF(UNITS.EQ.'MM') THEN
        CONVERT=X*0.001
    ELSE IF(UNITS.EQ.'CM') THEN
        CONVERT=X*0.01
    ELSE IF(UNITS.EQ.'M '.OR.UNITS.EQ.' M') THEN
        CONVERT=X
    ELSE IF(UNITS.EQ.'IN') THEN
        CONVERT=X*0.0254
    ELSE IF(UNITS.EQ.'FT') THEN
        CONVERT=X*0.3048
    ELSE
        B900 WRITE(6,6900) UNITS
        FORMAT(' *** ERROR IN SUBROUTINE CONVERT: UNKNOWN UNIT ',
1          'NAME ',A2,'''')
        CONVERT=0.
    END IF
    RETURN
END

SUBROUTINE EP(JEL,ELDATA,F,AZS,AZE,NAZ,ELS,ELE,NEL,GE1,GE2,
2      ALPHA1,ALPHA2,UNITS)
C
C COMPUTES ELEMENT PATTERN
C WRITTEN DEC.2/85 - S.KAVANAGH
C PRELIMINARY VERSION - ISOTROPIC ELEMENTS ONLY
C UPDATED JAN.21/85 - S.KAVANAGH
C ACCEPTS ISOTROPIC OR RECTANGULAR PATCH ELEMENTS
C
    CHARACTER*2 UNITS
    REAL GE1(20,20),ALPHA1(20,20),GE2(20,20),ALPHA2(20,20)
    REAL K,KO,ELDATA(10)
    COMPLEX ETH,EPH,ERC,ELC
    DATA C/300./,PI/3.1415926535/
C
C ISOTROPIC ELEMENTS
C
    IF(JEL.EQ.0) THEN
        DO 120 I=1,NAZ
            DO 110 J=1,NEL
                GE1(I,J)=1.
                ALPHA1(I,J)=0.
                GE2(I,J)=0.
                ALPHA2(I,J)=0.
110             CONTINUE
120             CONTINUE
        RETURN
C
C RECTANGULAR PATCH ELEMENTS
C
    ELSE IF(JEL.EQ.1) THEN
        IPOL=NINT(ELDATA(1))
        XX=CONVERT(ELDATA(2),UNITS)
        YY=CONVERT(ELDATA(3),UNITS)
        T=CONVERT(ELDATA(4),UNITS)
        ER=ELDATA(5)
        KO=2.*PI*F/C

```

```

      K=KO*SQRT(ER)
C
C BEGIN ANGLE LOOP
C
      DAZ=(AZE-AZS)/(NAZ-1)
      DEL=(ELE-ELS)/(NEL-1)
      DO 190 I=1,NAZ
        AZ=AZS+(I-1)*DAZ
        DO 180 J=1,NEL
          EL=ELS+(J-1)*DEL
          CALL CHANGE(AZ,EL,TH,PH)
          CP=COS(PH)
          SP=SIN(PH)
          CT=COS(TH)
          ST=SIN(TH)
          C1=COS(K*T*CT)/COS(K*T)
C
C COMPUTE THETA,PHI COMPONENTS FOR AZ AND/OR EL EXCITATIONS
C
      IF(IPOL.EQ.1.OR.IPOL.EQ.3.OR.IPOL.EQ.4)
        2 CALL PATCH1(YY,XX,CP,CT,SP,ST,C1,KO,ETHAZ,EPHAZ)
      IF(IPOL.EQ.2.OR.IPOL.EQ.3.OR.IPOL.EQ.4)
        2 CALL PATCH2(YY,XX,CP,CT,SP,ST,C1,KO,ETHEL,EPHEL)
C
C LINEAR AZIMUTH POLARIZATION
C
      IF(IPOL.EQ.1) THEN
        CALL XVCOMP(ETHAZ,EPHAZ,AZ,EL,TH,PH,EAZ,EEL)
        GE1(I,J)=EAZ**2
        GE2(I,J)=EEL**2
        ALPHA1(I,J)=0.
        IF(EAZ.LT.0.) ALPHA1(I,J)=PI
        ALPHA2(I,J)=0.
        IF(EEL.LT.0.) ALPHA2(I,J)=PI
C
C LINEAR ELEVATION POLARIZATION
C
      ELSE IF(IPOL.EQ.2) THEN
        CALL XVCOMP(ETHEL,EPHEL,AZ,EL,TH,PH,EAZ,EEL)
        GE1(I,J)=EEL**2
        GE2(I,J)=EAZ**2
        ALPHA1(I,J)=0.
        IF(EEL.LT.0.) ALPHA1(I,J)=PI
        ALPHA2(I,J)=0.
        IF(EAZ.LT.0.) ALPHA2(I,J)=PI
C
C RIGHT-HAND CIRCULAR POLARIZATION
C
      ELSE IF(IPOL.EQ.3) THEN
        ETH=CMPLX(ETHAZ,0.)-CMPLX(0.,ETHEL)
        EPH=CMPLX(EPHAZ,0.)-CMPLX(0.,EPHEL)
        ERC=0.5*(ETH+CMPLX(0.,1.)*EPH)
        ELC=0.5*(ETH-CMPLX(0.,1.)*EPH)
        GE1(I,J)=CABS(ERC)**2
        GE2(I,J)=CABS(ELC)**2
        ALPHA1(I,J)=PHASE(ERC)+PH
        IF(ALPHA1(I,J).LT.-PI) ALPHA1(I,J)=ALPHA1(I,J)+2.*PI
        IF(ALPHA1(I,J).GT.PI) ALPHA1(I,J)=ALPHA1(I,J)-2.*PI
        ALPHA2(I,J)=PHASE(ELC)-PH
        IF(ALPHA2(I,J).LT.-PI) ALPHA2(I,J)=ALPHA2(I,J)+2.*PI
        IF(ALPHA2(I,J).GT.PI) ALPHA2(I,J)=ALPHA2(I,J)-2.*PI
C
C LEFT-HAND CIRCULAR POLARIZATION
C
      ELSE IF(IPOL.EQ.4) THEN
        ETH=CMPLX(ETHAZ,0.)+CMPLX(0.,ETHEL)
        EPH=CMPLX(EPHAZ,0.)+CMPLX(0.,EPHEL)
        ERC=0.5*(ETH+CMPLX(0.,1.)*EPH)
        ELC=0.5*(ETH-CMPLX(0.,1.)*EPH)
        GE1(I,J)=CABS(ELC)**2
        GE2(I,J)=CABS(ERC)**2
        ALPHA1(I,J)=PHASE(ELC)-PH
        IF(ALPHA1(I,J).LT.-PI) ALPHA1(I,J)=ALPHA1(I,J)+2.*PI
        IF(ALPHA1(I,J).GT.PI) ALPHA1(I,J)=ALPHA1(I,J)-2.*PI
        ALPHA2(I,J)=PHASE(ERC)+PH
        IF(ALPHA2(I,J).LT.-PI) ALPHA2(I,J)=ALPHA2(I,J)+2.*PI
        IF(ALPHA2(I,J).GT.PI) ALPHA2(I,J)=ALPHA2(I,J)-2.*PI
      END IF

```

180 CONTINUE

190 CONTINUE

```

      RETURN
C
C ERROR CONDITION
C
      ELSE
        WRITE(6,6900) JEL
6900      FORMAT(' *** ERROR IN SUBROUTINE EP: ELEMENT TYPE ',I2,
              1      ' UNKNOWN. ')
      END IF
      RETURN
      END

```

```

      SUBROUTINE PATCH1(A,B,CP,CT,SP,ST,C1,KO,ETHAZ,EPHAZ)
C
C IMPLEMENTS CARVER + MINK EQUATIONS (45,46) FROM AP JAN.81
C "A" IS LENGTH OF RADIATING EDGE ( PARALLEL TO Y AXIS )
C BASED ON SUBROUTINE PATCH IN PROGRAM JPCMA3F
C WRITTEN JAN.20/86 - S.KAVANAGH
C

```

```

      REAL KO
C
      G1=KO*0.5*A*ST*SP
      IF(ABS(G1).LT.0.0001) THEN
        G=1.
      ELSE
        G=SIN(G1)/G1
      END IF
      H=COS(KO*0.5*B*ST*CP)
      ETHAZ=-C1*G*H*CP
      EPHAZ=C1*G*H*CT*SP
C
      RETURN
      END

```

```

      SUBROUTINE PATCH2(A,B,CP,CT,SP,ST,C1,KO,ETHEL,EPHEL)
C
C SIMILAR TO CARVER + MINK EQUATIONS (45,46) FROM AP JAN.81
C EXCEPT FOR Y(ELEVATION) POLARIZED PATCH.
C "B" IS LENGTH OF RADIATING EDGE ( PARALLEL TO X AXIS )
C BASED ON SUBROUTINE PATCH IN PROGRAM JPCMA3F
C WRITTEN JAN.20/86 - S.KAVANAGH
C

```

```

      REAL KO
C
      G1=KO*0.5*B*ST*CP
      IF(ABS(G1).LT.0.0001) THEN
        G=1.
      ELSE
        G=SIN(G1)/G1
      END IF
      H=COS(KO*0.5*A*ST*SP)
      ETHEL=-C1*G*H*SP
      EPHEL=-C1*G*H*CT*CP
C
      RETURN
      END

```

```

      FUNCTION PHASE(C)
C
C FINDS ANGLE OF POLAR FORM OF COMPLEX ARGUMENT C.
C IF RE(C) AND IM(C) ARE BOTH ZERO THEN THE RESULT IS ZERO.
C RESULT IS IN RADIANS
C
C WRITTEN JAN.21/86 - S.KAVANAGH
C

```

```

      COMPLEX C
      DATA PI/3.141592654/
C
      CR=REAL(C)
      CI=AIMAG(C)
      IF(ABS(CR).LT.0.00001.AND.ABS(CI).LT.0.00001) THEN
        PHASE=0.
        RETURN
      END IF
      PHASE=ATAN2(CI,CR)
      RETURN
      END

```

```

SUBROUTINE READEL(JEL,ELDATA)
C
C READS DATA DESCRIBING ELEMENT
C WRITTEN DEC.2/85-S.KAVANAGH
C PRELIMINARY VERSION: ISOTROPIC ELEMENTS ONLY
C MODIFIED JAN.20/86-S.KAVANAGH
C ACCEPTS ISOTROPIC OR RECTANGULAR PATCH ELEMENTS
C
      REAL ELDATA(10)
C
      READ(5,*) JEL
      IF(JEL.EQ.0) RETURN
      IF(JEL.EQ.1) THEN
        READ(5,*) IPOL,(ELDATA(I),I=2,5)
        ELDATA(1)=FLOAT(IPOL)
        RETURN
      END IF
      WRITE(6,6900) JEL
6900 FORMAT(' *** ERROR IN SUBROUTINE READEL: ELEMENT TYPE ',
1         I2,' UNKNOWN. ISOTROPIC USED.')
      JEL=0
      RETURN
      END

SUBROUTINE READEX(JEX,NX1,NY1,A,XI,XID,AX,AY,XIXD,XIYD)
C
C READS DATA DESCRIBING AMPLITUDE AND PHASE EXCITATIONS AND
C COMPUTES ACTUAL ELEMENT EXCITATIONS.
C
C WRITTEN DEC.3/85-S.KAVANAGH
C
      DIMENSION A(35,35),XI(35,35),XID(35,35)
      DIMENSION AX(35),AY(35),XIXD(35),XIYD(35)
      DATA RAD/57.29577951/
C
      READ(5,*) JEX
      50 CONTINUE
C
C UNIFORM IN-PHASE DISTRIBUTION
C
      IF(JEX.EQ.1) THEN
        DO 150 MM=1,NX1
          AX(MM)=1.
          XIXD(MM)=0.
          DO 140 NN=1,NY1
            A(MM,NN)=1.
            XI(MM,NN)=0.
            XID(MM,NN)=0.
140          CONTINUE
150        CONTINUE
          DO 160 NN=1,NY1
            AY(NN)=1.
            XIYD(NN)=0.
160          CONTINUE
          RETURN
        END IF
C
C UNIFORM AMPLITUDE DISTRIBUTION WITH CONSTANT
C ELEMENT-TO-ELEMENT PHASE DIFFERENCE
C
      IF(JEX.EQ.2) THEN
        READ(5,*) DXIXD,DXIYD
        DO 210 MM=1,NX1
          M=MM-(NX1+1)/2
          AX(MM)=1.
          XIXD(MM)=M*DXIXD
210        CONTINUE
          DO 220 NN=1,NY1
            N=NN-(NY1+1)/2
            AY(NN)=1.
            XIYD(NN)=N*DXIYD
220          CONTINUE
          DO 250 MM=1,NX1
            DO 240 NN=1,NY1
              A(MM,NN)=1.
              XID(MM,NN)=XIXD(MM)+XIYD(NN)
              XI(MM,NN)=XID(MM,NN)/RAD
            
```



```

240         CONTINUE
250         CONTINUE
          RETURN
        END IF
C
C READ X- AND Y- AMPLITUDE DISTRIBUTIONS
C
      IF(JEX.EQ.3.OR.JEX.EQ.4) THEN
        READ(5,*) (AX(MM),MM=1,NX1)
        READ(5,*) (AY(NN),NN=1,NY1)
        DO 350 MM=1,NX1
          DO 340 NN=1,NY1
            A(MM,NN)=AX(MM)*AY(NN)
          CONTINUE
        CONTINUE
      340
      350         CONTINUE
        END IF
C
C READ CONSTANT ELEMENT-TO-ELEMENT PHASE DIFFERENCES
C
      IF(JEX.EQ.3) THEN
        READ(5,*) DXIXD,DXIYD
        DO 360 MM=1,NX1
          M=MM-(NX1+1)/2
          XIXD(MM)=M*DXIXD
        360         CONTINUE
          DO 370 NN=1,NY1
            N=NN-(NY1+1)/2
            XIYD(NN)=N*DXIYD
          CONTINUE
        370         DO 390 MM=1,NX1
          DO 380 NN=1,NY1
            XID(MM,NN)=XIXD(MM)+XIYD(NN)
            XI(MM,NN)=XID(MM,NN)/RAD
          CONTINUE
        380         CONTINUE
        390         CONTINUE
          RETURN
        END IF
C
C READ X- AND Y- PHASE DISTRIBUTIONS (DEGREES)
C
      IF(JEX.EQ.4) THEN
        READ(5,*) (XIXD(MM),MM=1,NX1)
        READ(5,*) (XIYD(NN),NN=1,NY1)
        DO 450 MM=1,NX1
          DO 440 NN=1,NY1
            XID(MM,NN)=XIXD(MM)+XIYD(NN)
            XI(MM,NN)=XID(MM,NN)/RAD
          CONTINUE
        440         CONTINUE
        450         CONTINUE
          RETURN
        END IF
C
C ARBITRARY EXCITATIONS
C
      IF(JEX.EQ.5) THEN
        DO 520 NN=1,NY1
          READ(5,*)( A(MM,NN),MM=1,NX1)
        520         CONTINUE
          DO 540 NN=1,NY1
            READ(5,*) (XID(MM,NN),MM=1,NX1)
            DO 530 MM=1,NX1
              XI(MM,NN)=XID(MM,NN)/RAD
            CONTINUE
          CONTINUE
        530         CONTINUE
        540         CONTINUE
          RETURN
        END IF
C
C ERROR PROCESSING
C
      WRITE(6,6900) JEX
6900  FORMAT(' *** ERROR IN SUBROUTINE READEX: EXCITATION TYPE ',I4,
1      ' UNKNOWN. UNIFORM IN-PHASE ASSUMED')
      JEX=1
      GO TO 50
C
      END

```

SUBROUTINE WRITAD(IPAO,NX1,DX1,NY1,DY1,A,XID,AX,AY,XIXD,XIYD,
1. UNITS,JEX)

RPT/MST/2500/001

C
C WRITES DATA DESCRIBING ELEMENT POSITIONS AND EXCITATIONS TO TAPES
C
C WRITTEN NOV.29/85 - S.KAVANAGH
C MODIFIED MAR.17/86 - S.KAVANAGH - MINOR CHANGE IN OUTPUT FORMAT
C

```

      CHARACTER*2 UNITS
      REAL A(35,35),XID(35,35),AX(35),AY(35),XIXD(35),XIYD(35)
C
      IF(IPAD.EQ.0) THEN
        WRITE(6,6100) NX1
        6100  FORMAT(16X,'NO.DF ELEMENTS IN X-DIRECTION: ',I3)
        WRITE(6,6110) DX1,UNITS
        6110  FORMAT(16X,'X-DIRECTION ELEMENT SPACING: ',F7.3,1X,A)
        WRITE(6,6120) NY1
        6120  FDMAT(16X,'NO.DF ELEMENTS IN Y-DIRECTION: ',I3)
        WRITE(6,6130) DY1,UNITS
        6130  FDMAT(16X,'Y-DIRECTION ELEMENT SPACING: ',F7.3,1X,A)
        IF(JEX.EQ.1) THEN
          WRITE(6,6140)
          6140  FORMAT(16X,'UNIFORM IN-PHASE APERTURE DISTRIBUTION')
        ELSE
          WRITE(6,6150)
          6150  1  FORMAT(/16X,'DISTRIBUTION IN X-DIRECTION'//16X,' M',T20,
            'AMPLITUDE',T34,'DB',T40,'PHASE(DEG.)'//)
          DO 165 MM=1,NX1
            AXDB=20.*BLOG10(AX(MM),1.E-5)
            M=MM-(NX1+1)/2
            WRITE(6,6160) M,AX(MM),AXDB,XIXD(MM)
            6160  165  FORMAT(15X,I3,T20,F8.5,T31,F7.2,T41,F7.2)
            CONTINUE
          WRITE(6,6170)
          6170  1  FDMAT(/16X,'DISTRIBUTION IN Y-DIRECTION'//16X,' N',T20,
            'AMPLITUDE',T34,'DB',T40,'PHASE(DEG.)'//)
          DO 180 NN=1,NY1
            AYDB=20.*BLOG10(AY(NN),1.E-5)
            N=NN-(NY1+1)/2
            WRITE(6,6160) N,AY(NN),AYDB,XIYD(NN)
            180    CONTINUE
          END IF
        ELSE
          WRITE(6,6210) UNITS
          6210  1  FORMAT(/25X,'ELEMENT POSITIONS AND EXCITATIONS'//,T16
            'ELEMENT',T28,'POSITION(',A2,')',T51,'AMPLITUDE',
            2    T71,'PHASE'/T17,'M',T21,'N',T30,'X',T40,'Y',T47,
            3    'NUMERICAL',T61,'DB',T70,'DEGREES'//)
          DO 270 MM=1,NX1
            M=MM-(NX1+1)/2
            X=M*DX1
            DO 260 NN=1,NY1
              N=NN-(NY1+1)/2
              ADB=20.*BLOG10(A(MM,NN),1.E-5)
              Y=N*DY1
              WRITE(6,6220) M,N,X,Y,A(MM,NN),ADB,XID(MM,NN)
              6220  1  FORMAT(T15,I3,T20,I3,T26,F8.3,T36,F8.3,T48,F8.5,
                T58,F7.2,T69,F8.3)
              260    CONTINUE
            270    CONTINUE
          END IF
          RETURN
        END

```

SUBROUTINE WRITEL(JEL,ELDATA,UNITS)

C
C WRITES DESCRIPTION OF ELEMENT
C WRITTEN DEC.2/85 - S.KAVANAGH
C PRELIMINARY VERSION - ISOTROPIC ELEMENTS ONLY
C MODIFIED JAN.20/86 - S.KAVANAGH
C ACCEPTS ISOTROPIC AND RECTANGULAR PATCH ELEMENTS
C

```

      REAL ELDATA(10)
      CHARACTER*2 UNITS
      CHARACTER*4 POLNAME(4)
      DATA POLNAME/'AZIM','ELEV','RHCP','LHCP'/

```

C
C ISDTROPIC ELEMENTS
C

```

      IF(JEL.EQ.0) THEN
        WRITE(6,6010)

```

RPT/MST/2500/001

```

6010    FORMAT(/,16X,'ELEMENTS ARE ISOTROPIC RADIATORS')
        RETURN
C
C RECTANGULAR MICROSTRIP PATCH ELEMENTS
C
        ELSE IF(JEL.EQ.1) THEN
            WRITE(6,6110)
6110    FORMAT(/,16X,'ELEMENTS ARE RECTANGULAR MICROSTRIP PATCHES')
            IPOL=NINT(ELDATA(1))
            WRITE(6,6120) POLNAME(IPOL)
6120    FORMAT(18X,'POLARIZATION : ',T40,A4)
            WRITE(6,6130) ELDATA(2),UNITS
6130    FORMAT(18X,'AZIM.DIMENSION : ',T40,F7.3,2X,A2)
            WRITE(6,6140) ELDATA(3),UNITS
6140    FORMAT(18X,'ELEV.DIMENSION : ',T40,F7.3,2X,A2)
            WRITE(6,6150) ELDATA(4),UNITS
6150    FORMAT(18X,'SUBSTRATE THICKNESS : ',T40,F7.3,2X,A2)
            WRITE(6,6160) ELDATA(5)
6160    FORMAT(18X,'SUBSTR.DIEL.CONST. : ',T40,F7.3,2X,A2)
C
C UNKNOWN ELEMENT TYPE
C
        ELSE
            WRITE(6,6900) JEL
6900    FORMAT(' ***ERROR IN SUBROUTINE WRITEL: ELEMENT TYPE ',
1          I2,' UNKNOWN.')
            END IF
            RETURN
            END

        SUBROUTINE WRITEL(AZSD,AZED,NAZ,ELSD,ELED,NEL,GE1,GE2,ALPHA1,
2          ALPHA2)
C
C WRITES ELEMENT GAIN AND PHASE MATRICES 'GE' AND 'ALPHA' TO TAPE6
C WRITTEN NOV.29/85 - S.KAVANAGH
C MODIFIED JAN.21/86 - S.KAVANAGH - INCORPORATES CO- AND CROSS-POL
C
        REAL GE1(20,20),GEDB(20,20),ALPHA1(20,20),ALPHAD(20,20)
        REAL GE2(20,20),ALPHA2(20,20)
C
        WRITE(6,6100)
6100    FORMAT(/T15,'CO-POLARIZED ELEMENT PATTERN GAIN TABLE (DBI)')
        DO 120 I=1,NAZ
            DO 110 J=1,NEL
                GEDB(I,J)=10.*BLOG10(GE1(I,J),1.E-10)
                ALPHAD(I,J)=57.29577951*ALPHA1(I,J)
110        CONTINUE
120    CONTINUE
        CALL WRITGT(AZSD,AZED,NAZ,ELSD,ELED,NEL,GEDB,6)
        WRITE(6,6130)
6130    FORMAT(/T15,'CO-POLARIZED ELEMENT PATTERN PHASE TABLE(DEG.)')
        CALL WRITGT(AZSD,AZED,NAZ,ELSD,ELED,NEL,ALPHAD,6)
C
        WRITE(6,6200)
6200    FORMAT(/T15,'CROSS-POLARIZED ELEMENT PATTERN GAIN TABLE (DBI)')
        DO 220 I=1,NAZ
            DO 210 J=1,NEL
                GEDB(I,J)=10.*BLOG10(GE2(I,J),1.E-10)
                ALPHAD(I,J)=57.29577951*ALPHA2(I,J)
210        CONTINUE
220    CONTINUE
        CALL WRITGT(AZSD,AZED,NAZ,ELSD,ELED,NEL,GEDB,6)
        WRITE(6,6230)
6230    FORMAT(/T15,'CROSS-POLARIZED ELEMENT PATTERN PHASE TABLE(DEG.)')
        CALL WRITGT(AZSD,AZED,NAZ,ELSD,ELED,NEL,ALPHAD,6)
        RETURN
        END

        SUBROUTINE WRITGT(AZS,AZE,NAZ,ELS,ELE,NEL,G,ITAPE)
C
C WRITES A TABLE OF VALUES WITH ROWS AND COLUMNS LABELLED
C WITH VALUES OF ELEVATION AND AZIMUTH TO TAPE-ITAPE.
C
C WRITTEN NOV.29/85 - S.KAVANAGH
C
        CHARACTER*8 DASH8
        REAL AZ(20),EL(20),G(20,20)
        DATA DASH8/'-----'/

```


```

C
C SET UP LISTS OF AZIM., ELEV. VALUES
C
    DAZ=(AZE-AZS)/(NAZ-1)
    DEL=(ELE-ELS)/(NEL-1)
    DO 100 I=1,NAZ
        AZ(I)=AZS+(I-1)*DAZ
    100 CONTINUE
    DO 110 J=1,NEL
        EL(J)=ELS+(J-1)*DEL
    110 CONTINUE
C
C WRITE TABLE WITH LABELS
C
    WRITE(ITAPE,210)
    210 FORMAT(/,T30,'AZIMUTH',/,T30,'-----')
    WRITE(ITAPE,220) (AZ(I),I=1,NAZ)
    220 FORMAT(T5,'ELEV. ',T13,20(1X,F7.2))
    WRITE(ITAPE,225) ( DASH8,L=1,NAZ)
    225 FORMAT(T13,15A8)
    DO 250 J=NEL,1,-1
        WRITE(ITAPE,230) EL(J),(G(I,J),I=1,NAZ)
    230 FORMAT(T3,F7.2,T11,':',T13,20(1X,F7.2),/)
    250 CONTINUE
    RETURN
    END

    SUBROUTINE XVCOMP(ETH,EPH,AZ,EL,TH,PH,EAZ,EEL)
C
C TRANSFORMS THETA, PHI COMPONENTS OF A FIELD TO EQUIVALENT
C AZIMUTH, ELEVATION COMPONENTS. (REAL ARGUMENTS ONLY)
C FOR COORDINATE TRANSFORMATIONS SEE: W.H.HAYT, JR.,
C "ENGINEERING ELECTROMAGNETICS", MCGRAW-HILL, 1981.
C WRITTEN JAN.21/86 - S.KAVANAGH
C
    TE=1.570796327-EL
    CP=COS(PH)
    SP=SIN(PH)
    CT=COS(TH)
    ST=SIN(TH)
    CA=COS(AZ)
    SA=SIN(AZ)
    CE=COS(TE)
    SE=SIN(TE)
C
    EX=ETH*CT*CP-EPH*SP
    EY=ETH*CT*SP+EPH*CP
    EZ=-ETH*ST
C
    ETE=EZ*CE*CA-EX*CE*SA-EY*SE
    EAZ=-EZ*SA-EX*CA
    EEL=-ETE
C
    RETURN
    END

```

APPENDIX C

DOCUMENT No.	REV.	 COM DEV
RPT/MST/2500/001	—	
		SHEET 196

JMPAT1F
Computer Program to Calculate
Gain and Bandwidth of a Rectangular
Microstrip Antenna

Prepared by: S. Kavanagh
Date: June 1986

RPT/MST/2500/001

PROGRAM DESCRIPTION

JMPAT1F is a program to compute the bandwidth and gain that can be obtained from a rectangular microstrip antenna operating in its first mode (half-wave resonance). The computations are based on a paper by Pues and Van de Capelle [1]. The program accepts data describing an antenna interactively and routes the output to the user's terminal and to a local file (TAPE6). Figure 1 defines the physical input variables. The user is also prompted for a choice of measurement units, frequency, VSWR for which bandwidth is to be evaluated, and an assumed efficiency to take into account antenna losses.

Microstrip effective dielectric constant and effective width are calculated according to Hammerstad and Jensen [2] and the open end extension is found using the method of Kirschning, Jansen and Koster [3]. The sine integral is evaluated using a rational approximation or a series expansion, depending on the value of the argument. Both approximations are found in the handbook by Abramowitz and Stegun [4]. Bessel functions are computed using a subroutine from the IMSL library [5].

RUNNING JMPAT1F UNDER NOS AT COM DEV

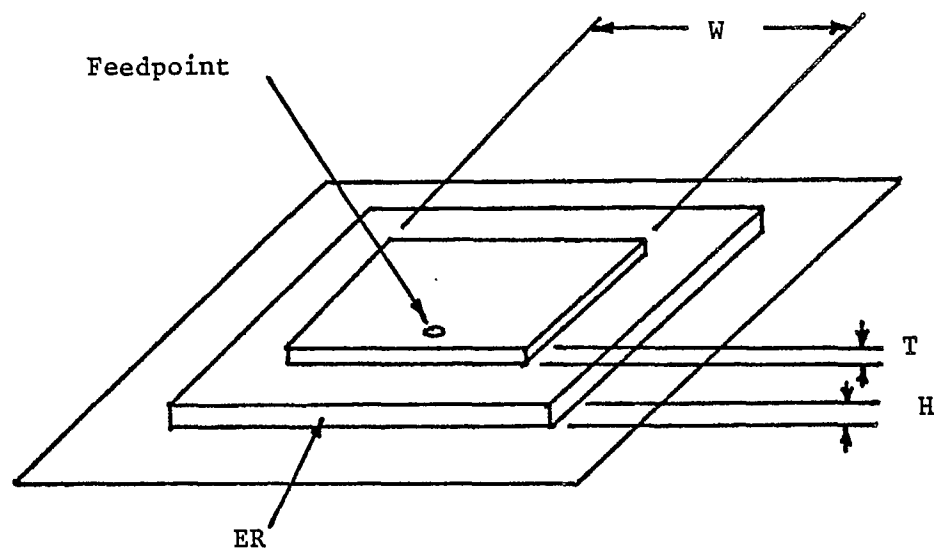
The files JMPAT1F (or KMPAT1B) and IMSLIB (the IMSL Library) must be available. The source program JMPAT1F is compiled using FTN5 and the binary (relocatable) file is saved as KMPAT1B. This must be loaded with the necessary IMSL routines to create an absolute file which may be run. The procedure file KMPAT1P shown below performs the loading and produces an absolute file KMPAT1A which is maintained as a local file (non-auto-drop) for the current terminal session. To run the procedure type "- ,KMPAT1P". Then to run the program type "KMPAT1A".

Procedure File KMPAT1P

```
.PROC,KMPAT1P.  
GET,KMPAT1B.  
ATTACH,IMSLIB/UN=APPLLIB.  
LDSET,LIB=IMSLIB.  
LOAD,KMPAT1B.  
NOGD,KMPAT1A.  
SETFS,KMPAT1A/FS=NAD.  
RETURN,KMPAT1B,IMSLIB.
```

REFERENCES

1. Pues, H. and A. Van de Capelle, "Functional Dependence of the Bandwidth and Gain of a Rectangular Microstrip Antenna on its Structural Parameters", IEEE 1982 AP-S International Symposium Digest, pp 77 - 80.
2. Hammerstad, E. and O. Jensen, "Accurate Models for Microstrip Computer Aided Design", IEEE 1980 MTT-S Symposium Digest, pp 407-409.
3. Kirschning, M., R.H. Jansen and N.H.L. Koster, "Accurate Model for Open End Effect of Microstrip Lines", Electronics Letters, Vol. 17, No. 3, 5 February 1981, pp 123 - 125.
4. Abramowitz, M. and I.A. Stegun, Handbook of Mathematical Functions, U.S. National Bureau of Standards, 1964.
5. IMSL General Information Manual (Revision E), Publication No. 84000150, Control Data Corporation, Minneapolis, 1983.



W : Radiating edge length
 T : Conductor thickness
 H : Substrate thickness
 ER : Substrate dielectric constant

FIGURE 1: ANTENNA GEOMETRY

Typical Output to TAPE6

LINEAR UNITS ARE INCHES
RADIATING EDGE LENGTH " 6.500
SUBSTRATE THICKNESS " .250
CONDUCTOR THICKNESS " .080
SUBSTRATE DIELECTRIC CONSTANT " 1.020
FREQUENCY(GHZ) " .850
BANDWIDTH IS FOR VSWR " 2.000
ANTENNA EFFICIENCY " 1.000

COMPUTED BANDWIDTH = 1.950 PERCENT
COMPUTED GAIN(DBI) = 9.912
QRAD= 38.285

```

MODULE NAME : JMPAT1F
LANGUAGE    : CDC FORTRAN 5
PURPOSE     : COMPUTES BANDWIDTH AND GAIN OF RECTANGULAR
              MICROSTRIP PATCH ANTENNA

```

DATE	VERSION	AUTHOR	REASON
-----	-----	-----	-----
OCT.21/85	JMPAT1F	S. KAVANAGH	ORIGINAL VERSION

BASED ON PUES AND VAN DE CAPELLE, IEEE AP-S DIGEST 1982

I/O UNITS USED : INTERACTIVE I/O TAPE4,5, OUTPUT TAPE6

EXTERNAL REFERENCES : MMBSJN (IMSL)

```
PROGRAM JMPAT1F(INPUT,OUTPUT,TAPE4=OUTPUT,TAPE5=INPUT,TAPE6)
```

REAL K, LN
DATA PI/3. 1415926535/, ETA/376.7/

100 CONTINUE

```

WRITE(4,4010)
4010 FORMAT(' ENTER LINEAR UNITS: 0=MM, 1=INCHES')
READ(5,*) IUNITS
WRITE(4,4020)
4020 FORMAT(' ENTER RADIATING EDGE LENGTH')
READ(5,*) W
WRITE(4,4030)
4030 FORMAT(' ENTER SUBSTRATE THICKNESS, CONDUCTOR THICKNESS')
READ(5,*) H,T
WRITE(4,4040)
4040 FORMAT(' ENTER SUBSTRATE DIELECTRIC CONSTANT')
READ(5,*) ER
WRITE(4,4050)
4050 FORMAT(' ENTER FREQUENCY (GHZ)')
READ(5,*) FREQ
WRITE(4,4060)
4060 FORMAT(' ENTER BAND-EDGE VSWR, EFFICIENCY(MAX.=1)')
READ(5,*) S,Q

```

150 CONTINUE

```

      IF(IUNITS.EQ.0) THEN
        WRITE(4,6010)
        WRITE(6,6010)
      END IF
6010  FORMAT(T10,'LINEAR UNITS ARE MILLIMETRES')
      IF(IUNITS.EQ.1) THEN
        WRITE(4,6011)
        WRITE(6,6011)
      END IF
6011  FORMAT(T10,'LINEAR UNITS ARE INCHES')
      WRITE(4,6020) W
      WRITE(6,6020) W
6020  FORMAT(T10,'RADIATING EDGE LENGTH',T40,'=',F8.3)
      WRITE(4,6030) H
      WRITE(6,6030) H
6030  FORMAT(T10,'SUBSTRATE THICKNESS',T40,'=',F8.3)

```

RPT/MST/2500/001


```

WRITE(4,8035) T
WRITE(6,8035) T
8035 FORMAT(T10,'CONDUCTOR THICKNESS',T40,'=',F8.3)
WRITE(4,8040) ER
WRITE(6,8040) ER
8040 FORMAT(T10,'SUBSTRATE DIELECTRIC CONSTANT',T40,'=',F8.3)
WRITE(4,8050) FREQ
WRITE(6,8050) FREQ
8050 FORMAT(T10,'FREQUENCY(GHZ)',T40,'=',F8.3)
WRITE(4,8060) S
WRITE(6,8060) S
8060 FORMAT(T10,'BANDWIDTH IS FOR VSWR',T40,'=',F8.3)
WRITE(4,8065) Q
WRITE(6,8065) Q
8065 FORMAT(T10,'ANTENNA EFFICIENCY',T40,'=',F8.3)
C
IF(IUNITS.EQ.0) K=2.*PI*FREQ/299.7925
IF(IUNITS.EQ.1) K=2.*PI*FREQ/11.80283
CALL HJMIC(W,H,T,ER,EEFF,WEFF,U)
CALL KJKLOC(EEFF,ER,U,H,DLOC)
WN=K*WEFF
LN=PI/SQRT(EEFF)
DLN=K*DLOC
CALL PVDG(WN,LN,DLN,GRAD)
QRAD=WN*LN*EEFF/(2.*K*H*ETA*GRAD)
BW=100.*(S-1.)/(Q*QRAD*SQRT(S))
GAIN=4.*Q*WN*WN/(PI*ETA*GRAD)
DBGAIN=10.*ALOG10(GAIN)
C
WRITE(4,8100) BW
WRITE(6,8100) BW
8100 FORMAT(/,T10,'COMPUTED BANDWIDTH =',F8.3,' PERCENT')
WRITE(4,8110) DBGAIN
WRITE(6,8110) DBGAIN
8110 FORMAT(T10,'COMPUTED GAIN(DBI) =',F8.3)
C
WRITE(4,8120) QRAD
WRITE(6,8120) QRAD
8120 FORMAT(T10,'QRAD=',F8.3,///)
C
200 CONTINUE
WRITE(4,4100)
4100 FORMAT(' 0 STOP'/' 1 GO'/' 2 CHANGE UNITS'/' 3 CHANGE',
2 ' RADIATING EDGE LENGTH'/' 4 CHANGE SUBSTRATE ',
3 ' THICKNESS'/' 5 CHANGE CONDUCTOR THICKNESS'/'
4 ' 6 CHANGE DIELECTRIC CONSTANT'/' 7 CHANGE FREQUENCY'
5 ' /' 8 CHANGE VSWR'/' 9 CHANGE EFFICIENCY'/' 10 RESTART'
6 ' //' ENTER CHOICE')
READ(5,*) IOPT
IF(IOPT.EQ.1) GO TO 150
IF(IOPT.EQ.2) THEN
WRITE(4,4010)
READ(5,*) IUNITS
GO TO 200
END IF
IF(IOPT.EQ.3) THEN
WRITE(4,4020)
READ(5,*) W
GO TO 200
END IF
IF(IOPT.EQ.4) THEN
WRITE(4,4131)
4131 FORMAT(' ENTER SUBSTRATE THICKNESS')
READ(5,*) H
GO TO 200
END IF
IF(IOPT.EQ.5) THEN
WRITE(4,4132)
4132 FORMAT(' ENTER CONDUCTOR THICKNESS')
READ(5,*) IUNITS
GO TO 200
END IF
IF(IOPT.EQ.6) THEN
WRITE(4,4040)
READ(5,*) ER
GO TO 200
END IF
IF(IOPT.EQ.7) THEN
WRITE(4,4050)
READ(5,*) FREQ

```

RPT/MST/2500/001

```

      GO TO 200
      END IF
      IF(IOPT.EQ.8) THEN
        WRITE(4,4161)
4161    FORMAT(' ENTER BAND-EDGE VSWR')
        READ(5,*) S
        GO TO 200
      END IF
      IF(IOPT.EQ.9) THEN
        WRITE(4,4162)
4162    FORMAT(' ENTER EFFICIENCY(MAX.=1)')
        READ(5,*) Q
        GO TO 200
      END IF
      IF(IOPT.EQ.10) GO TO 100
C
      RETURN
      END
C
CCCCCCCCCCCCCCCCCCCCCCCCCCCCCCCCCCCCCCCCCCCCCCCCCCCCCCCCCCCCCCCCCCCC
C
      FUNCTION COTH2(X)
C
      COTH2=1./(TANH(X))**2
      RETURN
      END
C
CCCCCCCCCCCCCCCCCCCCCCCCCCCCCCCCCCCCCCCCCCCCCCCCCCCCCCCCCCCCCCCCCCCC
C
      SUBROUTINE HJMIC(W,H,T,ER,EEFF,WEFF,U)
C
C COMPUTES EFFECTIVE DIELECTRIC CONSTANT EEFF AND WIDTH WEFF FROM
C HAMMERSTAD AND JENSEN, 'ACCURATE MODELS FOR MICROSTRIP COMPUTER-
C AIDED DESIGN', IEEE MTT-S DIGEST 1980.
C
C WRITTEN OCT.15/85-S.KAVANAGH
C
      DATA PI/3.1415938535/
C
      U=W/H
      TH=T/H
      V=10.87312731/(TH*COTH2(SQRT(6.517*U)))
      DU1=(TH/PI)*ALOG(1.+V)
      U1=U+DU1
      UR=U+(0.5+0.5/COSH(SQRT(ER-1.)))*DU1
      B=0.584*((ER-0.9)/(ER+3.))**0.053
      A1=(UR**4+(UR/52.))**2)/(UR**4+0.432)
      A2=1.+(UR/18.1)**3
      A=1.+ALOG(A1)/49.+ALOG(A2)/18.7
      EE=0.5*(ER+1.+(ER-1.)*(1.+10./UR)**(-A*B))
      EEFF=EE*(Z01(U1)/Z01(UR))**2
      WEFF=UR*H
C
      RETURN
      END
C
CCCCCCCCCCCCCCCCCCCCCCCCCCCCCCCCCCCCCCCCCCCCCCCCCCCCCCCCCCCCCCCCCCCC
C
      SUBROUTINE KJKLOC(EEFF,ER,U,H,DLOC)
C
C COMPUTES OPEN END EXTENSION OF MICROSTRIP LINE FROM KIRSCHNING,
C JANSEN AND KOSTER, 'ACCURATE MODEL FOR OPEN END EFFECT OF
C MICROSTRIP LINES', ELECTRONICS LETTERS, FEB. 5, 1981.
C
C WRITTEN OCT.15/85-S.KAVANAGH
C
      Z1=(EEFF**0.81+0.26)/(EEFF**0.81-0.189)
      Z2=(U**0.8544+0.236)/(U**0.8544+0.87)
      X1=0.434907*Z1*Z2
      X2=1.+(U**0.371)/(2.358*ER+1.)
      Z3=0.084*U*(1.9413/X2)
      X3=1.+0.5274*ATAN(Z3)/EEFF**0.9236
      X4=1.+0.0377*ATAN(0.067*U**1.456)*(6.-5.*EXP(0.038*(1.-ER)))
      IF(U.GT.3.) THEN
        X5=1.
      ELSE
        X5=1.-0.218*EXP(-7.5*U)
      END IF
      DLOC=X1*X3*X5*H/X4
C

```

RPT/MST/2500/001

```

      RETURN
      END
C
CCCCCCCCCCCCCCCCCCCCCCCCCCCCCCCCCCCCCCCCCCCCCCCCCCCCCCCCCCCCCCCC
C
      SUBROUTINE PVDCG(W,L,S,GRAD)
C
C COMPUTES RADIATION CONDUCTANCE OF RECTANGULAR MICROSTRIP PATCH
C FROM PUES AND VAN DE CAPELLE, IEEE AP-S DIGEST 1982.
C USES IMSL ROUTINE MMBSJN.
C
C WRITTEN OCT. 15/85-S.KAVANAGH
C
      REAL L,BESSEL(3)
      DATA PI/3.1415926535/,ETA/376.7/
C
      S2=S*S
      SW=SIN(W)
      CW=COS(W)
      F1=(W*SI(W)+CW+SW/W-2.)*(1.-S2/24.)
      F1=F1+(S2/12.)*(1./3.+CW/W**2-SW/W**3)
      CALL MMBSJN(L,3,BESSEL,IER)
      IF (IER.GE.129) PRINT 1,IER
1  FDMAT(' MMBSJN ERROR PARAMETER IER =',I4)
      F2=1.+BESSEL(1)+(S2/(24.-S2))*BESSEL(3)
      GRAD=2.*F1*F2/(PI*ETA)
C
      RETURN
      END
C
CCCCCCCCCCCCCCCCCCCCCCCCCCCCCCCCCCCCCCCCCCCCCCCCCCCCCCCCCCCCCCCC
C
      FUNCTION SI(X)
C
C COMPUTES SINE INTEGRAL ACCORDING TO RATIONAL APPROXIMATION
C GIVEN IN ABRAMOWITZ AND STEGUN (FOR X.GE.1) OR SERIES
C EXPANSION FROM SAME BOOK FOR X.LT.1.
C
C WRITTEN OCT. 15/85 S.KAVANAGH
C MODIFIED OCT. 18/85-S.KAVANAGH-TO ADD X.LT.1 SERIES.
C
      REAL A(4),B(4),C(4),D(4)
      DATA A/38.027264,265.187033,335.677320,38.102495/
      DATA B/40.021433,322.624911,570.236280,157.105423/
      DATA C/42.242855,302.757865,352.018498,21.821899/
      DATA D/48.196927,482.485984,1114.978885,449.690326/
      DATA PI/3.1415926535/
C
      IF(X.LT.1.) THEN
        SI=X-X**3/18.+X**5/600.-X**7/35280.+X**9/3265920.
C
      ELSE
        Y=X*X
        UP=((Y+A(1))*Y+A(2))*Y+A(3))*Y+A(4)
        DOWN=((Y+B(1))*Y+B(2))*Y+B(3))*Y+B(4)
        F=UP/(X*DOWN)
        UP=((Y+C(1))*Y+C(2))*Y+C(3))*Y+C(4)
        DOWN=((Y+D(1))*Y+D(2))*Y+D(3))*Y+D(4)
        G=UP/(Y*DOWN)
        SI=PI/2.-F*COS(X)-G*SIN(X)
C
      END IF
      RETURN
      END
C
CCCCCCCCCCCCCCCCCCCCCCCCCCCCCCCCCCCCCCCCCCCCCCCCCCCCCCCCCCCCCCCC
C
      FUNCTION ZO1(U)
C
C COMPUTES ZO1(U) FROM HAMMERSTAD AND JENSEN, 'ACCURATE MODELS
C FOR MICROSTRIP COMPUTER AIDED DESIGN', IEEE MTT-S DIGEST 1980.
C
C WRITTEN OCT. 15/85-S.KAVANAGH
C
      DATA PI2/6.283185308/,ETA/376.7/
C
      X=(30.686/U)**0.7528
      F=6.+(PI2-6.)*EXP(-X)
      R=SQRT(1.+4./(U*U))
      ZO1=(ETA/PI2)*ALOG(F/U+R)

```

RPT/MST/2500/001

C

RETURN
END

 COM DEV

RPT/MST/2500/001

APPENDIX D



JATLM1F

Computer Program to Model the Input
Impedance of a Coaxial Probe Fed Rectangular
Microstrip Antenna

Prepared by: S. Kavanagh

Date: April 1986

RPT/MST/2500/001

PROGRAM DESCRIPTION

JATLM1F is a program to implement the model for a rectangular microstrip antenna with coaxial probe feed given by Pues and Van de Capell [1]. It computes the input impedance as a function of frequency, assuming no losses in the antenna. Input data is entered interactively from the terminal and output is provided to the terminal and also to a local file (TAPE6). The input variables describing the antenna are shown in Figure 1.

Microstrip effective dielectric constant and effective width are computed according to Hammerstad and Jensen [2] and the open end effect is found using the model of Kirschning, Jansen and Koster [3]. The probe reactance is modelled using the formulation of Sengupta [4]. Several Bessel functions are computed using routines from the International Mathematical and Statistical Library [6]. The program is written in CDC Fortran 5.

RUNNING JATLM1F UNDER NOS AT COM DEV

The files JATLM1F (or KATLM1B) and IMSLIB (the IMSLIB Library) must be available. The program is compiled using FTN5 and the binary (relocatable) file is saved as KATLM1B. This must be loaded with the necessary IMSL routines to create an absolute file which may be run. The procedure file KATLM1P shown below performs the loading (using KATLM1B in user account STEVEK) and produces an absolute file KATLM1A which is maintained as a local file (non-auto-drop) for the current terminal session. To run the procedure type "-",KATLM1P". Then run the program type "KATLM1A".

Procedure file KATLM1P

```
.PROC,KATLM1P.  
GET,KATLM1B/UN=STEVEK.  
ATTACH,IMSLIB/UN=APPLLIB.  
LDSET,LIB=IMSLIB.  
LOAD,KATLM1B.  
NOGO,KATLM1A.  
SETFS,KATLM1A/FS=NAD.  
RETURN,KATLM1B,IMSLIB.
```

RPT/MST/2500/001

REFERENCES

1. Pues, H. and A. Van de Capelle, "Accurate Transmission-Line Model for the Rectangular Microstrip Antenna", Proc. IEE, Vol. 131, Part H, No. 6, December 1984, pp 334-340.
2. Hammerstad, E. and O. Jensen, "Accurate models for Microstrip Computer-Aided Design", IEEE 1980 MTT-S Symposium Digest, pp 407-409.
3. Kirschning, M., R.H. Jansen and N.H.L. Koster, "Accurate Model for Open End Effect of Microstrip Lines", Electronics Letters, Vol. 17, No. 3, 5 February 1981, pp 123-125.
4. Sengupta, D.L., "The transmission Line Model for Rectangular Patch Antennas", IEEE 1983 AP-S Symposium Digest, pp 158-161.
5. Abramowitz, M. and I.A. Stegun, Handbook of Mathematical Functions, U.S. National Bureau of Standards, 1964.
6. IMSL General Information Manual (Revision E), Publication No. 84000150, Control Data Corporation, Minneapolis, 1983.

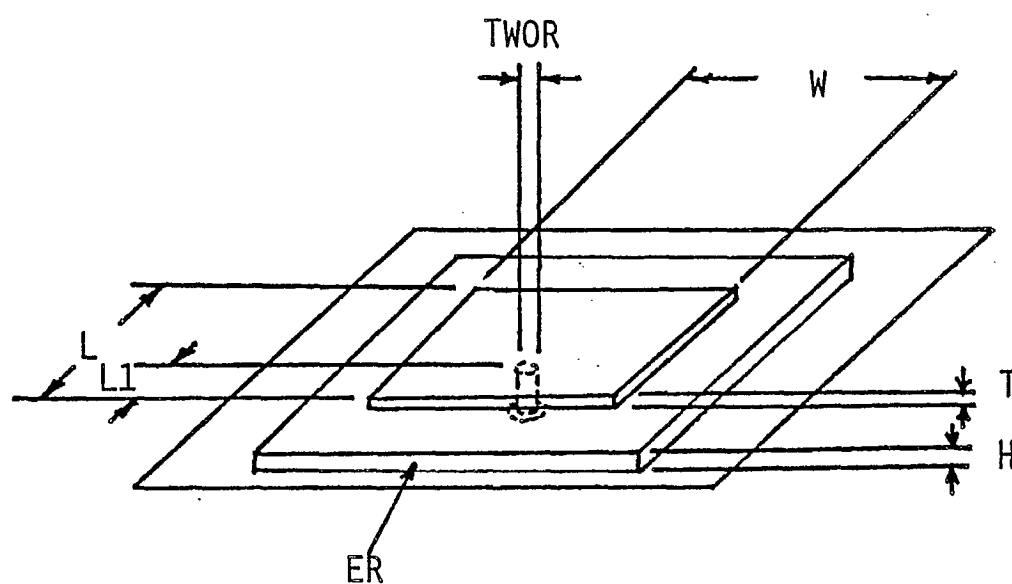


FIGURE 1: ANTENNA GEOMETRY

TYPICAL OUTPUT TO TAPE6

JATLM1F: RECTANGULAR PATCH INPUT IMPEDANCE

 COM DEV

LENGTH(RESONANT DIMENSION) = 6.400 INCHES
 FEED-TO-EDGE DISTANCE = 1.700 INCHES
 WIDTH(RADIATING EDGE) = 5.700 INCHES
 CONDUCTOR THICKNESS = .050 INCHES
 SUBSTRATE THICKNESS = .400 INCHES
 SUBSTRATE DIELECTRIC CONSTANT = 1.030
 MINIMUM FREQUENCY = .700 GHZ
 MAXIMUM FREQUENCY = 1.000 GHZ
 NUMBER OF FREQUENCY POINTS = 31
 REFERENCE FEED IMPEDANCE = 50.000 OHMS
 FEED PROBE DIAMETER = .120 INCHES

FREQ. (GHZ)	Z(OHMS)		RETURN LOSS	PROBE
	REAL	IMAG.	(DB)	XL(OHMS)
.700	2.2	55.4	.35	42.3
.710	2.7	57.8	.39	42.7
.720	3.2	60.6	.45	43.2
.730	3.9	63.7	.52	43.6
.740	5.0	67.3	.61	44.0
.750	6.4	71.7	.73	44.5
.760	8.6	77.1	.88	44.9
.770	11.9	83.9	1.08	45.4
.780	17.6	92.6	1.35	45.8
.790	27.9	104.0	1.74	46.2
.800	48.6	117.6	2.31	46.6
.810	91.5	124.0	3.16	47.1
.820	152.0	80.5	4.47	47.5
.830	138.7	-8.1	6.53	47.9
.840	80.2	-33.0	9.54	48.3
.850	45.5	-24.5	11.96	48.8
.860	28.3	-12.6	10.00	49.2
.870	19.2	-2.8	7.01	49.6
.880	13.9	4.8	4.93	50.0
.890	10.7	10.8	3.58	50.4
.900	8.5	15.6	2.70	50.8
.910	7.0	19.5	2.10	51.2
.920	5.9	22.8	1.69	51.7
.930	5.0	25.7	1.39	52.1
.940	4.4	28.1	1.16	52.5
.950	3.9	30.3	1.00	52.9
.960	3.5	32.3	.87	53.3
.970	3.2	34.0	.77	53.7
.980	3.0	35.6	.68	54.1
.990	2.8	37.1	.62	54.5
1.000	2.6	38.5	.56	54.9

RPT/MST/2500/001

CCCCCCCCCCCCCCCCCC

SOFTWARE SYSTEM DEVELOPMENT DOCUMENTATION

```

MODULE NAME : JATLM1F
LANGUAGE    : CDC FORTRAN 5
PURPOSE     : COMPUTES INPUT IMPEDANCE OF RECTANGULAR MICROSTRIP
              PATCH ANTENNA WITH COAXIAL PROBE FEED.

```

REVISION HISTORY

DATE	VERSION	AUTHOR	REASON
OCT.28/85	JATLM1F	S.KAVANAGH	ORIGINAL VERSION

DESCRIPTION

COMPUTES COMPLEX INPUT IMPEDANCE OF RECTANGULAR PATCH ANTENNA WITH COAXIAL PROBE FEED AS FUNCTION OF FREQUENCY. BASED ON PUES AND VAN DE CAPELLE, 'ACCURATE TRANSMISSION-LINE MODEL FOR THE RECTANGULAR MICROSTRIP ANTENNA', IEE PROC., PART H, DEC. 1984. ONLY THE LOSSLESS CASE ($\alpha=0$) IS CONSIDERED.

COMMON BLOCKS : NONE

```

I/O UNITS USED : TAPE4 : INTERACTIVE OUTPUT TO TERMINAL
                  TAPE5 : INTERACTIVE INPUT FROM TERMINAL
                  TAPE6 : OUTPUT TO FILE

```

EXTERNAL REFERENCES : MMBSJ0,MMBSJ1,MMBSJN (IMSL)

```
PROGRAM JATLM1F(INPUT,OUTPUT,TAPE4=OUTPUT,TAPE5=INPUT,TAPE6)
```

```

CHARACTER*8 UNIT(2),UN
CHARACTER*15 FLAG(2)
REAL L,L1,K0,LEFF,LN,KB,JN(3),CONVERT(2)
COMPLEX G,YS,YM,CTL,CSL,COD,YC2,YS2,YM2,PMC,PSC,A1,A2,ZIN,RC
COMPLEX CCOSH,CCOTH,CCSCH
DATA ETA/378.7/,PI/3.1415926535/
DATA UNIT/'MM. ','INCHES'/
DATA FLAG/' ','SURF.WAVE.COND.'/
DATA CONVERT/.001,.0254/

```

C INPUT DATA

```

WRITE(4,4010)
4010 FORMAT(' ENTER UNITS: 0=MM,1=INCHES')
READ(5,*) IUNITS
WRITE(4,4020)
4020 FORMAT(' ENTER LENGTH(RESONANT DIMENSION)')
READ(5,*) L
WRITE(4,4030)
4030 FORMAT(' ENTER LENGTH FROM FEEDPOINT TO EDGE')
READ(5,*) L1
WRITE(4,4040)
4040 FORMAT(' ENTER WIDTH(RADIATING EDGE)')
READ(5,*) W
WRITE(4,4050)
4050 FDMAT(' ENTER CONDUCTOR THICKNESS')
READ(5,*) T
WRITE(4,4060)
4060 FORMAT(' ENTER SUBSTRATE THICKNESS')
READ(5,*) H
WRITE(4,4070)
4070 FORMAT(' ENTER DIELECTRIC CONSTANT')
READ(5,*) ER
WRITE(4,4080)
4080 FORMAT(' ENTER MIN.FREQ.,MAX.FREQ.(GHZ),NO.OF PDINTS')
READ(5,*) FMIN,FMAX,NF

```

RPT/MST/2500/001

```

WRITE(4,4090)
4090 FORMAT(' ENTER DESIRED FEED IMPEDANCE(OHMS)')
READ(5,*) ZO
WRITE(4,4095)
4095 FORMAT(' ENTER FEED PROBE DIAMETER')
READ(5,*) TWOR

C
C ECHO DATA TO TERMINAL AND TAPE6
C
UN=UNIT(IUNITS+1)
WRITE(6,6005)
6005 FORMAT(/T9,'JATLM1F: RECTANGULAR PATCH INPUT IMPEDANCE'/)
WRITE(4,6020) L,UN
WRITE(6,6020) L,UN
6020 FORMAT(T10,'LENGTH(RESONANT DIMENSION)',T40,'=',F8.3,A7)
WRITE(4,6030) L1,UN
WRITE(6,6030) L1,UN
6030 FORMAT(T10,'FEED-TO-EDGE DISTANCE',T40,'=',F8.3,A7)
WRITE(4,6040) W,UN
WRITE(6,6040) W,UN
6040 FORMAT(T10,'WIDTH(RADIATING EDGE)',T40,'=',F8.3,A7)
WRITE(4,6050) T,UN
WRITE(6,6050) T,UN
6050 FORMAT(T10,'CONDUCTOR THICKNESS',T40,'=',F8.3,A7)
WRITE(4,6060) H,UN
WRITE(6,6060) H,UN
6060 FORMAT(T10,'SUBSTRATE THICKNESS',T40,'=',F8.3,A7)
WRITE(4,6070) ER
WRITE(6,6070) ER
6070 FORMAT(T10,'SUBSTRATE DIELECTRIC CONSTANT',T40,'=',F8.3)
WRITE(4,6080) FMIN,FMAX
WRITE(6,6080) FMIN,FMAX
6080 FORMAT(T10,'MINIMUM FREQUENCY',T40,'=',F8.3,' GHZ')
2 T10,'MAXIMUM FREQUENCY',T40,'=',F8.3,' GHZ')
WRITE(4,6082) NF
WRITE(6,6082) NF
6082 FORMAT(T10,'NUMBER OF FREQUENCY POINTS',T40,'=',I4)
WRITE(4,6090) ZO
WRITE(6,6090) ZO
6090 FORMAT(T10,'REFERENCE FEED IMPEDANCE',T40,'=',F8.3,' OHMS')
WRITE(4,6095) TWOR,UN
WRITE(6,6095) TWOR,UN
6095 FORMAT(T10,'FEED PROBE DIAMETER',T40,'=',F8.3,A7)

C
C CONVERT DIMENSIONS TO METRES
C
CF=CONVERT(IUNITS+1)
L=L*CF
L1=L1*CF
W=W*CF
H=H*CF
T=T*CF
R=0.5*TWOR*CF

C
C COMPUTE FREQUENCY INDEPENDENT VALUES: EEFF,WEFF,YC,DLOC,D
C
CALL HJMIC(W,H,T,ER,EEFF,WEFF,U)
CALL KJKLOC(EEFF,ER,U,H,DLOC)
LEFF=L+DLOC
YC=SQRT(EEFF)*WEFF/(ETA*H)
D=ABS(0.5*L-L1)

C
C LOOP THROUGH FREQUENCY RANGE
C
FSTEP=(FMAX-FMIN)/(NF-1)
WRITE(4,6100)
WRITE(6,6100)
6100 FORMAT(/T10,'FREQ.(GHZ)',T26,'Z(OHMS)',T40,'RETURN LOSS',
2 T53,'PROBE'/ T23,'REAL',T32,'IMAG.',T43,'(DB)',T53,'XL(OHMS)'/)
DO 300 I=1,NF
IFLAG=0
F=FMIN+FSTEP*FLOAT(I-1)
KO=2.*PI*F/.2997925
BETA=KO*SQRT(EEFF)
G=CMPLX(0.,BETA)
WN=KO*WEFF
S=KO*DLOC

C
C COMPUTE SLOT SELF-ADMITTANCE YS
C

```

[illegible]


```
C RETURN  
C END  
CCCCCCCCCCCCCCCCCCCCCCCCCCCCCCCCCCCCCCCCCCCCCCCCCCCCCCCCCCCCCCCCCCCCCC  
C  
C COMPLEX FUNCTION CCOTH(Z)  
C COMPUTES HYPERBOLIC COTANGENT OF COMPLEX ARGUMENT  
C WRITTEN OCT.24/85-S.KAVANAGH  
C  
C COMPLEX T1,T2,Z  
C  
C U=REAL(Z)  
C V=AIMAG(Z)  
C T1=CMPLX(COSH(2.*U)+COS(2.*V),0.)  
C T2=CMPLX(SINH(2.*U),SIN(2.*V))  
C CCOTH=T1/T2  
C  
C RETURN  
C END  
CCCCCCCCCCCCCCCCCCCCCCCCCCCCCCCCCCCCCCCCCCCCCCCCCCCCCCCCCCCCCCCCCCCCCC  
C  
C COMPLEX FUNCTION CCSCH(Z)  
C COMPUTES HYPERBOLIC COSECANT OF COMPLEX ARGUMENT  
C WRITTEN OCT.24/85-S.KAVANAGH  
C  
C COMPLEX Z  
C  
C U=REAL(Z)  
C V=AIMAG(Z)  
C CCSCH=1./CMPLX(SINH(U)*COS(V),COSH(U)*SIN(V))  
C  
C RETURN  
C END  
CCCCCCCCCCCCCCCCCCCCCCCCCCCCCCCCCCCCCCCCCCCCCCCCCCCCCCCCCCCCCCCCCCCCCC  
C  
C FUNCTION COTH2(X)  
C  
C COTH2=1./(TANH(X))**2  
C RETURN  
C END  
CCCCCCCCCCCCCCCCCCCCCCCCCCCCCCCCCCCCCCCCCCCCCCCCCCCCCCCCCCCCCCCCCCCCCC  
C  
C SUBROUTINE HJMIC(W,H,T,ER,EFF,WEFF,U)  
C COMPUTES EFFECTIVE DIELECTRIC CONSTANT EFF AND WIDTH WEFF FROM  
C HAMMERSTAD AND JENSEN,'ACCURATE MODELS FOR MICROSTRIP COMPUTER  
C AIDED DESIGN', IEEE MTT-S DIGEST 1980.  
C WRITTEN OCT.15/85-S.KAVANAGH  
C  
C DATA PI/3.1415938535/  
C  
C U=W/H  
C TH=T/H  
C V=10.87312731/(TH*COTH2(SQRT(6.517*U)))  
C DU1=(TH/PI)*ALOG(1.+V)  
C U1=U+DU1  
C UR=U+(0.5+0.5/COSH(SQRT(ER-1.)))*DU1  
C B=0.584*((ER-0.9)/(ER+3.))*0.053  
C A1=(UR**4+(UR/52. )**2)/(UR**4+0.432)  
C A2=1.+(UR/18.1)**3  
C A=1.+ALOG(A1)/49.+ALOG(A2)/18.7  
C EE=0.5*(ER+1.+(ER-1.)*(1.+10./UR)**(-A*B))  
C EEFF=EE*(Z01(U1)/Z01(UR))**2  
C WEFF=UR*H  
C  
C RETURN  
C END  
CCCCCCCCCCCCCCCCCCCCCCCCCCCCCCCCCCCCCCCCCCCCCCCCCCCCCCCCCCCCCCCCCCCCCC  
C  
C SUBROUTINE KJKLDC(EFF,ER,U,H,DLOC)
```

RPT/MST/250

```

C COMPUTES OPEN END EXTENSION OF MICROSTRIP LINE FROM KIRSCHNING,
C JANSEN AND KOSTER, 'ACCURATE MODEL FOR OPEN END EFFECT OF
C MICROSTRIP LINES', ELECTRONICS LETTERS, FEB. 5, 1981.
C
C WRITTEN OCT.15/85-S.KAVANAGH
C
      Z1=(EEFF**0.81+0.26)/(EEFF**0.81-0.189)
      Z2=(U**0.8544+0.236)/(U**0.8544+0.87)
      X1=0.434907*Z1*Z2
      X2=1.+(U**0.371)/(2.358*ER+1.)
      Z3=0.084*U**(1.9413/X2)
      X3=1.+0.5274*ATAN(Z3)/EEFF**0.9236
      X4=1.+0.0377*ATAN(0.067*U**1.456)*(6.-5.*EXP(0.036*(1.-ER)))
      IF(U.GT.3.) THEN
        X5=1.
      ELSE
        X5=1.-0.218*EXP(-7.5*U).
      END IF
      DLOC=X1*X3*X5*H/X4
C
      RETURN
      END
C
CCCCCCCCCCCCCCCCCCCCCCCCCCCCCCCCCCCCCCCCCCCCCCCCCCCCCCCCCCCCCCCC
C
      SUBROUTINE PROBEX(R,W,H,BETA,YC,XL)
C
C COMPUTES PROBE INDUCTANCE ACCORDING TO SENGUPTA,IEEE AP-S DIGEST 1983,
C EQUATION 3.
C
C WRITTEN OCT.24/85-S.KAVANAGH
C
      DATA GAM/1.78107/,PI/3.1415926535/
C
      U=W/H
      ALPHA=1.+1.393/U+0.667*ALOG(U+1.444)/U
      XL=0.5*BETA*W*ALPHA*ALOG(2./(GAM*BETA*R))/(PI*YC)
C
      RETURN
      END
C
CCCCCCCCCCCCCCCCCCCCCCCCCCCCCCCCCCCCCCCCCCCCCCCCCCCCCCCCCCCCCCCC
C
      FUNCTION SI(X)
C
C COMPUTES SINE INTEGRAL ACCORDING TO RATIONAL APPROXIMATION
C GIVEN IN ABRAMOWITZ AND STEGUN (FOR X.GE.1) OR SERIES
C EXPANSION FROM SAME BOOK FOR X.LT.1.
C
C WRITTEN OCT.15/85 S.KAVANAGH
C MODIFIED OCT.18/85-S.KAVANAGH
C
      REAL A(4),B(4),C(4),D(4)
      DATA A/38.027264,285.187033,335.877320,38.102495/
      DATA B/40.021433,322.824911,570.236280,157.105423/
      DATA C/42.242855,302.757885,352.018498,21.821899/
      DATA D/48.196927,482.485984,1114.978885,449.890328/
      DATA PI/3.1415926535/
C
      IF(X.LT.1.) THEN
        SI=X-X**3/18.+X**5/800.-X**7/35280.+X**9/3265920.
C
      ELSE
        Y=X*X
        UP=((Y+A(1))*Y+A(2))*Y+A(3))*Y+A(4)
        DOWN=((Y+B(1))*Y+B(2))*Y+B(3))*Y+B(4)
        F=UP/(X*DOWN)
        UP=((Y+C(1))*Y+C(2))*Y+C(3))*Y+C(4)
        DOWN=((Y+D(1))*Y+D(2))*Y+D(3))*Y+D(4)
        G=UP/(Y*DOWN)
        SI=PI/2.-F*COS(X)-G*SIN(X)
C
      END IF
      RETURN
      END
C
CCCCCCCCCCCCCCCCCCCCCCCCCCCCCCCCCCCCCCCCCCCCCCCCCCCCCCCCCCCCCCCC
C
      FUNCTION Y(N,X)
C

```

RPT/MST/2500/001

```

C COMPUTES BESSEL FUNCTION OF SECOND KIND, ORDER 0,1 OR 2, FOR
C POSITIVE REAL ARGUMENT. USES POLYNOMIAL APPROXIMATIONS FROM
C ABRAMOWITZ AND STEGUN. REQUIRES IMSL FUNCTIONS MMBSJO AND
C MMBSJ1.
C
C WRITTEN OCT.23/85-S.KAVANAGH
C
      REAL MMBSJO,MMBSJ1
      DATA PI/3.1415926535/
C
      IF(X.LT.0.0001) THEN
        Y=0.
        PRINT 10
10      FORMAT(' ***ERROR IN FUNCTION Y: ARGUMENT .LT. .001')
        RETURN
      END IF
      P=X/3.
      Q=3./X
      P2=P*P
      P4=P**4
      P6=P**6
      P8=P**8
      P10=P**10
      P12=P**12
      Q2=Q*Q
      Q3=Q**3
      Q4=Q**4
      Q5=Q**5
      Q6=Q**6
C
C COMPUTE YO
C
      IF(N.EQ.0.OR.N.EQ.2) THEN
        IF(X.LE.3.) THEN
          YO=2.*ALOG(X/2.)*MMBSJO(X,IER)/PI+.36748691+.80559366
2          *P2-.74350384*P4+.25300117*P6-.04281214*P8+
3          .00427916*P10-.00024848*P12
          IF(IER.GT.129) PRINT 20
20         FORMAT(' ***ERROR IN FUNCTION Y: MMBSJO IER .GT. 129')
        ELSE
          FO=.79788456-.00000077*Q-.00552740*Q2-.00009512*Q3
2          +.00137237*Q4-.00072805*Q5+.00014476*Q6
          TO=X-.78539816-.04186397*Q-.00003954*Q2+.00262573*Q3
2          -.00054125*Q4-.00029333*Q5+.00013558*Q6
          YO=FO*SIN(TO)/SQRT(X)
        END IF
      IF(N.EQ.0) THEN
        Y=YO
        RETURN
      END IF
C
      END IF
C
C COMPUTE Y1
C
      IF(N.EQ.1.OR.N.EQ.2) THEN
        IF(X.LE.3) THEN
          Y1=-.6366198+.2212091*P2+2.1882709*P4-1.3184827*P6
2          +.3123951*P8-.0400978*P10+.0027873*P12
          Y1=Y1/X+2.*ALOG(X/2.)*MMBSJ1(X,IER)/PI
          IF(IER.GT.129) PRINT 30
30         FORMAT(' ***ERROR IN FUNCTION Y: MMBSJ1 IER .GT. 129')
        ELSE
          F1=.79788456+.00000156*Q+.01659867*Q2+.00017105*Q3
2          -.00249511*Q4+.00113653*Q5-.00020033*Q6
          T1=X-2.35819449+.12499812*Q+.00005650*Q2
2          -.00637879*Q3+.00074348*Q4+.00079824*Q5
3          -.00029168*Q6
          Y1=F1*SIN(T1)/SQRT(X)
        END IF
      IF(N.EQ.1) THEN
        Y=Y1
        RETURN
      END IF
C
      END IF
C
C COMPUTE Y2

```

RPT/MST/2500/001

```
C      IF(N.EQ.2) THEN  
          Y=2.*Y1/X-Y0  
          RETURN  
      END IF  
  
C      PRINT 40,N  
40    FORMAT(' ***ERROR IN FUNCTION Y: INVALID ORDER=',I5)  
      Y=0  
  
C      RETURN  
      END  
  
C  
CCCCCCCCCCCCCCCCCCCCCCCCCCCCCCCCCCCCCCCCCCCCCCCCCCCCCCCCCCCCCCCCCC  
C  
      FUNCTION Z01(U)  
  
C  COMPUTES Z01(U) FROM HAMMERSTAD AND JENSEN, 'ACCURATE MODELS  
C  FOR MICROSTRIP COMPUTER AIDED DESIGN', IEEE MTT-S DIGEST 1980.  
C  
C  WRITTEN OCT.15/85-S.KAVANAGH  
C  
      DATA PI2/6.283185308/,ETA/376.7/  
  
C      X=(30.886/U)**0.7528  
      F=6.+(PI2-6.)*EXP(-X)  
      R=SQRT(1.+4./(U*X))  
      Z01=(ETA/PI2)*ALOG(F/U+R)  
  
C      RETURN  
      END
```

LKC

P91 .C654 D49 1986

Development of microstrip
antenna technology for the
Canadian MSAT programme :
final report.

DATE DUE

A blank sheet of white graph paper with a black grid pattern. The grid consists of 10 columns and 20 rows. The paper is slightly tilted and placed on a light-colored surface.

CRC LIBRARY/BIBLIOTHEQUE CRC
P91.C654 D48631 1986

INDUSTRY CANADA / INDUSTRIE CANADA



208056

**COM DEV PRODUCTS AND SERVICES
FOR
COMMUNICATIONS AND RADAR SYSTEMS**

HIGH POWER MICROWAVE PRODUCTS

- High Power Filters, Diplexers, Combiners
- High Power Isolators, Circulators
- High Power Couplers, Splitters, Terminations
- Low Loss Transmit Reject Filters
- Variable Power Combiners
- High Power Antenna Co-polarized Diplexers
- Amplitude Equalizers
- Group Delay Equalizers

COMMUNICATIONS SATELLITE PRODUCTS

- Low Loss, High Order Dual Mode Output Multiplexers
- Beam Switching and Beam Reconfiguring Networks
- High Power Microwave Components and Subsystems
- Waveguide and Coax Isolators, Circulators
- Low Pass Receive Band and Harmonic Band Reject Filters
- Low Loss Preselect Filters
- Group Delay and Amplitude Equalized Input Multiplexers
- Waveguide to SMA Adaptors and Monitor Couplers
- Telemetry and Command Filters
- Variable Power Dividers

CONSULTING SERVICES

- Conceptual, hardware and systems of Microwave transponders and Communications Subsystems for Communications Satellites.
- Tradeoff analyses, layout and hardware design of high power combining and multiplexing networks for Satellite Earth Terminals.
- All software and hardware aspects of devices and subsystems involving microwave filtering networks and ferrite devices for both terrestrial and satellite communications systems.



COM DEV LTD.

155 SHELDON DRIVE,
CAMBRIDGE, ONTARIO, CANADA N1R 7H6
TEL.: (519) 622-2300 • TWX: 610-366-3164

MICROWAVE DEVICES AND SUBSYSTEMS FOR TERRESTRIAL AND SATELLITE COMMUNICATIONS